UNIVERSITA' DEGLI STUDI DI VERONA

DEPARTMENT OF

Biotechnology

GRADUATE SCHOOL OF

Natural Sciences and Engineering

DOCTORAL PROGRAM IN

Biotechnology

Cycle / year XXXI/2015

TITLE OF THE DOCTORAL THESIS

Evolution and regulation of photoprotective mechanisms in microalgae

S.S.D. BIO/04

Coordinator: Prof. Matteo Ballottari

Tutor: Prof. Matteo Ballottari

Doctoral Student: Dott.ssa Laura Girolomoni

Table of contents

1. Riassunto

La fotosintesi ossigenica è un processo per mezzo del quale l'energia solare e l'anidride carbonica (CO_2) sono utilizzate per produrre ossigeno (O_2) e biomassa. La conversione dell'energia luminosa in energia chimica è condotta da complessi multiproteici denominati Fotosistema II (PSII) e Fotosistema I (PSI). Il PSII e il PSI mediano la separazione di carica, la raccolta della luce e il trasporto di elettroni dall'acqua, producendo il potere riducente necessario per fissare la CO_2 in carboidrati (ATP e NADPH). I Fotosistemi sono composti da due unità principali: il centro di reazione, sito in cui avvengono le reazioni biochimiche e la separazione di carica, e il sistema antenna, costituito da complessi proteici di raccolta della luce (LHC), coinvolti principalmente nella raccolta della luce e nel trasferimento dell'energia d'eccitazione al centro di reazione. Gli organismi fotosintetici sfruttano la radiazione fotosinteticamente attiva (PAR) a fini metabolici. Variazioni nell'irradianza, quali l'eccesso di luce, possono determinare condizioni limitanti o di stress, portando alla formazione di specie reattive dell'ossigeno (ROS), le quali, influenzando la crescita delle piante e ne riducono la produttività. L'attivazione del processo di dissipazione termica, denominato *Non-Photochemical Quenching* (NPQ), ha un ruolo fondamentale nella reazione di *quenching* (smorzamento) degli stati eccitati di singoletto della clorofilla, dissipando l'energia di eccitazione sotto forma di calore, prevenendo quindi lo stress foto-ossidativo. Nelle microalghe fino all'80% dell'energia luminosa assorbita può essere riemessa sotto forma di calore con conseguente riduzione della produttività totale di biomassa.

Questa tesi è incentrata sullo studio della regolazione dell'NPQ in diverse specie di alghe. A tale scopo sono stati applicati diversi approcci quali la trasformazione genetica, la caratterizzazione fenotipica e spettroscopica di cellule intere e di complessi proteici isolati. La regolazione dell'NPQ a livello del PSII e del PSI è stata ampiamente studiata anche in relazione alle proteine LHC nell'organismo modello per le alghe verdi, *Chlamydomonas reinhardtii*, in cui è stata evidenziata un'attività di *quenching* in entrambi i Fotosistemi. Nella specie di microalga di uso commerciale, *Chlorella vulgaris*, la regolazione dell'NPQ è stata studiata in relazione all'accumulo di zeaxantina, evidenziandone una forte dipendenza. Infine, la regolazione fotosintetica è stata monitorata in cellule intere e in complessi isolati nella microalga *Haematococcus*

pluvialis, in presenza di forti stress indotti dall'eccesso di energia luminosa e dalla carenza di nutrienti.

CAPITOLO I

Il Capitolo I di questa tesi è stato incentrato sullo studio del regolamento dell'NPQ nell'organismo modello *Chlamydomonas reinhardtii*. In questa microalga l'NPQ è principalmente regolato da LHCSR1 e LHCSR3, ma, la maggior parte delle informazioni presenti in letteratura, riportano un'attività di *quenching* su complessi LHCII-PSII, mentre sono presenti poche informazioni sul PSI. Nella sezione A del Capitolo I, è stata studiata l'attività di *quenching* delle subunità LHCSRs sui super-complessi LHCII-PSII e PSI. Il contributo di fluorescenza dal PSI è stato valutato registrando gli spettri di emissione e di eccitazione ed eseguendo analisi risolte nel tempo a 77K di cellule intere in stato "smorzato" e "non smorzato". Le proprietà di *quenching* sono state misurate in mutanti sull'espressione dei prodotti genici LHCSR1 o LHCSR3 e/o sulle transizioni stato-1-stato 2. Da questo lavoro è stato possibile concludere che l'NPQ si verifica attraverso il PSII e attraverso le proteine LHCII legate al PSI con un meccanismo velocemente reversibile che richiede LHCSRs e dipende dal pH lumenale delle membrane tilacoidali. I sistemi antenna hanno un ruolo cruciale in questo processo e una conoscenza dettagliata della famiglia proteica LHC è di particolare importanza nell'addomesticazione delle alghe unicellulari. Nella sezione B di questo capitolo è stata data maggiore attenzione alle LHCII e al loro contributo sulla regolazione dell'NPQ. Le proteine LHCII sono complessi trimerici, codificati da nove geni altamente conservati e funzionalmente specializzati chiamati *LHCBM1-LHCBM9*. In questa sezione è stata determinata la funzione di tre proteine antenna (LHCBM4/6/8) con un duplice approccio. I prodotti genici sono stati analizzati mediante ricostituzione *in vitro* e analizzando le loro caratteristiche biochimiche e spettroscopiche. Inoltre, la loro funzione fisiologica è stata studiata producendo ceppi mutanti silenziati e caratterizzandoli *in vivo*. Da questo lavoro concludiamo che le subunità LHCBM4/6/8 possono essere trovate nei super-complessi del PSII liberi nelle membrane o scarsamente connessi al PSII. La riduzione dell'accumulo delle subunità LHCBM4/6/8 ha inoltre causato una riduzione significativa dell'attività di NPQ e della fotoprotezione.

CAPITOLO II

Nel Capitolo II, è stata rivolta maggiore attenzione a specie di microalghe di uso industriale quali, *C. vulgari*s e *H. pluvialis*. *Chlorella vulgaris* è un'alga verde coltivata per la produzione di cibo e biocarburanti, ma sono presenti poche informazioni sulla sua genetica. Nella sezione A del Capitolo II sono stati presentati i genomi nucleari e degli organelli di *Chlorella vulgaris* 211/11P. A tale scopo, il *next generation sequencing* e l'*optical mapping* di molecole di DNA isolate sono stati combinati con dati di RNAseq di cellule cresciute in alta o bassa luce per l'annotazione funzionale del genoma. Il genoma nucleare è stato assemblato in 14 pseudo-molecole e sono stati riconosciuti 10746 geni. L'annotazione funzionale delle sequenze genomiche del nucleo, del cloroplasto e del mitocondrio mostra un trasferimento genico orizzontale dal cloroplasto al genoma mitocondriale. È interessante notare che, inoltre, è stato identificato un singolo grande gene codificante per un complesso multi-subunità fungal/animal fatty-acid-synthase type I. Grazie alle informazioni riportate nella sezione A di questo capitolo, siamo stati in grado di focalizzare la nostra attenzione su un altro meccanismo coinvolto nella regolazione dell'NPQ nelle piante superiori: il ciclo delle xantofille. In questo ciclo, in condizioni di stress, la violaxantina viene de-epossidata in zeaxantina dall'enzima violaxantina de-epossidasi (VDE) che non è conservata tra piante superiori e le alghe verdi. Nella sezione B del Capitolo II, abbiamo identificato e caratterizzato l'enzima VDE in *C. vulgaris*. L'allineamento multiplo delle sequenze di VDE, da *C. vulgaris* e da altri organismi, ha consentito l'identificazione di quasi tutti i residui chiave necessari per l'attività enzimatica nelle piante superiori. L'attività catalitica della VDE è stata valutata mediante saggio *in vitro* della proteina ricombinante e *in vivo* utilizzando un inibitore specifico per la sua attività (DL-Dithiothreitol; DTT), dimostrando l'esistenza dell'attivazione e della funzione del ciclo delle xantofille simile alle piante in *C. vulgaris*, diversamente dagli altri Chlorophyta come *C. reinhardtii*. Nel Capitolo II, sezione C e D, abbiamo analizzato la regolazione fotosintetica dell'alga *H. pluvialis* in condizioni di stress. *H. pluvialis* è una microalga verde, studiata per la sua capacità di accumulare alti livelli di astaxantina, un potente ketocarotenoide con una forte attività antiossidante, prodotta in condizioni di stress. Nella sezione C sono state studiate le influenze della crescita in condizione di alta luce e/o di carenza d'azoto sulle proprietà fotosintetiche. Si è dimostrato che la carenza di azoto stimola la degradazione della

clorofilla b, la clororespirazione e il trasporto ciclico degli elettroni con la conseguente inibizione della biosintesi delle clorofille, mentre elevate concentrazioni di luce determinano una destabilizzazione del PSII. Inoltre, la combinazione di entrambe queste condizioni di stress induce una risposta fotoprotettiva più rapida e una massima produzione di astaxantina. Nella sezione D sono state analizzate le proprietà biochimiche e spettroscopiche di complessi proteici leganti pigmenti di *H. pluvialis* responsabili della raccolta della luce e della conversione dell'energia. In particolare, è stato dimostrato che la transizione dalla fase verde a quella rossa non migliora la fotoprotezione dei Fotosistemi, mentre inducendo la sostituzione parziale del β-carotene nel PSI e nel PSII porta alla destabilizzazione entrambi. Inoltre, l'astaxantina legandosi ai Fotosistemi riduce l'efficienza di trasferimento dell'energia di eccitazione ai centri di reazione.

1. Summary

Oxygenic photosynthesis is a process by which sunlight energy and CO_2 are used to produce O_2 and biomass. The light energy conversion into chemical energy is carried forth by multiproteic complexes called Photosystem II (PSII) and Photosystem I (PSI). PSII and PSI drive charge separation, light harvesting and electron transport from water, producing the reducing power necessary to fix CO_2 into carbohydrates (ATP and NADPH). Photosystems are composed by two moieties: a core reaction center, site of biochemical reactions and charge separation, and an antenna system constituted by Light Harvesting Complex (LHC) proteins mainly involved in light harvesting and excitation energy transfer to the reaction center. Photosynthetic organisms use the photosynthetically active radiation (PAR) for their metabolic processes but irradiance undergo changes and light excess becomes a limit or even a stressor leading to the formation of Reactive Oxygen Species (ROS) which influence plant growth and could decrease crop productivity. Photo-oxidative stress can be prevented by activation of thermal dissipation process called Non-Photochemical Quenching (NPQ), which has an important role in quenching chlorophylls singlet excited states dissipating the excitation energy in form of heat. In microalgae, up to 80% of absorbed light energy can be re-emitted as heat with a consequent reduction of total biomass productivity. This thesis was focused into the investigation of NPQ regulation in several algae species. For this purpose, different approaches were applied including genetic transformation, phenotypic and spectroscopic characterization of entire cells and of isolated complexes. The NPQ regulation at the level of both PSII and PSI also in relation with LHC proteins was fully investigated in the model green alga *Chlamydomonas reinhardtii* evidencing a quenching activity in both Photosystems. In the commercial microalga specie, *Chlorella vulgaris*, the NPQ regulation was studied in relation with zeaxanthin accumulation evidencing a strong dependency. Finally, in the microalga *Haematococcus pluvialis*, the photosynthetic regulation was also monitored in entire cells and isolated complexes, in presence of strong stresses induced by light excess and nutrients depletion.

CHAPTER I

The Chapter I of this thesis was focused on study of the NPQ regulation in the model organism *Chlamydomonas reinhardtii*. In this microalga NPQ is mainly regulated by

LHCSR1 and LHCSR3 but, most of the information present in literature, report a quenching activity on LHCII-PSII complexes, while few information about PSI are present. In the Chapter I section A, the quenching activity of LHCSRs subunits on LHCII-PSII and PSI supercomplexes was investigated. The PSI fluorescence contribution was evaluated by recording emission and excitation spectra, and by performing time-resolved analysis at 77K of whole cells in quenched and unquenched states. The quenching properties were measured in mutants affected on the expression of LHCSR1 or LHCSR3 gene products and/or state-1-state 2 transitions. From this work we conclude that NPQ occurs through PSII and LHCII bound to PSI with a fast-reversible mechanism which requires LHCSRs and is dependent on thylakoid lumenal pH. The antenna systems have a crucial role in this process and a detailed knowledge of LHC protein family is of special importance in the domestication of unicellular algae. In the section B of this Chapter more attention was given to LHCII and their contribution on NPQ regulation. LHCII are trimeric protein complexes, encoded by nine highly conserved genes called *LHCBM1–LHCBM9* and each protein component is functionally specialized. In this Chapter we analyzed the role of three antenna proteins (LHCBM4/6/8) with a double approach. The gene products were analyzed by *in vitro* refolding and by analyzing their biochemical and spectroscopic characteristics. Furthermore, their physiologic function was studied by producing of knock down mutant strains and characterizing them *in vivo*. From this work we conclude that LHCBM4/6/8 subunits could be found in the PSII supercomplexes free in the membranes or poorly connected to PSII. The reduction of LHCBM4/6/8 subunits caused a significant reduction of the NPQ activity and photoprotection.

CHAPTER II

In the Chapter II, more attention was given to commercial species of microalgae strains like *C. vulgaris* and *H. pluvialis*, due to their industrial application. *Chlorella vulgaris* is a green alga cultivated at industrial level for food and biofuel production, but few information about its genetic are present. In the Chapter II section A, the *Chlorella vulgaris 211/11P* nuclear and organelle genomes were presented. For this aim, next generation sequencing and optical mapping of isolated DNA molecules were combined with RNAseq data of low or high light grown cells for the genome functional annotation. Nuclear genome was assembled into 14 pseudo-molecules and 10746 genes were

recognized. The functional annotation of nuclear, chloroplast and mitochondrial genome sequences demonstrate a horizontal gene transfer from chloroplast to mitochondrial genome. Interestingly, a single large gene encoding for a fungal/animal-like fatty-acid-synthase type I multi-subunit complex was also identified. Thanks to the information reported in the section A of this Chapter, we were able to focus our attention on another mechanism involved in the regulation of NPQ in higher plants: the xanthophyll cycle. In this cycle, upon stress condition, violaxanthin is de-epoxidated into zeaxanthin by the violaxanthin de-epoxidase (VDE) enzyme which is not conserved among higher plants and green algae. In the Chapter II section B, we identified and characterized the VDE enzyme in *C. vulgaris*. Multiple alignment of VDE sequences, from *C. vulgaris* and other organisms, allow us to identify almost all the key residues required for the enzymatic activity in higher plants. The VDE catalytic activity was evaluated by *in vitro* assay of the recombinant protein, and *in vivo* by using a specific inhibitor for its activity (DL-Dithiothreitol; DTT), demonstrating the existence of plant-like xanthophyll cycle activation and function in *C. vulgaris*, differently from other Chlorophyta as *C. reinhardtii.* In the Chapter II section C and D, we analysed the photosynthetic regulation of the alga *H. pluvialis* under stress conditions. *H. pluvialis* is a green microalga, studied for its ability to accumulate high levels of astaxanthin, a potent ketocarotenoid with a strong anti-oxidant activity, produced upon stress conditions. In the section C, the influence of high irradiances and/or nitrogen starvation on the photosynthetic properties were investigated. We showed that nitrogen starvation stimulates the chlorophyll b degradation, chlororespiration and cyclic electron transport with the concomitant chlorophyll biosynthesis repression, while high light induced a PSII destabilization. Moreover, the combination of these two stresses induced the fastest photoprotective response and highest astaxanthin production. In the section D, the biochemical and spectroscopic properties of the *H. pluvialis* pigment binding complexes responsible for light harvesting and energy conversion were analysed. We showed that the transition from the green to red phase does not improve the Photosystem photoprotection, while induce the partial β-carotene substitution in PSI and II destabilizing both. The astaxanthin binding to the Photosystems also reduces the efficiency of excitation energy transfer to the reaction centers.

2. Introduction

2.1. Microalgae
Subcellular organization and sexual cycle

Algae are the first oxygen-releasing photosynthetic organisms, with a simple cellular organization, appeared on Earth. Microalgae are described as “lower plants” without a cellular differentiation like stems, roots and leaves mainly living in aquatic ecosystems. Currently, more than 246,000 species are knew but this number is continuously increasing. Algae group comprehends both eukaryotic and prokaryotic organisms. The first group is composed by green algae (Chloropyceae), diatoms (Bacillariophyceae), yellow-green algae (Xanthophyceae), golden algae (Chrysophyceae), red algae (Rodophyceae), brown algae (Phaeophyceae), dinoflagellates (Dinophyceae) and pico-plankton (Prasinophyceae and Eustigmatophyceae). The prokaryotic algae are represented by cyanobacteria (Cyanophyceae). The size of algal cells is highly variable (1µm-60m); the smallest described is *Ostreococcus tauri* (Prasinophyceae), characterized by a cell diameter of less than 1µm; in contrast the largest is a brown alga *Macrocystis pyrifera* (Phaeophyceae) which grows up to 60m and is often the prevailing organism in kelp forests (Hallmann, 2007) (Figure 1).

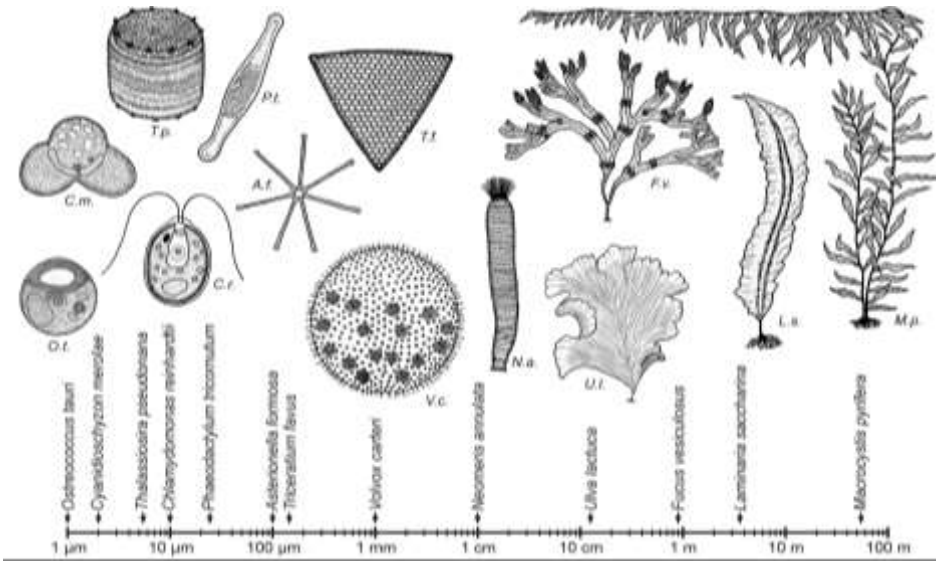

Figure 1 *Example of different phenotypes and size of algae species. In this figure a logarithmic scale of cells dimension is showed. (Hallmann, 2007).*

Microalgae have different morphologies not only in relation to species but also to different life stages. There are various cellular organization structures such as ameboid, palmelloid (capsoid), coccoid, filamentous, flagellate and sarcinoid. The internal algae cell structure is characterized by high variability. The cyanobacteria or blue-green algae have a prokaryotic organization which closely resembles bacteria. Eukaryotic algae have a nucleus, one or more chloroplasts, mitochondria, endoplasmic reticulum, Golgi bodies and other typical eukaryotic organelles. The model species, for the study of microalgae, is *Chlamydomonas reinhardtii*, a unicellular flagellate alga of *Volvaceae* family and *Chlorophyta* division. Its cultivation is simple, it has a short mitotic cycle, small cell dimension (10 µm diameter) and both mitochondrial and chloroplastic genomes have been sequenced (Harris, 2001; Merchant *et al.*, 2007). Moreover, the techniques for its sexual cycle manipulation and both nuclear and chloroplastic genome transformation are well knew (Harris, 2001; Remacle *et al.*, 2006; Purton, 2007). *C. reinhardtii* grows on liquid and solid media, with neutral pH and without vitamins or other additional factors in both autotrophic and heterotrophic environments; it lives at temperature between 20-25°C with a light intensity of 200-400 µmol photons $m^{-2}sec^{-1}$. *C. reinhardtii* has a cell wall mainly composed by seven layers of proteoglycans, hydroxyproline-rich glycoproteins, from which two anterior flagella of 10-12 µm in length, protrude (Woessner and Goodenough, 1994). Nuclear membranes are near one of the four Golgi bodies in continuous with the endoplasmic reticulum (Figure 2).

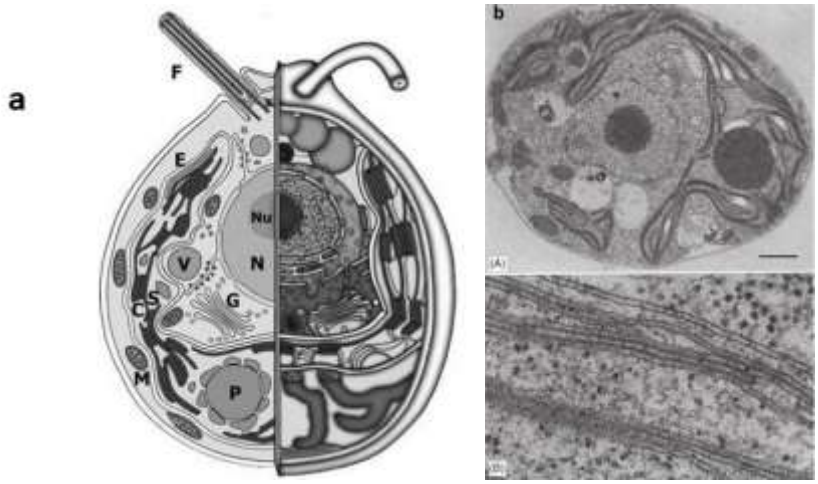

Figure 2 *A scheme (a) of C. reinhardtii cell. (E, eyespot; G, Golgi bodies; L, lipid bodies; M, mitochondrion; P, pyrenoid; S, starch granules; N, nucleus; Nu, nucleolus. Section (b) of C. reinhardtii WT grow mixotrophically (entire cell A and portion of the same cell at higher magnification B) (Harris, 2009).*

There are two contractile vacuoles located at the anterior of the cell which pulsate alternately at intervals of 10-15 seconds depending on the conditions while the chloroplast, site of photosynthesis, occupies two thirds of the cell (Luykx *et al.*, 1997). The chloroplast is the result of an endosymbiotic process deriving from a photosynthetic prokaryote (a cyanobacterium-like cell) engulfed by a mitochondriate eukaryote (Raven and Allen, 2003). This organelle has become fully integrated into the biology of the host eukaryotic cell resulting in loss of most plastid genes, whose functions were substituted by nucleus-encoded proteins. Many chloroplast multi-protein complexes contain subunits encoded by both the plastid and the nucleus and their assembly requires the expression of both chloroplast and nuclear genes (Martin and Herrmann, 1998). Chloroplast is delimited by two membranes called envelope: the external membrane is permeable and the internal is more selective due to the presence of specialized transporter systems. Within the chloroplast, there are complex lipoprotein membrane systems called thylakoids which divide the organelle's volume into two compartments: the lumen and the stroma (Staehelin, 1986). In the stroma, Calvin-Benson cycle enzymes are located together with the chloroplastic genome and the machineries for protein synthesis and plastome replication (Benson and Calvin, 2000). Differently from higher plants in the chloroplast of microalgae single pyrenoid is located in the broad basal area. Pyrenoid is a spherical body with a high Rubisco concentration, the dominant protein involved in the Calvin-Benson cycle where inorganic CO_2 is fixed to organic sugars. An additional important variance with higher plants is the thylakoid membranes organization, which can be either single or arranged in stacks of 2-10 discs, but multidisc grana are not present. The eyespot (or stigma), orange in colour due to the high carotenoids concentration, represents a specialized lipid accumulation site associated with flagellum. With the eyespot, cell detects incident light direction and swim toward or away from the light source (Harris, 2009). The nuclear genome of *C. reinhardtii* is haploid, composed by 17 chromosomes and the size is estimated to be $1.2*10^{\wedge 5}$ Kbp with a GC composition of 64% (Merchant *et al.*, 2007). The chloroplastic genome is circular and composed by approximately 200 Kbp (Maul *et al.*, 2002); the mitochondrial genome is linear and smaller (15.8 Kbp) (Michaelis *et al.*, 1990). *C. reinhardtii* is a haploid organism which replicate by mitosis, but it can start a sexual reproduction cycle to survive under stress conditions (Figure 3).

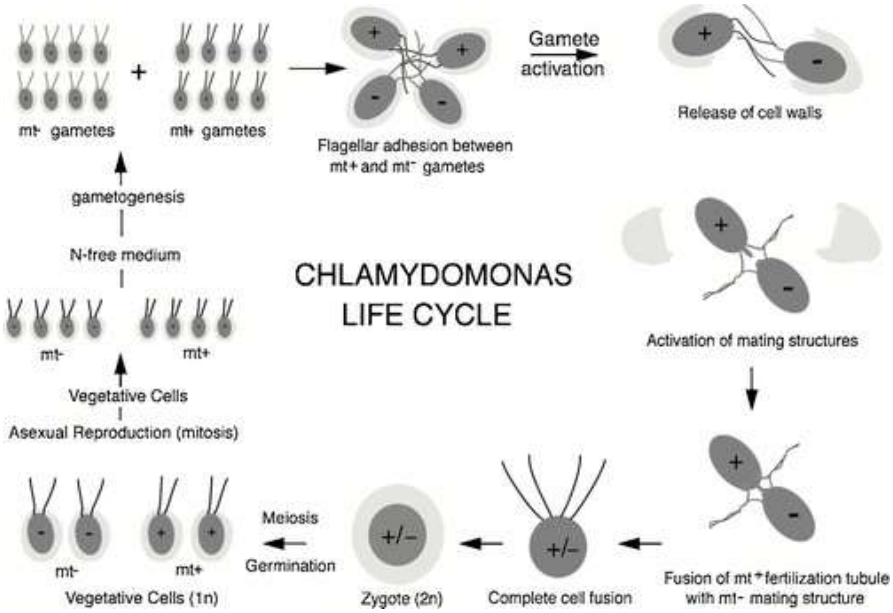

Figure 3. *Life cycle of C. reinhardtii. In the asexual reproduction cycle cells divide by fission, the protoplast divide forming 4-8 zoospores similar to the parent. During stress condition cells became isogametes starting the sexual reproduction. Gametes fuse in pairs forming a zygote, which lose flagella and produces a thick wall until the environmental conditions return favourable. The zygote undergoes meiosis to form 4 haploid zoospores (Harris, 2001).*

Cells have a *mating type* locus with two different alleles, plus (mt+) or minus (mt-), which are expressed in stress condition such as nitrogen starvation. Contact between a plus and minus gamete is mediated by agglutinin molecules, exposed on the flagella surface. This adhesion generates a transduction signal involving cAMP, which allows for gamete fusion with the activation of a transcription factor for zygote differentiation. Nuclei fuse, flagella are reabsorbed, and a thick cell wall is assembled around the zygote to increase stress resistance. When the environmental conditions are advantageous, meiotic division occurs to generate four haploid cells with mitochondria from *minus* gamete and chloroplast from *plus* gamete (Goodenough *et al.*, 2007). Microalgae are interesting organisms for their ability to produce high value chemicals and pharmaceuticals (Spolaore *et al.*, 2006; Hallmann, 2007) and for their use as bioenergetic resource (Hannon *et al.*, 2010). Moreover *C. reinhardtii* has been studied for the possibility to use as a substrate for anaerobic fermentation in the biogas production (Mussgnug *et al.*, 2010) and to photobiologically generate molecular hydrogen (Melis *et al.*, 1999; Zhang and Melis, 2002; Kruse *et al.*, 2005).

2.2. Oxygenic photosynthesis

Photosynthesis is a process in which sunlight energy and CO_2 are converted into organic matter. The first photosynthetic organism, evolving this mechanism about 3 billion years ago, was a bacterium which used light in order to pump protons across a membrane driving electrons from electron donor as Fe^{2+} or H_2S to CO_2. The development of oxygenic photosynthesis was one of the most important event in Earth's history for it changed the redox balance, and allowed for development of an aerobic metabolism. The key, in developing oxygenic photosynthesis, was the development of the OEC (Oxygen Evolving Complex) manganese complex, capable of water oxidation. Prokaryotic cyanobacteria and, later, eukaryotic algae created oxygenic atmosphere starting about 2 billion years ago. In photosynthesis, water is used as reducing substrate to produce carbohydrates (CH_2O) and molecular oxygen (O_2) through a series of redox reactions collectively summarized as (1):

$$6H_2O + 6CO_2 \rightarrow C_6H_{12}O_6 + 6O_2 \qquad (1)$$

This endergonic reaction causes an increase of free energy by +2840 kJ per mole of esose produced. The measurement of photosynthetic activity is based on detection of oxygen evolution versus light intensity, in the so called light-response (*P*/*I*) curve (Figure 4) (A., Richmond; H., 2013).

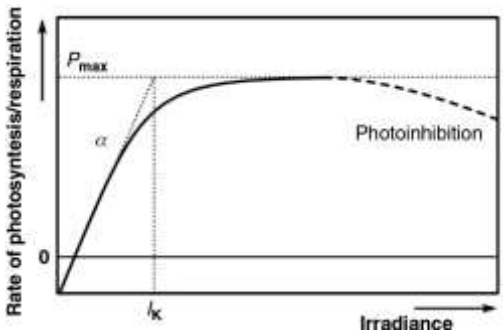

Figure 4. *Photosynthesis light response curve (A., Richmond; H., 2013).*

The initial slope ($\alpha = P_{max}/I_k$) represents the maximum rate of photosynthesis where I_k is the saturation irradiance. In the dark, the net oxygen consumption is a consequence of respiration (negative part of the curve, Figure 4). With low irradiance the rate of photosynthesis has a linear correlation with light intensity, while increasing light intensity photosynthesis becomes less efficient. The maximum rate P_{max} it's defined as

the light intensity at which plateau is reached. Under continuous supra-optimal irradiance, the rate of photosynthesis declines from the light-saturated value due to photoinhibition. The photosynthesis process is functionally divided in two main units, light reactions and dark reactions. In the light reactions, which occurs in the photosynthetic membranes, the light energy is converted into chemical energy with the final production of $NADPH_2$ and ATP. In the dark reactions, which takes place in the stroma, $NADPH^+$, H^+ and ATP are used in the sequential biochemical reduction of CO_2 to carbohydrates.

2.2.1. The light phase

Five proteins complexes, located in the thylakoids membrane, are involved in the light phase reactions: light-harvesting antennae, Photosystem II (PSII), Photosystem I (PSI), cytochrome b_6/f and ATP synthase (ATPase). All these complexes, together, represent the photosynthetic electron transport chain and the photophosphorylation system for solar energy conversion into chemical energy and reducing power (Figure 5).

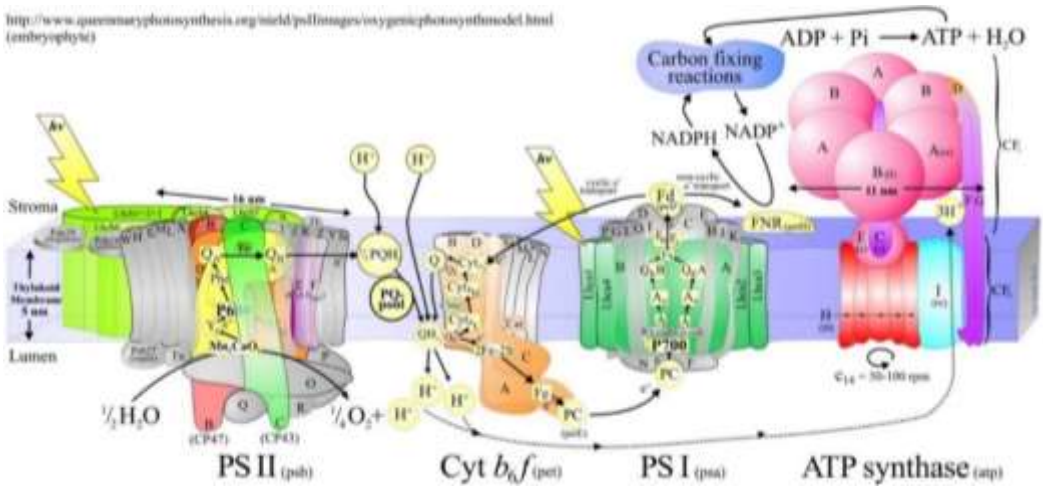

Figure 5. *A schematic model detailing the main photosynthetic complexes engaged in oxygenic photosynthesis. (http://macromol.sbcs.qmul.ac.uk/oldsite/psIIimages/oxygenicphotosynthmodel.html)*

PSII and PSI are responsible for energy conversion, cytochrome b_6/f mediates electron transport between PSII and PSI and contributes to proton translocation in the lumen (Hill and Bendall, 1960). ATPase catalyses ATP synthesis using the proton-motive force (*pmf*), generated during the light reactions and by the cytochrome b_6/f. PSI and PSII bound pigments which absorb photons used for charge transfer. Basing on the redox

potential of reagents and products, the energy required for the production of $NADPH_2$ cannot be provided by only one photon in the visible range of light: for this reason the photosystems work in series in the so called "Z" scheme (Figure 6) (Hill and Bendall, 1960).

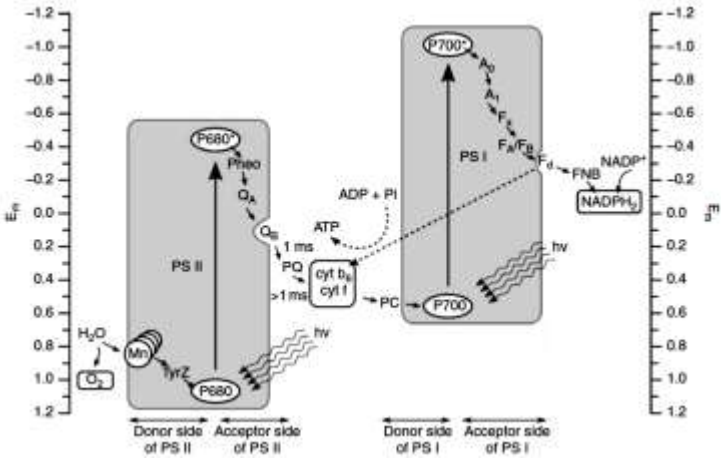

Figure 6. *The "Z" scheme of electron transport chain from water to $NADPH_2$. Cofactors and redox potentials are indicated* (A., Richmond; H., 2013).

In the "Z" scheme, the electron transport goes on from lower to higher values of equilibrium midpoint potential of the individual redox components. In the reaction centers, when a chlorophyll *a* dimer (special couple) is excited, a separation charge event is generated, and one electron is transferred to specific transporters in the thylakoid membranes. When the PSII reaction center is excited by light (λ = 680nm), a strong oxidant ($P680^+$) and a strong reductant (plastosemiquinone, Q_A^-) are produced, leading a charge separation of 1.2V. The positive charge on P680 is neutralized by electron transport from the Mn cluster of OEC via Tyr Z. Four manganese ions, in turn, oxidize water upon accumulation of 4 charges as a consequence of 4 consecutive photo-reactions. Subsequently, the quinone cycle is activated to carry on the electron transport in the cyt b_6/f and the proton translocation to the *lumen.* In detail, after plastosemiquinone (Q_A) reduction by the pheophytin, two electrons are sequentially transferred from Q_A to a secondary acceptor Q_B, which is oxidized by the cyt b_6/f complex. Cytochrome b6f (plastohydroquinone:plastocyanin oxidoreductase) works with a mechanism called Q-cycle in which electrons are transferred from PQH_2 and protons are translocated with a generation of a transmembrane electrochemical H^+ gradient

($\Delta\mu H^+$) (Stroebel *et al.*, 2003). The Q-cycle represents the limitation step of the electronic transport, it requests 1-2ms due to the diffusion of PQH_2 across the membrane. From PQH_2 two protons are released at the Qo site at the lumenal side of the membrane. One electron is transferred, through an iron–sulphur cluster (Fe_2S_2) attached to the Rieske protein to haem f, in the cytochrome f, where it is taken by plastocyanin (PC) (Kurisu *et al.*, 2003). The second electron, through haems bL and bH, is conducted to reduce quinone at the Qi site near the stroma side of the membrane; after two consecutive reduction events, at the Qi site, two protons are taken up from the stroma. From this cycle two plastoquinols are oxidised and 4 H^+ are translocated for every 2 electrons transported to PSI; moreover, an electro-chemical gradient is formed across the membrane. Through PC, a small copper-containing protein, one electron is carried to the P700 in the reaction center of the PSI. The PSI excitation by light (λ = 700nm) produces a strong and stable reductant (Fe-S center, F_X^-) and a weak oxidant ($P700^+$). On the acceptor site of PSI, electrons are transferred from a series of transporters to the ferredoxin. Finally, the reductant ferredoxin transfers the electrons to $NADP^+$ to produce NADPH. The transportation of electrons through thylakoid membranes is coupled with the proton movement from the stroma to the lumen, with the creation of a pH gradient used by the ATPase to produce ATP (Mitchell, 1961). ATPase (ADP kinase ΔpH dependent) is composed by nine subunits arranged into two main subunits CF0 and CF1. The CF0 subunit, inside the thylakoid membranes, is involved in the protons translocation across the thylakoid membrane. Proton movement through CF0 is coupled to ATP synthesis/hydrolysis at the CF1 catalytic site which is exposed to the stroma. When the ratio between $NADPH_2$ and $NADP^+$ is high the electron transport chain can works in a cyclic way in order to generate a proton gradient without PSII involvement. This process is called cyclic photophosphorylation or cyclic electron flow and is used to accumulate ATP but with no $NADPH_2$ and oxygen production. In this mechanism electrons from ferredoxin are transferred to the cytochrome b6f complex through the ferredoxin-plastoquinone oxidoreductase (NADH dehydrogenase); producing a proton gradient and transferring the electrons to PC with the regeneration of the P700 reaction center (Harbinson and Foyer, 1991).

The general reactions of the light phase can be described as (2, 3):

$$2NADP^+ + 2H_20 + \text{light} \rightarrow 2NADPH + O_2 + 2H^+ \qquad (2)$$

$$ADP + Pi + \text{energy} \rightarrow ATP \qquad (3)$$

2.2.2. Dark phase

In the dark phase, $NADPH_2$ and ATP, produced during the light phase of photosynthesis, are used to fix O_2 to sugars through the Calvin-Benson cycle (Figure 7) (Benson and Calvin, 2000). The reaction is expressed as:

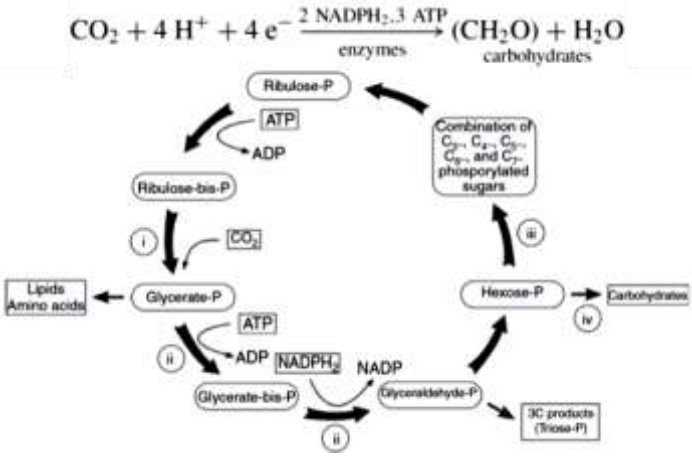

Figure 7. *The Calvin-Banson cycle (A., Richmond; H., 2013).*

The Calvin-Benson cycle can be subdivided in four phases: carboxylation, reduction, regeneration and production. During the carboxylation the ribulose bisphosphate carboxylase/oxygenase (Rubisco) catalyses the addiction of two CO_2 molecules to ribulose bisphosphate (Ribulose-bis-P) to produce two molecules of phosphoglycerate (Glycerate-P). During the reduction the glycerate-P is converted in a Triose-P by using $NADPH_2$ and ATP. In the regeneration, the ribulose-P is regenerated for further CO_2 fixation in several reactions. Lastly the final photosynthesis products such as carbohydrates, fatty acids and organic acids are produced. The carboxylation phase has a competing process, the photorespiration. In the photorespiration the phosphoglicolate, produced by oxygenation of RubP in the presence of the competitive inhibitor O_2, organic carbon is converted into CO_2 without metabolic gain. Photorespiration depends on the relative O_2/CO_2 ratio; for this reason, microalgae had evolved carbon-concentrating mechanism to provide Rubisco with high levels of CO_2.

2.2.3. Photosynthetic pigments

In the light phase, photosynthetic complexes use pigments for light harvesting and for use of excitation energy. Pigments absorb light at the wavelength corresponding to a

quantum jump in their energy levels, to produce excited states. Microalgae contain three major classes of pigments: Chlorophylls (Chl), Carotenoids (Car) and phycobilines. Algae classification is based on their pigments composition. Green algae (Chlorophyta, Charophyta, Euglenophyta) such as *C. reinhardtii* have a pigments composition similar to higher plants, with Chl a, Chl b, xanthophylls and *β*-carotene (*β*-Car). Eustigmatophyceae lack Chl b and have only Chl a and *β*-Car. The brown algae (Phaeophyta, Chrysophyta, Pyrrhophyta e Cryptophyta) are rich in Chl a, Chl c and xanthophylls.

2.2.3.1. Chlorophylls

Chlorophylls are characterized by a tetrapyrrole ring structure (porphyrin) with a central magnesium atom coordinated by four nitrogen atoms. Chls are classified in five main types depending on their side-group substituents: Chl a, b, c d and f. The number of double conjugated bonds on the porphyrin and the side-group substituents, change the light absorption ability in the visible region and, therefore, their spectroscopic properties. In higher plants and green algae are present Chl a and b, which are distinguished by the carbon substitute in the second pyrrolic ring: Chl a has a methyl group ($-CH_3$), Chl *b* has a formyl group (-COH) (Figure 8A).

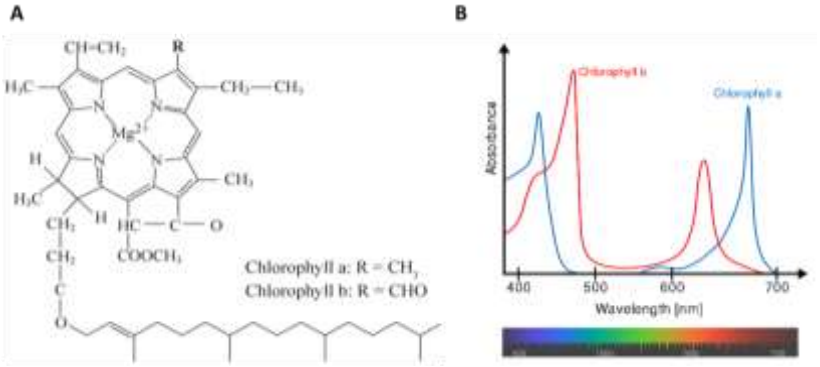

Figure 8. *A) Structure and B) absorption spectrum of Chl a and b.*

Their synthesis starts from a glutamic acid and occurs inside the chloroplast; moreover ,except for Chl c, a terpenoid alcohol chain, important for their stability in membranes (20 carbon atoms phytol chain), is presents (Malkin and Niyogi, 2000). Chlorophylls absorb in the Soret region (450-475nm) and in the Qy region (630-675nm) and are characterized by a high molar coefficient of extinction ($<10^5$ M^{-1} cm^{-1}) (Figure 8B). Qy

region corresponds to the S0 to S1 electron transition while the Soret band is related to higher transition states. These pigments have an important role also in protein stabilization by water or lipid molecules or with the central Mg which bound nucleophilic amino acids residues like histidine (Jordan *et al.*, 2001; Liu *et al.*, 2004). Chl a is present in all oxygenic photoautotrophs, in the core and reaction center pigment-protein complexes. In the light-harvesting antennae, it is present together with Chl b or Chl c, and are necessary for the correct proteins folding, like for LHC (Light harvesting complex) (Paulsen *et al.*, 1993).

2.2.3.2. Carotenoids

Carotenoids are polyisoprenoid composed by 40 carbons atoms produced in plants, algae, some bacteria and fungi. These pigments are synthetized in the chloroplast by eight isoprene molecules condensation, and are characterized by a polyenic chain, two terminal rings with six carbons atoms. The chromophoric system is constituted by a central light-absorbing conjugated polyene compound, which absorb light between 400-500nm in the visible region of the electromagnetic spectrum. Carotenoids are divided into two classes: carotenes which are composed by carbon and hydrogen, and xhantophylls which include also oxygen, responsible for the higher molecule polarity (Bhosale and Bernstein, 2005). Carotenes are mainly found connected to the core complex of both photosystems, while xanthophylls to the antenna complexes (Bassi *et al.*, 1993; Ruban *et al.*, 1999; Caffarri *et al.*, 2001). In higher plants carotenoids include α and β carotene and the xanthophylls lutein, violaxanthin, neoxanthin and zeaxanthin. *C. reinhardtii*, also contains another carotenoid, absents in higher plants, called loroxanthin which is synthesized in the α-carotene branch (Figure 9A). Another important keto-carotenoid is astaxanthin which is accumulated in high level in the green alga *Haematococcus pluvialis* (Boussiba, 2000; Lemoine and Schoefs, 2010; Han *et al.*, 2013). Astaxanthin is mainly used as colouring agent in aquaculture, for the animal red pigmentation, but has been also reported its strong effect in preventing reactive oxygen species (ROS) production and lipids peroxidation in solution and in several membrane systems (Terao, 1989; Lorenz and Cysewski, 2000; Guerin *et al.*, 2003; Stahl and Sies, 2005) (Figure 9B).

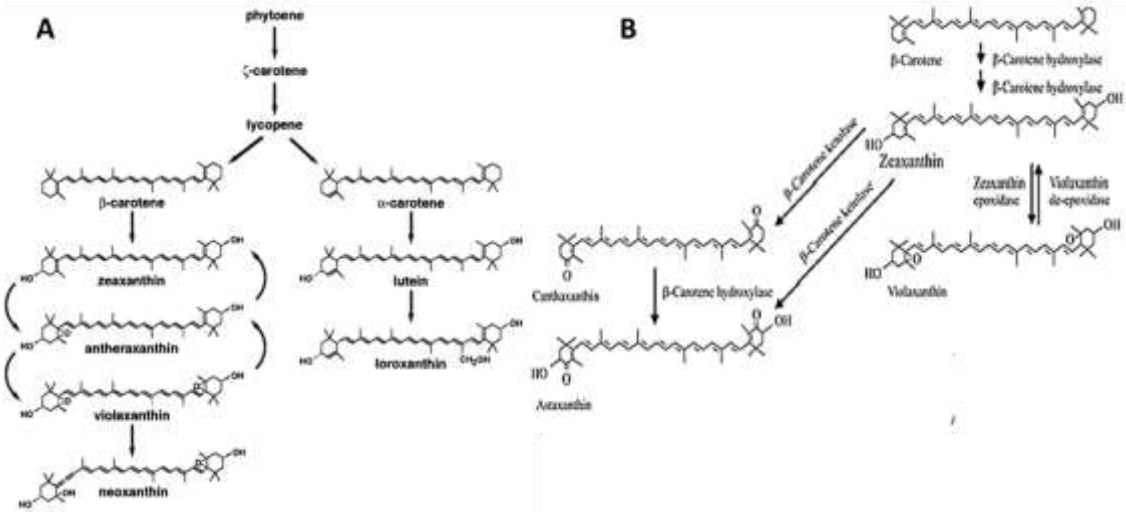

Figure 9. *A) Carotenoids biosynthetic pathway in C. reinhardtii B) Astaxanthin biosynthetic pathway.*

Carotenoids have different roles in the photosynthetic apparatus: they are accessory light-harvesting pigments for transferring excitation energy to Chl a and are necessary, like Chls, for the right assembly and stabilization of proteins complexes in thylakoids membranes (Plumley and Schmidt, 1987; Mimuro and Katoh, 1991; Paulsen *et al.*, 1993). Carotenoids interact with proteins through non-covalent bounds, across hydrophobic interaction (Gastaldelli *et al.*, 2003). They are also important for photo-protection dissipating energy excess to bring back chlorophylls to the ground state and for oxygen free radicals (ROS) scavenging (Moore *et al.*, 1982; Havaux and Niyogi, 1999).

2.2.3.3. Xanthophyll cycle

The xanthophyll or violaxanthin (Vx) cycle is a group of reactions in which Vx is de-epoxidated into zeaxanthin (Zx) (Figure 10).

Figure 10. *Violaxanthin cycle. The enzymes, substrates and cofactor involved are show in the figure. Simbol + indicates that high amount of substrates needed for enzymatic activity. VDE violaxanthin de-epoxidase, e, ZEP zeaxanthin epoxidase, Asc ascorbate, MGDG, monogalactosyl-diacylglycerole (Goss and Jakob, 2010)*

The conversion of Vx into Zx is important for the excess excitation energy dissipation in the PSII antenna system, in order to prevent the photodamage of the photosynthetic apparatus, through for example non- photochemical quenching (NPQ) (Demmig-Adams *et al.*, 1990; Horton and Ruban, 1992; Gilmore and Yamamoto, 1993). The xanthophylls cycle is presents in higher plants, green and brown algae (Yamamoto *et al.*, 1962). The Vx is converted into Zx across two de-epoxidation steps, catalysed by the enzyme violaxanthin de-epoxidase (VDE); while the reverse reaction is catalysed by the enzyme zeaxanthin epoxidase (Yamamoto and Kamite, 1972). The intermediate of the reaction is antheraxanthin (Ax) which contains one epoxy group. VDE is a nuclear encoded protein, transported in the thylakoid lumen through a transit peptide. This enzyme is activated by lumenal acidification upon transmembrane proton gradient formation, consequence of an high light environment (Gilmore and Yamamoto, 1993). The de-epoxidation reactions require ascorbate to reduce the epoxy group producing water (A., Richmond; H., 2013). VDE activity is inhibited by dithiothreitol (DTT) which reduces one or more disulfide bonds formed by cysteine residues (Yamamoto and Kamite, 1972). In microalgae, unlike higher plants, the role of xanthophyll cycle seems to be not homogeneous. In the model green alga *C. reinhardtii* was seen that the Zx production is not required for the ApH-dependent NPQ (Niyogi *et al.*, 1997*a*). Instead *Chlorella vulgaris* and *Chlorella saccharophila* show a zeaxanthin-dependent NPQ (Quaas *et al.*, 2015).

2.2.4. Photosystems

Photosystems are multisubunit transmembrane pigment protein complexes involved in light energy conversion and electrons transport, composed by a core reaction center and antenna complexes (Boekema *et al.*, 1995; Ben-Shem *et al.*, 2003). The core reaction center is the site of biochemical reactions and charge separation and binds β-carotene and chlorophyll a. Antenna complexes are mainly involved in light harvesting and excitation energy transfer to the reaction center, placed energetically downhill, bounding xanthophylls, chlorophyll a and b. Core complexes work as energy trap for the excitation energy derived from the peripheral antenna promoting the excitation transfer to the electron transport chain. This behaviour is allowed by their spectroscopic characteristics and in particular by their absorption spectra which are shifted to higher wavelengths compared to antenna proteins. PSII and PSI show differences in light absorption and in charge separation quantum efficiency. The PSI absorbs far-red light with a quantum

efficiency of charge separation around 1; the PSII absorbs red light and its quantum efficiency is more variable also depending on the antenna system (Wientjes *et al.*, 2013). Genes encoding core proteins are called *Psa* and *Psb* for the PSI and the PSII, respectively. Encoding genes are located in both plastidial and nuclear genome and the polypeptides, which codified, show homology between photosynthetic organisms (Ballottari *et al.*, 2012). The antenna complexes, belong to LHC (Light Harvesting Complex) family, are called LHCI or LHCII depending on the principal association with the PSI or PSII and are codified by *Lhca* or *Lhcb* genes respectively for the PSI and PSII, showing more variability through the evolution (Jansson, 1999; Dekker and Boekema, 2005). LHCs proteins are encoded by nuclear genes and translated in the cytoplasm, after which they are targeted to the two translocons traversing the outer (Toc) and inner (Tic) envelope membranes, which catalyse proteins import into the stroma. In the stroma, the transit peptide is removed and the proteins assemble with chlorophylls and carotenoids in the thylakoids membrane (Oreb *et al.*, 2008).

2.2.4.1. Photosystem II

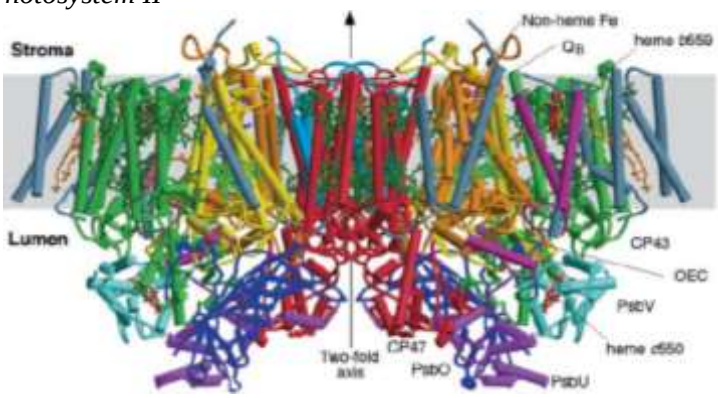

Figure 11. *3D crystal structure of PSII core complex from the cynobacterium T. elongatus (Ferreira et al., 2004).*

PSII is a homodimeric multiproteic complex that catalyse electron transfer from water to PQ producing oxygen. It's located in the thylakoid membranes and is composed by 20-30 subunits with a relative molecular mass of about 350 kDa (Figure 11). The precise number of subunits which composed this complex is unknown and is species-specific. PSII is composed by a quinone type reaction center (6Q-type/type II), an Oxygen-Evolving Complex (OEC) and by an inner light-harvesting complexes. PSII core complex of *C. reinhardtii* is predicted to have a dimeric structure as plants and

cyanobacteria. The PSII reaction center contains D1 and D2 proteins, and the α and β subunits of cyt b_{559} (PsbE and PsbF). D1 and D2, encoded by the plastidial genes *PsbA* and *PsbD*, carry all prosthetic groups for charge separation, and also binds the special Chl a pair of P680 and the cofactors necessary for electron transport (pheophytin, Q_A, Q_B). D1 and D2 bind 6 Chl a, 2 pheophytins, 2 β-carotenes, 2 phylloquinones and iron. In the lumenal side the OEC is composed by the gene products PsbO, PsbP, PsbQ, PsbR, which stabilize the manganese cluster (4 Mn). Inner antenna proteins CP47 and CP43, important for excitation energy transfer from peripheral antenna to the reaction center, are located on either sides of D1 and D2 and bind 29 Chl a and β-carotene. PSII core binds about 45 Chl a and 11-12 β-carotenes (Ferreira *et al.*, 2004; Umena *et al.*, 2011; Caffarri *et al.*, 2014). LHCII antenna proteins, mainly associated with PSII, include monomeric and trimeric isoforms. Monomeric minor antenna in *C. reinhardtii* are LHCB5 (CP26) and LHCB4 (CP29) which are located near the PSII core complex, binding CP43 and CP47 (Bassi *et al.*, 1993). These proteins contribute in PSII-LHCII super complexes formation with three LHCII trimers attached to both sides of the dimeric core ($C_2S_2M_2L_2$) (Tokutsu *et al.*, 2012; Drop *et al.*, 2014). In *C. reinhardtii* about six LHCII trimers for monomeric PSII core are present and are encoded by nine *Lhcbm* genes called *Lhcbm1-Lhcbm9* (Figure 12) (Merchant *et al.*, 2007; Drop *et al.*, 2014).

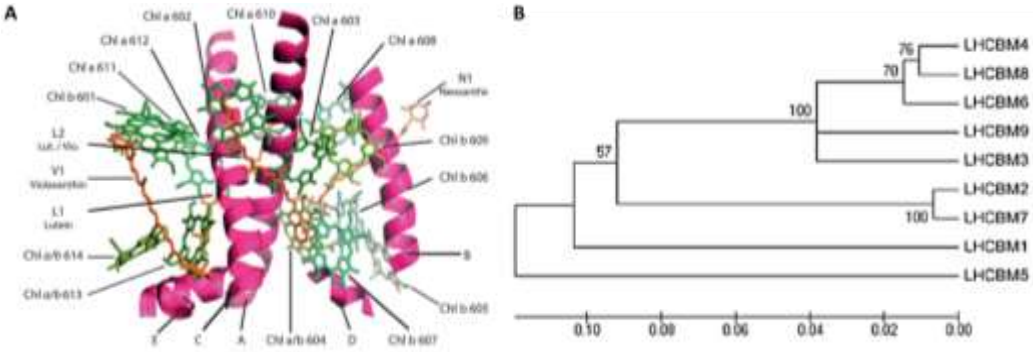

Figure 12. *A) Model of LHCII monomer binding chlorophylls and carotenoids. Pink: polypeptide, Green: chlorophylls, Orange: Carotenoids. (Ballottari et al., 2012) B) Phylogenetic tree of LHCBM CDSs (Ferrante et al., 2012).*

LHC proteins are characterized by three α-helical membrane spanning domains named A-B-C connected by stroma and lumen exposed loops and two amphipathic helices exposed on the luminal surface, with a Chl-binding motif of approximately 25 residues

(Kühlbrandt *et al.*, 1994; Green and Durnford, 1996; Ballottari *et al.*, 2012). Each protein binds 9-13 Chl a and b and xanthophylls (2 luteins, 1 neoxanthin and 1 violaxanthin, converted into zeaxanthin in the xanthophyll cycle). Carotenoids bind to the monomer are important for chlorophyll tripled excited states quenching and ROS scavenging. Trimerization and stability of LHCII is given by lipid molecules of phosphatidyl glycerol (PG) and digalactosyl diacyl glycerol (DGDG). LHCII trimerization is coordinated my a motif (WYGPDR) which is similar or identical to higher plants (Hobe *et al.*, 1995). Trimeric LHCII complexes in *C. reinhardtii* are encoded by nine *Lhcb-m* genes called *Lhcbm1-Lhcbm9*, with M referring to "major" antenna complex (Merchant *et al.*, 2007) (Figure 12B). Four *Lhcbm* genes are localized on chromosome 6 (*Lhcbm4*, *6*, *8* and *9*), two on chromosome 12 (*Lhcbm 2 and 7*), one on chromosome 3 (*Lhcbm5*) whereas the isoforms *Lhcbm1* and *Lhcbm3* have not yet be mapped. All these proteins show a high identity degree in amino acid sequences, except for the N-terminal region. The LHCBM proteins are subdivided into four groups depending on their sequences identity (Figure 12B): Type I (LHCBM3, LHCBM4, LHCBM6 LHCBM8 and LHCBM9), Type II (LHCBM5), Type III (LHCBM 2 and LHCBM7) and Type IV (LHCBM1). Function of almost all LHCBM proteins have been already clarified using mutagenesis or iRNA technologies. LHCBM1 inactivation in *C. reinhardtii* causes a decrease in the thermal dissipation of excess light energy acting like an excitation energy quencher (Elrad, 2002). The preferential expression of *Lhcbm9* under sulphur and nitrogen starvation and anaerobiosis was shown to be important in preventing stress-dependent reduction of LHCII content, and its presence results in faster chlorophyll fluorescence decay and reduced production of singlet oxygen (Nguyen *et al.*, 2008; Grewe *et al.*, 2014). LHCBM2/7 are encoded by two highly homologous genes, which codify identical mature polypeptides, and their function were investigated with microRNA (amiRNA) silencing technology, showing an alteration in state transitions (Ferrante *et al.*, 2012). Similar phenotype was observed for LHCBM5 (Takahashi *et al.*, 2006; Tokutsu *et al.*, 2009). Finally LHCBM4/6/8 were found to be important in photoprotection showing a NPQ alternated phenotype in knock down mutants (Girolomoni *et al.*, 2016). In *C. reinhardtii*, PSII supercomplexes organization was clarified using electron microscopy and single particle analysis (Drop *et al.*, 2014). LHCII trimers are classified depending on their position and on their strong (S), moderate (M) or loose (L) association with the core (C) (Boekema *et al.*, 1995). Has

been reported that in *C. reinhardtii* at least six LHCII trimers per monomeric PSII core complex can be found in the conformation C2S2M2N2, differently in *A. thaliana* only four LHCII were observed (C2S2M2), resulting in a higher harvesting capacity of the green alga (Figure 13).

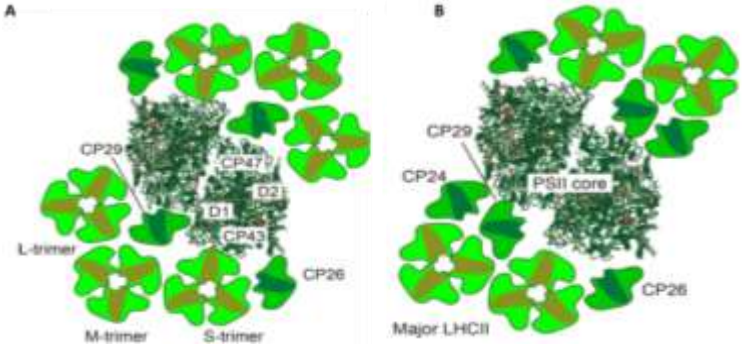

***Figure 13**. Supramolecular organization of PSII-LHCII in A) C. reinhardtii and B) A. thaliana (Minagawa and Tokutsu, 2015)*

Structural analysis indicate that LHCBM1, LHCBM2/7 and LHCBM3 are the dominant LHCBM proteins and represent the main components of PSII supercomplexes while LHCBM5 and LHCBM4/6/8 belong to the "extra" LHCII poll loosely associated to the PSII core and free in the membrane (Drop *et al.*, 2014; Girolomoni *et al.*, 2016).

2.2.4.2. Photosystem I

PSI in *C. reinhardtii* was predicted to be a monomeric complex as plants with an iron-sulphur reaction center (type I) with a terminal acceptor more reducing then the type II. PSI generates the low redox potential used for reducing ferredoxin and producing $NADPH_2$. High resolution structure has been resolved for both cyanobacteria and higher plants (Figure 14) (Jordan *et al.*, 2001; Amunts *et al.*, 2010).

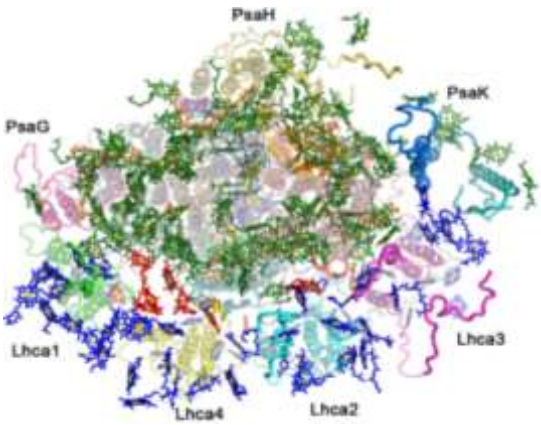

***Figure 14.** Structural model of PSI from Pisum sativum at 3.4 Å resolution (Amunts et al., 2010).*

Core complex is composed by 17 polypeptides, PsaB and PsaA are the larger (80 KDa) and bind cofactors for light harvesting (80 Chl a and 20 β-carotenes) and cofactors involved in electron transfer (6 Chl a, 2 phylloquinones and a Fe-S cluster). PSI contains also smaller subunits (4-18 KDa) which include, PsaF involved in plastocyanin docking, PsaC binds the terminal electron acceptor (Fe-S cluster), PsaC, PsaD and PsaE involved in ferredoxin docking in the stroma side. PsaK and PsaG are involved in LHCI stabilization, PsaH and PsaO are important for LHCII interaction during state transitions. PSI bind at least 173 Chls (100 Chls bound to the core) with a Chl a/b ratio of about 8,2/9,7 and 33-34 carotenoids (12 bound to LHCA and 22 β-carotenes bound to the core) (Amunts *et al.*, 2010; Galka *et al.*, 2012). In the PSI of higher plants are also present 8-10 low energy Chls which absorb at wavelengths above those of P700 that are absent in the PSII. These red forms are mostly associated with LHCA and their function seems to be associated with light harvesting shading light conditions (Morosinotto *et al.*, 2003; Caffarri *et al.*, 2014).

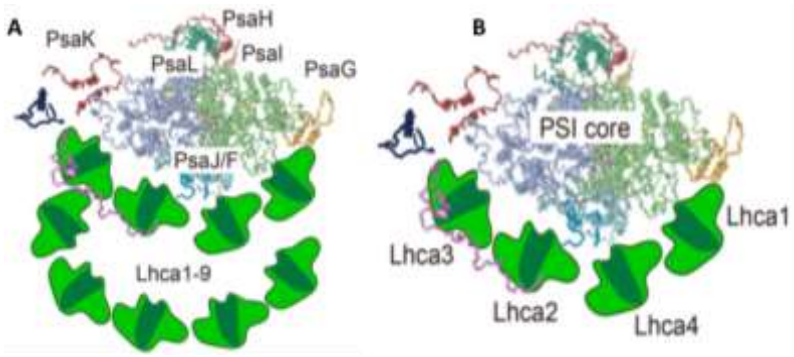

Figure 15. *Supramolecular organization of PSI-LHCI in A) C. reinhardtii and B) A. thaliana (Minagawa and Tokutsu, 2015)*

Nine *lhca* genes encoding LHCI have been identified in *C. reinhardtii* form a double-layered LHCI bind to the site of PsaJ/F/G in low light condition (Drop *et al.*, 2011). *Lhca* have been divided into three subclasses based on their content of high wavelength adsorbing Chls (red forms) which affect their fluorescence emission peak. The first subclass is the "blue LHCA" which include LHCA1, LHCA3 and LHCA7 with emission maxima at 682.5-683.5nm; the second group, called "intermediate LHCA", is composed by LHCA5, LHCA6 and LHCA8 with peaks between 694.5 and 697.5nm. Finally, the

third class, “red LHCA” is composed by LHCA2, LHCA4 and LHCA9 with emission maxima between 707 and 715nm (Mozzo *et al.*, 2010).

2.2.5. Alternative pathways

The basic mechanism of photosynthesis is represented by the Linear Electron Flow (LEF) in which PSII, Cyt b_6f, PSI and ATPase work in series to produce ATP and $NADPH_2$ subsequently used in the Calvin Benson cycle. The ratio of ATP and $NADPH_2$ produced with this process is not sufficient to sustain the nitrogen, lipids, amino acids, pigments and proteins metabolisms, meaning that other mechanisms must work to provide extra ATP for the carbon assimilation. Those processes include the water-water cycle mediated by the Mehler reaction or by PTOX and the Cyclic Electron Flow (CEF) (Cardol *et al.*, 2011).

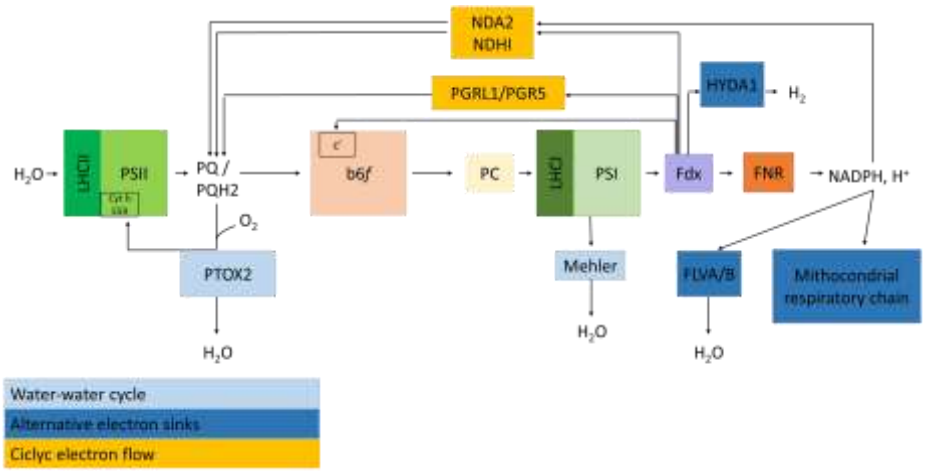

Figure 16. *Alternative pathways of electron transport chain.*

In microalgae, unlike higher plants, most of oxygen consumption is not due by photorespiration but is a result of oxygen reduction at the acceptor site of PSI through the Mehler reaction (Mehler, 1951). In the Mehler reaction molecular oxygen is converted into superoxide (O_2^-) which is then used by the superoxide dismutase (SOD) enzyme to produce H_2O_2. In *C. reinhardtii* was reported the activity of the ascorbate peroxide (APX) to produce H_2O and monodehydroascorbate (MDA) from hydrogen peroxide and ascorbate (Takeda *et al.*, 1997). MDA is finally reduced by PSI core by the MDA reductase. Flavodiiron (Flv) proteins, which in cyanobacteria catalyse the oxygen reduction using $NADPH_2$, was proposed to be involved as catalyst of the Mehler reaction

(Zhang *et al.*, 2009; Peltier *et al.*, 2010). In the water-water cycle oxygen is reduce to water by the plastoquinone terminal oxidase (PTOX) which uses electrons derived from the reduced phanquinone. When this cycle is active the LEF is reduced to prevent the formation of $NADPH_2$ by electrons from PSI but maintaining the ATP synthesis (Kuntz, 2004). The over-reduction of PSI could be balance by the Cyclic Electron Flow (CEF) that in *C. reinhardtii* is enhanced when cells are in state 2 (Finazzi, 2005). Interestingly by reducing this mechanism in microalgae, not significant effects were observed if not also coupled with a reduction of respiration (Cardol *et al.*, 2009). CEF could acts through the activity of the NAD(P)H dehydrogenase (Ndh) which is present in higher plants, but the same reaction is catalyse by Nda2 in microalgae (Jans *et al.*, 2008). Another possibility could by the reduction of the plastoquinone pool by the ferredoxin-quinone reductase via the $c_{'}$ heme of the cytochrome, which could correspond to cytochrome b_6f complex or to a membrane complex formed by PGR5 and PGRL1 (DalCorso *et al.*, 2008; Iwai *et al.*, 2010). The reducing power produced during photosynthesis could be transferred across the malate-oxaloacetate or aspartate oxaloacetate shuttle in the mitochondria. Finically when *C. reinhardtii* cells are stressed with anaerobiosis the hydrogenase HydA1 is activated and catalyse the H_2 production by taking electrons from ferredoxin and preventing the oxidative damage (Hemschemeier and Happe, 2011).

2.3. Photoinhibition and photoprotection

Photosynthetic process is strongly influenced by environmental conditions such as temperature, light intensity and nutrients availability. Photosynthetic organisms use the Photosynthetically Active Radiation (PAR) for their metabolic processes but irradiances quality and intensity changes during seasons, a single day or within the day. Algae developed several strategies to tune light absorption and/or utilization, but light can be a limit or even a stressor. This typically occurs when the light phase products are not fully consumed by the Calvin-Benson cycle and accumulate in the chloroplast. Additionally, environmental conditions might cause limitations in the electron transport chain, thus in photon energy. When the light energy absorbed exceed the capacity for photochemistry utilization and ATP and $NADPH_2$ are over-accumulated, the electron transport chain is over-reduced and the PSII chlorophyll excited states ($^1Chl^*$), increase their life time. The

excitation energy associated to the chlorophylls cannot be used in photochemistry, which is saturated. Thus, it can be re-emitted as fluorescence in small fraction or decay via the triplet excited state (^{3}Chl*) in the intersystem crossing process. ^{3}Chl* has a longer lifetime (ms) compared to ^{1}Chl* (ns) and thus have a higher probability to react with molecular oxygen ($^3O_2$) producing singlet oxygen ($^1O_2$*). $^1O_2$* is highly reactive and can modify lipids, nucleic acids and proteins causing photoinhibition. All these events lead to the photo-oxidative stress unless de-excited by activation of thermal dissipation processes. In the photosynthetic transport chain one of the central site of ROS formation is the PSII. Usually after the primary charge transfer, P_{680}^+ and Ph^- species are formed; after electron transfer to Q_A Ph^- return to Ph, while P_{680}^+ is reconverted to P_{680} through Tyr oxidation. In light excess conditions Q_A is fully reduced and electron transport is impaired, which can lead to recombination between P_{680}^+ and Ph^-, producing $^3P_{680}^*$, which can generate singlet oxygen leading to damage of D1 core protein (Aro *et al.*, 1993). Compared to PSII, the PSI reaction center P_{700}^+ is more stable acting as a quencher of the excitation energy (Dau, 1994). Instead ferredoxin, the acceptor site of PSI, can reduce the O_2 to O_2^- that can be metabolize as H_2O_2 or OH^*, which are strong ROS. Oxygenic photosynthetic organisms have developed different strategies to contrast over-excitation which can be classified in short (minutes or seconds) and long (hours or days) term responses (Figure 17).

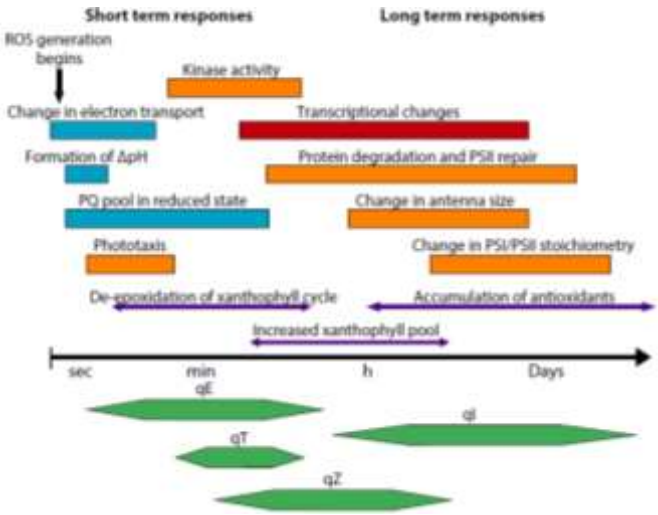

Figure 17. *Relative time scale of short and long term response to high light stress (Erickson et al., 2015).*

The first response to high light stress triggered in *C. reinhardtii* is the escape from light by activating the negative phototaxis. If this mechanism in not enough to avoid stress the excess of light can be dissipated by heat thought Non-Photochemical Quenching (NPQ) and/or carotenoids, modulating the antenna size of photosystems or changing the electron transport (see paragraph 2.2.5.). After longer exposure to high light long term response mechanisms are activated such as PSII turnover or changing in genes expression (Erickson *et al.*, 2015).

2.3.1. Short term response

2.3.1.1. Non-Photochemical quenching

The main mechanism in preventing ROS formation is a set of mechanisms called Non-Photochemical Quenching (NPQ) which dissipate excess energy absorbed as heat and that can be monitored as quenching of Chls fluorescence (Demmig-Adams and Adams, 1992). NPQ is measured by delivering a saturating light pulse (>3000 µmol photon m^{-2} sec^{-1}) in order to saturate photosynthetic light reactions and reach the maximum fluorescence level (F_m). Treating with continuous saturating light intensity the dissipation mechanisms remain active and the value of maximal fluorescence, in these conditions called F_m', decreases and is used for NPQ quantification. Switching off the light, a recovery of F_m' for the relaxation of NPQ is induced (Müller *et al.*, 2001) (Figure 18).

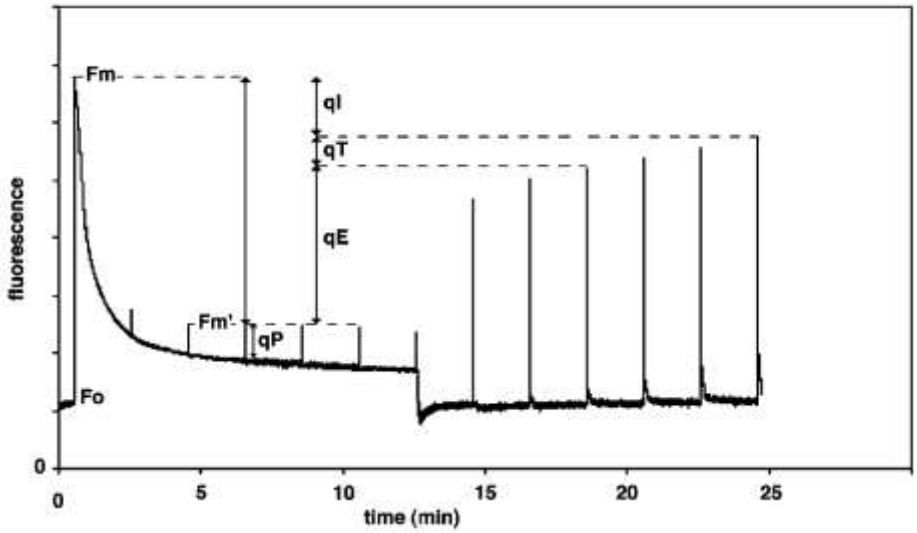

Figure 18. *Chl fluorescence measurement from Arabidopsis leaf (Müller et al., 2001).*

NPQ is composed by at least three different components depending on the kinetics of their rise upon illumination and decay at dark. The first component is the pH- or energy-dependent component, qE, which is turned on and off in few seconds or minutes and is related to changes in luminal acidification (ApH) when thylakoids membranes are exposed to high light. The second is qT, more important in algae compared to higher plants, related to the phenomenon of the state transition. The last and slowest component is related to photoinhibition of photosynthesis (damaged of PSII centers) and/or zeaxanthin accumulation and is called qI (Dall'Osto *et al.*, 2005).

ApH dependent NPQ (qE)

qE has a triple role in photoprotection by reducing the $^{1}Chl^{*}$ life time, preventing the over-reduction of the plastoquinone pool and the over-acidification of the thylakoids lumen. In *C. reinhardtii* the qE activation requires the ApH formation and the expression of the stress related LHC protein called LHCSR (Peers *et al.*, 2009). In the chromosome 8 of *C. reinhardtii* three genes which encode for LHCSR isoforms are present (*Lhcsr3.1*, *Lhcsr3.2* and *Lhcsr1*) (Merchant *et al.*, 2007). *Lhcsr3.1* and *Lhcsr3.2* encode the same polypeptide and are overexpressed in high light conditions, while *Lhcsr1* is overexpressed with high CO_2 concentration (Maruyama *et al.*, 2014). LHCSR isoforms bind Chl a, Chl b (six or seven per polypeptide; Chl a/b ratio 6,3 ± 0,3) and carotenoids (lutein and violaxanthin) (Bonente *et al.*, 2011). LHCSR3 has a key role as quencher of $^{1}Chl^{*}$ and in pH sensing through aspartic and glutamic residues present in its C-terminal domain (Liguori *et al.*, 2013). In particular, when algal cells are stressed with high light LHCSR3 expression is induced and associated with the supercomplex PSII-LHCII forming the complex PSII-LHCII-LHCSR3. In dark or low light the supercomplex PSII-LHCII-LHCSR3 is in a light harvesting state but when the thylakoids lumen is acidified it becomes energy dissipative (Minagawa and Tokutsu, 2015). Two mutants altered in LHCSR accumulation are present. The *npq4* mutant lack in LHCSR3 showing a strong reduce in qE capacity while in the *npq4 lhcsr1* mutant no qE is present (Peers *et al.*, 2009). In vascular plant the Lhc-like complex involved in NPQ is PSBS which act as a sensor of lumen pH but doesn't binds pigments, instead LHCSR3 wasn't found (Li *et al.*, 2000). An important finding was the identification of both LHCSR and PSBS in the moss *Physcomitrella patents*, an intermediate between vascular plants and algae

(Alboresi *et al.*, 2010). Recently in *C. reinhardtii* a transiently PSBS expression under high light was observed suggesting its role in photoprotection (Tibiletti *et al.*, 2016).

State transition (qT)

In plants and algae the excess of excitation energy on PSII can be reduced by moving LHCII antenna from PSII to PSI where excitation is quenched by PSI in the so called state transition (qT). During the "State 1" the excitation energy is balanced between the two photosystem and LHCII are bound to PSII and LHCI are bound to PSI. If the light quality changes to PSII favour (blue) the plastoquinone pool becomes reduced activating the STT7 serine/threonine kinase (Lemeille *et al.*, 2009). STT7 phosphorylates LHCII inducing the dissociation from PSII to PSI in the "State 2" thus increasing the PSI antenna size and re-equilibrating energy distribution between the two photosystems. This process is reversible through the phosphatase that dephosphorylates the LHCII which return to the PSII (Depege *et al.*, 2003). STT7 kinase is also one of the most important agent in LHCSR3 phosphorylation, but is not needed for NPQ activity (Bonente *et al.*, 2011).

Zeaxanthin dependent quenching (qZ)

As described in paragraph 2.2.3.3 zeaxanthin is accumulated in high light condition by the activity of the VDE enzyme. In *C. reinhardtii* the VDE enzyme is different from higher plants and no ortholog of the plant gene was found in its genome. The role of this xanthophyll, in *C. reinhardtii* was studied by producing the *npq1* mutant which is unable to accumulate zeaxanthin and shows a decrease of the second phase of NPQ compared to WT (Niyogi, 1997*a*). Carotenoids act as scavenger of $^1O_2$* and quencher of ^{3}Chl* (5, 6).

$$^3\text{Chl}^* + {}^1\text{Car} \rightarrow {}^1\text{Chl} + {}^3\text{Car}^* \qquad (5)$$

$$^3\text{Car}^* \rightarrow {}^1\text{Car} + \text{heat} \qquad (6)$$

Inhibitory quenching (qI)

The main target of the photo-oxidative damage is D1 protein of PSII reaction center, its photodamage shows a linear correlation with light intensity. In photosynthetic organism the damage D1 is degraded and reassemble with new synthesized PSII proteins (Aro *et al.*, 1993). The speed of repair is regulated by environmental changes and by the energetic state of the chloroplast. The PSII photodamage is correlated with qI quenching helping in control electron flow to PSI.

2.3.2. Long term response

2.3.2.1. Light harvesting antenna size modulation

When plants or algae are stressed for a long period long-term photoprotective mechanisms are activated. In this case are induced changes in plant architecture through expression or repression of specific proteins. Examples are regulation of LHC genes expression or degradation. The light harvesting antenna size is strictly regulated in response to the growth environment requiring a balance between the light need for the photochemistry and minimizing the light damage. During acclimation from low light to high light several regulation pathways are activated such as halve the Chls content and double up two times the carotenoids amount (Niyogi *et al.*, 1997*b*; Shapira *et al.*, 1997).

2.4. Microalgae for biofuel and high values products production

Microalgae are used as factories for producing biofuels, food, feed and high-value bioactive substances. The potential of biofuels production from algae had been already discovered in the ‘60s but the incentive for its production began with the oil crisis in the ‘70s (Oswald and Golueke, 1960). Microalgae present many advantages, such us no competition with food production (growth in non-arable lands), fast life cycle, a completely photosynthetically active biomass (10-40% in higher plants), high oil accumulation, no contribution in atmospheric CO_2 accumulation, no relevant environment impact and algae can also use nutrients from different wastewater resources providing an additional benefit on bio-remediation. Microalgae produce high amount of lipids between 20-50% of the dry weight, these values can be increased by optimizing the growth determining factors such as nitrogen levels, light intensity, temperature, salinity, CO_2 concentration and harvesting procedure. Microalgae, usually, are cultivated with three different systems: batch, continuous and immobilized cultures. In the batch culture system, medium and algal inoculum are placed in a vessel and incubated with favourable environmental growth conditions. Agitation is necessary to ensure nutrients and gaseous exchanges. In photo-autrophic or mixotrophic cultures, CO_2 enriched air is added, and the cultures are illuminated by natural, artificial light source or sunlight by optical fibers. In continuous system, fresh medium is added to the culture mixed

homogeneously and the growth inhibitory products are removed or, diluted continuously or intermittently. In the immobilized system, algae are entrapped or absorbed on a support to avoid the inhibition by the substrate or to eliminate contamination by other algae strains (A., Richmond; H., 2013). Solar to mass conversion efficiency of algae was estimated to be 8-10% with a maximum productivity of 77 g biomass $m^{-2}day^{-1}$ (280 ton $ha^{-1}year^{-1}$), yet the real conversion does not exceed 3% in the best case (73-146 ton dry weight $ha^{-1}year^{-1}$) (Melis, 2009). Mass culture conditions, whit high cell density, are preferred but they differ from natural habitats explaining the gap between the theoretical and present biomass productivities of algae. The light saturation curve of *C. reinhardtii*, shows that when the light irradiance overcomes the rate of downstream dark phase reactions and increases beyond saturation, photoprotective mechanisms are activated and leads to decrease photosynthesis quantum yield and, consequently, to reduced biomass (Figure 4). In natural water environments, algae escape from light excess by swimming in the water column. The excess of sunlight absorption is due to the high number of chlorophylls antenna molecules per reaction center in the photosynthetic apparatus. Up to 600 Chl a and Chl b are associated to the PSII and PSI reaction centers (Melis, 1996). In high density cultivations or mass cultivations, the individual cells at the surface of the culture would over-adsorb sunlight and dissipate most of energy via NPQ, limiting biomass productivity. One possibility to reduce this phenomenon, is minimize sunlight adsorption by individual chloroplast in the surface of the culture to ensure a greater transmittance of irradiance through a high density cultivation (Kirst *et al.*, 2012). When the Chl concentration exceeds the optimum value a decline of integrated net photosynthesis is observed due to excessive shading leading to increased respiration. Another strategy suggests for improve the light conversion efficiency for biomass production by reducing dissipative mechanisms like NPQ (Berteotti *et al.*, 2016). Biofuel production from algae seems to be an important alternative to fossil fuels but the production systems have high costs for the production equipment and for the biomass treatment. To optimize the productivity, it is necessary to develop bio-refinery systems where the biofuels production is combined with high value product synthesis.

2.4.1. Biotechnological tools for microalgae strains manipulation

Most of problems regarding biomass production from microalgae derive from using wild-type algal strains; they are evolved to adapt in their natural habitat, and some of their characteristics do not allow for an optimal growth in mass culture conditions. For this reason, it is necessary a new "green revolution", not only for increase productivity but also to study the microalgae biology and physiology. The algae domestication is easier than higher plants because the genetic manipulation is more rapid thanks to their short life-cycle, and the phenotypic selection can be faster for their haploid nature and absence of cellular differentiation. Strategies for algae domestication include searching of new strains, breeding and selection, mutagenesis and genetic engineering. Currently, about 25 algal species are accessible to genetic transformation, but these do not include many algae of commercial interest and only *C. reinhardtii* is accessible to genetic analysis by breeding. Transformation techniques in microalgae mainly depend on cell wall presence or absence. In the green alga *C. reinhardtii*, mutants deficient in the cell wall are present but their vitality is lower compare to WT strains. In this case the most convenient methods are based on using of glass beads (used with *C. reinhardtii* and *Dunaliella salina*) and electroporation (used with *C. reinhardtii*, *Nannochloropsis spp*. and *Phaeodactyum tricomutum*). Microalgae with a thick cell wall need more invasive methods or need to be treated before use electroporation or glass beads. Stronger methods include bio-transformation (mediated by *A. tumefaciens* or *E.coli*) and biolistic method such as particle bombardment (used with *H. pluvialis*) (Kathiresan *et al.*, 2009; Vazquez-Villegas *et al.*, 2018). Metabolic engineering of microalgae is limited also by the few information about genomes sequences, promoters and markers. In order to generate mutants library or studying specific genes function the most simple and used technique is based on random integration of DNA sequences (usually with an antibiotic resistance). The truncated gene or DNA sequence can be identified easily by PCR. This method is used in all the organisms with well know transformation techniques including algae were the genome is not sequenced. Another possibility to study genes functions could be to replace them with a modified sequence using the Homologous Recombination (HR). In algae HR has produced positives results in *C. reinhardtii* and *N. gaditana* (Zorin *et al.*, 2009; Kilian *et al.*, 2011). Alternatively to HR is also possible to

the decrease the genes expression by using RNA interference (RNAi) and antisense RNA. In the RNAi, subclasses of small complementary RNAs (microRNA or miRNA) are generated inhibiting the translation or inducing the transcript degradation (Valencia-Sanchez *et al.*, 2006). Instead, RNA antisense sequences paired targeted genes obscuring the translation machinery. The main problems related with those techniques are, the stability of the genes silencing due to the high duplication rate of microalgae, the availability of RNA transcriptome and the identification of target sequences for small RNAs. Microalgae are very efficient proteins expression systems due to their low cost production with high yield. The metabolic engineering of microalgae, in particular for *C. reinhardtii*, can be developed at the chloroplast or nucleus level. Examples of heterologous proteins expression include expression of human antibodies, oils, novel carotenoids, (Mayfield and Franklin, 2005; León-Bañares *et al.*, 2004). Improving genetic tools is an important challenge to generate new and more productive mutants not only for biofuels production but also for clinical and nutritional aims in particular for those algae that are marked as GRAS (generally recognized as safe). For this reason, expanding the number of transformable species is the most important challenge for the next years of algal-based research.

2.5 Bibliography

A., Richmond; H. Q. 2013. *Handbook of Microalgal Culture*.

Alboresi A, Gerotto C, Giacometti GM, Bassi R, Morosinotto T. 2010. *Physcomitrella patens* mutants affected on heat dissipation clarify the evolution of photoprotection mechanisms upon land colonization. Proceedings of the National Academy of Sciences **107**, 11128–11133.

Amunts A, Toporik H, Borovikova A, Nelson N. 2010. Structure determination and improved model of plant photosystem I. Journal of Biological Chemistry **285**, 3478–3486.

Aro EM, Virgin I, Andersson B. 1993. Photoinhibition of Photosystem II. Inactivation, protein damage and turnover. BBA - Bioenergetics **1143**, 113–134.

Ballottari M, Girardon J, Dall'Osto L, Bassi R. 2012. Evolution and functional properties of Photosystem II light harvesting complexes in eukaryotes. Biochimica et Biophysica Acta - Bioenergetics **1817**, 143–157.

Bassi R, Pineau B, Dainese P, Marquardt J. 1993. Carotenoid-binding proteins of photosystem II. European Journal of Biochemistry **212**, 297–303.

Ben-Shem A, Frolow F, Nelson N. 2003. Crystal structure of plant photosystem I. Nature **426**, 630–635.

Benson AA, Calvin M. 2000. Carbon dioxide fixation. , 1–34.

Berteotti S, Ballottari M, Bassi R. 2016. Increased biomass productivity in green algae by tuning non-photochemical quenching. Scientific reports **6**, 21339.

Bhosale P, Bernstein PS. 2005. Microbial xanthophylls. Applied Microbiology and Biotechnology **68**, 445–455.

Boekema EJ, Hankamert B, Baldt D, Kruipt J, Nieldt J, Boonstra AF, Barbert J, Rognert M. 1995. Supramolecular structure of the photosystem II complex from green plants and cyanobacteria (transmission electron microscopy/image analysis/subunit positioning). Cell Biology **92**, 175–179.

Bonente G, Ballottari M, Truong TB, Morosinotto T, Ahn TK, Fleming GR, Niyogi KK, Bassi R. 2011. Analysis of LHcSR3, a protein essential for feedback de-excitation in the green alga *Chlamydomonas reinhardtii*. PLoS Biology **9**, e1000577.

Boussiba S. 2000. Carotenogenesis in the green alga *Haematococcus pluvialis*: Cellular physiology and stress response. Physiologia Plantarum **108**, 111–117.

Caffarri S, Croce R, Breton J, Bassi R. 2001. The major antenna complex of Photosystem II has a xanthophyll binding site not involved in Light Harvesting. Journal of Biological Chemistry **276**, 35924–35933.

Caffarri S, Tibiletti T, Jennings R, Santabarbara S. 2014. A Comparison between plant Photosystem I and Photosystem II architecture and functioning. Current Protein & Peptide Science

15, 296–331.

Cardol P, Alric J, Girard-Bascou J, Franck F, Wollman F-A, Finazzi G. 2009. Impaired respiration discloses the physiological significance of state transitions in *Chlamydomonas*. Proceedings of the National Academy of Sciences **106**, 15979–15984.

Cardol P, Forti G, Finazzi G. 2011. Regulation of electron transport in microalgae. Biochimica et Biophysica Acta - Bioenergetics **1807**, 912–918.

DalCorso G, Pesaresi P, Masiero S, Aseeva E, Schünemann D, Finazzi G, Joliot P, Barbato R, Leister D. 2008. A complex containing PGRL1 and PGR5 is involved in the switch between Linear and Cyclic Electron Flow in *Arabidopsis*. Cell **132**, 273–285.

Dall'Osto L, Caffarri S, Bassi R. 2005. A mechanism of nonphotochemical energy dissipation, independent from PsbS, revealed by a conformational change in the antenna protein CP26. The Plant cell **17**, 1217–1232.

Dau H. 1994. New trends in photobiology. Short-term adaptation of plants to changing light intensities and its relation to Photosystem II photochemistry and fluorescence emission. Journal of Photochemistry and Photobiology, B: Biology **26**, 3–27.

Dekker JP, Boekema EJ. 2005. Supramolecular organization of thylakoid membrane proteins in green plants. Biochimica et Biophysica Acta - Bioenergetics **1706**, 12–39.

Demmig-Adams B, Adams WW. 1992. Responses of plants to high light stress. Annu. Rev. Plant Physiol. Plant Mol. Biol. **43**, 599–626.

Demmig-Adams B, Adams WW, Heber U, Neimanis S, Winter K, Kruger A, Czygan F-C, Bilger W, Bjorkman O. 1990. Inhibition of zeaxanthin formation and of rapid changes in radiationless energy dissipation by dithiothreitol in spinach leaves and chloroplasts. Plant Physiology **92**, 293–301.

Depege N, Bellafiore S, Rochaix JD. 2003. Rote of chloroplast protein kinase Stt7 in LHCII phosphorylation and state transition in *Chlamydomonas*. Science **299**, 1572–1575.

Drop B, Webber-Birungi M, Fusetti F, Kouril R, Redding KE, Boekema EJ, Croce R. 2011. Photosystem I of *Chlamydomonas reinhardtii* contains nine light-harvesting complexes (Lhca) located on one side of the core. Journal of Biological Chemistry **286**, 44878–44887.

Drop B, Webber-Birungi M, Yadav SKN, Filipowicz-Szymanska A, Fusetti F, Boekema EJ, Croce R. 2014. Light-harvesting complex II (LHCII) and its supramolecular organization in *Chlamydomonas reinhardtii*. Biochimica et biophysica acta **1837**, 63–72.

Elrad D. 2002. A major Light-Harvesting polypeptide of Photosystem II functions in thermal Dissipation. the Plant Cell **14**, 1801–1816.

Erickson E, Wakao S, Niyogi KK. 2015. Light stress and photoprotection in *Chlamydomonas reinhardtii*. Plant Journal **82**, 449–465.

Ferrante P, Ballottari M, Bonente G, Giuliano G, Bassi R. 2012. LHCBM1 and LHCBM2/7 polypeptides, components of major LHCII complex, have distinct functional roles in photosynthetic antenna system of *Chlamydomonas reinhardtii*. Journal of Biological Chemistry **287**, 16276–16288.

Ferreira KN, Iverson TM, Maghlaoui K, Barber J, Iwata S. 2004. Architecture of the Photosynthetic Oxygen-Evolving Center. Science **43**, 1831–1839.

Finazzi G. 2005. The central role of the green alga *Chlamydomonas reinhardtii* in revealing the mechanism of state transitions. Journal of Experimental Botany **56**, 383–388.

Galka P, Santabarbara S, Khuong TTH, Degand H, Morsomme P, Jennings RC, Boekema EJ, Caffarri S. 2012. Functional Analyses of the plant Photosystem I-Light-Harvesting Complex II supercomplex reveal that Light-Harvesting Complex II loosely bound to Photosystem II is a very efficient antenna for Photosystem I in State II. The Plant Cell **24**, 2963–2978.

Gastaldelli M, Canino G, Croce R, Bassi R. 2003. Xanthophyll binding sites of the CP29 (Lhcb4) subunit of higher plant photosystem II investigated by domain swapping and mutation analysis. Journal of Biological Chemistry **278**, 19190–19198.

Gilmore AM, Yamamoto HY. 1993. Linear models relating xanthophylls and lumen acidity to non-photochemical fluorescence quenching. Evidence that antheraxanthin explains zeaxanthin-independent quenching. Photosynthesis Research **35**, 67–78.

Girolomoni L, Ferrante P, Berteotti S, Giuliano G, Bassi R, Ballottari M. 2016. The function of LHCBM4/6/8 antenna proteins in *Chlamydomonas reinhardtii*. Journal of experimental botany **68**, 627–641.

Goodenough U, Lin H, Lee JH. 2007. Sex determination in *Chlamydomonas*. Seminars in Cell and Developmental Biology **18**, 350–361.

Goss R, Jakob T. 2010. Regulation and function of xanthophyll cycle-dependent photoprotection in algae. Photosynthesis Research **106**, 103–122.

Green BR, Durnford DG. 1996. The chlorophyll-carotenoid proteins of oxygenic photosynthesis. Annual Review of Plant Physiology and Plant Molecular Biology **47**, 685–714.

Grewe S, Ballottari M, Alcocer M, D'Andrea C, Blifernez-Klassen O, Hankamer B, Mussgnug JH, Bassi R, Kruse O. 2014. Light-Harvesting Complex protein LHCBM9 is critical for Photosystem II activity and hydrogen production in *Chlamydomonas reinhardtii*. The Plant cell **26**, 1598–1611.

Guerin M, Huntley ME, Olaizola M. 2003. *Haematococcus* astaxanthin: applications for human health and nutrition. Trends in Biotechnology **21**, 210–216.

Hallmann A. 2007. Algal transgenics and biotechnology. Transgenic Plant J **1**, 81–98.

Han D, Li Y, Hu Q. 2013. Astaxanthin in microalgae: Pathways, functions and biotechnological implications. Algae **28**, 131–147.

Hannon M, Gimpel J, Tran M, Rasala B, Mayfield S. 2010. Biofuels from algae: challenges and potential. Biofuels **1**, 763–784.

Harbinson J, Foyer CH. 1991. Relationships between the efficiencies of Photosystems I and II and stromal redox state in CO(2)-free air. Plant physiology **97**, 41–49.

Harris EH. 2001. *Chlamydomonas* as a odel rganism. Molecular Biology **52**, 363–406.

Harris EH. 2009. *The Chlamydomonas Sourcebook: introduction to Chlamydomonas and its laboratory use.* (Elsevier, Ed.).

Havaux M, Niyogi KK. 1999. The violaxanthin cycle protects plants from photooxidative damage by more than one mechanism. Proceedings of the National Academy of Sciences **96**, 8762–8767.

Hemschemeier A, Happe T. 2011. Alternative photosynthetic electron transport pathways during anaerobiosis in the green alga *Chlamydomonas reinhardtii*. Biochimica et Biophysica Acta - Bioenergetics **1807**, 919–926.

Hill R, Bendall F. 1960. Function of the Two cytochrome components in chloroplasts: A Working Hypothesis. Nature **186**, 136–137.

Hobe S, Förster R, Klingler J, Paulsen H. 1995. N-proximal sequence motif in light-harvesting Chlorophyll a/b-binding protein is essential for the trimerization of Light-Harvesting Chlorophyll alb complex. Biochemistry **34**, 10224–10228.

Horton P, Ruban A V. 1992. Regulation of Photosystem II. Photosynthesis Research **34**, 375–385.

Iwai M, Takizawa K, Tokutsu R, Okamuro A, Takahashi Y, Minagawa J. 2010. Isolation of the elusive supercomplex that drives cyclic electron flow in photosynthesis. Nature **464**, 1210–1213.

Jans F, Mignolet E, Houyoux P-A, Cardol P, Ghysels B, Cuine S, Cournac L, Peltier G, Remacle C, Franck F. 2008. A type II NAD(P)H dehydrogenase mediates light-independent plastoquinone reduction in the chloroplast of *Chlamydomonas.* Proceedings of the National Academy of Sciences **105**, 20546–20551.

Jansson S. 1999. A guide to the Lhc genes and their relatives in *Arabidopsis*. Trends in Plant Science **4**, 236–240.

Jordan P, Fromme P, Witt HT, Klukas O, Saenger W, Krauß N. 2001. Three-dimensional structure of cyanobacterial photosystem I at 2.5 Å resolution. Nature **411**, 909–917.

Kathiresan S, Chandrashekar a., Ravishankar G a., Sarada R. 2009. *Agrobacterium*-mediated transformation in the green alga *Haematococcus pluvialis* (chlorophyceae, volvocales). Journal of Phycology **45**, 642–649.

Kilian O, Benemann CSE, Niyogi KK, Vick B. 2011. High-efficiency homologous recombination in the oil-producing alga *Nannochloropsis* sp. Proceedings of the National Academy of Sciences **108**, 21265–21269.

Kirst H, Garcia-Cerdan JG, Zurbriggen A, Ruehle T, Melis A. 2012. Truncated Photosystem chlorophyll antenna size in the green microalga *Chlamydomonas reinhardtii* upon deletion of the TLA3-CpSRP43 gene. Plant Physiology **160**, 2251–2260.

Kruse O, Rupprecht J, Bader KP, Thomas-Hall S, Schenk PM, Finazzi G, Hankamer B. 2005. Improved photobiological H2 production in engineered green algal cells. Journal of Biological Chemistry **280**, 34170–34177.

Kühlbrandt W, Wang DN, Fujiyoshi Y. 1994. Atomic model of plant light-harvesting complex by electron crystallography. Nature **367**, 614–621.

Kuntz M. 2004. Plastid terminal oxidase and its biological significance. Planta **218**, 896–899.

Kurisu G, Zhang H, Smith JL, Cramer WA. 2003. Structure of the Cytochrome b 6 f complex of oxygenic Photosynthesis : Tuning the Cavity. **302**, 1009–1015.

Lemeille S, Willig A, Depège-Fargeix N, Delessert C, Bassi R, Rochaix JD. 2009. Analysis of the chloroplast protein kinase Stt7 during state transitions. PLoS Biology **7**, 0664–0675.

Lemoine Y, Schoefs B. 2010. Secondary ketocarotenoid astaxanthin biosynthesis in algae: a multifunctional response to stress. Photosynthesis research **106**, 155–177.

León-Bañares R, González-Ballester D, Galván A, Fernández E. 2004. Transgenic microalgae as green cell-factories. Trends in Biotechnology **22**, 45–52.

Li X-P, Björkman O, Shih C, Grossman AR, Rosenquist M, Jansson S, Niyogi KK. 2000. A pigment-binding protein essential for regulation of photosynthetic light harvesting. Nature **403**, 391.

Liguori N, Roy LM, Opacic M, Durand G, Croce R. 2013. Regulation of Light Harvesting in the green alga *Chlamydomonas reinhardtii*: The C-Terminus of LHCSR is the knob of a dimmer switch. Journal of the American Chemical Society **135**, 18339–18342.

Liu Z, Yan H, Wang K, Kuang T, Zhang J, Gui L, An X, Chang W. 2004. Crystal structure of spinach major light-harvesting complex at 2.72 Å resolution. Nature **428**, 287–292.

Lorenz RT, Cysewski GR. 2000. Commercial potential for *Haematococcus* microalgae as a natural source of astaxanthin. Trends in Biotechnology **18**, 160–167.

Luykx P, Hopenrath M, Robinson DG. 1997. Osmoregulatory mutants that affect the function of the contractile vacuole in *Chlamydomonas reinhardtii*. Protoplasma **200**, 99–111.

Malkin R, Niyogi K. 2000. Photosynthesis. Biochemistry and Molecular Biology of Plants, Buchanan B, Gruissem W, Jones R,.pp 568-628.

Martin W, Herrmann RG. 1998. Gene Transfer from Organelles to the Nucleus: How Much, What Happens, and Why? Plant Physiology **118**, 9–17.

Maruyama S, Tokutsu R, Minagawa J. 2014. Transcriptional regulation of the stress-responsive light harvesting complex genes in C*hlamydomonas reinhardtii*. Plant and Cell Physiology **55**, 1304–1310.

Maul JE, Lilly JW, Cui L, dePamphilis CW, Miller W, Harris EH, Stern DB. 2002. The *Chlamydomonas reinhardtii* plastid chromosome: islands of genes in a sea of repeats. The Plant cell **14**, 2659–79.

Mayfield SP, Franklin SE. 2005. Expression of human antibodies in eukaryotic micro-algae. Vaccine **23**, 1828–1832.

Mehler AH. 1951. Studies on reactions of illuminated chloroplasts. II. Stimulation and inhibition of the reaction with molecular oxygen. Archives of Biochemistry and Biophysics **34**, 339–351.

Melis A. 1996. Excitation Energy transfer: functional and dynamic aspects of Lhc (cab) proteins. In: Ort DR,, In: Yocum CF,, In: Heichel IF, eds. Oxygenic Photosynthesis: The Light Reactions. Dordrecht: Springer Netherlands, 523–538.

Melis A. 2009. Solar energy conversion efficiencies in photosynthesis: Minimizing the chlorophyll antennae to maximize efficiency. Plant Science **177**, 272–280.

Melis A, Zhang L, Forestier M, Ghirardi ML, Seibert M. 1999. Sustained photobiological hydrogen gas production upon reversible inactivation of oxygen evolution in the green alga *Chlamydomonas reinhardtii*. **2**, 1–19.

Merchant SS, Prochnik SE, Vallon O, *et al.* 2007. The *Chlamydomonas* Genome reveals the evolution of key animal and plant functions. Science **318**, 245–250.

Michaelis G, Vahrenholz C, Pratje E. 1990. Mitochondrial DNA of *Chlamydomonas reinhardtii*: the gene for apocytochrome b and the complete functional map of the 15.8 kb DNA. Molecular & general genetics : MGG **223**, 211–216.

Mimuro M, Katoh T. 1991. Carotenoids in photosynthesis: absorption, transfer and dissipation of light energy. Pure and Applied Chemistry **63**, 123–130.

Minagawa J, Tokutsu R. 2015. Dynamic regulation of photosynthesis in *Chlamydomonas reinhardtii*. Plant Journal **82**, 413–428.

Mitchell P. 1961. Coupling of phosphorylation to electron and hydrogen transfer by a chemi-osmotic type of mechanism. Nature **191**, 144–148.

Moore AL, Joy A, Tom R, Gust D, Moore TA, Bensasson R V, Land EJ. 1982. Photoprotection by carotenoids during photosynthesis: motional dependence of intramolecular energy transfer. Science **216**, 982 LP-984.

Morosinotto T, Breton J, Bassi R, Croce R. 2003. The nature of a chlorophyll ligand in Lhca proteins determines the far red fluorescence emission typical of photosystem I. The Journal of biological chemistry **278**, 49223–49229.

Mozzo M, Mantelli M, Passarini F, Caffarri S, Croce R, Bassi R. 2010. Functional analysis of Photosystem I light-harvesting complexes (Lhca) gene products of *Chlamydomonas reinhardtii*. Biochimica et Biophysica Acta - Bioenergetics **1797**, 212–221.

Müller P, Li X-P, Niyogi KK. 2001. Non-Photochemical Quenching. A response to excess light energy. Plant Physiology **125**, 1558 LP-1566.

Mussgnug JH, Klassen V, Schlüter A, Kruse O. 2010. Microalgae as substrates for fermentative biogas production in a combined biorefinery concept. Journal of Biotechnology **150**, 51–56.

Nguyen AV, Thomas-Hall SR, Malnoë A, Timmins M, Mussgnug JH, Rupprecht J, Kruse O, Hankamer B, Schenk PM. 2008. Transcriptome for photobiological hydrogen production induced by sulfur deprivation in the green alga *Chlamydomonas reinhardtii*. Eukaryotic Cell **7**, 1965–1979.

Niyogi KK, Bjorkman O, Grossman AR. 1997*a*. *Chlamydomonas* xanthophyll cycle mutants identified by video imaging of chlorophyll fluorescence quenching. the Plant Cell **9**, 1369–1380.

Niyogi KK, Bjorkman O, Grossman AR. 1997*b*. The roles of specific xanthophylls in photoprotection. Proceedings of the National Academy of Sciences **94**, 14162–14167.

Oreb M, Tews I, Schleiff E. 2008. Policing Tic 'n' Toc, the doorway to chloroplasts. Trends in Cell Biology **18**, 19–27.

Oswald WJ, Golueke CG. 1960. Biological transformation of solar energy. Advances in Applied Microbiology **2**, 223–262.

Paulsen H, Finkenzeller B, Kühlein N. 1993. Pigments induce folding of light-harvesting chlorophyll a/b-binding protein. European Journal of Biochemistry **215**, 809–816.

Peers G, Truong TB, Ostendorf E, Busch A, Elrad D, Grossman AR, Hippler M, Niyogi KK. 2009. An ancient light-harvesting protein is critical for the regulation of algal photosynthesis. Nature **462**, 518–521.

Peltier G, Tolleter D, Billon E, Cournac L. 2010. Auxiliary electron transport pathways in chloroplasts of microalgae. Photosynthesis Research **106**, 19–31.

Plumley FG, Schmidt GW. 1987. Reconstitution of chlorophyll a/b light-harvesting complexes: Xanthophyll-dependent assembly and energy transfer. Cell Biology **84**, 146–150.

Purton S. 2007. Tools and techniques for chloroplast transformation of C*hlamydomonas*. Advances in Experimental Medicine and Biology **616**, 34–45.

Quaas T, Berteotti S, Ballottari M, Flieger K, Bassi R, Wilhelm C, Goss R. 2015. Non-photochemical quenching and xanthophyll cycle activities in six green algal species suggest mechanistic differences in the process of excess energy dissipation. Journal of Plant Physiology **172**, 92–103.

Raven J a, Allen JF. 2003. Genomics and chloroplast evolution: what did cyanobacteria do for plants? Genome biology **4**, 209.

Remacle C, Cardol P, Coosemans N, Gaisne M, Bonnefoy N. 2006. High-efficiency biolistic transformation of *Chlamydomonas* mitochondria can be used to insert mutations in complex I genes. Proceedings of the National Academy of Sciences **103**, 4771–4776.

Ruban A V., Lee PJ, Wentworth M, Young AJ, Horton P. 1999. Determination of the stoichiometry and strength of binding of xanthophylls to the photosystem II light harvesting complexes. Journal of Biological Chemistry **274**, 10458–10465.

Shapira M, Lers A, Heifetz PB, Irihimovitz V, Osmond CB, Gillham NW, Boynton JE. 1997. Differential regulation of chloroplast gene expression in *Chlamydomonas reinhardtii* during photoacclimation: Light stress transiently suppresses synthesis of the Rubisco LSU protein while enhancing synthesis of the PS II D1 protein. Plant Molecular Biology **33**, 1001–1011.

Spolaore P, Joannis-Cassan C, Duran E, Isambert A. 2006. Commercial applications of microalgae. Journal of Bioscience and Bioengineering **101**, 87–96.

Staehelin LA. 1986. *Chloroplast structure and supramolecular organization of photosynthetic membranes. Photosynthesis III. Encyclopedia of Plant Physiology* (New Series). Springer, Berlin, Heidelberg, Vol 19.

Stahl W, Sies H. 2005. Bioactivity and protective effects of natural carotenoids. Biochimica et Biophysica Acta - Molecular Basis of Disease **1740**, 101–107.

Stroebel D, Choquet Y, Popot J-L, Picot D. 2003. An atypical haem in the cytochrome b6f complex. Nature **426**, 413–418.

Takahashi H, Iwai M, Takahashi Y, Minagawa J. 2006. Identification of the mobile light-harvesting complex II polypeptides for state transitions in *Chlamydomonas reinhardtii*. Proceedings of the National Academy of Sciences of the United States of America **103**, 477–482.

Takeda T, Ishikawa T, Shigeoka S. 1997. Metabolism of hydrogen peroxide by the scavenging system in *Chlamydomonas reinhardtii*. Physiologia Plantarum **99**, 49–55.

Terao J. 1989. Antioxidant activity of beta-carotene-related carotenoids in solution. Lipids **24**, 659–661.

Tibiletti T, Auroy P, Peltier G, Caffarri S. 2016. *Chlamydomonas reinhardtii* PsbS protein is functional and accumulates rapidly and transiently under high light. Plant Physiology **171**, 2717–2730.

Tokutsu R, Iwai M, Minagawa J. 2009. CP29, a monomeric light-harvesting complex II protein, is essential for state transitions in *Chlamydomonas reinhardtii*. Journal of Biological Chemistry **284**, 7777–7782.

Tokutsu R, Kato N, Bui KH, Ishikawa T, Minagawa J. 2012. Revisiting the supramolecular organization of photosystem II in *Chlamydomonas reinhardti*i. Journal of Biological Chemistry **287**, 31574–31581.

Umena Y, Kawakami K, Shen JR, Kamiya N. 2011. Crystal structure of oxygen-evolving photosystem II at a resolution of 1.9Å. Nature **473**, 55–60.

Valencia-Sanchez MA, Liu J, Hannon GJ, Parker R. 2006. Control of translation and mRNA degradation by miRNAs and siRNAs. Genes and Development **20**, 515–524.

Vazquez-Villegas P, Torres-Acosta MA, Garcia-Echauri SA, Aguilar-Yanez JM, Rito-Palomares M, Ruiz-Ruiz F. 2018. Genetic manipulation of microalgae for the production of bioproducts. Frontiers in bioscience (Elite edition) **10**, 254–275.

Wientjes E, Van Amerongen H, Croce R. 2013. LHCII is an antenna of both photosystems after long-term acclimation. Biochimica et Biophysica Acta - Bioenergetics **1827**, 420–426.

Woessner JP, Goodenough UW. 1994. Volvocine cell walls and their constituent glycoproteins: An evolutionary perspective. Protoplasma **181**, 245–258.

Yamamoto HY, Kamite L. 1972. The effects of dithiothreitol on violaxanthin de-epoxidation and absorbance changes in the 500-nm region. Biochimica et Biophysica Acta (BBA) - Bioenergetics **267**, 538–543.

Yamamoto HY, Nakayama TO, Chichester CO. 1962. Studies on the light and dark interconversions of leaf xanthophylls. Archives of biochemistry and biophysics **97**, 168–173.

Zhang P, Allahverdiyeva Y, Eisenhut M, Aro E-M. 2009. Flavodiiron proteins in oxygenic photosynthetic organisms: photoprotection of Photosystem II by Flv2 and Flv4 in Synechocystis sp. PCC 6803. PLoS ONE **4**, e5331.

Zhang L, Melis A. 2002. Probing green algal hydrogen production. , 1499–1509.

Zorin B, Lu Y, Sizova I, Hegemann P. 2009. Nuclear gene targeting in *Chlamydomonas* as exemplified by disruption of the PHOT gene. Gene **432**, 91–96.

3.Chapter I

NPQ regulation in C. reinhardtii

Section A

LHCSR3 is a nonphotochemical quencher of both photosystems in *Chlamydomonas reinhardtii*[1]

In this chapter's thesis was investigated the role of LHCSR1 and LHCSR3 in NPQ activation in *Chlamydomonas reinhardtii,* in order to verify whether these proteins are involved in thermal dissipation of PSI excitation energy. To this aim we measured the fluorescence emitted at 77K by whole cells in quenched or unquenched state using Green Fluorescence Protein (GFP) as internal standard. We show that NPQ activation by high light treatment in *Chlamydomonas reinhardtii* leads to energy quenching in both PSI and PSII antenna systems. By analyzing quenching properties of mutants affected on the expression of LHCSR1 or LHCSR3 gene products and/or state-1-state 2 transitions or zeaxanthin accumulation, namely *npq4, stt7, stt7 npq4, npq4 lhcsr1, lhcsr3*-complemented *npq4 lhcsr1* and *npq1*, we showed that NPQ of Photosystem I occurs through quenching of associated LHCII antenna. This quenching event is fast-reversible upon switching light off, requires LHCSRs and is dependent on thylakoid lumenal pH, and could be observed in absence of zeaxanthin or STT kinase activity.

In this work I've performed all the experiments excluding the life time measurements analysis.

Abbreviations**:** PSI/II, Photosystem I/II; NPQ, Non-Photochemical Quenching; LHC, Light Harvesting Complex; ROS, Reactive Oxygen Species; GFP, Green Fluorescent Protein; DAS, Decay Associated Spectral Components.

---

[1]This section is based on the published article: **Girolomoni L,** Cazzaniga S, Pinnola A, Perozeni F, Ballottari M and Bassi R; LHCSR3 is a nonphotochemical quencher of both photosystems in *Chlamydomonas reinhardtii*. *Proceedings of the National Academy of Sciences* Volume 116, Issue 10, 5 March 2019, Pages 4212-4217

Introduction

Photosystem II (PSII) and I (PSI) are pigment-protein complexes, located in the thylakoid membranes, composed of a core complex, hosting photochemical reactions, and a peripheral antenna system formed by Light Harvesting Complexes (LHC) (Wei *et al.*, 2016; Mazor *et al.*, 2017). PSI and PSII fuel a light dependent electron transport chain from water to NADPH coupled with proton transport to the lumen driving ATP synthesis. ATP and NADPH are then used by the Calvin-Benson-Bassham cycle (CBB) to reduce CO2 into sugars. In excess light, rate of CBB reactions is saturated, ATP and NADPH are produced in excess compared to their metabolic demand, leading to ATPase limitation from lack of ADP substrate, which reduces the return of H+ to the stroma compartment and causes lumen acidification. Lack of electron acceptors causes charge recombination in PSII with triplet chlorophyll (Chl) excited states formation and reaction with oxygen, forming toxic Reactive Oxygen Species (ROS) (Niyogi, 1999). A major photoprotective mechanism, Non-Photochemical Quenching (NPQ) is activated when lumenal pH drops, safely dissipating up to 80% of the excitation energy absorbed into heat (Rees *et al.*, 1992). In *Chlamydomonas reinhardtii*, NPQ activity requires LHCSR1 and LHCSR3 proteins which are triggered to a quenching state upon sensing low lumenal pH (Peers *et al.*, 2009). Both LHCSR1 and LHCSR3 subunits are over-expressed upon prolonged high light treatment while LHCSR1 expression depends on high CO2 (Peers *et al.*, 2009; Maruyama *et al.*, 2014). LHCSRs expression has been reported to be triggered by blue light, involving phototropins as photoreceptor which activate a signal transduction pathway leading to LHCSR3 accumulation (Petroutsos *et al.*, 2016). LHCSR1 has been reported to be triggered by UV light through the activity of the UVR8 photoreceptor. LHCSR3 is accumulated to a far higher level than LHCSR1, making the former the major player in NPQ activity (Berteotti *et al.*, 2016; Dinc *et al.*, 2016). The *npq4* mutant lacks LHCSR3 and retains a low NPQ, which is abolished in *npq4 lhcsr1* also lacking LHCSR1 (Peers *et al.*, 2009; Berteotti *et al.*, 2016). In high light, violaxanthin is converted to zeaxanthin, a strong NPQ enhancer in plants (Niyogi *et al.*, 1998; Ware *et al.*, 2015) but not in *C. reinhardtii* (*npq1*) (Bonente *et al.*, 2011). Photoprotection is also favoured by reversible phosphorylation of PSII antenna subunits LHCII and CP29, upon which they are released from PSII and connect to PSI, enhancing its cross-section and balancing PSI vs PSII electron transport rates. This process, called

State1 to State2 transition depends on the STT7 kinase (Depege *et al.*, 2003; Bellafiore *et al.*, 2005) which, in turn, is activated by interaction with Cytochrome b_6f complex upon reduction of the PQ pool (Lemeille *et al.*, 2009, 2010; Shapiguzov *et al.*, 2016; Dumas *et al.*, 2017). Despite STT7 activity decreases under high light (Lemeille *et al.*, 2009), a photoprotective effect of state transitions was reported based on enhanced photoinhibition observed in the *stt7 npq4* double mutant respect to *npq4* under high light (Allorent *et al.*, 2013). Evidence for interaction between NPQ and state transitions rely on LHCSR3 being phosphorylated by STT7 (Bonente *et al.*, 2011; Bergner *et al.*, 2015) and interacting with the mobile LHCII fraction (Allorent *et al.*, 2013; Roach and Na, 2017). However, STT7-independent phosphorylation sites have also been reported in LHCSR3 and LHCSR1 (Bergner *et al.*, 2015). LHCSR3 was reported to interact with both PSI and PSII complexes (Tokutsu and Minagawa, 2013; Xue *et al.*, 2015; Bergner *et al.*, 2015), with phosphorylation negatively affecting LHCSR3 binding to PSI (Bergner *et al.*, 2015). Phosphorylation of LHCSR3 and LHCII was reported not to affect NPQ (Bonente *et al.*, 2011). While both LHCSR1 and LHCR3 have been reported to be quenchers for LHCII and PSII complexes (Dinc *et al.*, 2016; Roach and Na, 2017; Semchonok *et al.*, 2017), their involvement in PSI photoprotection is still under debate. In the moss *Physcomitrella patens*, LHCSR1 was found to be localized in stroma membranes and to be a quencher of both Photosystems (Pinnola *et al.*, 2015). Recently, LHCSR1 was reported to be involved in PSI quenching via excitation energy transfer from LHCII in *C. reinhardtii* (Kosuge *et al.*, 2018). In this work we investigated the quenching properties of LHCSR proteins towards LHCII, PSII and PSI-LHCII complexes in *C. reinhardtii*.

Materials and Methods

Strains and culture conditions

C. reinhardtii cells were grown at 25 °C in flask with white light (70 μE m^{-2} s^{-1}, 16h light/8h dark photoperiod) in TAP medium. High light acclimation was induced by growing cells at 400 μE m^{-2} s^{-1} in HS medium. *npq4 lhcsr1* complementation was performed as described in Ballottari *et al.* (2016).

NPQ measurements at room temperature

NPQ measurements were performed with a PAM-101 (Waltz, Germany) with actinic and saturating light of 1500 μE m^{-2} s^{-1} and 4000 μE m^{-2} s^{-1} respectively. The far-red LED was kept on during dark recovery. During dark adaptation cells were shaken in HS medium.

Quenching measurements at low temperature

77K fluorescence emission and excitation spectra were recorded using a Fluoromax3 (Horiba scientific) on whole C. reinhardtii cells dark adapted or HL treated (1500 μE m^{-2} s^{-1}) as described in the text. GFP protein was added to the sample as internal standard for normalization of fluorescence emission spectra. Additional details on fluorescence spectra acquisition and analysis are reported on SI Appendix.

Time-resolved fluorescence

Time-resolved fluorescence measurements were performed at 77K using a Chronos BH ISS Photon Counting instrument with picosecond laser excitation at 447 nm operating at 50 MHz. Laser power was kept below 0.1μW. Fluorescence decay maps were then globally fitted with exponential functions as previously reported (Van Stokkum *et al.*, 2004) using Glotaran v.1.5.1 software (Snellenburg *et al.*, 2012).

SDS-PAGE and immunoblotting

SDS-PAGE and immunoblotting were performed as described in (Bonente *et al.*, 2011). LHCSR1 and LHCSR3 specific antibodies (AS142819 and AS142766 respectively) were acquired from Agrisera company (Sweden).

Results

NPQ at room temperature

While room temperature fluorescence analysis is effective as a probe for NPQ of PSII, the low quantum yield of PSI makes its fluorescence a poor signal. As reported in Figure 1, the *npq4* mutant showed low residual NPQ activity from LHCSR1 when the effect of excess light was measured at room temperature, i.e. in conditions specific for detection of fluorescence from PSII.

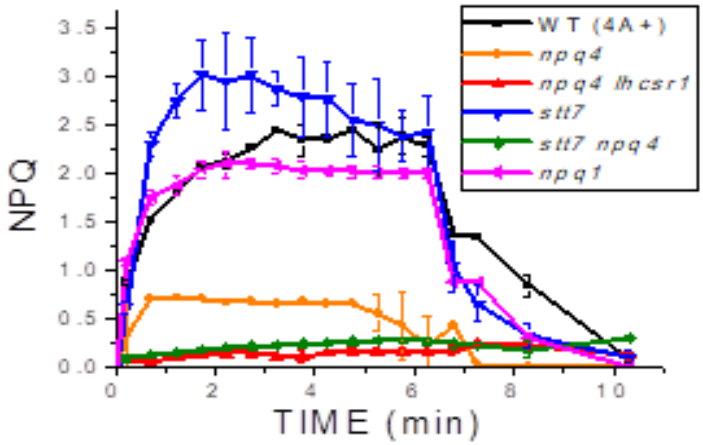

Figure 1. *NPQ induction kinetics measured at room temperature. Pulse-amplitude fluorometric time course at room temperature of WT and npq4, npq4 lhcsr1, stt7, stt7 npq4 and npq1 mutants. Standard deviations are reported as error bars (n=5).*

NPQ activity was further reduced in the double mutant *npq4 lhcsr1*. NPQ induction of the *stt7* mutant was faster than in WT and its amplitude was enhanced, suggesting STT7 kinase is not essential for NPQ. Interestingly, *stt7 npq4* mutant exhibited lower NPQ compared to *npq4* suggesting that the LHCSR1-dependent quenching might depend on STT7 activity, despite LHCSR1 was not a STT7 substrate. Analysis of WT vs *npq1* mutant (Niyogi *et al.*, 1997) showed NPQ in was independent from zeaxanthin (Figure 1), in agreement with previous reports (Bonente *et al.*, 2011). Since the amplitude of NPQ in *C. reinhardtii* is modulated by the amount of LHCSR subunits, their accumulation was quantified in the genotypes investigated by immunoblotting. LHCSRs content per PSI or PSII was similar in WT, *npq1* and *stt7* mutants. In WT and *npq1* strains LHCSR3 appeared as a double band, related to the presence of the phosphorylated form, increasing its apparent molecular weight. The LHCSR3 phosphorylated form was lost in absence of the STT7 kinase. In stt7 mutant, LHCSR1 accumulation was rather increased compared to WT, as in the case of npq4 and stt7 npq4 (Supplementary data, Figure S1).

Light dependent quenching of PSII and PSI in C. reinhardtii measured by 77K fluorescence emission spectra

PSI fluorescence contribution to the overall fluorescence emitted by *C. reinhardtii* can be investigated at 77K, where the PSI photochemistry is essentially blocked, and the

fluorescence quantum yield is significantly increased (Cho and Govindjee, 1970). Fluorescence emission spectra at low temperature of the WT shows two peaks at 687 nm and 710 nm which can be mainly attributed to PSII and PSI contribution respectively. Spectral deconvolution with Gaussian forms allowed for extrapolating the contributions of the different emitting components (Supplementary data, Figure S2): two Gaussians peaking at 684 and 694 nm can be associated to PSII-LHCII complexes, while the Gaussian form peaking at 712 nm can associated to PSI contribution. The last Gaussian function peaking at 735 nm is used for fitting optimization due to the red tail of Chl emission forms. These attributions were then confirmed by deconvolution analysis on 77K fluorescence emission spectra obtained from mutants with reduced amount of PSI (*psaB* mutant) (Lee *et al.*, 1996), or depleted of PSII (*psbD* mutant) (Erickson *et al.*, 1986) or LHCI and LHCII complexes (*cbs3)* (Tanaka *et al.*, 1998).

To investigate the role of LHCSR proteins in quenching of PSI and PSII, *C. reinhardtii* cells from WT, *npq4, npq4 lhcsr1, stt7, npq1* and *stt7 npq4* mutants were acclimated to high light (HL, 400 μE m^{-2} s^{-1}) for at least ten generations to induce LHCSR1 and LHCSR3 expression in the genotypes were the genes were expressed. Dark adapted, HL acclimated, cells were added with Green Fluorescent Protein (GFP) as internal fluorescence intensity standard and split into aliquots for different treatments upon which samples were rapidly frozen in liquid nitrogen and stored in the dark at 77K until fluorescence measurement were performed. As reported in Supplementary data, Figure S3, HL treatment for 6 minutes with strong light (1500 uE) did not change the GFP fluorescence emission spectrum or amplitude, enabling its use as internal standard, as previously reported (Pinnola *et al.*, 2015). Since a light-independent trans-thylakoidal ΔpH was previously reported to form in green algae especially in presence of high reducing power in the mitochondria (Finazzi and Rappaport, 1998), in order to exclude any potential quenching on PSII or PSI in dark adapted cells, 77K fluorescence emission spectra were measured in presence of the uncoupler nigericin, obtaining no significant effect on fluorescence emission spectra (Supplementary data, Figure S4). HL treatment gave a similar reduction of both PSI and PSII peaks in WT and *npq1* (Figure 2A, B).

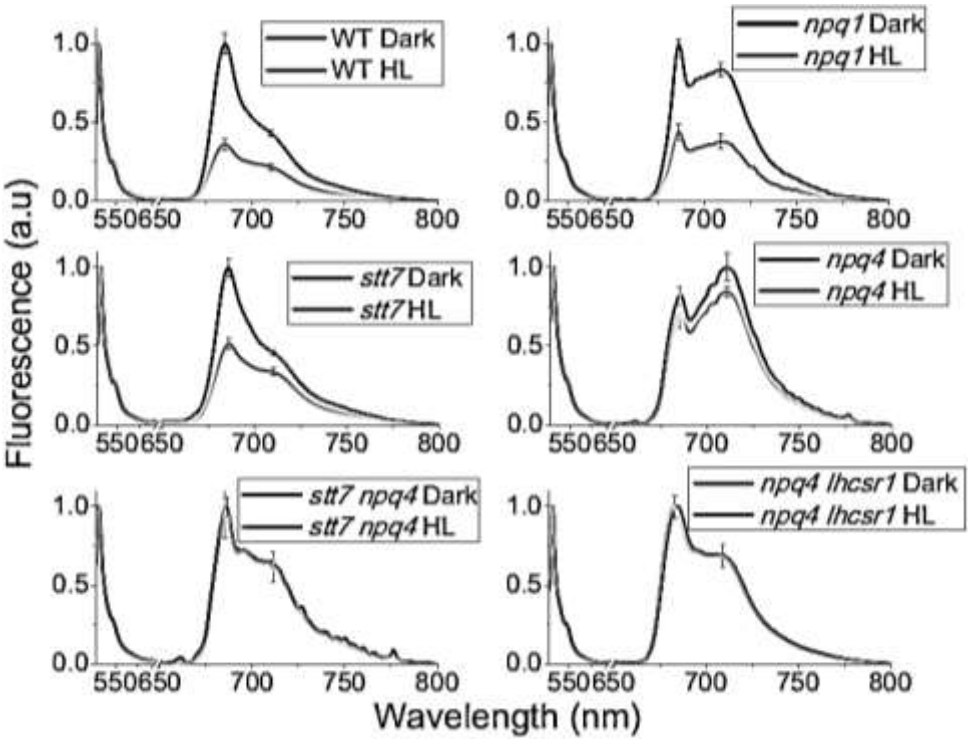

Figure 2. *77K fluorescence emission spectra of C. reinhardtii cells normalized to GFP before and after high light exposure. Fluorescence emission spectra of C. reinhardtii were recorded for whole cells dark adapted (black) or high light treated (1500 $\mu E\ m^{-2}\ s^{-1}$) for 6' (grey). GFP was added as internal standard for normalization. Standard deviations are reported as error bars (n=4).*

The quenching on PSI and PSII observed were confirmed by deconvolution of WT and *npq1* 77K fluorescence emission spectra into Gaussian components, as described in Supplementary data, Figure S2, resulting into a reduced amplitude for both PSI and PSII spectral components (Figure 3A, B).

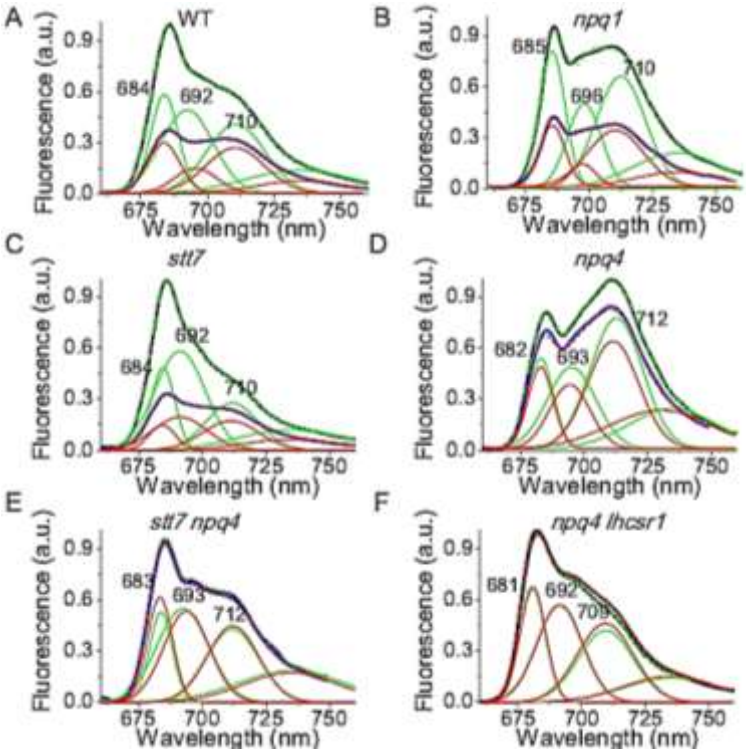

Figure 3. *Spectral deconvolution of 77K fluorescence emission spectra. Fluorescence emission spectra of dark adapted (black) or high light treated cells (blue) were reconstructed by spectral deconvolution with Gaussians: cumulative fit results are reported in dashed green (dark adapted samples) or dashed red (high light treated samples), while the different Gaussians used are reported in green (dark adapted samples) or red (high light treated samples). GFP was added as internal standard for normalization.*

In the case of *stt7*, the overall fluorescence emission of PSI was reduced in *stt7* mutant, likely due to the deplation of phosphorylated LHCII contributing to PSI emission in this mutant (Allorent *et al.*, 2013), where HL treatment caused a more evident quenching of the main peak (PSII) rather than on the 709 nm shoulder from PSI (Figure 2C). Gaussian deconvolution analysis, however, allowed for detection of decreased emission from PSI (Figure 3C), implying the onset of a STT7-independent quenching on PSI. In the case of *npq4*, only a minor effect was detected on PSII components upon HL treatment (Figure 2D, Figure 3D), while a more evident reduction of PSI contribution at 709 nm was detected (Figure 2D). These results suggest that while PSII and PSI quenching were still active in *npq4*, where LHCSR1 is the only LHCSR subunit, even if to a reduced extent compared to WT. It is worth to note that the highest PSI/PSII fluorescence ratio was

detected in *npq4* consistently with previous findings (Allorent *et al.*, 2013; Berteotti *et al.*, 2016). This residual quenching on PSI was, however, absent in the double mutant *stt7 npq4* (Figure 2E, Figure 3E). Both PSI and PSII quenching activities were absent in *npq4 lhcsr1* (Figure 2F, Figure 3F). In order to further investigate the possible role of LHCSR1 in PSI and PSII quenching, a genotype with only LHCSR3 subunit was generated by complementation of *npq4 lhcsr1* mutant with the *lhcsr3.1* gene under the control of its endogenous promoter, as previously described (Ballottari *et al.*, 2016). Complemented lines, herein called *C-lhcsr3-4* and *C-lhcsr3-24*, were characterized by a similar level of LHCSR3 compared to WT, but no LHCSR1 (Supplementary data, Figure S1). The resulting NPQ at room temperature was similar to the WT (SI Appendix Fig. S5), as previously reported (Ballottari *et al.*, 2016). 77K fluorescence emission spectra demonstrated that both PSI and PSII contributions were quenched upon HL treatment even in absence of LHCSR1 in *C-lhcsr3-4* and *C-lhcsr3-24* lines, obtaining similar results compared to WT (Supplementary data, Figure S5).

To characterize the kinetics of quenching, 77K fluorescence emission spectra were followed upon HL treatment for 2, 4, 6 minutes and following 2, 5 or 10 minutes of dark recovery in the presence of far red light. As reported in Supplementary data, Figure S6-8, HL treatment of WT, *stt7*, *npq1* and complemented lines *C-lhcsr3-4* and *C-lhcsr3-24* induced a progressive decrease of fluorescence emissions from both the main PSII peak (685 nm) and the PSI peak (709 nm). Upon dark recovery in dim far-red light to maintain plastoquinone pool oxidized, fluorescence emission of pre-illuminated WT samples nearly recovered the amplitude observed in dark adapted cells (Supplementary data, Figure S6). Differently, *npq4* and *stt7 npq4* mutants only underwent a transient decrease of both 686 and 710/711 nm emission peaks during the first 4' HL, while a slight reduction of 711 nm peak was observed in the case of the npq4 mutant only, with poor, if any recovery in the dark (Supplementary data, Figure S7). No significant quenching could be observed in the case of *npq4 lhcsr1* mutant neither on 682 nor on 709 nm peaks (Supplementary data, Figure S6D-E). Rather, a minor reduction of 682 nm peak was detected during dark recovery in presence of far red light, possibly related to activation of PSII repair system. To reconstruct the kinetics of PSI and PSII quenching from the fluorescence emission spectra, spectral deconvolution into Gaussians components was performed, as described in Figure 3, for the 77K fluorescence emission spectra obtained at different times of illumination or dark recovery. Fitting analysis on

WT, *C-lhcsr3-4* and *C-lhcsr3-24*, *stt7* and *npq1* curves showed similar quenching kinetics for all the components retrieved, with the 692-696 nm component (PSII) showing the highest quenching amplitude upon light treatment (Supplementary data, Figure S9-S13). In *npq4* and *stt7 npq4* mutants, small and virtually irreversible quenching effects were detected for the different components (Supplementary data, Figure S14 and Figure S15). In *npq4 lhcsr1*, instead, no quenching was observed in any component upon HL treatment (Supplementary data, Figure S16). Based on the amplitude of the PSII and PSI Gaussians the quenching on PSII vs PSI was estimated (Figure 4): the amplitude at time X (A_X) of the different Gaussians components was then used to calculate the quenching on PSI or PSII according to the formula $(A_{Dark} - A_X)/A_X$.

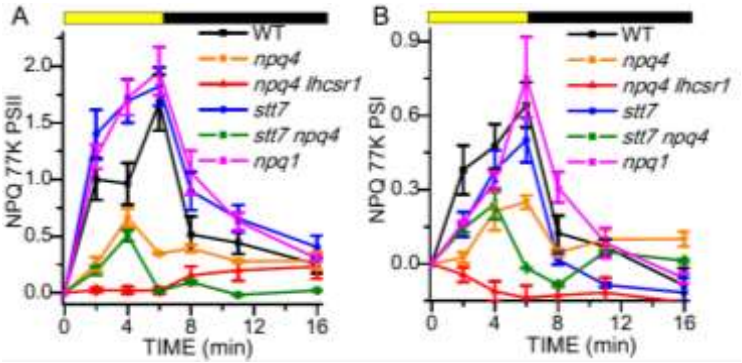

Figure 4. *Calculated NPQ induction kinetics at 77K. The NPQ curves were calculated from the area of the sum of the Gaussians used for the fitting according to the formula* $(A_{Dark} - A_X)/A_X$ *where* A_X *and* A_{Dark} *are respectively the amplitude at time X* (A_X) *or at time 0* (A_{Dark}*, dark adapted samples) of the different Gaussians attributable to PSII or PSI. Standard deviations are reported as error bars (n=4).*

PSII quenching estimated from Gaussian deconvolution was faster in *stt7*, *npq1* and *C-lhcsr3-4* and *C-lhcsr3-24* lines compared to WT while was strong reduced in *npq4*, *stt7 npq4* mutants and negligible in *npq4 lhcsr1* (Figure 4A; Supplementary data, Figure S17), consistent with the NPQ kinetics at room temperature (Figure 1; Supplementary data, Figure S5). PSI quenching was observed in WT, *stt7*, *C-lhcsr3-4* and *C-lhcsr3-24 lines* and *npq1* strains, with a faster induction kinetic in the case of WT and *C-lhcsr3-4* and *C-lhcsr3-24* lines. PSI quenching was partially detectable in *npq4* and in *stt7 npq4* even if strongly reduced, but absent in the *npq4 lhcsr1* mutant. These results imply that mainly LHCSR3 is involved in quenching of both PSI and PSII, while STT7 activity and zeaxanthin have a minor effect. In absence of LHCSR3a small LHCSR1 dependent quenching could be also measured.

77K fluorescence excitation spectra: PSI quenching is specifically located on antenna complexes

LHCSRs dependent quenching can be active specifically on LHC antenna proteins, acting as an alternative trap of excitation energy, or on the whole PSI or PSII supercomplexes. To discriminate between these two possibilities, the fluorescence excitation spectra were measured for PSI (emission at 710 nm) or PSII (emission at 685 nm) in dark adapted or HL treated cells. 77K excitation spectra were characterized by two main peaks: 435 nm, (Chl *a*) and 480 nm, (Chl *b*). Since LHC antenna proteins bind both Chl *a* and Chl *b*, while core complexes bind Chl *a* only, a preferential quenching of LHC antenna in HL is expected to yield excitation spectra with a decreased Chl *b* peak amplitude. In WT, NPQ induction did not change the PSII excitation spectrum compared to dark adapted sample but reduced the Chl *b* peak in PSI excitation spectrum (Figure 5A, B).

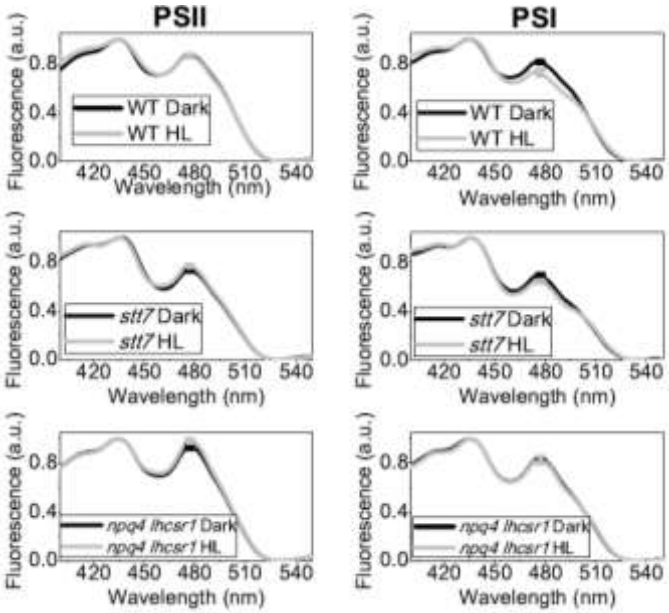

Figure 5. *77K fluorescence excitation spectra. Fluorescence excitation spectra were recorded following the fluorescence emission at 710 nm, where mainly PSI emits, and 685 nm, where mainly PSII emits. Fluorescence excitation spectra were measured in the case of dark adapted (black) and high light treated (grey) cells and normalized to the Chl a contribution at 436 nm. Standard deviations are reported as error bars (n=4).*

This result indicates that in the case of PSII, NPQ activation quenches the overall PSII-LHCII supercomplex, while in the case of PSI the HL treatment specifically reduces the

contribution of LHC complexes to the fluorescence emission of PSI. This observation was even more striking when the 480 nm/440 nm ratio observed in 77K fluorescence excitation spectra was corrected for the partial overlapping of PSII and PSI emission at 710 nm, according to the Gaussian deconvolution of 77K fluorescence emission spectra (Supplementary data, Table S1). Similar results were then obtained in the case of *C-lhcsr3-4* and *C-lhcsr3-24* or *npq1* (Supplementary data, Figure S18-19). In the case of *stt7* mutant HL treatment caused a decrease of Chl b contribution in PSI excitation spectrum, although smaller compared to WT (Figure 5C, D). No decrease in Chl b contribution was observed in *npq4 lhcsr1* (Figure 5E, F), *npq4* and *stt7npq4* (Supplementary data, Figure S19), consistent with LHCSR being involved in specifically quenching LHC proteins connected to PSI while homogeneously quenching LHCII-PSII core pigment bed

77K time resolved analysis

Time-resolved fluorescence analysis at 77K was performed on WT and *npq4 lhcsr1* strain in dark adapted state or upon activating quenching by HL treatment. Fluorescence decay traces were then submitted to global analysis as previously described (Van Stokkum *et al.*, 2004) in order to identify the different spectral components and relative decay time constants associated. Four DAS (Decay associated spectral components) were required for best fit of the fluorescence decay maps (Figure 6).

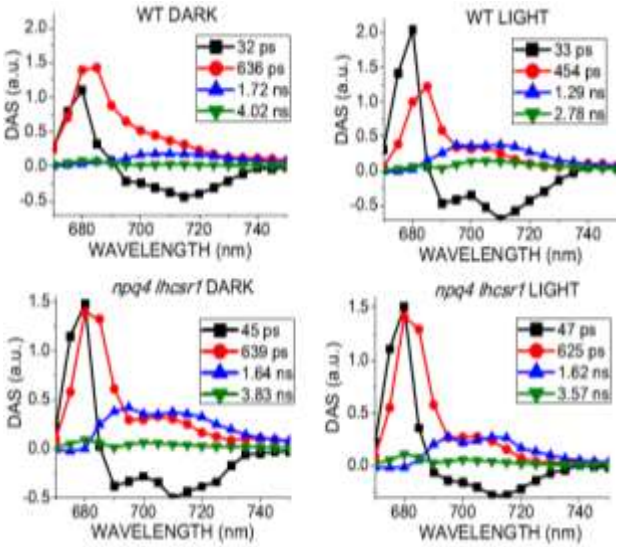

Figure 6. *Global analysis of time resolved fluorescence kinetics at 77K. Fluorescence decay kinetics of dark adapted or high light treated WT and npq4 lhcsr1 mutant were acquired at 77K in the 670 – 750 nm range with 5 nm step and globally fitted with 4 exponentials. The decay associated spectra (DAS) obtained are reported normalized to the same total area for each sample, while the associated time constants are indicated the legend. Standard deviation associated to time constants is less than 5% for each component.*

The first component (DAS 1) was characterized by a positive/negative DAS and a time constant of 32-47 ps: this component reflects the excitation energy transfer from LHC proteins to PSII and PSI core complex, which is not significantly affected by activation of NPQ mechanisms (Chukhutsina *et al.*, 2014). The second component (DAS 2) peaked in the 680-690 nm region with a shoulder at 710 nm and a decay constent of 630 ps in dark adapted WT and in *npq4 lhcsr1*. Differently, in the case of HL treated WT, DAS 2 showed a shorter time constant of 454 ps. DAS 2 is principally related to PSII (680-690nm emission) with a small contribution from PSI (emission at 710 nm), in agreement with reports of sub-ns component at 77K from both PSII and PSI (Wlodarczyk *et al.*, 2016). The third DAS (DAS 3) showed a wide emission in the 690-740 nm, best fitting with PSI. The decay constant was 1.72 ns, reduced to 1.29 ns in HL. In the *npq4 lhcsr1* mutant the decay constant of this DAS 3 was not significantly affected by light treatment. These results agree with a LHCSR dependent activation of quenching mechanisms for both PSI and PSII upon HL treatment. Finally, a small component (DAS 4) with a decay constant of 2.7 – 4 ns was observed in all samples: this component has been previously attributed to loosely bound LHCII and to the longest decay contribution from PSI at 77K (Wlodarczyk *et al.*, 2016). In WT, DAS 4 was shortened upon HL exposure, from 4.01 ns to 2.70 ns. It should be noticed that *npq4 lhcsr1* mutant, also underwent a limited reduction in DAS 4 lifetime from 3.8 to 3.6 ns. WT DAS 4, however, was specifically decreased at 685 nm respect to *npq4 lhcsr1* mutant, suggesting a preferential LHCSR-dependent quenching of loosely bound LHCII. Time resolved fluorescence analysis was also performed on *stt7, npq1, npq4, stt7 npq4* and *C-lhcsr3-4* and *C-lhcsr3-24* strains (Supplementary data, Figure S20): in the case of dark-adapted samples, global analysis yielded similar results compared to WT and *npq4 lhcsr1* genotypes. Upon HL treatment only *stt7, npq1* and *C-lhcsr3-4* and *C-lhcsr3-24* strain exhibited a shortening of the decay constants of DAS2, 3 and 4 as in the case of WT. A minor shortening of decay constant of DAS3 from 1.77 ns to 1.49 nm was also observed also for *npq4*, in agreement with a minor quenching activity on PSI from residual LHCSR1.

Discussion

LHCSR3 and LHCSR1 are pigment binding proteins involved in NPQ activation in *C. reinhardtii* (Peers *et al.*, 2009; Berteotti *et al.*, 2016; Dinc *et al.*, 2016; Kosuge *et al.*,

2018). NPQ measurements have been mainly based on room temperature fluorescence measurements monitoring changes of PSII fluorescence while the low fluorescence quantum yield of PSI prevents analysis in presence of strong emissions by PSII. At 77K, fluorescence quantum yield is high for both PSI and PSII allowing for proper quantification of both emissions. Moreover, freezing samples in liquid nitrogen preserves the conformations previously induced by actinic light thus allowing for spectral characterization of quenched states (Pinnola *et al.*, 2015, Wlodarczyk *et al.*, 2018). The direct involvement of LHCSR in activating quenching is evident from Figure 2 and Figure 3, showing that HL was effective in reducing the amplitude of both PSII and PSI emissions in presence of LHCSR subunits. Deconvolution of fluorescence emission spectra in Gaussians components allowed to isolate the contributions of PSI from PSII and showing both were quenched upon HL treatment (Figure 3). Indeed, time resolved fluorescence analysis, also at 77K, on dark adapted *vs* HL treated cells, showed a strong reduction of time constants decay of both PSI and PSII in presence of LHCSR subunits only (Figure 6). The activity of LHCSR subunits as quenchers for LHCII trimers either components of PSII or PSI supercomplexes or loosely bound, is consistent with previous reports: LHCSR1 was found active vs LHCII, either free or bound to PSI (Dinc *et al.*, 2016; Kosuge *et al.*, 2018), while LHCSR3 subunit was found to bind to both PSI and PSII in *C. reinhardtii* (Tokutsu and Minagawa, 2013; Xue *et al.*, 2015; Bergner *et al.*, 2015) and to be active in quenching purified PSII-LHCII supercomplexes (Tokutsu and Minagawa, 2013). Interestingly, the absence of LHCSR1 in *C-lhcsr3-4* and *C-lhcsr3-24* lines did not affect PSI or PSII quenching (Supplementary data, Figure S17), while only a partial quenching was observed upon LHCSR1 upregulation in npq4 or stt7 npq4 mutant (Figure 4): these results indicate that LHCSR3 is the major actor in PSI and PSII quenching, while only a minor role, if any, can be attributed to LHCSR1. Nevertheless, the residual quenching observed in *npq4* and *stt7 npq4* indicates that LHCSR1 might be a quencher for both Photosystems, even if with a much lower efficiency compared to LHCSR3. The increased quenching activity of LHCSR3 compared to LHCSR1 might be related simply to a dose effect and/or to some specific interactions with potential partners and/or to a specific intrinsic quenching activity. Quenching activity toward PSI or PSII by LHCSR differs: while the fluorescence excitation spectra of PSII-LHCII complex was similar in dark adapted or HL-treated samples, suggesting homogeneous quenching in HL, a specific reduction of Chl b

contribution to PSI emission was observed in the case of LHCSR3-dependent quenching of PSI (Figure 5, Supplementary data, Table S1). This result suggests that in the case of PSI, LHCSR3 subunits quenches preferentially antenna proteins, rather than PSI core complex. Both LHCSR1 and LHCSR3 have been previously reported to interact with the "mobile" fraction of LHCII, preferentially involved in state transitions: LHCSR3 was suggested to modulate coupling/decoupling of this LHCII population to PSII (Roach and Na, 2017), while LHCSR1 to modulate the excitation energy transfer from LHCII to PSI (Kosuge *et al.*, 2018). The results herein reported are consistent with the above reports, highlighting a specific role of LHCSR subunits, in particular LHCSR3, in quenching "mobile" LHCII trimers thus reducing the fraction of LHC subunits involved in efficient ET to PSI (Figure 6). At variance with results reported by Kosuge *et al.* (2018), 77K fluorescence excitation spectra and time resolved fluorescence analysis suggest that the LHCSR-dependent quenching on LHCII trimers does not correlate with increased excitation energy transfer to PSI. This interpretation is supported by several evidences: a) Chl b contribution to PSI fluorescence emission was reduced, while an increased excitation energy transfer to PSI would be expected to increase the contribution of antenna proteins to PSI emission; b) the amplitude of the shortest DAS (DAS 1, ~30 ps) obtained by time resolved fluorescence analysis, from excitation energy transfer to PSI, did not increase upon HL treatment as expected from increasing the antenna size; c) time constants of DAS attributable to both PSII and PSI in WT dark adapted cells were reduced upon HL treatment, consistent with the onset of a quenching mechanism, rather than as result of excitation energy transfer to PSI reaction centre; d) PSI fluorescence was observed at 77K i.e. with photochemical activity strongly reduced, if any. This finding implies that the possible LHCSR dependent quenching mechanism at room temperature should be extremely fast in order to compete with PSI photochemistry: a quenching conformation decaying in 80 ps was reported *in vitro* in the case of LHCSR1 from the moss *Physcomitrella patens* (Pinnola *et al.*, 2017). This time scales are consistent with competition with PSI photochemical traps, even if further investigation is required to properly evaluate this point. Nevertheless, we cannot fully rule out the possibility that LHCSR-dependent quenching might in part involve energy transfer to PSI reaction centres as suggested by Kosuge *et al.* (2018). or detachment of antenna proteins from PSI core, which could account for the preferential loss of Chl b contribution to PSI excitation spectra (Figure 5).

Kinetics of NPQ on PSII and PSI were reconstructed based on Gaussian deconvolution at different illumination times (Figure 4). Zeaxanthin accumulation upon HL treatment had little effect on PSII quenching, while PSI quenching was only slightly affected in terms of decay kinetics (Figure 4). These results are consistent with a minor role, if any, of zeaxanthin in increasing the kinetic for activation of PSI quenching in *C. reinhardtii* (Bonente *et al.*, 2011). In the case of *stt7* mutant, the absence of an active STT7 kinase did not impair NPQ induction at the level of either PSI or PSII (Figure 4): while LHCII phosphorylation is dependent on STT7 activity and related to state transitions (Depege *et al.*, 2003), LHCSR3 was also reported to harbour phosphorylation sites which are not substrates for STT7 and the binding of LHCSR3 to PSI was negatively affected by its phosphorylation (Bergner *et al.*, 2015). The results herein presented and previous findings, together, suggest that LHCSR3-dependent quenching of PSI occur on LHC proteins bound to PSI-complex which could be either identified as phosphorylated LHCII trimers or LHCI proteins (Figure 7), thus explaining the different Chl b contribution observed in fluorescence excitation spectra in *stt7* mutant upon HL treatment.

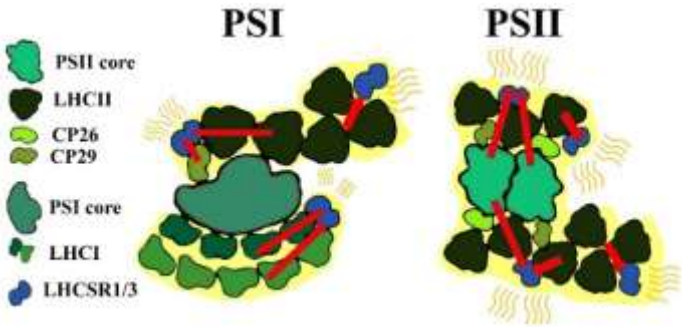

***Figure 7**. Model for LHCSRs quenching on PSI and PSII. LHCSR1 and LHCSR3 interaction with PSI an PSII supercomplexes is schematically reported as a model for their quenching activity. LHCSR3 has the major role in quenching, while a residual LHCSR1 dependent quenching activity can be observed in absence of LHCSR3. Red arrows indicate excitation energy transfer. Peripheral LHCII trimers loosely connected to PSI or PSII are also reported. In the model, the PSI and PSII subunits quenched by LHCR proteins are highlighted in yellow.*

We conclude that in *C. reinhardtii* LHCSR3 subunits are involved in quenching both PSI and PSII, by both directly interacting with PSII supercomplexes, and with PSI-bound LHCII (Figure 7). Since in *C. reinhardtii* PSBS is only transiently expressed (Tibiletti *et al.*, 2016; Correa-Galvis *et al.*, 2016) and not detected in the conditions hetein applied (Supplementary data, Figure S1), LHCSR3 proteins appear to account for

most or all NPQ activity as shown by lack of quenching in *npq4 lhcsr1*. Quenching activity occurs at different sites: (i) PSII complexes, where LHCSR3 was found docking to LHCII trimers or CP26 (Semchonok *et al.*, 2017); (ii) LHC complexes bound to PSI complexes, and (iii) LHCII "mobile" pool loosely connected to Photosystems (Figure 7). In the WT, upon HL stress, PSII quenching rapidly occurred while PSI quenching was slower (Figure 4), possibly due to a time lag for LHCSR-dependent detachment of LHCII proteins from PSI. The photoprotective relevance for the observed fluorescence quenching on PSI was confirmed by the strong PSI photoinhibition observed when PSI quenching was completely abolished in the *stt7 npq4* mutant (Allorent *et al.*, 2013).

References

Allorent G, Tokutsu R, Roach T, *et al.* 2013. A Dual Strategy to Cope with High Light in *Chlamydomonas reinhardtii*. The Plant Cell **25**, 545–557.

Ballottari M, Truong TB, Re De E, Erickson E, Stella GR, Fleming GR, Bassi R, Niyogi KK. 2016. Identification of ph-sensing sites in the light harvesting complex stress-related 3 protein essential for triggering non-photochemical quenching in *Chlamydomonas reinhardtii*. Journal of Biological Chemistry **291**, 7334–7346.

Bellafiore S, Barneche F, Peltier G, Rochaix J-D. 2005. State transitions and light adaptation require chloroplast thylakoid protein kinase STN7. Nature **433**, 892–895.

Bergner SV, Scholz M, Trompelt K, *et al.* 2015. STATE Transition7-dependent phosphorylation is modulated by changing environmental conditions, and its absence triggers remodeling of photosynthetic protein complexes. Plant physiology **168**, 615–634.

Berteotti S, Ballottari M, Bassi R. 2016. Increased biomass productivity in green algae by tuning non-photochemical quenching. Scientific reports **6**, 21339.

Bonente G, Ballottari M, Truong TB, Morosinotto T, Ahn TK, Fleming GR, Niyogi KK, Bassi R. 2011. Analysis of LHcSR3, a protein essential for feedback de-excitation in the green alga *Chlamydomonas reinhardtii*. PLoS Biology **9**, e1000577.

Cho F, Govindjee. 1970. Low-temperature (4-77 degrees K) spectroscopy of *Chlorella*: temperature dependence of energy transfer efficiency. Biochimica et biophysica acta **216**, 139–150.

Chukhutsina VU, Buchel C, van Amerongen H. 2014. Disentangling two non-photochemical quenching processes in *Cyclotella meneghiniana* by spectrally-resolved picosecond fluorescence at 77K. Biochimica et biophysica acta **1837**, 899–907.

Correa-Galvis V, Redekop P, Guan K, Griess A, Truong TB, Wakao S, Niyogi KK, Jahns P. 2016. Photosystem II Subunit PsbS is involved in the induction of LHCSR protein-dependent energy dissipation in *Chlamydomonas reinhardtii*. The Journal of biological chemistry **291**, 17478–17487.

Depege N, Bellafiore S, Rochaix J-D. 2003. Role of chloroplast protein kinase Stt7 in LHCII phosphorylation and state transition in *Chlamydomonas*. Science **299**, 1572–1575.

Dinc E, Tian L, Roy LM, Roth R, Goodenough U, Croce R. 2016. LHCSR1 induces a fast and reversible pH-dependent fluorescence quenching in LHCII in *Chlamydomonas reinhardtii* cells. Proceedings of the National Academy of Sciences of the United States of America **113**, 7673–7678.

Dumas L, Zito F, Blangy S, Auroy P, Johnson X, Peltier G, Alric J. 2017. A stromal region of cytochrome b6f subunit IV is involved in the activation of the Stt7 kinase in *Chlamydomonas*. Proceedings of the National Academy of Sciences of the United States of America **114**, 12063–12068.

Erickson JM, Rahire M, Malnoe P, Girard-Bascou J, Pierre Y, Bennoun P, Rochaix JD. 1986. Lack of the D2 protein in a *Chlamydomonas reinhardtii* psbD mutant affects photosystem II stability and D1 expression. The EMBO journal **5**, 1745–1754.

Finazzi G, Rappaport F. 1998. *In vivo* characterization of the electrochemical proton gradient generated in darkness in green algae and its kinetic effects on cytochrome b6f turnover. Biochemistry **37**, 9999–10005.

Kosuge K, Tokutsu R, Kim E, Akimoto S, Yokono M, Ueno Y, Minagawa J. 2018. LHCSR1-dependent fluorescence quenching is mediated by excitation energy transfer from LHCII to photosystem I in *Chlamydomonas reinhardtii*. Proceedings of the National Academy of Sciences of the United States of America **115**, 3722–3727.

Lee H, Bingham SE, Webber AN. 1996. Function of 3' non-coding sequences and stop codon usage in expression of the chloroplast psaB gene in *Chlamydomonas reinhardtii*. Plant molecular biology **31**, 337–354.

Lemeille S, Turkina M V, Vener A V, Rochaix J-D. 2010. Stt7-dependent phosphorylation during state transitions in the green alga *Chlamydomonas reinhardtii*. Molecular & cellular proteomics **9**, 1281–1295.

Lemeille S, Willig A, Depège-Fargeix N, Delessert C, Bassi R,

Rochaix JD. 2009. Analysis of the chloroplast protein kinase Stt7 during state transitions. PLoS Biology **7**, 0664–0675.

Maruyama S, Tokutsu R, Minagawa J. 2014. Transcriptional regulation of the stress-responsive light harvesting complex genes in *Chlamydomonas reinhardtii*. Plant & cell physiology **55**, 1304–1310.

Mazor Y, Borovikova A, Caspy I, Nelson N. 2017. Structure of the plant photosystem I supercomplex at 2.6 A resolution. Nature plants **3**, 17014.

Niyogi KK. 1999. Photoprotection revisited: Genetic and Molecular Approaches. Annual review of plant physiology and plant molecular biology **50**, 333–359.

Niyogi KK, Bjorkman O, Grossman AR. 1997. *Chlamydomonas* xanthophyll cycle mutants identified by Video Imaging of chlorophyll fluorescence quenching. the Plant Cell **9**, 1369–1380.

Niyogi KK, Grossman AR, Bjorkman O. 1998. *Arabidopsis* mutants define a central role for the xanthophyll cycle in the regulation of photosynthetic energy conversion. The Plant cell **10**, 1121–1134.

Peers G, Truong TB, Ostendorf E, Busch A, Elrad D, Grossman AR, Hippler M, Niyogi KK. 2009. An ancient light-harvesting protein is critical for the regulation of algal photosynthesis. Nature **462**, 518–521.

Petroutsos D, Tokutsu R, Maruyama S, *et al.* 2016. A blue-light photoreceptor mediates the feedback regulation of photosynthesis. Nature **537**, 563–566.

Pinnola A, Ballottari M, Bargigia I, Alcocer M, D'Andrea C, Cerullo G, Bassi R. 2017. Functional modulation of LHCSR1 protein from *Physcomitrella patens* by zeaxanthin binding and low pH. Scientific reports **7**, 11158.

Pinnola A, Cazzaniga S, Alboresi A, Nevo R, Levin-Zaidman S, Reich Z, Bassi R. 2015. Light-Harvesting Complex Stress-Related proteins catalyze excess energy dissipation in both photosystems of *Physcomitrella patens*. Plant Cell **27**, 3213–3227.

Pinnola A, Dall'Osto L, Gerotto C, Morosinotto T, Bassi R, Alboresi A. 2013. Zeaxanthin binds to Light-Harvesting Complex Stress-Related protein to enhance nonphotochemical quenching in *Physcomitrella patens*. The Plant Cell **25**, 3519–3534.

Rees D, Noctor G, Ruban A V, Crofts J, Young A, Horton P. 1992. pH dependent chlorophyll fluorescence quenching in spinach thylakoids from light treated or dark adapted leaves. Photosynthesis research **31**, 11–19.

Roach T, Na CS. 2017. LHCSR3 affects de-coupling and re-coupling of LHCII to PSII during state transitions in *Chlamydomonas reinhardtii*. Scientific reports **7**, 43145.

Semchonok DA, Sathish Yadav KN, Xu P, Drop B, Croce R, Boekema EJ. 2017. Interaction between the photoprotective protein LHCSR3 and C2S2 Photosystem II supercomplex in *Chlamydomonas reinhardtii*. Biochimica et biophysica acta. Bioenergetics **1858**, 379–385.

Shapiguzov A, Chai X, Fucile G, Longoni P, Zhang L, Rochaix J-D. 2016. Activation of the Stt7/STN7 kinase through dynamic interactions with the Cytochrome b6f Complex. Plant physiology **171**, 82–92.

Snellenburg JJ, Laptenok SP, Seger R, Mullen KM, van Stokkum IHM. 2012. Glotaran : A Java -Based Graphical User Interface for the R Package TIMP. Journal of Statistical Software **49**, 1–22.

Van Stokkum IHM, Larsen DS, Van Grondelle R. 2004. Global and target analysis of time-resolved spectra. Biochimica et Biophysica Acta - Bioenergetics **1657**, 82–104.

Tanaka A, Ito H, Tanaka R, Tanaka NK, Yoshida K, Okada K. 1998. Chlorophyll a oxygenase (CAO) is involved in chlorophyll b formation from chlorophyll a. Proceedings of the National Academy of Sciences **95**, 12719–12723.

Tibiletti T, Auroy P, Peltier G, Caffarri S. 2016. *Chlamydomonas reinhardtii* PsbS protein is functional and accumulates rapidly and transiently under high light. Plant Physiology **171**, 2717–2730.

Tokutsu R, Minagawa J. 2013. Energy-dissipative supercomplex of photosystem II associated with LHCSR3 in *Chlamydomonas reinhardtii*. Proceedings of the National Academy of Sciences of the United States of America **110**, 10016–10021.

Ware MA, Belgio E, Ruban A V. 2015. Comparison of the protective effectiveness of NPQ in Arabidopsis plants deficient in PsbS protein and zeaxanthin. Journal of experimental botany **66**, 1259–1270.

Wei X, Su X, Cao P, Liu X, Chang W, Li M, Zhang X, Liu Z. 2016. Structure of spinach photosystem II-LHCII supercomplex at 3.2 A resolution. Nature **534**, 69–74.

Wlodarczyk LM, Dinc E, Croce R, Dekker JP. 2016. Excitation energy transfer in *Chlamydomonas reinhardtii* deficient in the PSI core or the PSII core under conditions mimicking state transitions. Biochimica et biophysica acta **1857**, 625–633.

Wlodarczyk LM, Snellenburg JJ, Dekker JP, Stokkum IHM. 2018. Development of fluorescence quenching in *Chlamydomonas reinhardtii* upon prolonged illumination at 77 K. Photosynthesis Research **137**, 503–513.

Xue H, Tokutsu R, Bergner SV, Scholz M, Minagawa J, Hippler M. 2015. Photosystem II subunit R is required for efficient binding of Light-Harvesting Complex Stress-Related Protein3 to photosystem II-light-harvesting supercomplexes in *Chlamydomonas reinhardtii*. Plant physiology **167**, 1566–1578.

Supplementary material and data

Quenching measurements at low temperature and Gaussians deconvolution of fluorescence emission spectra

Algal cells were washed twice with water and kept in dark for 1 hour; 1 μM of recombinant GFP was used as an internal standard. During dark adaptation cells were shacked in tap water at the concentration of 75 μg/ml of chlorophylls. When needed, nigericin was added in the dark 10 minutes before the measurements. The final concentration of nigericin was 15μM. Samples were collected before the illumination, after treatment with 1500 μE m−2 s−1 or following a 5-min recovery in the dark. All samples were frozen in liquid nitrogen. Fluorescence at low temperature were recorded using a Fluoromax3 equipped with an optical fiber (Horiba scientific). Emission spectra were performed by exciting the sample at 475 nm and recording emission from 500 to 800 nm, normalizing to the GFP signal at 508 nm. Excitation spectra were performed by recording the emission derived from PSII at 685 nm and PSI at 709 nm for excitation in the 400- to 550-nm range. The contribution of PSI and PSII was evaluated through the deconvolution of the emission spectra using four Gaussians peaking at 681-685 (LHCII-PSII), 692-696 (PSII), 710-712 (PSI), and 735 nm (used for the fitting optimization) nm. The spectra analysis was performed using OriginPro 9.0 software (OriginLab).

Table S1: Contribution of Chl b to PSI and PSII fluorescence.

Chl b and Chl a contribution to 685 and 710 nm emission were determined on the base of fluorescence excitation spectra reported in Figure 6 for WT, stt7 and npq4 lhcsr1, in Figure S18 for complemented lines C-lhcsr3-4 and C-lhcsr3-24 and in Figure S19 for mutants npq4, npq1 and stt7 npq4 dark adapted (D) or high light treated (HL). The contribution of PSII or PSI emission to 685 or 710 nm fluorescence emission is reported as based on the Gaussians deconvolution reported in Figure 6 and Figure S12. Due to some overlapping of Gaussians attributed to PSI or PSII at 710 nm, the real 480/440 nm ratio in PSI excitation spectra (480/440 nm ex PSI) was calculated by considering the contribution of PSII to 710 nm emission and the 480/440 nm ratio observed in the excitation spectra at 685 nm. the contribution of PSI emission to 685 nm was assumed to be negligible.*

	685 nm emission			710 nm emission				
	480/440 nm ex	dev st	% PSII	480/440 nm ex	dev st	%PSI	480/440 nm ex PSI*	dev st
WT *D*	0.875	0.005	95.4%	0.813	0.009	70.0%	0.786	0.010
WT *HL*	0.866	0.014	90.5%	0.728	0.025	80.1%	0.693	0.027
stt7 D	0.735	0.009	98.0%	0.693	0.012	65.2%	0.670	0.015
stt7 HL	0.769	0.010	95.6%	0.646	0.011	72.4%	0.600	0.015
npq4 lhcsr1 D	0.936	0.016	95.9%	0.843	0.004	75.9%	0.813	0.016
npq4 lhcsr1 HL	0.983	0.015	95.0%	0.828	0.026	79.2%	0.788	0.029
npq1 D	0.820	0.006	97.3%	0.774	0.008	77.4%	0.760	0.008
npq1 HL	0.819	0.006	88.7%	0.716	0.006	84.0%	0.697	0.009
npq4 D	0.920	0.000	94.2%	0.854	0.012	75.8%	0.833	0.017
npq4 HL	0.980	0.021	91.3%	0.856	0.021	74.7%	0.814	0.030
stt7 npq4 D	0.975	0.005	96.6%	0.823	0.007	67.5%	0.749	0.009
stt7 npq4 HL	0.982	0.031	97.7%	0.825	0.030	72.3%	0.765	0.054
C-lhcsr3-4 D	0.896	0.020	99.0%	0.822	0.015	60.9%	0.774	0.024
C-lhcsr3-4 HL	0.879	0.022	97.1%	0.753	0.031	69.2%	0.697	0.038
C-lhcsr3-4 D	0.890	0.000	97.8%	0.815	0.006	70.0%	0.783	0.020
C-lhcsr3-24 HL	0.915	0.015	88.4%	0.735	0.011	79.2%	0.687	0.017

Figure S1 *Accumulation of LHCSR subunits. Panel A: LHCSR1 and LHCSR3 accumulation in high light (400 µmol photons m−2 s−1) acclimated WT, npq1, npq4, stt7, stt7 npq4, npq4 lhcsr1 mutants and npq4 lhcsr1 complemented lines with lhcsr3 gene (C-lhcsr3-4 and C-lhcsr3-24 lines) were investigated by immunoblotting using specific α-LHCSR1 and α-LHCSR3 antibodies recognizing respectively LHCSR1 (https://www.agrisera.com/en/artiklar/lhcsr1.html) or LHCSR3 (https://www.agrisera.com/en/artiklar/lhcsr3.html). Total protein extracts were loaded on SDS-PAGE on a chlorophyll basis loading 1, 0.5 and 0.25 µg of chlorophyll for each sample analysed. In the case of LHCSR3, both the phosphorylated (LHCSR3-P) and unphosphorylated form (LHCSR3, with lower apparent molecular weight) were detected by the α-LHCSR3 antibody. Specific antibodies recognizing PSI and PSII subunits PsaA and CP43 as described in (1) were also used to determine the PSI and PSII relative content respectively. In addition, PsbS accumulation was investigated using specific α-PsbS antibody (2), but no traces of this subunit were detected in the different strains herein analysed when acclimated to high light conditions. Panel B: positive control for PsbS detection. PsbS subunit was detected upon exposure of low light (LL) acclimated WT to 4 hours of high light (1200 µmol photons m−2 s−1) as reported in (3). Panel C: relative LHCSR content was retrieved from immunoblots reported in Panel A by densitometry (in the case of LHCSR3, the amount of the phosphorylated and unphosphorylated forms were added up) and normalized to PSI or PSII content setting the LHCSR/PsaA or LHCSR/CP43 ratios to 100 in the case of WT. The LHCSR/CP43 and LHCSR/PsaA ratios obtained for the other genotypes were then normalized to the WT ratios. Data are expressed as mean ± s.d. (n = 3). The significantly different value from the WT are marked with an asterisk. (*) (p<0,01).*

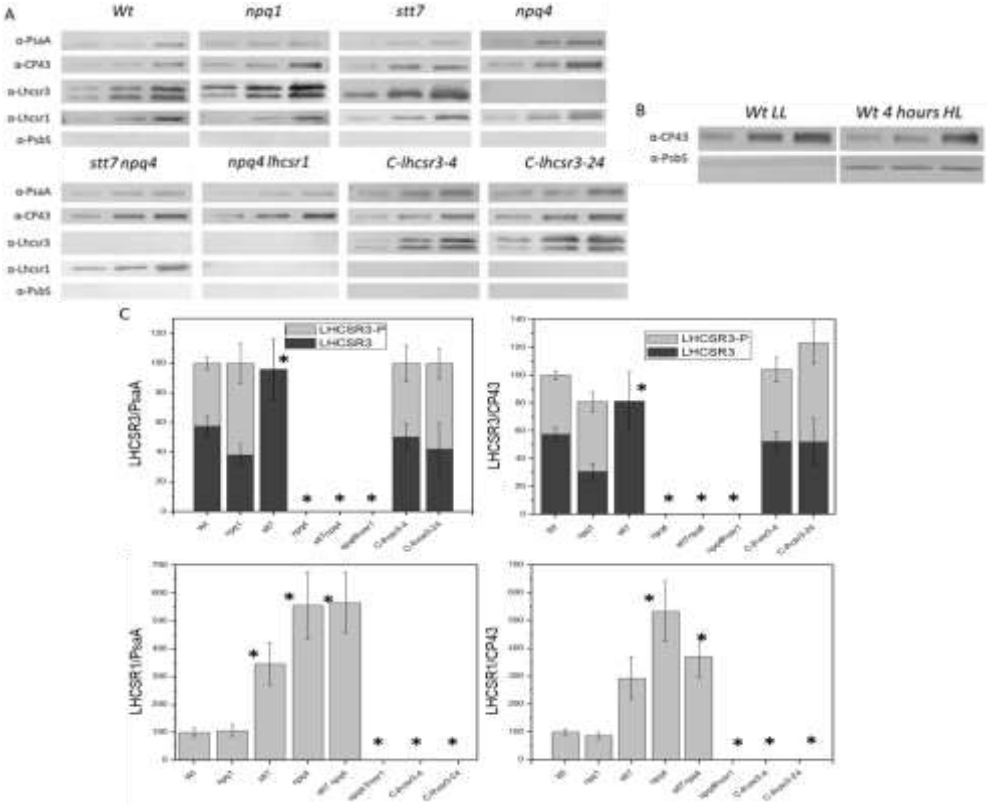

Figure S2. Fluorescence emission spectra of WT and of the mutant psbD, psaB and cbs.

Fluorescence emission spectra measured at 77K were analysed by spectral deconvolution with Gaussian forms to extrapolate the contribution of the different components. Differently from the other experiments reported in this work, the fluorescence emission spectra were measured from low light adapted strain (70 $\mu E\ m^{-2}\ s^{-1}$) grown in TAP medium due to high light sensitivity of the mutant strains herein investigated. In the case of WT, two Gaussians peaking at 684 and 694 nm can be associated to PSII-LHCII complexes, while the Gaussian form peaking at 712 nm can associated to PSI contribution. The last Gaussian function peaking at 735 nm was used for fitting optimization due to the red tail of chlorophyll emission forms. In the case of psbD mutant a strong reduction of the Gaussian peaking at 693 nm was evident, confirming its attribution to PSII supercomplexes. Fluorescence emission of psaB mutant was instead characterized by a strong reduction of the Gaussian peaking at 714 nm, which can be thus attributable to PSI-LHCI complex. The cbs3 mutant was instead characterized by a strong reduction of the 685 nm Gaussian, suggesting that this contribution is mainly related to LHC complexes which are bound to PSII-LHCII complex or free in the membrane.

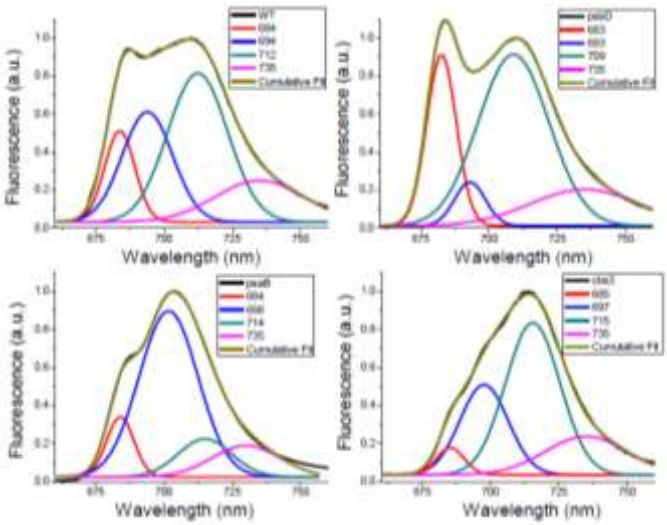

Figure S3. Absorption and emission spectra of Green Fluorescence Protein (GFP).

Panel A: Absorption and emission spectra of GFP in water; emission spectrum was recorded exciting at 475nm. Panel B: emission spectra of GFP before and after high light treatment for 6 minutes at 1500 uE.

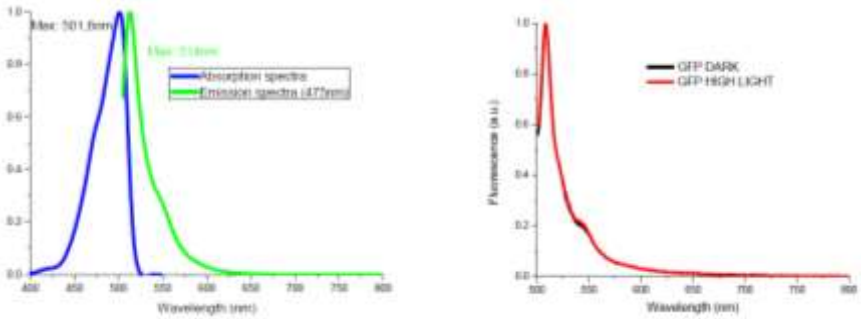

Figure S4. Influence of nigericin on 77K fluorescence emission spectra.

77K fluorescence emission spectra were measured in presence of GFP on dark adapted samples before and after addition of nigericin.

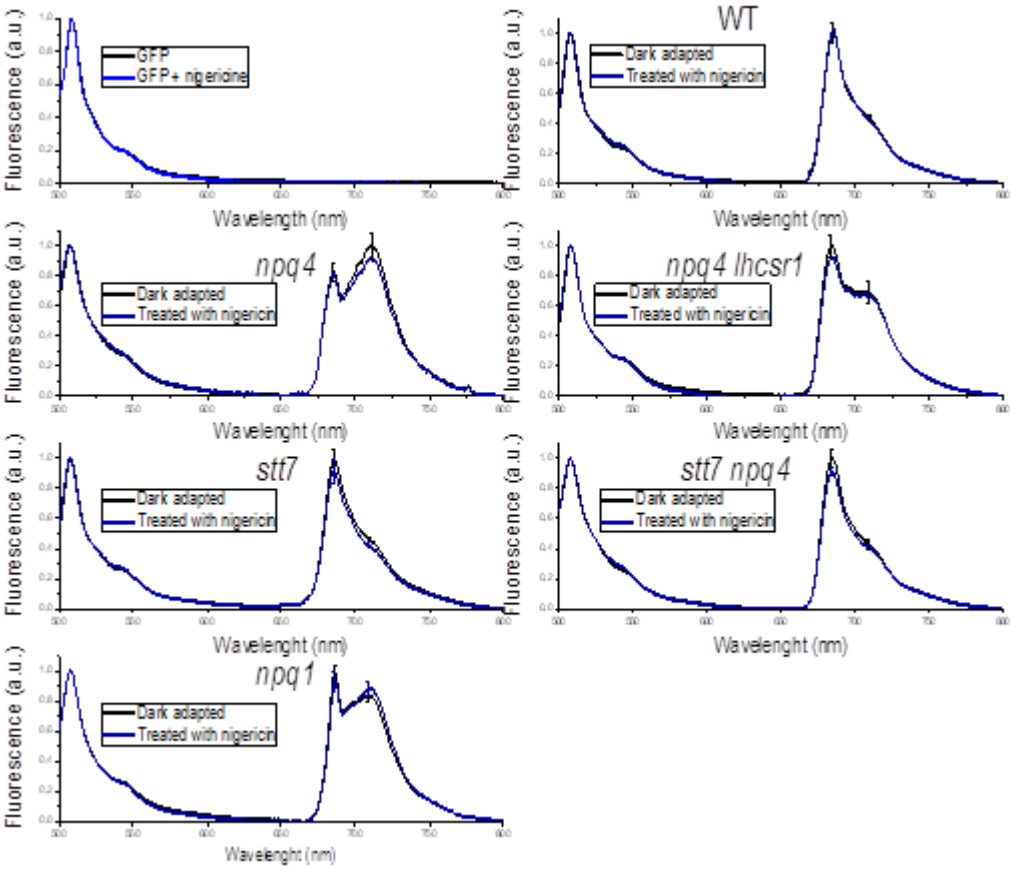

Figure S5. NPQ induction kinetics measured at room temperature and 77K fluorescence emission spectra of C-lhcsr3-4 and C-lhcsr3-24 complemented lines.

Panel A: pulse-amplitude fluorometric time course at room temperature of C-lhcsr3-4 and C-lhcsr3-24 complemented lines compare to WT. Standard deviations are reported as error bars (n=5). Panel B/C: fluorescence emission spectra of C-lhcsr3-4 (B) and C-lhcsr3-24 (C) complemented lines recorded for whole cells dark adapted (black) or high light treated (1500 μE m−2 s−1) for 6' (grey). GFP was added as internal standard for normalization. Standard deviations are reported as error bars (n=4).

A

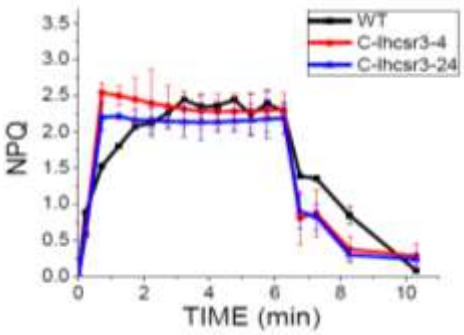

B

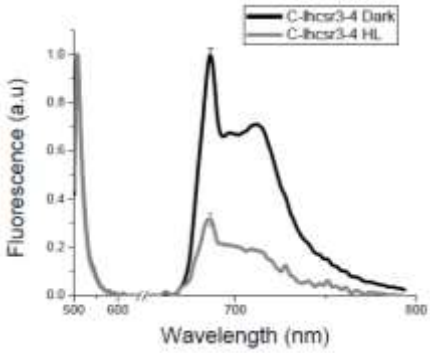

C

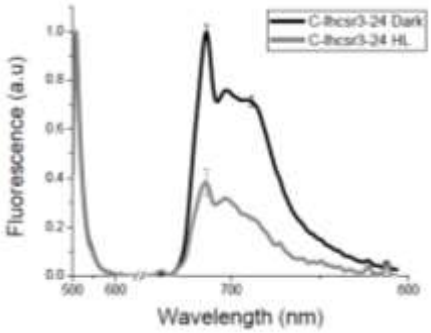

Figure S6. Changes in 77K florescence emission spectra during high light treatment and dark recovery.

77K fluorescence emission spectra of WT, npq4 lhcsr1 and stt7 mutants acquired for dark adapted samples or after different times of illumination (2', 4' and 6') followed by dark recovery in presence of far red light are reported normalized to GFP emission used as internal standard. Standard deviations are reported as error bars (n=4).

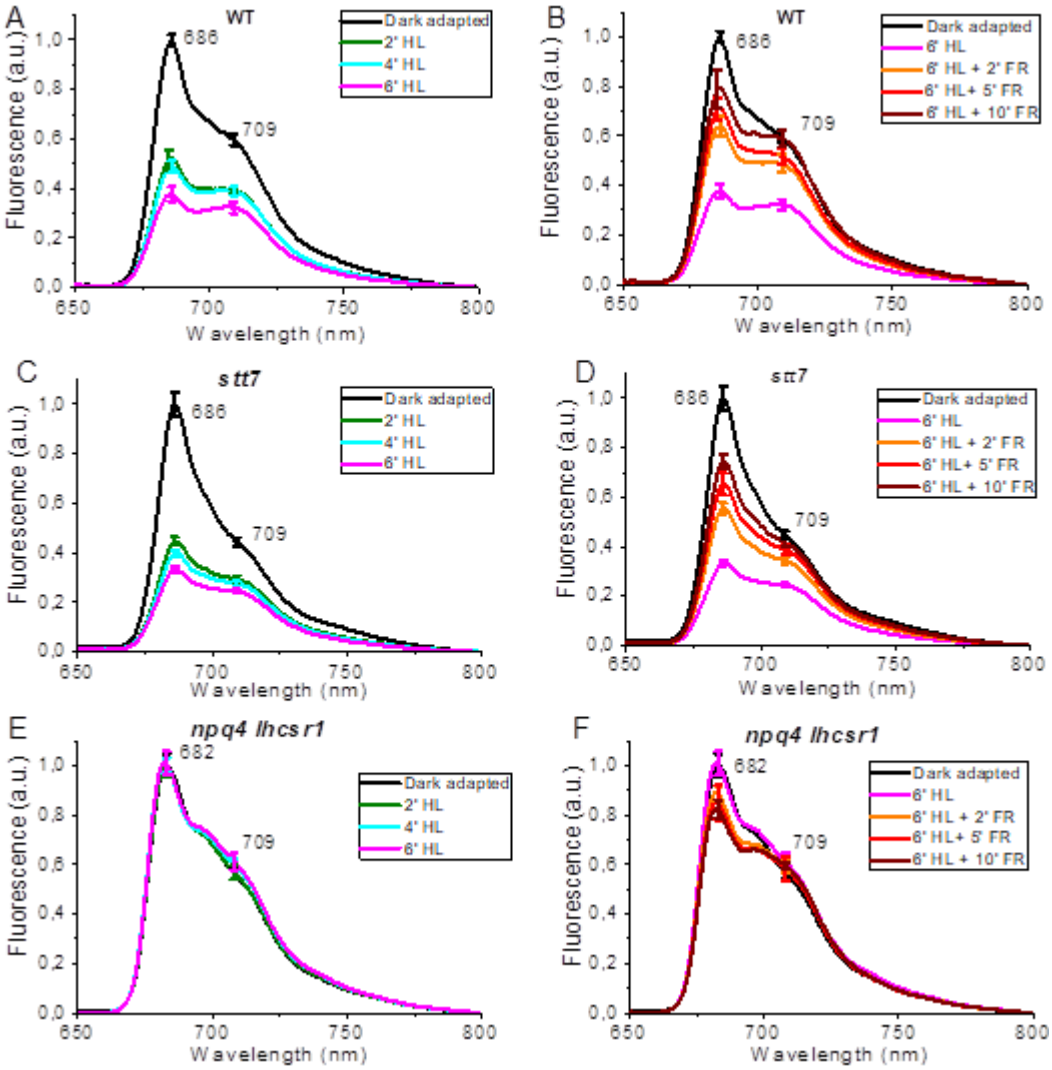

Figure S7. Changes in 77K florescence emission spectra during high light treatment and dark recovery in npq1, npq4 and stt7 npq4 mutants.

77K fluorescence emission spectra of WT, npq1, npq4 and stt7 npq4 mutants acquired for dark adapted samples or after different times of illumination (2', 4' and 6') followed by dark recovery in presence of far red light are reported normalized to GFP emission used as internal standard. Standard deviations are reported as error bars (n=4).

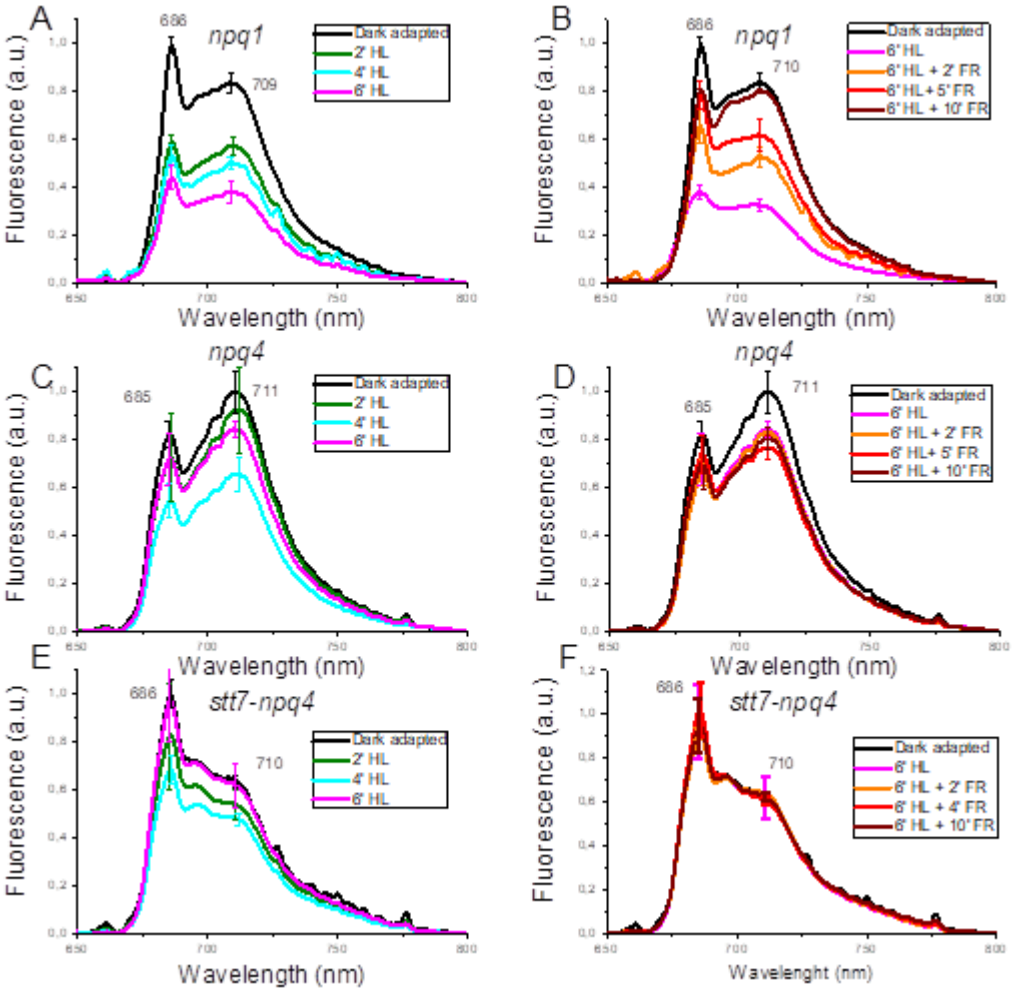

Figure S8. Changes in 77K florescence emission spectra during high light treatment and dark recovery in C-lhcsr3-4 and C-lhcsr3-24 complemented lines.

77K fluorescence emission spectra of C-lhcsr3-4 and C-lhcsr3-24 acquired for dark adapted samples or after different times of illumination (2', 4' and 6') followed by dark recovery in presence of far red light are reported normalized to GFP emission used as internal standard. Standard deviations are reported as error bars (n=4).

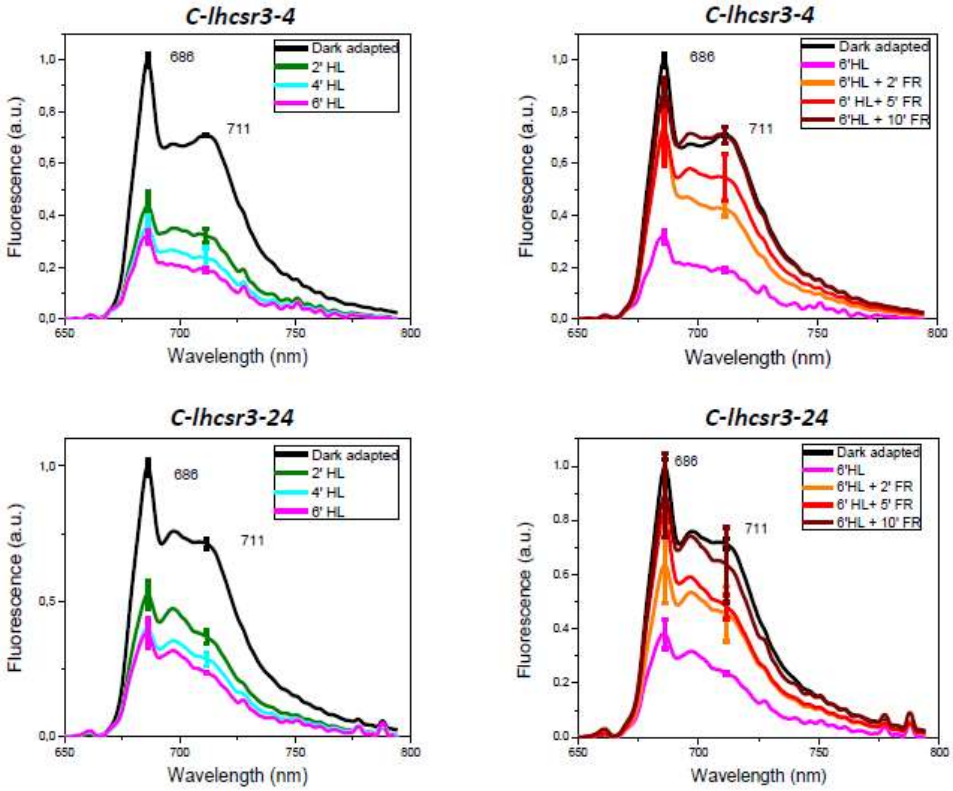

Figure S9. Deconvolution of fluorescence emission spectra from WT recorded at 77K.

a) Dark adapted; b) treated for 2 minutes with high light; c) treated for 4 minutes with high light d) treated for 6 minutes with high light; e) treated for 6 minutes with high light and for 2 minutes with far red light; f) treated for 6 minutes with high light and for 5 minutes with far red light; g) treated for 6 minutes with high light and for 10 minutes with far red light; h) NPQ curve reconstruction using the area of the gaussian curves used for the fitting.

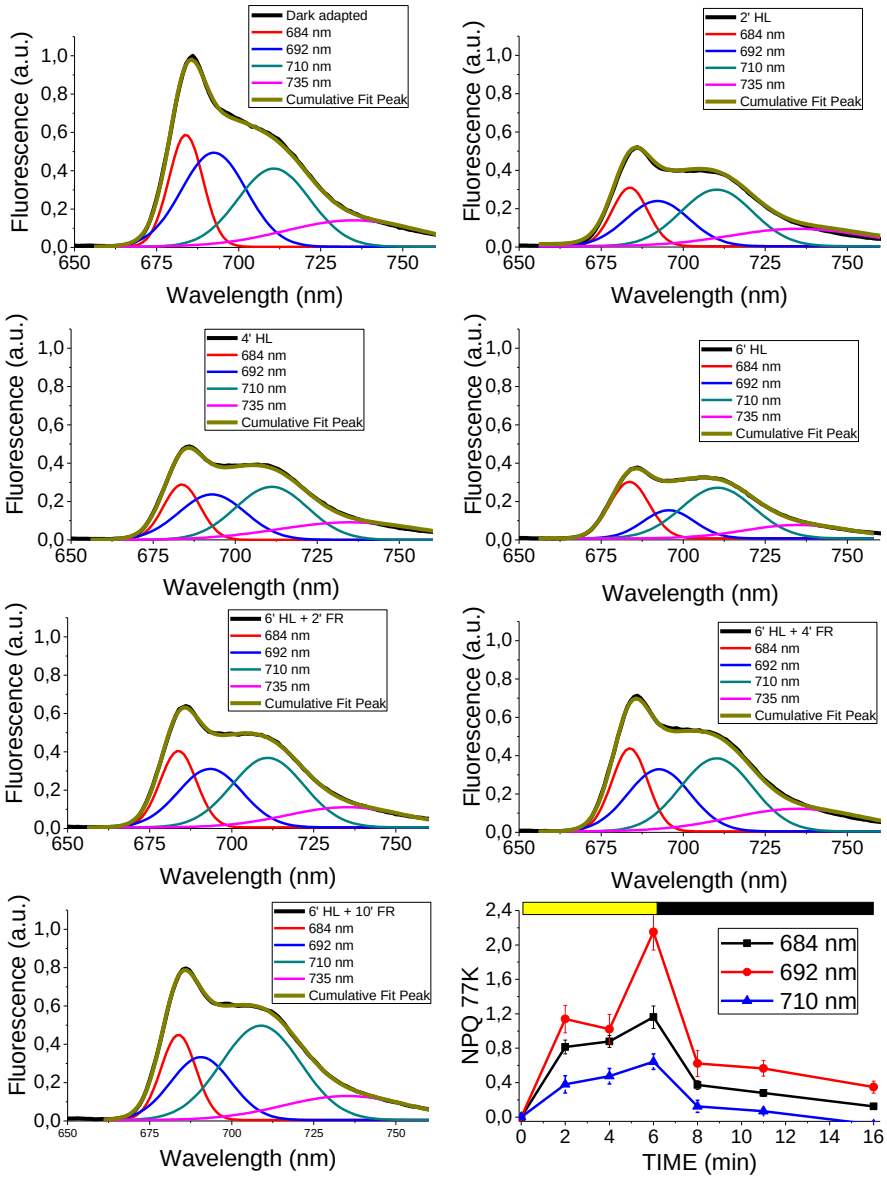

Figure S10. Spectra deconvolution of fluorescence emission spectra of C-lhcsr3-4 complemented line recorded at 77K.

a) Dark adapted; b) treated for 2 minutes with high light; c) treated for 4 minutes with high light; d) treated for 6 minutes with high light; e) treated for 6 minutes with high light and for 2 minutes with far red light; f) treated for 6 minutes with high light and for 5 minutes with far red light; g) treated for 6 minutes with high light and for 10 minutes with far red light; h)NPQ curved reconstruction using the area of the gaussian curves used for the fitting.

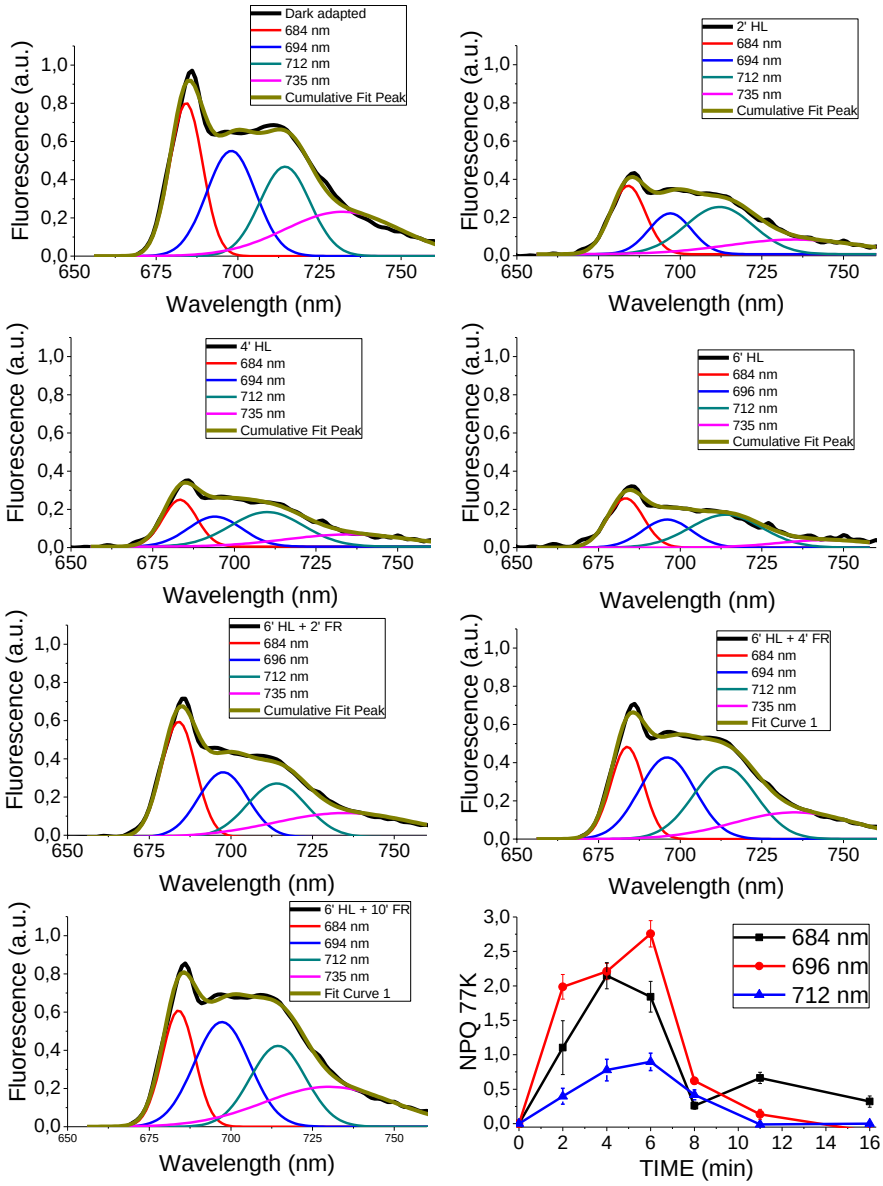

Figure S11. Spectra deconvolution of fluorescence emission spectra of C-lhcsr3-24 complemented line recorded at 77K.

a) Dark adapted; b) treated for 2 minutes with high light; c) treated for 4 minutes with high light; d) treated for 6 minutes with high light; e) treated for 6 minutes with high light and for 2 minutes with far red light; f) treated for 6 minutes with high light and for 5 minutes with far red light; g) treated for 6 minutes with high light and for 10 minutes with far red light; h)NPQ curved reconstruction using the area of the gaussian curves used for the fitting.

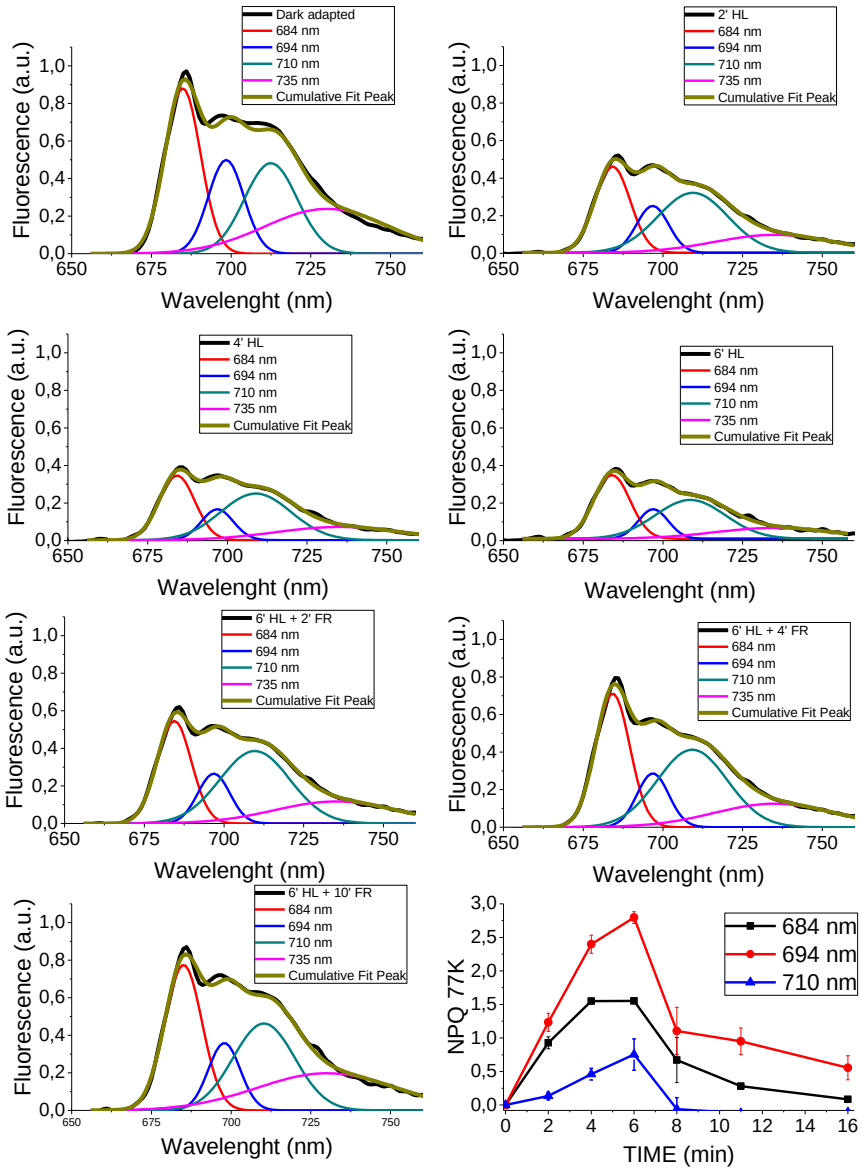

Figure S12. Spectra deconvolution of fluorescence emission spectra of stt7 mutant recorded at 77K.

a) Dark adapted; b) treated for 2 minutes with high light; c) treated for 4 minutes with high light; d) treated for 6 minutes with high light; e) treated for 6 minutes with high light and for 2 minutes with far red light; f) treated for 6 minutes with high light and for 5 minutes with far red light; g) treated for 6 minutes with high light and for 10 minutes with far red light; h) NPQ curved reconstruction using the area of the gaussian curves used for the fitting.

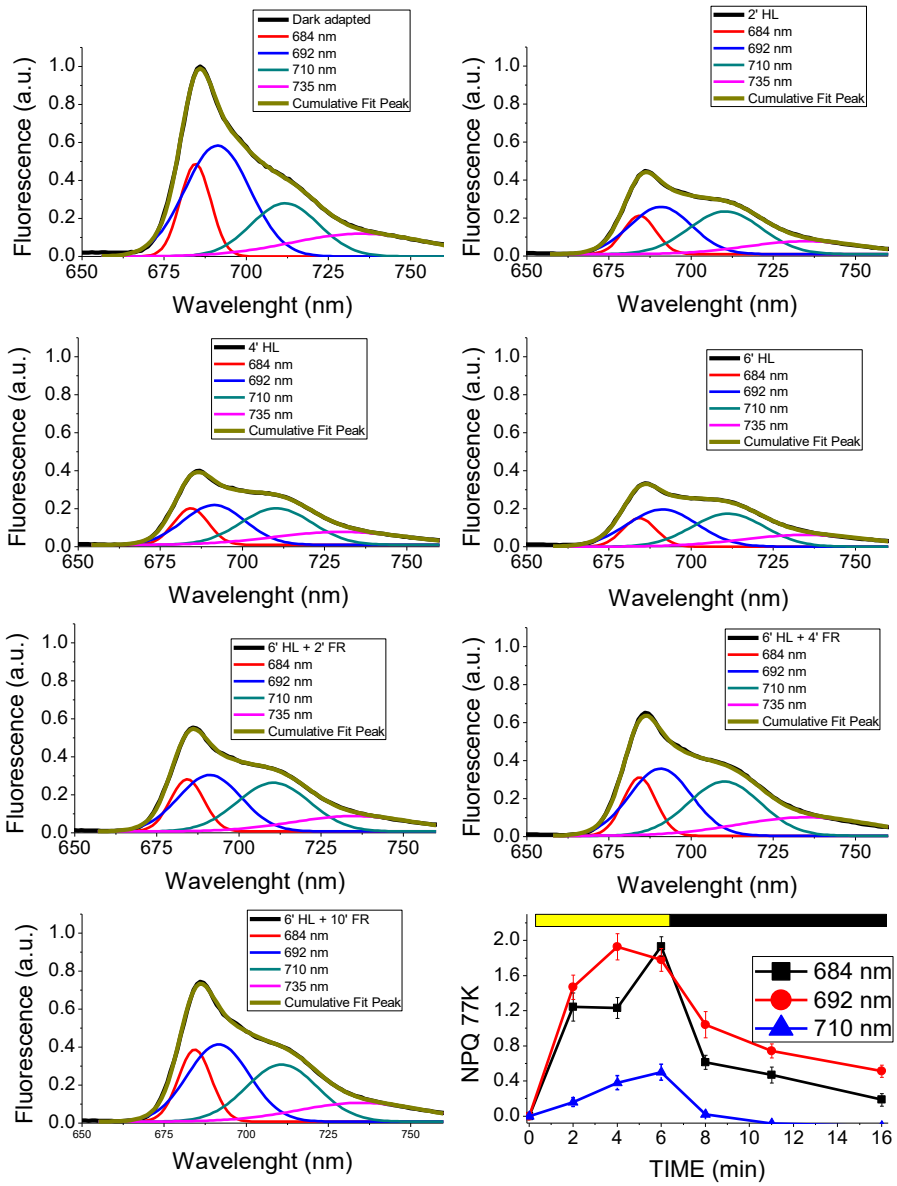

Figure S13. Spectra deconvolution of fluorescence emission spectra of npq1 mutant recorded at 77K.

a) Dark adapted; b) treated for 2 minutes with high light; c) treated for 4 minutes with high light; d) treated for 6 minutes with high light; e) treated for 6 minutes with high light and for 2 minutes with far red light; f) treated for 6 minutes with high light and for 5 minutes with far red light; g) treated for 6 minutes with high light and for 10 minutes with far red light; h)NPQ curved reconstruction using the area of the gaussian curves used for the fitting.

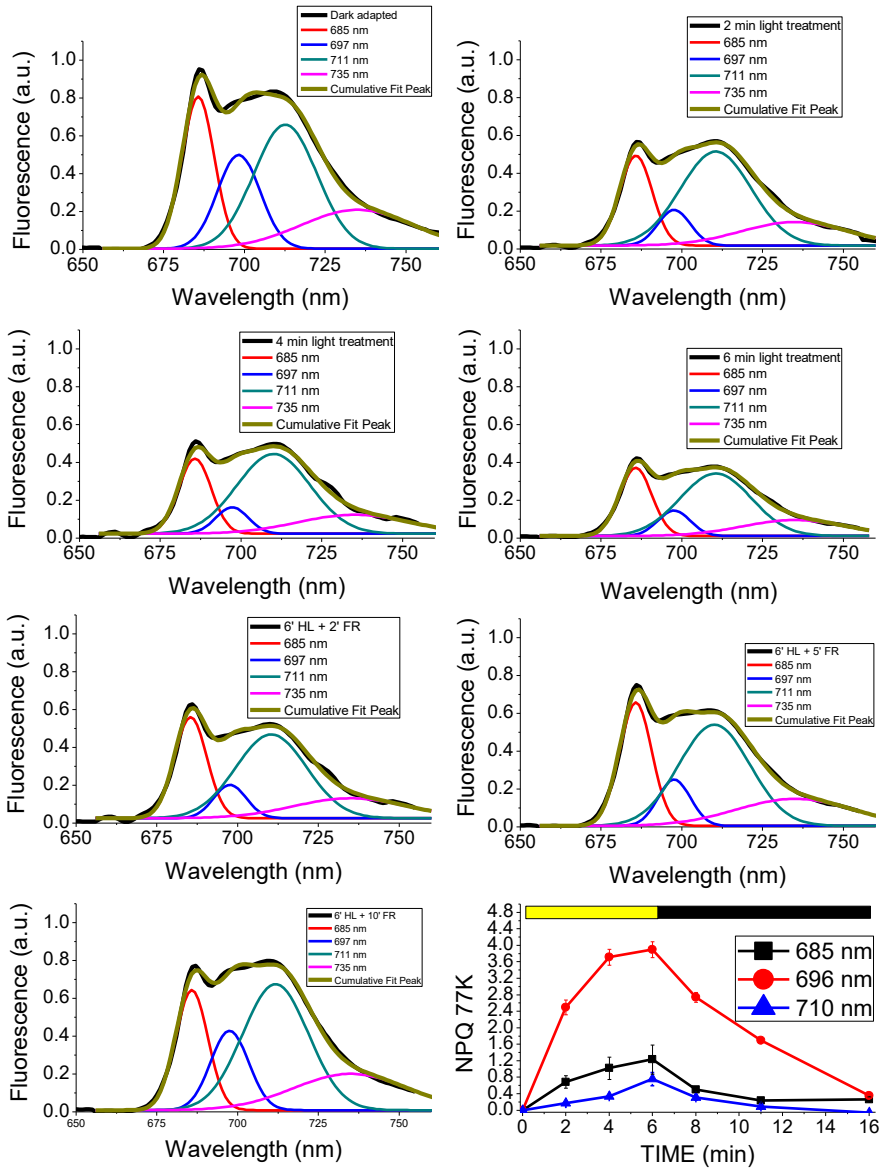

Figure S14. Spectra deconvolution of fluorescence emission spectra of npq4 mutant recorded at 77K

a) Dark adapted; b) treated for 2 minutes with high light; c) treated for 4 minutes with high light; d) treated for 6 minutes with high light; e) treated for 6 minutes with high light and for 2 minutes with far red light; f) treated for 6 minutes with high light and for 5 minutes with far red light; g) treated for 6 minutes with high light and for 10 minutes with far red light; h)NPQ curved reconstruction using the area of the gaussian curves used for the fitting.

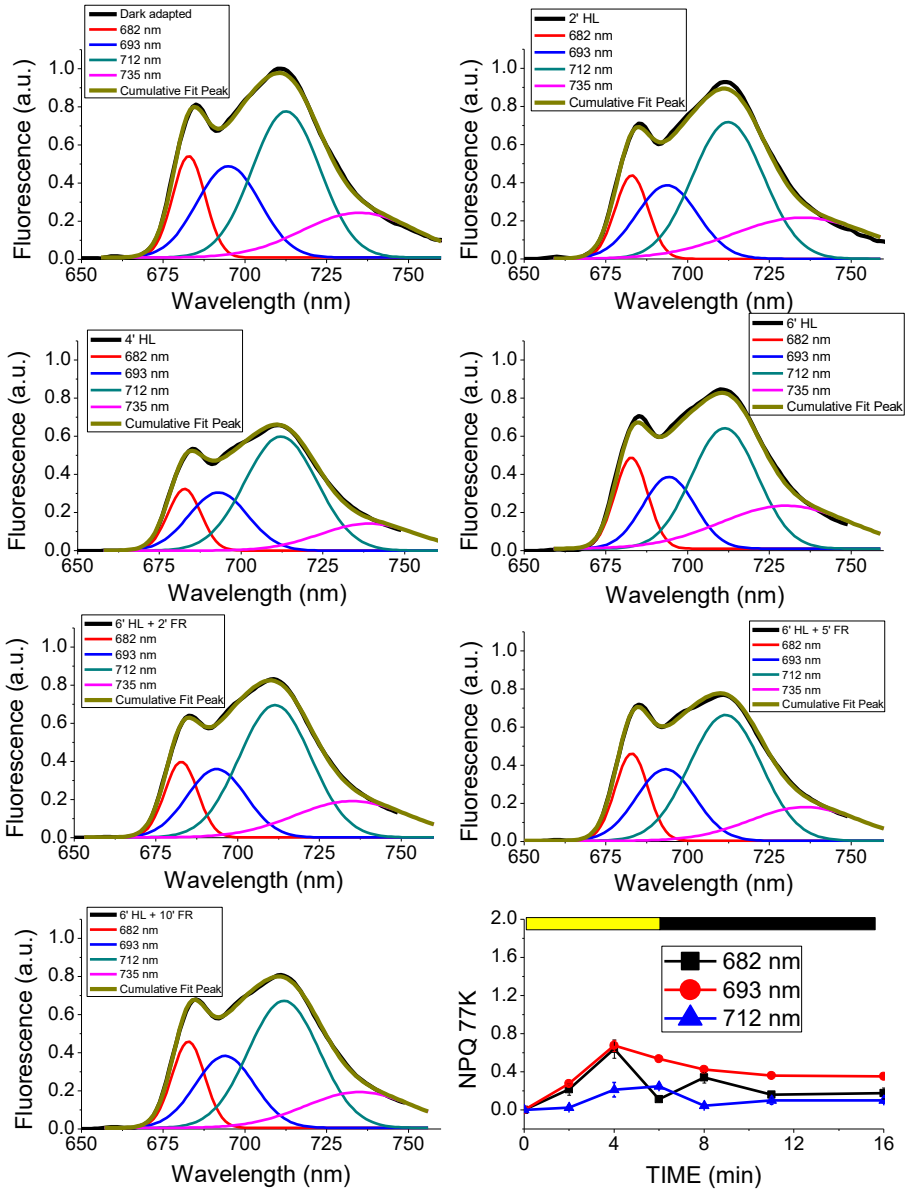

Figure S15. Spectra deconvolution of fluorescence emission spectra of stt7 npq4 mutant recorded at 77K.

a) Dark adapted; b) treated for 2 minutes with high light; c) treated for 4 minutes with high light; d) treated for 6 minutes with high light; e) treated for 6 minutes with high light and for 2 minutes with far red light; f) treated for 6 minutes with high light and for 5 minutes with far red light; g) treated for 6 minutes with high light and for 10 minutes with far red light; h)NPQ curved reconstruction using the area of the gaussian curves used for the fitting.

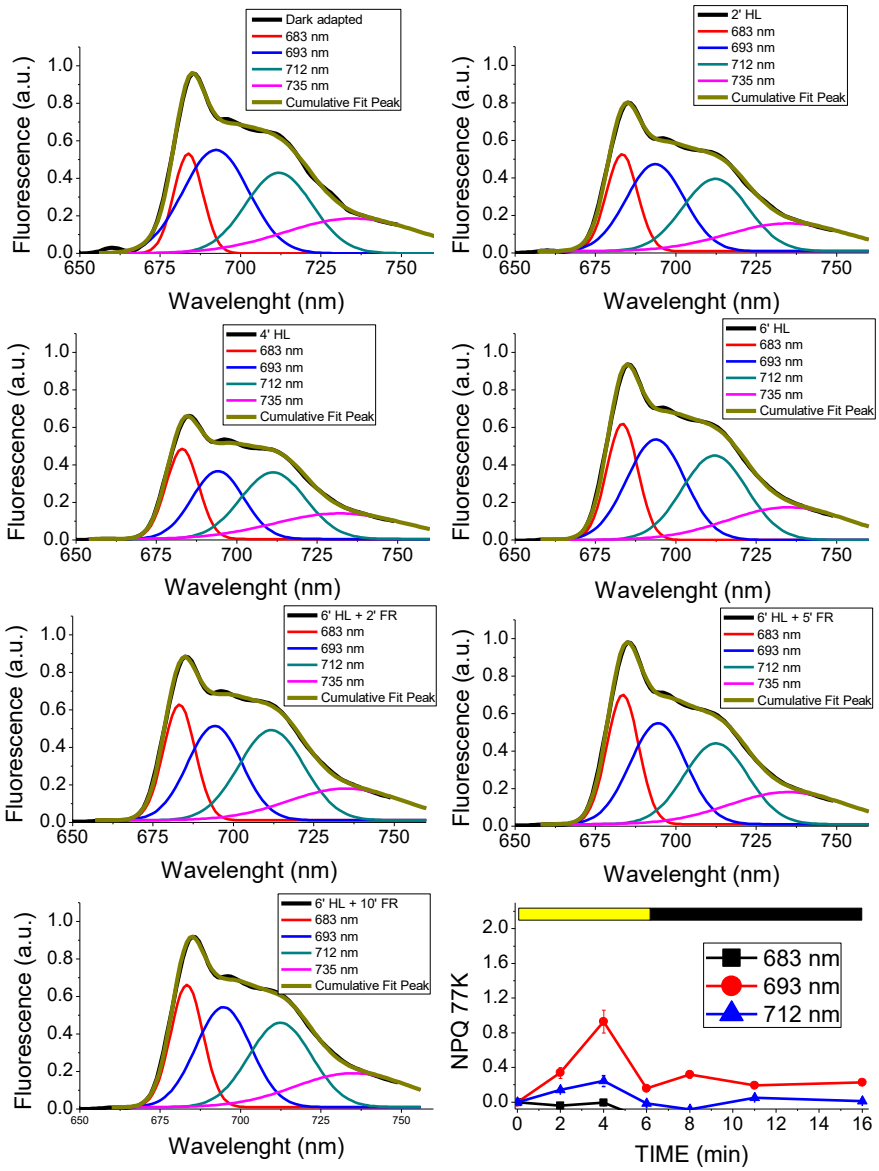

Figure S16. Spectra deconvolution of fluorescence emission spectra of npq4 lhcsr1 mutant recorded at 77K.

a) Dark adapted; b) treated for 2 minutes with high light; c) treated for 4 minutes with high light; d) treated for 6 minutes with high light; e) treated for 6 minutes with high light and for 2 minutes with far red light; f) treated for 6 minutes with high light and for 5 minutes with far red light; g) treated for 6 minutes with high light and for 10 minutes with far red light; h)NPQ curved reconstruction using the area of the gaussian curves used for the fitting

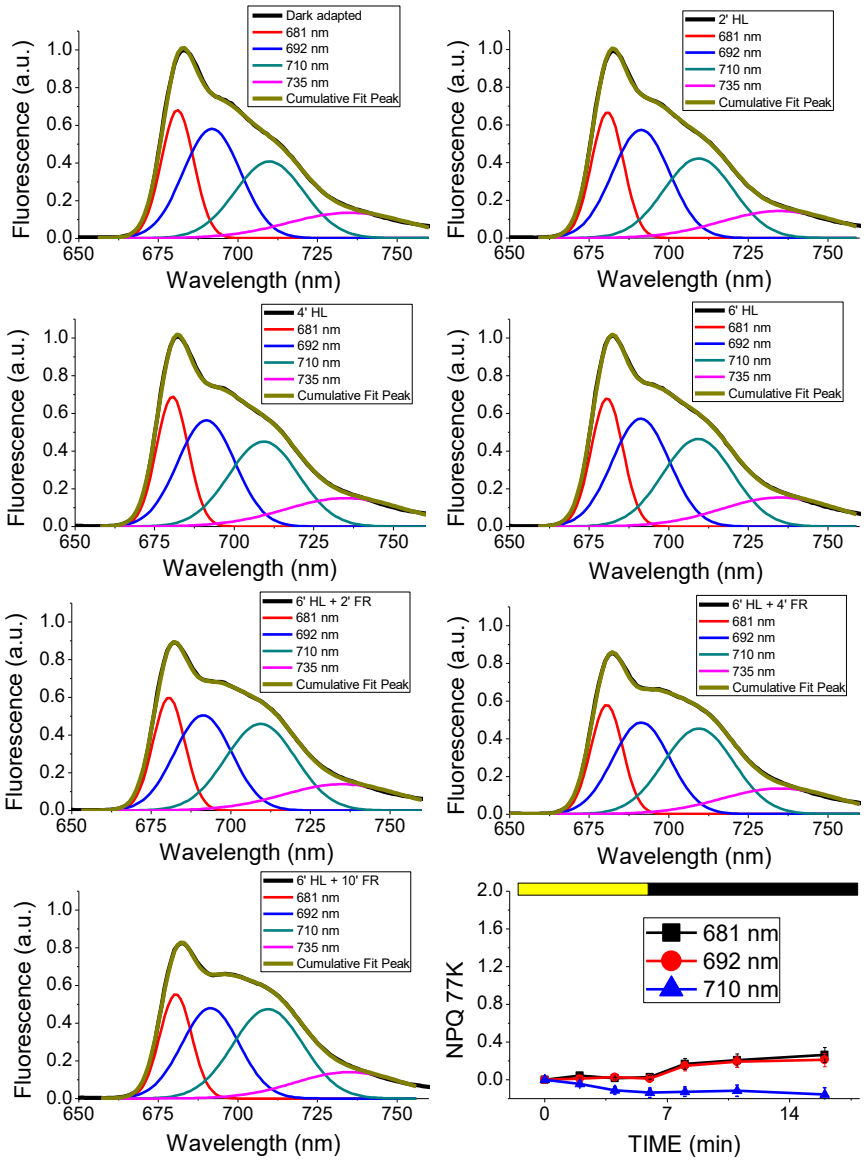

Figure S17. Calculated NPQ induction kinetics at 77K of C-lhcsr3-4 and C-lhcsr3-24 complemented lines.

The NPQ curves were calculated from the area of the sum of the Gaussians used for the fitting according to the formula $(A_{Dark} - A_X)/A_X$ *where* A_X *and* A_{Dark} *are respectively the amplitude at time X* (A_X) *or at time 0* (A_{Dark}, *dark adapted samples) of the different Gaussians attributable to PSII or PSI. Standard deviations are reported as error bars (n=4).*

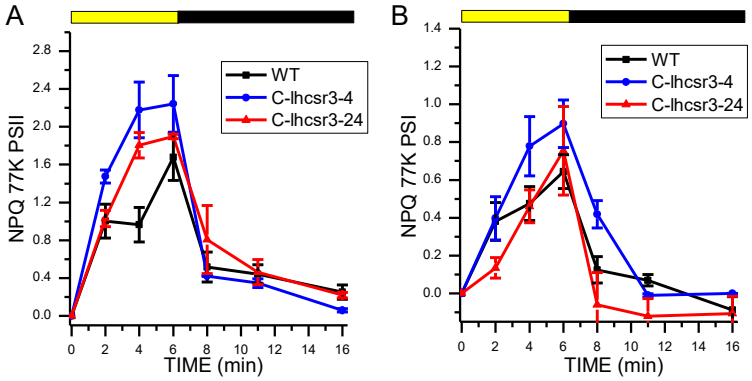

Figure S18. PSI and PSII excitation spectra in dark adapted and high light treated complemented lines C-lhcsr3-4 and C-lhcsr3-24.

77K fluorescence excitation spectra of PSI (fluorescence recorded at 710 nm) and PSII (fluorescence recorded at 685 nm) for dark adapted cells (black) and HL treated (grey) cells and normalized to the Chl a contribution at 436 nm. Standard deviations are reported as error bars (n=4).

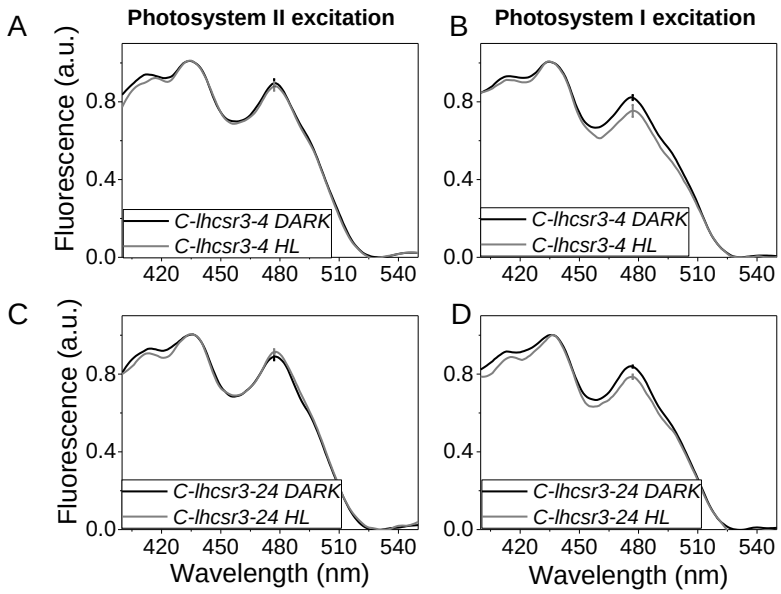

Figure S19. PSI and PSII excitation spectra in dark adapted and high light treated samples.

77K fluorescence excitation spectra of PSI (fluorescence recorded at 710 nm) and PSII (fluorescence recorded at 685 nm) for dark adapted cells (black) and HL treated (grey) cells and normalized to the Chl a contribution at 436 nm. Standard deviations are reported as error bars (n=4). The increased Chl b contribution upon high light treatment in npq4 might suggest a partial degradation of Chl a binding core complexes during high light treatment in this strain or a preferential LHCSR1 quenching on PSII core subunits, even if minor as observed in Fig. 1 and Fig. 5. Other possible explanations of this finding are a possible reorganization of PSII supercomplexes during high light treatment in npq4 with release of Chl b binding antenna proteins with higher fluorescence quantum yield.

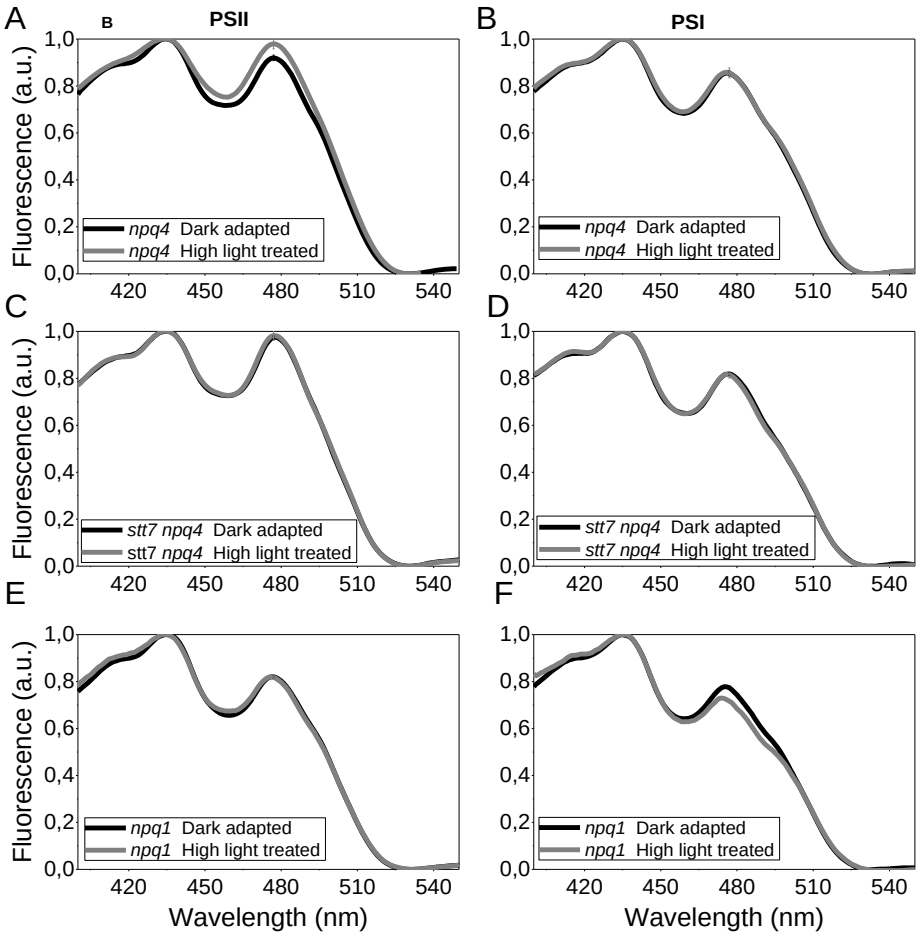

Figure S20. Global analysis of time resolved fluorescence kinetics at 77K of stt7, npq1, npq4, stt7 npq4 and C-lhcsr3 -4 and C-lhcsr3 -24 mutants.

Fluorescence decay kinetics of dark adapted or high light treated strains were acquired at 77K in the 670 – 750 nm range with 5 nm step and globally fitted with 4 exponentials. The decay associated spectra (DAS) obtained are reported normalized to the same total area for each sample, while the associated time constants are indicated the legend. Standard deviation associated to time constants is less than 5% for each component.

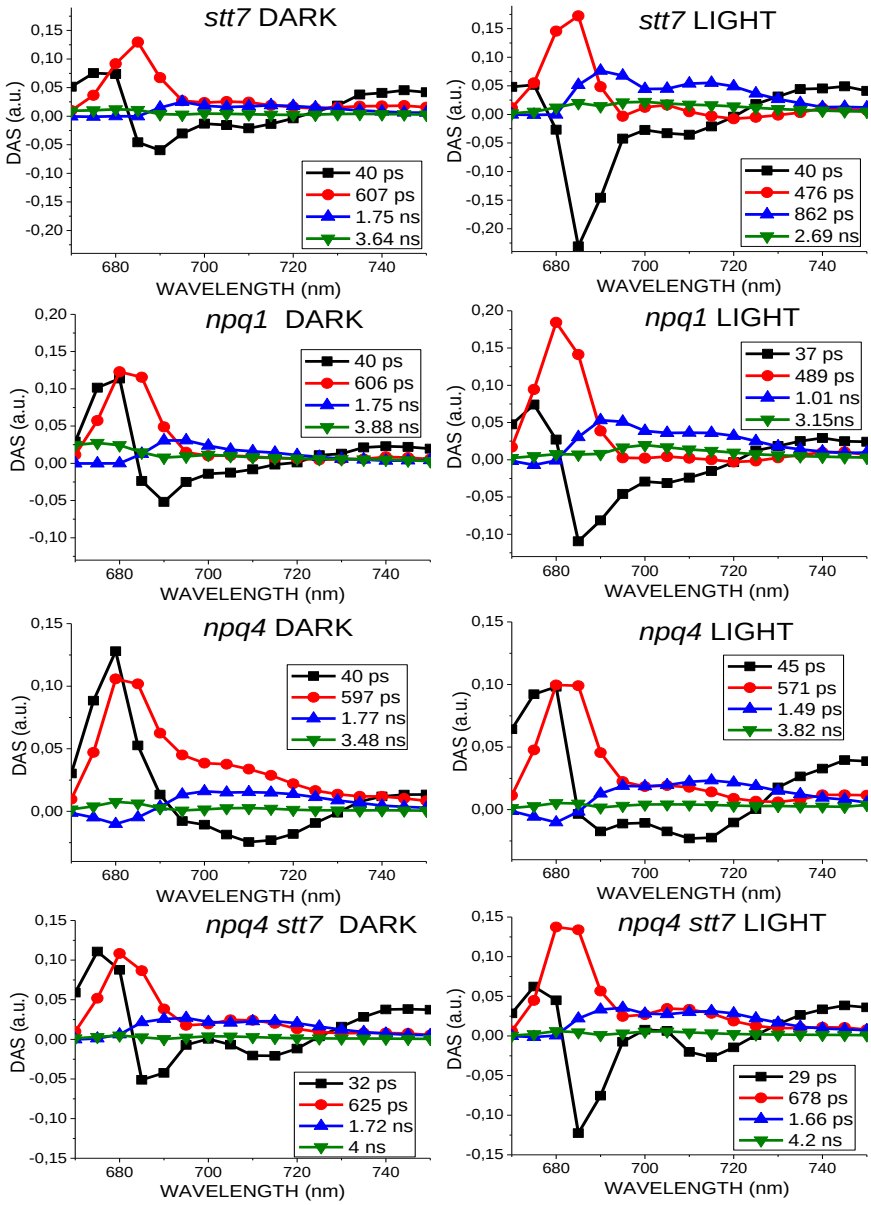

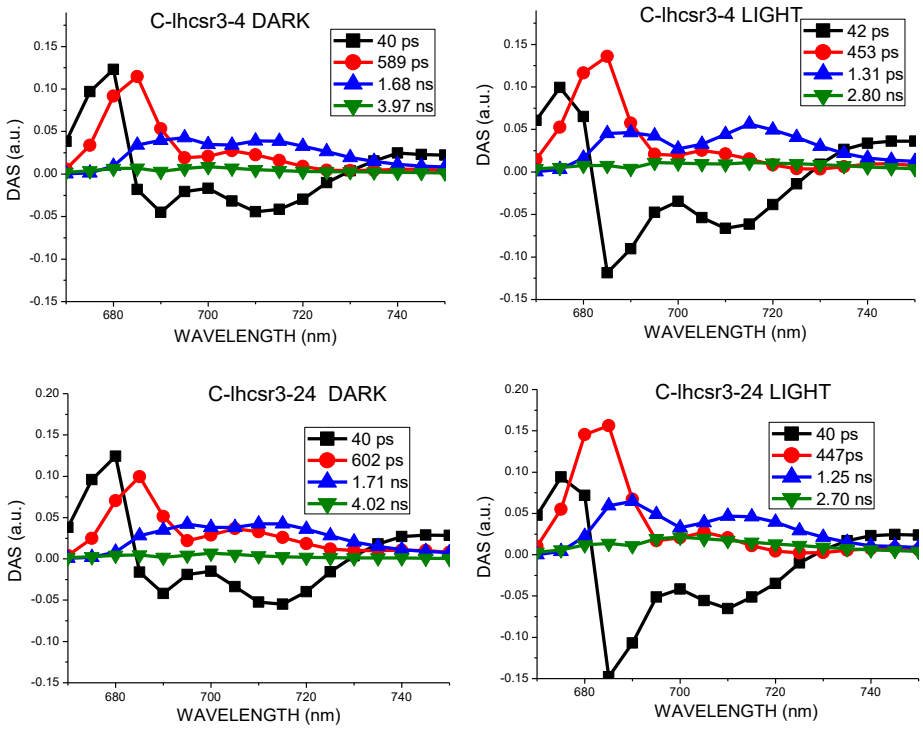
C-lhcsr3-4 DARK
40 ps
589 ps
1.68 ns
3.97 ns
DAS (a.u.)
WAVELENGTH (nm)
C-lhcsr3-4 LIGHT
42 ps
453 ps
1.31 ps
2.80 ns
DAS (a.u.)
WAVELENGTH (nm)
C-lhcsr3-24 DARK
40 ps
602 ps
1.71 ns
4.02 ns
DAS (a.u.)
WAVELENGTH (nm)
C-lhcsr3-24 LIGHT
40 ps
447ps
1.25 ns
2.70 ns
DAS (a.u.)
WAVELENGTH (nm)

Section B

The function of LHCBM4/6/8 antenna proteins in *Chlamydomonas reinhardtii*[2]

In this work we analyzed the function of three antenna proteins (LHCBM4/6/8) which are included in the group of major antenna of Photosystem II in *Chlamydomonas reinhardtii*. LHCBM4 and LHCBM6 gene products were analyzed *in vitro* by synthesizing recombinant apoproteins from individual sequences and refolding them with pigments. Biochemical and spectroscopic analysis on *in vitro* refolded proteins include: pigments analysis, absorption spectra and emission spectra at room and low (77K) temperature. Additionally, we characterized knock down strains *in vivo* for *Lhcbm4/6/8* genes. We show that LHCBM4/6/8 subunits could be found as component of Photosystem II supercomplexes with different size, although the largest pool was free in the membranes and poorly connected to PSII. Impaired accumulation of LHCBM4/6/8 caused a decreased LHCII content per Photosystem II and a reduction in the amplitude of state 1-state 2 transitions at low temperature. In addition, the reduction of LHCBM4/6/8 subunits caused a significant reduction of the Non-Photochemical Quenching activity and at the level of photoprotection.

In this work I've performed all the experiments excluding the mutants strains production and screening.

Abbreviations**:** PSI/II, Photosystem I/II; NPQ, Non-Photochemical Quenching; LHC, Light Harvesting Complex; amiRNA, artificial micro-RNA; DCMU, (3-(3,4-dichlorophenyl)-1,1-dimethylurea); CN, Clear Native; ROS, Reactive Oxygen Species; $^1O_2$, singlet oxygen; DI, de-epoxidation index.

[2]This section is based on the published article: **Girolomoni L**, Ferrante P, Berteotti S, Giuliano G, Bassi R, Ballottari M; The function of LHCBM4/6/8 antenna proteins in *Chlamydomonas reinhardtii*, *Journal of Experimental Botany*, Volume 68, Issue 3, 1 January 2017, Pages 627–641.

Introduction

Life on Earth is fueled by photon energy harvested by photosynthetic systems. In green algae and land plants photosynthesis occurs in chloroplasts, where two pigment binding protein complexes, Photosystem I and II (PSI and PSII) catalyze the light-dependent steps of electron transport from water to $NADP^+$ which is coupled to proton transport to the thylakoid lumen for ATP synthesis. Each photosystem includes two moieties: a core complex binding electron transport cofactors and a peripheral antenna system enhancing cross section and providing photoprotection. The PSII core complex is highly conserved in all photosynthetic organisms and is composed by the chlorophyll binding subunits D1 and D2, the chlorophyll *a*-binding antenna complexes CP43 and CP47, and the cytochrome b559. The outer antenna system of PSII is composed by pigment binding light-harvesting complexes called LHCII (Light Harvesting Complex II), a trimeric complex made by 22-26 kDa polypeptides with three transmembrane and two amphipatic *a*-helices exposed to the lumen (Kühlbrandt *et al.*, 1994; Liu *et al.*, 2004; Standfuss *et al.*, 2005), each binding up to 14 Chls and 4 xanthophylls. These chromophores are bound to multiple specific sites for xanthophylls (L1, L2, N1, and V1) as well as for chlorophylls (Chl601-614) (Croce *et al.*, 1999*a*, *b*; Caffarri *et al.*, 2001, 2004, 2007; Liu *et al.*, 2004; Ballottari *et al.*, 2012). LHC proteins harvest light energy and transfer excitons to the core complexes. LHCs also have a crucial role in photoprotection (Havaux and Tardy, 1997; Elrad *et al.*, 2002; Ballottari *et al.*, 2012; Dall'Osto *et al.*, 2010; Grewe *et al.*, 2014), provided by their carotenoid ligands: lutein, neoxanthin and violaxanthin, which are involved in quenching chlorophyll triplet excited states and ROS scavenging (Dall'Osto *et al.*, 2006, 2007, 2013; Li *et al.*, 2009; Ballottari *et al.*, 2012, 2013). In high light conditions, when absorbed energy exceeds the capacity of downstream metabolic reactions, photoprotection is enhanced by synthesis of zeaxanthin, which replaces violaxanthin (Havaux *et al.*, 2007; Ahn *et al.*, 2008; Dall'Osto *et al.*, 2010). Furthermore, LHC proteins are involved in fast regulative responses to unbalanced excitation of PSI vs PSII in limiting light, namely state 1- state 2 transitions (Allen and Pfannschmidt, 2000; Finazzi *et al.*, 2002; Depege *et al.*, 2003; Ferrante *et al.*, 2012; Galka *et al.*, 2012; Allorent *et al.*, 2013; Benson *et al.*, 2015) and in non-photochemical quenching of excitation energy (NPQ) (Elrad *et al.*, 2002; Ruban *et al.*, 2007; Peers *et al.*, 2009; de Bianchi *et al.*, 2011; Betterle *et al.*, 2015) in excess light.

Optimal use of limiting light is obtained by balancing PSII and PSI antenna sizes by transferring a subset of the LHCII from PSII to PSI whenever plastoquinone is over-reduced. Over-reduction of the plastoquinone pool activates a kinase (STT7) phosphorylating LHCII and favoring its migration to PSI (Allen and Pfannschmidt, 2000; Finazzi *et al.*, 2002; Depege *et al.*, 2003; Ferrante *et al.*, 2012; Galka *et al.*, 2012; Allorent *et al.*, 2013; Drop *et al.*, 2014*a*, *b*; Ünlü *et al.*, 2014; Benson *et al.*, 2015; Nawrocki *et al.*, 2016). In *Chlamydomonas reinhardtii*, trimeric LHCII is encoded by nine genes called *LHCBM1–LHCBM9*, with M referring to "major" antenna complex (Merchant *et al.*, 2007; Ferrante *et al.*, 2012). The *LHCBM4*, *6*, *8* and *9* genes are localized on chromosome 6, *LHCBM2* and *7* on chromosome 12, *LHCBM5* on chromosome 3, whereas the isoforms *LHCBM1* and *LHCBM3* have not yet been mapped (Drop *et al.*, 2014*a*). *LHCBM* gene products have sequence identity of ~70% and cluster into four groups: Type I (LHCBM3, LHCBM4, LHCBM6, LHCBM8, and LHCBM9), Type II (LHCBM5), Type III (LHCBM2 and LHCBM7), and Type IV (LHCBM1) (Drop *et al.*, 2014*a*) with members of the same sub-group showing identity up to 99% (Natali and Croce, 2015). Knowledge of LHCII structure and function is based on the orthologous complexes from higher plants. Common features include amino acid ligands for chlorophylls, the lumen-exposed tyrosine residue, essential for binding neoxanthin, and the N-terminal domain exposed to the chloroplast stroma which mediates interactions such as in trimerization (Hobe *et al.*, 1995; Natali and Croce, 2015). Despite their high similarity, LHCBM components are functionally specialized: reverse genetics applied to LHCBM2/7and LHCBM5 (Takahashi *et al.*, 2006; Ferrante *et al.*, 2012) suggest they are involved in state1-state2 transitions, while LHCBM1 (Elrad *et al.*, 2002) plays an important role in thermal energy dissipation likely as an interactor of LHCSR3, the trigger for NPQ (Peers *et al.*, 2009; Bonente *et al.*, 2011). A special case is LHCBM9, which is preferentially expressed in nutrient starvation or anaerobiosis (Nguyen *et al.*, 2008) to provide protection for PSII (Grewe *et al.*, 2014). Structural analysis suggests LHCBM1, LHCBM2 and LHCBM3 participate to PSII supercomplexes while LHCBM5 belongs to the "extra" LHCII pool more loosely associated to the core complexes (Drop *et al.*, 2014*a*). Here, we have studied the role of the LHCBM4, LHCBM6 and LHCBM8 proteins by using microRNA (amiRNA) silencing to coordinately silence genes sub-families sharing identical regions, while keeping the level of expression of others unaltered (Molnar *et al.*, 2009; Zhao *et al.*,

2009; Ferrante *et al.*, 2012; Grewe *et al.*, 2014). The phenotypic analysis was complemented by studying biochemical and spectroscopic proteins of pigment-protein subunits obtained by refolding *in vitro* the apoproteins expressed in bacteria, to yield a comprehensive explanation of the function of these three LHC subunits in *C. reinhardtii*.

Materials and methods

Strains and culture conditions

Unless indicated differently, *C. reinhardtii* cells were grown at 25°C with fluorescent white light (60 µE m^{-2} s^{-1}) with a 16h light: 8h dark photoperiod in HS medium. The cell wall less *cw15* strain was transformed with the recombinant pChlamyRNA3 vectors (Molnar *et al.*, 2009) containing the amiRNAs for silencing of *LHCBM6* or *LHCBM4*, *LHCBM6* and *LHCBM8*. Nuclear transformation was performed as described (Kindle, 1990). Transformants were selected on TAP agar plates containing paromomycin (10 µg/ml) as previously described (Ferrante *et al.*, 2012). To screen the silenced LHCBM6 and LHCBM4+6+8 transformants based on Chl *a*/*b* ratios, cells were grown in 96-well microtiter plates in 200 µl of TAP at 25 °C until the stationary phase ($2x10^7$cells ml^{-1}) with fluorescent white light (60 µE m^{-2} s^{-1}) with a 16h light: 8h dark photoperiod. Ninety transformants were analyzed for each construct. Chl *a*/*b* ratios were determined on pigment extracts as described in (Ferrante *et al.*, 2012). To perform quantitative real-time PCR, transformants showing increased Chl *a*/*b* ratios were grown in 4 ml of TAP medium in 24-well microtiter plates until the late-log phase with fluorescent white light (60 µE m^{-2} s^{-1}) with a 16h light: 8h dark photoperiod, and cells were harvested for RNA extraction.

Plasmid construction and q*uantitative Real Time RT-PCR*

amiRNAs used to silence *LHCBM* genes were designed using the WMD3 software (Web micro RNA designer Version3, http://wmd3.weigelworld.org/cgi-bin/webapp.cgi?page=Home;project=stdwmd) and verified using the EST database (http://est.kazusa.or.jp/en/plant/chlamy/EST/blast.html). Two amiRNAs were designed for silencing of *LHCBM6* gene, the former (LHCBM6A) annealing in the 3' UTR, the latter (LHCBM6B) annealing in the 5'UTR of the gene. Cloning of the amiRNAs in pChlamyRNA3 vector, total RNA extraction from *Chlamydomonas* transformants and Real Time RT-PCR were performed as previously described (Ferrante *et al.*, 2012). In

particular, cells were harvested for RNA extraction in the light period after 6 hours of light. Oligonucleotides used for RT-PCR are reported in Supplementary Table S1.

Protein purification and in vitro reconstitution.

LHCBM4 and LHCBM6 coding sequence for the mature proteins were cloned in pET28 expression vector and overexpressed in *Escherichia coli*. The signal peptide sequence was identify as described in the literature (Turkina *et al.*, 2006). Inclusion bodies we purified as previously described (Giuffra *et al.*, 1996) and *in vitro* refolding upon addition of pigments were performed previously reported (Giuffra *et al.*, 1996; Grewe *et al.*, 2014).

Pigment analysis

Pigments analysis were performed by HPLC as described in Lagarde *et al.* (2000). Chl *a/b* and Chl/Cars ratios were corrected through fitting analysis of the absorption spectrum (Croce *et al.*, 2002).

Thylakoid preparation from C. reinhardtii cells

Chlamydomonas reinhardtii stacked thylakoids were purified as described in Ferrante *et al.* (2012).

SDS-PAGE electrophoresis and immunoblotting

Denaturing SDS-PAGE was performed in the presence of 6 M Urea with the Tris-Tricine buffer systems (Schagger and von Jagow, 1987). Immunoblotting analysis were performed using α-CP43, α-PsaA and α-LHCBM5 (herein renamed α-LHCII) from Agrisera and using α-LHCSR3 described in Bonente *et al.* (2012) and α-LHCBM6 described in Berger *et al.* (2014) .

Native electrophoresis

Thylakoid membranes were solubilized in the presence of 1.2% α-dodecyl-maltoside and separated by Clear Native (CN)-PAGE as described in Grewe *et al.* (2014) .

PSI and PSII functional antenna size

Relative PSI antenna size was estimated from kinetics of P700 oxidation in limiting orange light (12 μE m^{-2} s^{-1}) in thylakoids treated with DCMU (3-(3,4-dichlorophenyl)-

1,1-dimethylurea), ascorbate and methyl-viologen, as described in Bonente *et al.* (2012). In particular the P700 oxidation kinetics were fitted with exponential functions and the reciprocal of rate constants extrapolated where used to estimate the PSI antenna size (Bonente *et al.*, 2012). PSII antenna size has been estimated in whole cells from F_m saturation kinetics ($1/t_{2/3}$) in the presence of DCMU 10^{-5}M (Cardol *et al.*, 2008).

State Transitions

The amplitude of State1-State2 transition was investigated by two approaches: (i) LHCII detachment from PSII upon State 2 induction was followed by measuring the differences in the maximal fluorescence emitted by PSII in state 1 or state 2 conditions as previously described (Fleischmann *et al.*, 1999; Bonente *et al.*, 2012; Ferrante *et al.*, 2012). The second method (ii) consisted into measuring the 77K fluorescence emission spectra of whole cells in state 1 or state 2 conditions: the extent of state transitions induction was expressed as the ratio between the peaks of PSI in state2/state1, prior to normalization to the peak of PSII in the two different conditions respectively.

NPQ measurements

NPQ measurements were performed on cells acclimated to high light conditions (400 μE m^{-2} s^{-1}) at exponential growth phase. Cells were pre-illuminated for 2 minutes with a weak (3 μE m^{-2} s^{-1}) far-red LED before NPQ analysis with a PAM-101 (Waltz, Effeltrich, Germany); actinic light was 1600 μE m^{-2} s^{-1} and saturating light 4080 μE m^{-2} s^{-1}. The far-red LED was kept on during dark recovery.

Singlet oxygen production

Singlet oxygen production was measured *in vivo* by following the 532 nm fluorescence emission of a singlet oxygen sensor green probe (Flors *et al.*, 2006).

Results

In vitro study of LHCBM4/6/8 proteins

LHCBM4, *LHCBM6*, and *LHCBM8* genes are paralogous, with a high level of identity to each other (Ferrante *et al.*, 2012). The protein sequences of LHCBM4 (XP_001695344.1), LHCBM6 (XP_001695353.1) and LHCBM8 (XP_001695467.1) are characterized by an identity of 97,63%, with only three substitutions in their amino acid

sequence (Figure 1), and one deletion in the case of LHCBM6 localized in the first 26 residues constituting the transit peptide for chloroplast import.

```
                                                                  Trim motif
LHCBM1      MAFALAKSSARAAVSRRSTVKVEARRTVKPASKASTPDSFWYGPERPLFL
LHCBM2      ---------MAAIMKSAVRSSVRPTVSGRSARVVPRAAIEWYGPDRPKFL
LHCBM4      ----MAFALATSRKALQVTCKATGKKTAAKAAAPKSSGVEFYGPNRAKWL
LHCBM6      -----MAFALASRKALQVTCKATGKKTAAKAAAPKSSGVEFYGPNRAKWL
LHCBM8      ----MAFALATSRKALQVTCKATGKKTAAKAAAPKSSGVEFYGPNRAKWL
                        :         ..    :   *      .   :***:*. :*
                                                        A4 A5 A1
LHCBM1      GAFTG-EPPSYLTGEFPGDYGWDTAGLSADPETFKRYRELELIHARWAML
LHCBM2      GPFSEGDTPAYLTGEFPGDYGWDTAGLSADPETFKRYRELELIHARWAML
LHCBM4      GPYSENSTPAYLTGEFPGDYGWDTAGLSADPETFKRYRELELIHARWAML
LHCBM6      GPYSENATPAYLTGEFPGDYGWDTAGLSADPETFKRYRELELIHARWAML
LHCBM8      GPYSENSTPAYLTGEFPGDYGWDTAGLSADPETFKRYRELELIHARWAML
            *.::    .*:*****************************************
                                                   N1
LHCBM1      GALGCIFPELLGSYGVPFGEAVWFKAGAQIFQEGGLDYLGNPNLVHAQSI
LHCBM2      GALGCITPELLAKNGIPFGEAVWFKAGAQIFAEGGLNYLGNENLIHAQSI
LHCBM4      GALGCLTPELLAKNGTKFGEAVWFKAGAQIFSEGGLDYLGNPSLVHAQNI
LHCBM6      GALGCLTPELLAKSGTKFGEAVWFKAGAQIFSEGGLDYLGNPSLVHAQNI
LHCBM8      GALGCLTPELLAKSGTKFGEAVWFKAGAQIFSEGGLDYLGNPSLVHAQNI
            ***** ****.. *  ************** ****:**** .*:***.*
                B6        B5  B5                  Lut motif
LHCBM1      LAILGTQVLLMGAIEGYRVNGGPLGEGLDKLYPGGSFDPLGLADDPDTFA
LHCBM2      IATLAFQVVVMGLAEAYRANGGPLGEGLDPLHPGGAFDPLGLADDPDTFA
LHCBM4      VATLAVQVILMGLIEGYRVNGGPAGEGLDPLYPGESFDPLGLADDPDTFA
LHCBM6      VATLAVQVILMGLIEGYRVNGGPAGEGLDPLYPGESFDPLGLADDPDTFA
LHCBM8      VATLAVQVILMGLIEGYRVNGGPAGEGLDPLYPGESFDPLGLADDPDTFA
            :* *. **::**  *.**.**** ***** *:** :***************
                A1 A2 A4          A3                B3
LHCBM1      ELKVKEIKNGRLAMFSMFGFFVQAIVTGKGPLQNLSDHLANPGTNNAFAY
LHCBM2      ELKVKEIKNGRLAMFSMFGFFVQAIVTGKGPIQNLDDHLANPTAVNAFAY
LHCBM4      ELKVKEIKNGRLAMFSMFGFFVQAIVTGKGPVQNLDDHLANPTVNNAFAF
LHCBM6      ELKVKEIKNGRLAMFSMFGFFVQAIVTGKGPVQNLDDHLANPTVNNAFAF
LHCBM8      ELKVKEIKNGRLAMFSMFGFFVQAIVTGKGPVQNLDDHLANPGVNNAFAF
            ********************************:***.****** . ****:

LHCBM1      ATKFTPQ-
LHCBM2      ATKFTPSA
LHCBM4      ATKFTPSA
LHCBM6      ATKFTPSA
LHCBM8      ATKFTPSA
            ******.
```

Figure 1*. Alignment of LHCBM1, LHCBM2, LHCBM4, LHCBM6 and LHCBM8 polypeptide sequences. Signal peptide is indicated in green, trimerization motif in blue, chlorophyll binding sites in red, lutein binding motif in purple and the tyrosine responsible for neoxanthin binding in the N1 site is indicated in orange.*

Alignment of LHCBM4, LHCBM6, LHCBM8 sequences with LHCBM1 and LHCBM2, suggested all the residues involved in chlorophyll and neoxanthin binding at the N1 site were conserved (Liu *et al.*, 2004; Caffarri *et al.*, 2007). Also, the DPLG motif which was previously associated with lutein binding (Kühlbrandt and Wang, 1991) is conserved in all the subunits herein considered. The trimerization motif WYxxxR was conserved in LHCBM1 and LHCBM2 but not in LHCBM4, 6, 8 due to replacement of W by F. The

LHCBM4 and LHCBM6 apoproteins were produced by expressing the gene sequences in *E. coli* and holocomplexes were obtained by in *vitro* refolding with pigments (Giuffra *et al.*, 1996). The absorption spectra of both holoproteins showed a red shift of the Qy transition compared to free pigments in detergent solution (Figure 2) while the Chl *b* > Chl *a* energy transfer efficiency was high as measured from overlapping fluorescence emission spectra with different excitation, namely 440, 475 and 500 nm for Chl *a*, *b* or carotenoids (Supplementary data, Figure S1), suggesting a correct folding of the protein-pigment complex (Giuffra *et al.*, 1996).

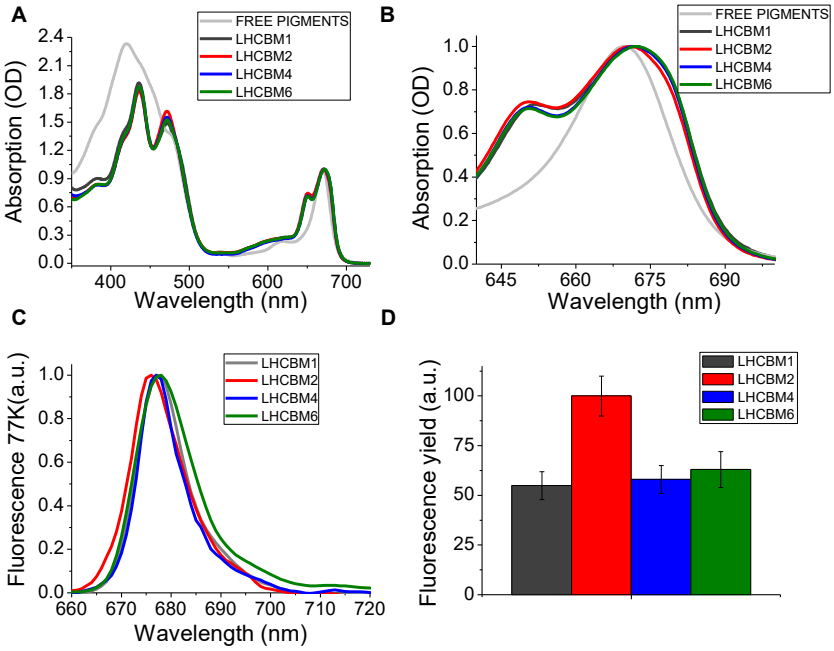

Figure 2 *Absorption spectra and fluorescence yield of LHCBM1, LHCBM2, LHCBM4 and LHCBM6 recombinant proteins. (A) Absorption spectra in the 350-750nm range normalized to the maximum peak in the Qy region. (B) Absorption spectra of LHCBM complexes zoomed in the 630-700 nm range. (C) 77K fluorescence emission spectra of LHCBM complexes upon excitation at 440 nm. (D) Relative fluorescence quantum yield of LHCBM1, LHCBM4 and LHCBM6 compared to LHCBM2, set to 100%. Standard deviations are reported for each sample (n=5).*

The fluorescence emission spectra at 77K of the LHCBM proteins revealed significant differences: LHCBM2 emission was blue-shifted, with emission peak at 677 nm, while LHCBM1 and LHCBM4 showed an intermediate behavior and LHCBM6 showed the red- most shifted subunit with a peak at 679 nm. “Red” emission forms are associated to chlorophyll ligands with low energy transitions. We thus proceeded to assess the relative

fluorescence quantum yield of the reconstituted LHCBM4 and LHCBM6 pigment-proteins. We used as a reference LHCBM1 and LHCBM2 subunits previously characterized as the gene products with, respectively, the lowest and the highest fluorescence quantum yield (Figure 2) (Grewe *et al.*, 2014; Natali and Croce, 2015). LHCBM4 and LHCBM6 showed an intermediate fluorescence yield, more similar to LHCBM1 than to LHCBM2. This result suggests a similar role for LHCBM4, LHCBM6 and LHCBM1 in defining the excited states lifetime of the antenna system. Pigment analysis of reconstituted proteins showed a Chl *a/b* molar ratio ranging between 1.1 and 1.4, while the number of xanthophylls ranged from 3 to 4 based on 14 chlorophylls bound by each subunit (Liu *et al.*, 2004; Grewe *et al.*, 2014; Natali and Croce, 2015). The number of lutein ligands varied from 1.21 to 1.81, violaxanthin was sub-stoichiometric (0.06 to 0.28) and neoxanthin ranged between 1.5 to 2.19. On this basis it can be inferred that all LHCBM proteins analyzed bind lutein in the L1 site, as previously reported for LHCII (Liu *et al.*, 2004), while the L2 site can be occupied by lutein, violaxanthin or neoxanthin, as previously reported for monomeric Lhcb subunits from higher plants (Ballottari *et al.*, 2009; Pan *et al.*, 2011). Neoxanthin is likely bound to the N1 site while the most peripheral site, V1, can be partially occupied by violaxanthin or by neoxanthin according to previous suggestions (Caffarri *et al.*, 2007; Natali and Croce, 2015). The high sequence similarity between LHCBM8 and LHCBM4 (Figure 1), suggests that conclusions drawn for LHCBM4 and LHCBM6 might hold true also for LHCBM8.

LHCBM4/6/8 accumulation in thylakoid membranes

Accumulation of LHCBM4/6/8 in thylakoid membranes in *C. reinhardtii* was investigated by immunoblotting using recombinant proteins refolded *in vitro* as standards. Immunoblot analysis was performed on thylakoid membranes purified from *C. reinhardtii* wild-type strain using an antibody recognizing all LHCBM proteins (α-LHCII) and a specific antibody for LHCBM4/6/8 subunits (Berger *et al.*, 2014). α-LHCBM4/6/8 antibody was tested for cross-reactivity with other LHCBM proteins, revealing only a minor cross reaction against LHCBM3 and LHCBM9, with signals respectively 16-, 40- and 18-fold weaker compared to LHCBM4 and LHCBM6 (Supplementary data, Figure S2). Immunoblotting reactions on thylakoid membranes using the α-LHCII antibody yielded three main bands with apparent molecular weights

of ~26, ~23 and ~22 KDa (Ferrante *et al.*, 2012) (Supplementary data, Figure S3). LHCBM1 was reported to be the only gene product in the band with intermediate mobility, LHCBM2 and LHCBM7 were reported to migrate with the most mobile band (Ferrante *et al.*, 2012), while LHCBM9 migrated with the upper band (Grewe *et al.*, 2014). Using the α-LHCBM6 antibody yielded a single band, with mobility corresponding to the LHCBM band with the highest apparent molecular weight. Recombinant LHCBM4 and LHCBM6 were recognized by α-LHCBM6 antibody with a slightly higher apparent molecular weight compared to the native LHCBM4/6/8 subunits in thylakoid membranes. The same behavior was observed in the case of recombinant LHCBM1 compared to the native LHCBM1: this is likely related to the presence of extra amino acids at the N-terminus in the recombinant proteins, part of the chloroplast transit peptide which are cleaved in the mature native proteins. By using recombinant LHCBM proteins and native LHCII trimers as standards it was possible to determine that LHCBM4/6/8 are present in the thylakoid membranes to a similar abundance as LHCBM1 contributing to a ~30% of the total pool of LHCII (Supplementary data, Figure S3).

Silencing of LHCBM genes

Chlamydomonas strains with reduced level of LHCBM4, LHCBM6 and LHCBM8 subunits were produced by artificial miRNA (amiRNA) silencing according to previous reports (Molnar *et al.*, 2009; Ferrante *et al.*, 2012; Grewe *et al.*, 2014). Two amiRNAs were designed to silence the *LHCBM6* gene (Supplementary data, Table S2 and Figure S4), while four different amiRNAs were selected for the simultaneous silencing of *LHCBM4*, *LHCBM6* and *LHCBM8*, but only one (Supplementary data, Table S2 and Figure S4) was effective in triggering silencing of this subgroup of genes (Supplementary data, Figure S4). The designed amiRNAs were expressed under the control of the *PSAD* constitutive promoter in the *cw15* strain (referred as the wild type in the following) and 90 transformants for each construct were screened based on their absorption spectra for Chl *a/b* ratios and confirmed by HPLC: since Chl *b* is bound to LHC proteins only while Chl *a* is bound to both LHC and core complexes, an increased Chl *a/b* ratio is a good indicator for reduced LHC protein content. A selection of transformants (about ten per construct) showing an increased Chl *a/b* ratio were investigated by Real-Time PCR, in order to confirm the silencing of the target genes.

From this analysis we selected the transformants showing the highest level of silencing: clones L6_A and L6_B (Supplementary data, Table S2 and Figure S5). As shown in Figure 3, the L6_A and L6_B transformants showed a ~40% decrease in *LHCBM6* mRNA level and a concomitant decrease of the *LHCBM4* mRNA level, while the *LHCBM8* gene in these strains was overexpressed as compared with wild type.

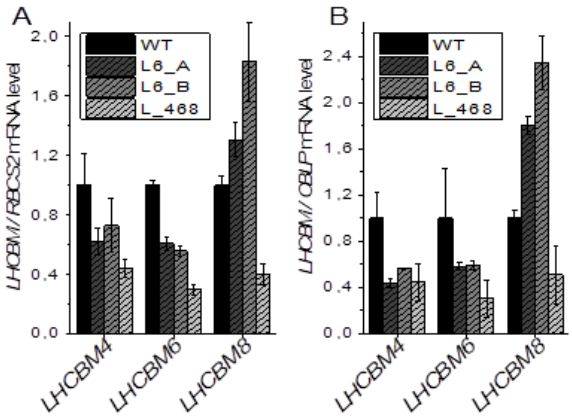

Figure 3: *Quantification of LHCBM mRNA levels in knock-down strains. LHCBM4, 6, 8 mRNA abundance was quantified through quantitative Real Time RT-PCR. The amounts of LHCBM mRNA are expressed using as reference the Ribulose Bisphosphate Carboxylase/Oxygenase Small Subunit 2 (RBCS2) mRNA level. Two different transformants silenced in the LHCBM6 gene (L6_A and L6_B) and one transformant silenced in LHCBM4, LHCBM6 and LHCBM8 genes were analyzed (L_468).*

The increased expression of LHCBM8 gene when LHCBM4 and LHCBM6 are down regulated suggests that the functions of these three subunits are redundant and that LHCBM8 accumulates likely in order to compensate for the reduction in LHCBM4 and LHCBM6. The L_468 transformant shows instead a decrease of ~65%, ~70% and ~50-60% respectively in the level of *LHCBM4, LHCBM6* and *LHCBM8* mRNAs. In order to evaluate the levels of off-target silencing, the expression level of all *LHCBM* genes was evaluated (Supplementary data, Figure S4). Some off-target silencing was found for *LHCBM3* in the L6_A transformant and for *LHCBM7* and LHCBM5 in L6_B transformant while the L_468, did not show statistically significant off-target silencing. The off-target effects were different in the different strains and were disregarded in case of consistent phenotype among the analyzed strains (Supplementary data, Figure S5). Interestingly, in the strain with a lower expression of LHCBM4, LHCBM6 and LHCBM8 genes, L_468 strain, an increased LHCBM1 and LHCBM9 expression was detected (Supplementary Figure S5).

Photosynthetic protein abundance in knock-down strains

Knock-down strains were analyzed by western blotting in order to evaluate the accumulation of LHCBM protein(s) compared to wild type. All knock-down mutants showed a decrease in LHCBM6/4/8 content per chlorophyll as compared to the wild type, especially in the case of L_468 strain. As reported in Figure 4B the accumulation of the different bands recognized by the α-LHCII antibody were similar in all cases, with the exception of L_468 where an increased accumulation of LHCBM1 was accompanied by a reduction of the signal at the higher apparent molecular weight, consistent with the strong reduction LHCBM4/6/8 subunits revealed by the α-LHCBM6 antibody (Figure 4).

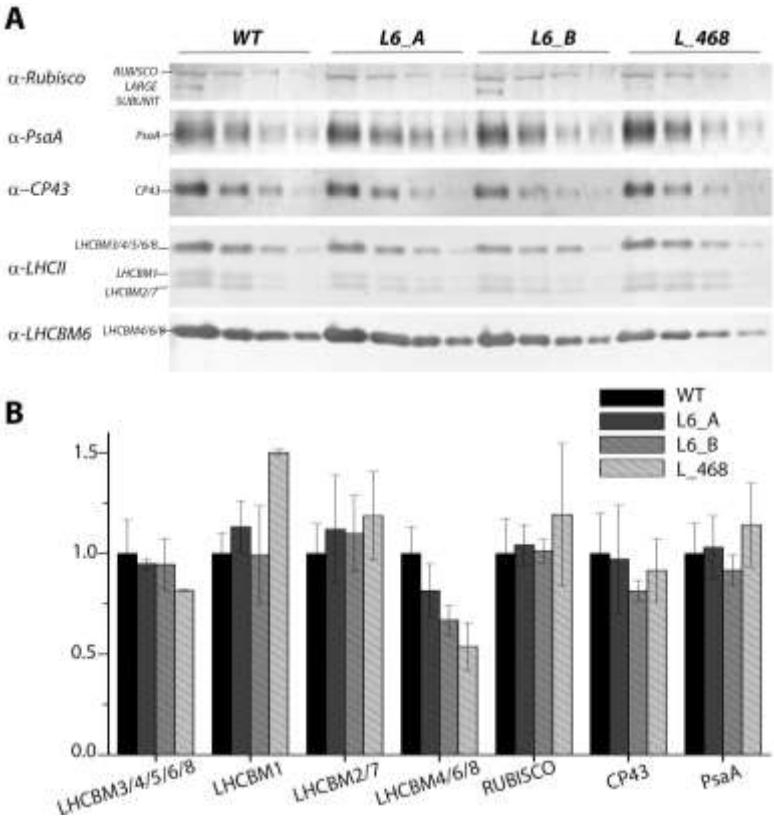

Figure 4. *Immunoblot analysis of photosynthetic proteins in knock-down strains. Immunoblot analysis was performed using specific antibody for PSI (α-PsaA), PSII (α -CP43), LHCs (α-LHCII) and LHCBM6 (α-LHCBM6). Three different sample amounts were loaded based on chlorophyll content (0.9, 0.3 and 0.015 µg of chlorophyll). Densitometric quantification of each band normalized to the wild type is reported in (B). Standard deviations are reported for each quantification (n=4).*

Partial compensation of LHCBM4/6/8 reduction by accumulation of LHCBM1 is consistent with the transcript analysis reported in Figure 3. Knock-down strains were characterized by a similar accumulation of CP43 and PsaA per chlorophyll compared to wild type. The amount of Rubisco was also investigated, as an indicator for the accumulation of Calvin-Benson cycle enzymes in the transformants compared to wild type, yielding a similar Rubisco/Chl ratio in wild type and knockdown strains. The organization of photosynthetic pigment-proteins was evaluated by 2D electrophoresis of solubilized thylakoid membranes on non-denaturing CN-PAGE as first dimension while the second dimension was run on SDS-PAGE (Grewe *et al.*, 2014) (Figure 5).

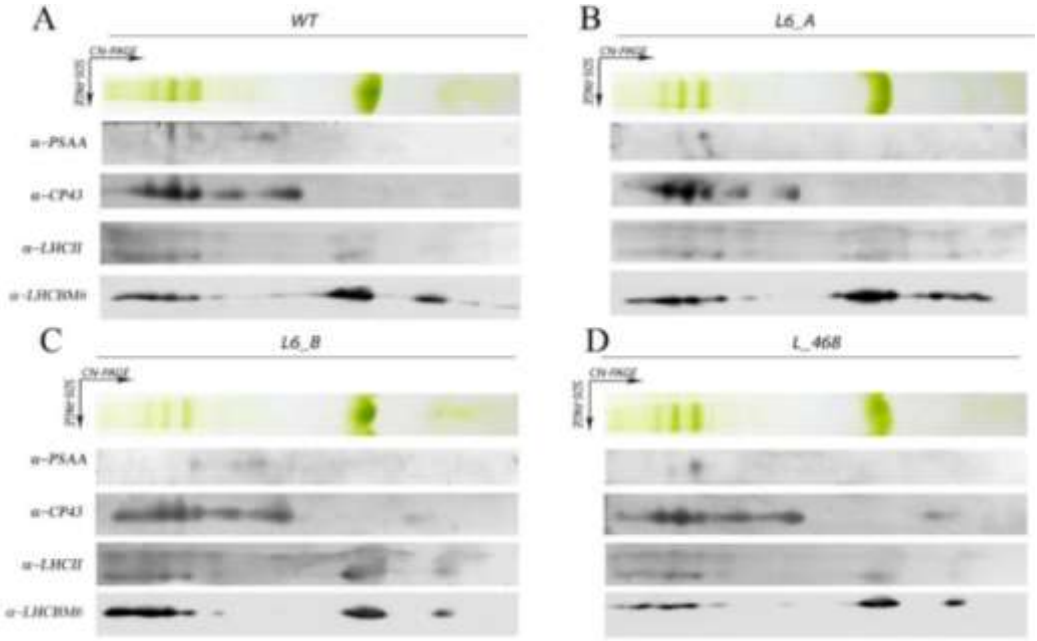

Figure 5. *Analysis of the thylakoid membrane pigment-protein complexes by 2D electrophoresis and immunoblotting. Thylakoid membranes of knock-down strains grown in control light, were solubilized with 1% dodecyl-maltoside (α-DM) and separated by CN-PAGE followed by a second-dimension separation by SDS-PAGE. Immunoblot detection of LHCBM4/6/8, LHCII, PSI (antibody α-PSAA) and PSII (antibody α-CP43) is also reported.*

Distinct subunits of the protein complexes were detected after 2D electrophoresis by immunoblotting with specific antibodies against PsaA (subunit of PSI), CP43 (subunit of PSII), LHCII and LHCBM4/6/8 (Figure 5). The chlorophyll distribution in the CN-PAGE and the levels of immunoblot signals were quantified by densitometry and reported in Supplementary data, Figure S6, for the wild type. PSII and PSI complexes

were resolved at high apparent molecular weight in CN-PAGE as PSI(I)-core, or as supercomplexes binding different amounts of LHC subunits. LHCII subunits could be found as monomers, trimers or in supercomplexes, together with PSI or PSII subunits (Figure 5 and Supplementary data, Figure S6). In the wild type, LHCBM4/6/8 subunit distribution was similar to other LHCII subunits and yet the intensity of the signal corresponding to trimers and monomers was clearly higher than that corresponding to PSII supercomplexes (Supplementary data, Figure S6). The pattern of PsaA, CP43, LHCII and LHCBM6 was not significantly altered in knockdown strains compared to the wild type, except for a reduced intensity of LHCBM4/6/8, as expected (Figure 5). This result suggests that LHCBM4/6/8 could be preferentially found as free LHCII trimers, even if a minor fraction of these subunits was associated to PSI and PSII supercomplexes of different size.

Roles of LHCBM4/6/8 in light harvesting and photoprotection

The effect of *LHCBM4/6/8* gene silencing on the stability of Photosystem II was monitored *in vivo* by measuring the maximum quantum efficiency of PSII, F_v/F_m, by pulse-amplitude fluorimetry. F_v/F_m values were found to be similar in wild type and knock-down strains, scoring between 0.6 and 0.7 in all genotypes (Table 1).

	F_v/F_m (CL)	F_v/F_m (HL)	NPQ_max
WT	0.712 ± 0.02	0.663 ± 0.01	1.57 ± 016
L6_A	0.701 ± 0.01	0.628 ± 0.01	0.96 ± 0.04
L6_B	0.703 ± 0.02	0.663 ± 0.01	1.12 ± 0.03
L_468	0.709 ± 0.01	0.660 ± 0.01	0.54 ± 0.01

The SD dis reported in the table (n=5).

Table 1. *F_v/F_m and NPQ parameter of wild-type (WT) and knock-down strains. Fv/Fm values were determined by PAM fluorimetery on cells grown in control light (CL) or high light (HL). NPQ values were measured by PAM fluorimetry on HL cells.*

Similar values were obtained when cells were grown under high irradiance (400 µmol $m^{-2}s^{-1}$), implying PSII was functional even at high excitation pressure (Table 1). In order to evaluate the role of LHCBM4/6/8 in light harvesting, PSI and PSII functional antenna size was measured in dark adapted wild-type and knock-down strains as previously described (Bonente *et al.*, 2012). In the case of PSI (Figure 6A), functional antenna size was measured from the kinetics of P700 oxidation in thylakoid membranes treated with DCMU and methyl-viologen.

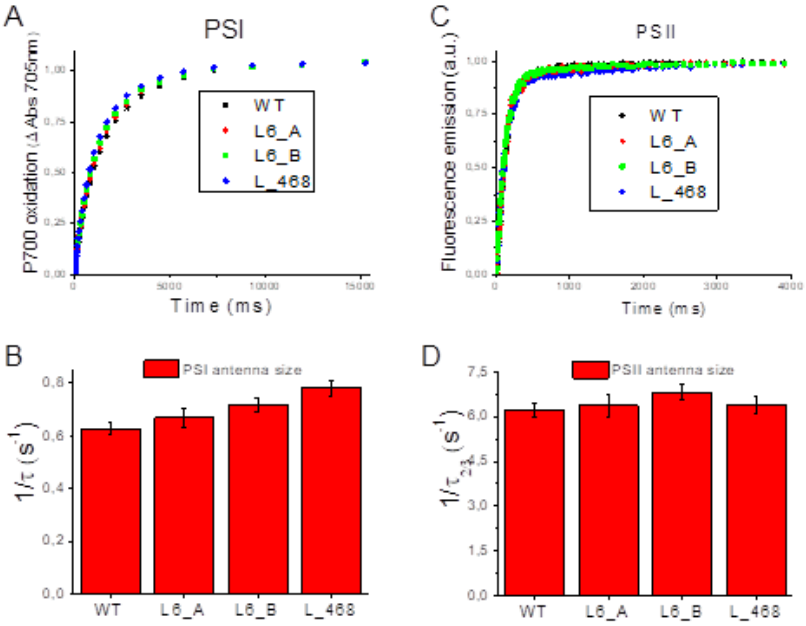

Figure 6: *PSI and PSII antenna size measurements. PSI antenna size (A) was measured in wild-type (WT) and knock-down strains by following the kinetics of P700 oxidation in limiting light conditions in DCMU, ascorbate and methyl viologen treated thylakoids. P700 oxidation kinetics were fitted with exponential functions and the reciprocal of time constants associated to fitting functions are reported in (B) normalized to WT as an estimate of PSI antenna size. PSII antenna size (C) was measured by following the fluorescence emission kinetics of PSII in DCMU treated cells. Fluorescence kinetics were fitted with exponential functions by which* $\tau_{2/3}$ *were calculated as the time required to reach two third of the maximum fluorescence emission: the reciprocal of* $\tau_{2/3}$ *is plotted in (D) as an estimation of PSII antenna size. Data reported in (B) and (D) were tested for their statistical significance compared to WT by Student t-test (n=3), obtaining in all cases P-values >0.05, indicating that the differences observed were not statistically significant.*

In particular PSI antenna size were estimated as the reciprocal of rate constant ($1/\tau$) obtained by fitting the oxidation kinetics with exponential function (Bonente *et al.*, 2012). The kinetics were similar in all genotypes analyzed and the ($1/\tau$) value obtained for silencing were not statistically significant compared to the wild type. The antenna size of PSII was measured from the kinetic of Chl *a* fluorescence emission in DCMU-treated cells: fluorescence kinetics were fitted with exponential function by which the time required to reach two third of the maximum fluorescence emission ($\tau_{2/3}$) were calculated. The reciprocal of the $\tau_{2/3}$ values were then used to estimate the PSII antenna size (Figure 6D) as previously reported (Cardol *et al.*, 2008). No significant difference was detected for $1/\tau_{2/3}$ values in silencing strains compared with the wild type,

suggesting that the LHCII trimers destabilized upon *LHBCM4/6/8* silencing are not essential for light harvesting function, consistent with the hypothesis it belongs to the extra-LHCII pool free in the thylakoid membranes (Drop *et al.*, 2014*a*). We then proceeded to verify the effects on regulative processes associated to antenna system. In particular we investigated if depletion in LHCBM4/6/8 affected the process of state1-state 2 transitions, namely the migration of LHCII from PSII to PSI. The amplitude of state transitions was evaluated by measuring the differences in fluorescence emission upon poising cells in either state 1 or state 2 at room temperature (Fleischmann *et al.*, 1999; Wollman, 2001) or at 77K (Allorent *et al.*, 2013). Room temperature florescence emission from whole cells is essentially coming from PSII, being the fluorescence quantum yield of PSI extremely low (Borisov and Il'ina, 1973): changes in maximum fluorescence emission at room temperature upon induction of state1 to state 2 transition is reported in Figure 7A, showing a similar amplitude for wild-type and knock-down strains.

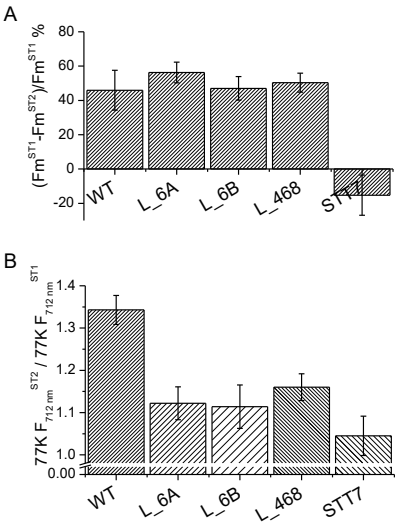

Figure 7. *State1-state 2 transition analysis. (A) Maximal capacity of switching LHCII antenna from PSII to PSI was analyzed in wild-type (WT) and knock down strains by measuring the variation in maximum fluorescence emission in state 1 (F_m^{ST1}) and state 2 (F_m^{ST2}) at room temperature. The changes in F_m are related to PSII fluorescence emission. (B) Fluorescence emission spectra of cells in state 1 or state 2 were measured at 77K, the spectra were normalized to PSII peaks (686 nm) and the ratio between the PSI peaks (712 nm) in state 2 and state 1 is reported as 77K F_{712} nm^{ST2}/77K F_{712} nm^{ST1}. The changes in 712 nm fluorescence emission are related to PSI. In both panels the stt7 mutant was used as negative control. Error bars indicate standard deviation (n=3).*

In order to investigate the effect of state transition on PSI, fluorescence emission spectra from whole cells in either state 1 or state 2 were also measured at 77K (Figure 7B): 77K fluorescence emission spectra were characterized by two major peaks at 682 nm and 715 nm (Supplementary data, Figure S7), related to PSII and PSI emissions respectively. When cells were induced to state 2, PSI fluorescence emission increased more, upon normalization to PSII fluorescence, in the wild type compared to knock-down strains, suggesting LHCBM4/6/8 is part of the mobile LHCII pool transferred upon state

transitions increasing the antenna size of PSI (Drop *et al.*, 2014*b*; Le Quiniou *et al.*, 2015). In particular, since the PSII fluorescence emission measured at room temperature decreased similarly in wild-type and knock-down strains upon transition to state2, the LHCBM4/6/8 subunits involved in state transitions are probably those located free in the membrane. The role of LHCBM4/6/8 in excess energy dissipation was evaluated by measuring the NPQ. Since in *C. reinhardtii* NPQ is fully activated upon acclimation to high light (Peers *et al.*, 2009; Bonente *et al.*, 2012; Allorent *et al.*, 2013), these measurements were performed upon acclimation to 400 µmol $m^{-2}s^{-1}$ light. In these conditions, the number of LHCBM4/6/8 subunits per PSII in the wild type was comparable to that of cells grown in control light, and the decrease of LHCBM4/6/8 in knockdown strains was maintained (Figure 8C, E). Knockdown strains acclimated to high light were characterized by a reduced NPQ activity (Figure 8D), which was more evident in strain L_468. This result suggests a possible role of LHCBM4/6/8 in NPQ activity.

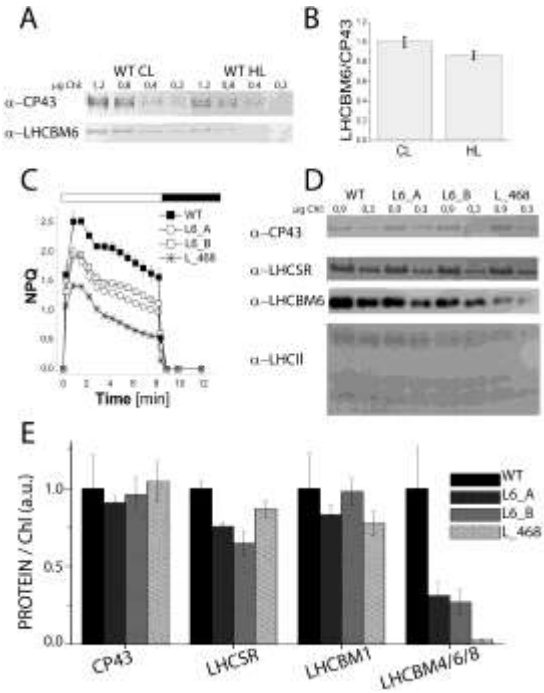

Figure 8. *LHCBM4/6/8 accumulation and non-photochemical quenching (NPQ) induction in high light. Accumulation of LHCBM4/6/8 in high light (HL) compared to control light (CL) was analyzed by western blot (A, chlorophyll loading in each lane is reported on the top of the figure) and estimated upon normalization to CP43 content (B). The NPQ induction kinetics were collected by using an actinic light of 1500 µmol photons*

m^{-2} s^{-1} on high light acclimated cells (C). Accumulation of LHCII, LHCSR3 and CP43 proteins in high light cells were determined using a specific antibody (D, chlorophyll loading in each lane is reported on the top of the figure). LHCBM4/6/8, LHCBM1 (the intermediate band recognized by α-LHCII antibody) and LHCSR level per PSII (normalized to CP43 content) are reported (E, F, G). The mean value of three independent measurements (n=3) and the respective SDs are shown.

Roles of LHCBM4/6/8 in stabilizing LHCSR3

Differences in NPQ induction could be related to a different accumulation of LHCSR1-LHCSR3, since LHCSR proteins are essential for triggering NPQ in *C. reinhardtii* (Peers *et al.*, 2009; Bonente *et al.*, 2011; Bonente *et al.*, 2012). The accumulation of LHCSR proteins was thus investigated by immunoblot analysis in samples grown in high light, yielding a slightly lower level of LHCSR3 in all knock-down strains as compared to wild type (Figure 8C, E), suggesting a possible role of LHCBM4/6/8 in stabilizing LHCSR3 in thylakoid membranes. LHCBM1 has been suggested to be partner for LHCSR3 since its depletion in the *npq5* mutant caused a strong reduction in NPQ activity (Elrad *et al.*, 2002; Peers *et al.*, 2009; Bonente *et al.*, 2011). The LHCBM1 level was measured by immunoblot analysis in the knock-down samples grown in high light, showing no significant difference as compared to the wild type (Figure 8C, E). As reported in Supplementary data, Figure S8, a positive linear correlation was found between the LHCBM4/6/8 accumulation and NPQ activation, but only for NPQ values >0.6. In contrast, no such linear correlation was found between NPQ induction and LHCBM1 or LHCSR accumulation, suggesting that the NPQ phenotype observed in silenced strains was specifically related to LHCBM4/6/8 subunits. The potential role of LHCBM4/6/8 as binding site for LHCSR protein was then investigated by 2D electrophoresis on CN-SDS PAGE of solubilized thylakoids from samples grown in high light conditions (Supplementary data, Figure S9) coupled with immunoblot analysis using antibodies directed to PSI and PSII core subunits (PsaA, CP43) and to antenna components (LHCBM4/68 and LHCSR). In all clones the LHCSR protein was detected with mobility corresponding to that of monomeric LHC proteins or higher. The appearance of LHCSR signals at high apparent molecular weight in CN-PAGE, although weak, suggests formation of oligomers and or interactions with other thylakoid components (Bonente *et al.*, 2011; Tokutsu and Minagawa, 2013; Xue *et al.*, 2015). It should be noticed that the LHCSR-specific reaction was very weak at the mobility corresponding to LHCII trimers, inconsistent with the presence of LHC heterotrimers

including LHCSR3. We cannot exclude, however, the formation of LHCSR3 homodimers or heterodimers with other LHC subunits, which might then interact with PSI and/or PSII supercomplexes. The distribution patterns of LHCSR3 and LHCBM4/6/8 in CN-PAGE were different in each strain investigated. Moreover, LHCBM4/6/8 strong reduction observed in L_468 strain did not significantly influence the LHCSR3 distribution compared with the wild type; these results suggest that LHCBM4/6/8 and LHCSR1/3 do not form stable interactions with each-other.

Roles of LHCBM4/6/8 in stress defense

In order to investigate further the role of LHCBM4/6/8 in stress defense, the production of singlet oxygen ($^1O_2$) was measured (Figure 9).

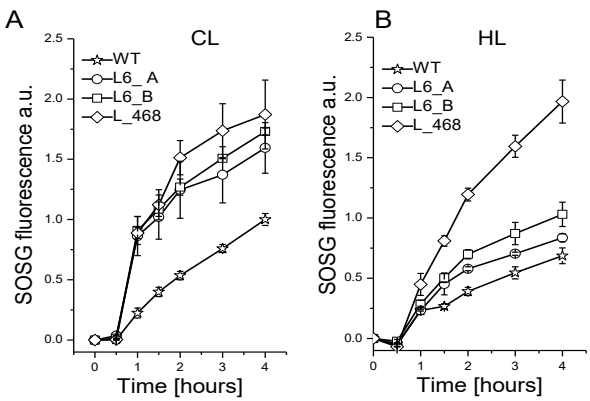

Figure 9. *Singlet oxygen ($^1O_2$) production in knock-down strains grown. Singlet oxygen production was measured in cells grown in control light (A) or high light (B) conditions upon exposure to red light at 840 µmol photons m^{-2} s^{-1} following the increase of the 530 nm fluorescence of the specific probe Singlet Oxygen Sensor Green (SOSG). SDs are reported for each sample (n=3).*

$^1O_2$ is produced from the reaction of molecular oxygen with chlorophyll triplet excited states and the which accumulate when the rate of excitation energy quenching is exceeded. $^1O_2$ production was measured by using a specific probe, SOSG, which increases its fluorescence at 530 nm proportionally to the accumulation of $^1O_2$ (Flors *et al.*, 2006). Cells acclimated in low light (60 µmol photons m^{-2} s^{-1}) and in high light (400 µmol photons m^{-2} s^{-1}) conditions were incubated in presence of SOSG and excited by a red (680 nm) light at 840 µmol photons m^{-2} s^{-1}. $^1O_2$ production was higher in the strains acclimated in low light than in high light, suggesting that the growth in high light activates several photoprotective mechanisms decreasing photo-oxidative stress, in agreement with previous reports (Baroli *et al.*, 2003; Bonente *et al.*, 2012; Allorent *et al.*, 2013). Increased $^1O_2$ production was observed in knock-down strains acclimated to both low and high light as compared to the wild type. In particular, strain L_468 showed

the highest $^1O_2$ production both in control light and in high light. These observations suggest a role of LHCBM4/6/8 in the mechanism of acclimation to high light conditions and photoprotection. One of the processes activated upon high light exposure is the xanthophyll cycle, during which violaxanthin is converted to zeaxanthin and anteraxanthin. The xanthophyll cycle activity can be estimated from the de-epoxidation index (DI), calculated as: (zeaxanthin+0.5*anteraxanthin)/(violaxanthin+zeaxanthin+anteraxanthin). A high DI was generally observed in high light-acclimated cells (Bonente *et al.*, 2012). Upon high light acclimation, a lower DI was observed in the silenced strains compared to the wild type (Table 2). This result suggests that the violaxanthin bound by LHCBM4/6/8 proteins can be more easily de-epoxidated to zeaxanthin as compared to the violaxanthin bound by other LHC proteins. The reduced DI observed in silenced strains in high light compared to the wild type could be related to the higher singlet oxygen production observed in these strains due to the high efficiency of zeaxanthin in scavenging ROS (Havaux and Niyogi, 1999).

	Nx	Vx	Ax	Lut	Zx	β-Car	Chl *a/b*	Car/Chl	DI	Chl/cell
WT CL	9.3 ± 1.2	4.2 ± 0.5	0.27 ± 0.03	7.5 ± 0.9	0.22 ± 0.03	4.6 ± 0.1	2,19 ± 0,03	0.26 ± 0.02	0.076 ± 0.002	2,7E-06 ± 6,7E-08
L6_A CL	10.2 ± 0.04	4.9 ± 0.01	0.3 ± 0.01	8.4 ± 0.09	0.34 ± 0.03	5.01 ± 0.08	2,23 ± 0,05	0.29 ± 0.002	0.089 ± 0.004	2,0E-06 ± 1,7E-07
L6_B CL	9.4 ± 1.2	4.7 ± 0.8	0.3 ± 0.06	8.4 ± 1.1	0.16 ± 0.08	5.2 ± 2.1	2,26 ± 0,02	0.28 ± 0.05	0.064 ± 0.016	2,7E-06 ± 2,8E-07
L_468 CL	8.7 ± 1.1	4.2 ± 0.5	0.27 ± 0.04	7.4 ± 0.9	0.25 ± 0.05	4.8 ± 0.1	2,36 ± 0,02	0.26 ± 0.03	0.08 ± 0.005	2,9E-06 ± 4,0E-07
WT HL	7,7 ± 2.3	4.4 ± 1.6	1.4 ± 0.5	16.1 ± 4.8	1.7 ± 0.8	2.7 ± 1.9	2,22 ± 0,00	0.35 ± 0.14	0.316 ± 0.01	1,5E-06 ± 7,7E-08
L6_A HL	7.1 ± 1.6	5.1 ± 1.4	0.9 ± 0.1	15.4 ± 2,0	0.9 ± 0.003	1.4 ± 0.001	2,31 ± 0,01	0.35 ± 0.0	0.196 ± 0.09	1,4E-06 ± 1,1E-07
L6_B HL	6.6 ± 0.9	4.9 ± 0.8	0.74 ± 0.1	13.2 ± 1.8	0.74 ± 0.1	4.99 ± 0.2	2,31 ± 0,07	0.31 ± 0.04	0.172 ± 0.0003	1,7E-06 ± 1,7E-07
L_468 HL	8.1 ± 1.4	5.7 ± 0.8	0.7 ± 0.08	14.2 ± 2.1	0.6 ± 0.04	4.5 ± 1.5	2,39 ± 0,00	0.34 ± 0.06	0.135 ± 0.002	2,0E-06 ± 2,1E-07

Nx, neoxanthin; Vx, violaxanthin; Ax, antheraxanthin, Lut, lutein, Zx, zeaxanthin, β-Car, β-carotene, Chl *a/b*, the ratio between Chl *a* and Chl *b*; Car/Chl, the ratio between the total carotenoid and chlorophyll content; DI, de-epoxidation index: DI=Zx+(0.5×Ax)/(Vx+Ax+Zx). The SD is reported in the table (n=3).

Table 2. *Pigment profiling of knock-down strains grown in control light (CL) and high light (HL). Pigment amounts quantified by HPLC are normalized on 100 Chl*

Discussion

LHCBM gene family is composed of nine members, which are highly similar to each other. The functional roles of LHCBM1, LHCBM2/7 and LHCBM9 have been previously described: LHCBM1 was reported to be involved in NPQ induction, while LHCBM2/7 in state transitions induction (Elrad *et al.*, 2002; Ferrante *et al.*, 2012). The LHCBM9 subunit was found to accumulate in stressing conditions only and was accompanied by an increased photoprotection activity (Nguyen *et al.*, 2008), as shown by the stabilization of both PSII supercomplexes and LHCII trimers (Grewe *et al.*, 2014). Little information was yet available for the remaining LHCBM subunits:

combined silencing of LHCBM1, LHCBM2 and LHCBM3 was reported to increase light-driven hydrogen production (Oey *et al.*, 2013). Recently LHCBM1, LHCBM2/7 and LHCBM3 were demonstrated to be the major components of the heterotrimers bound to PSII supercomplexes, while LHCBM5 was suggested to be mainly located in the "extra" LHCIIs which are not tightly connected to the PSII core complex (Drop *et al.*, 2014*a*). In agreement with these findings, LHCBM5 has been reported to be phosphorylated by STT7 kinase and was found in a complex with PSI upon state 2 induction (Takahashi *et al.*, 2006). It should be noted that, besides LHCBM5, also LHCBM1, LHCBM3, LHCBM4, LHCBM6, LHCBM8 and LHCBM9 can be phosphorylated by STT7, and all the different types of LHCBMs together with CP26 and CP29 were found in the PSI-LHCII supercomplex, even in non-phosphorylated form (Lemeille *et al.*, 2009; Drop *et al.*, 2014*b*). In this work we analyzed the functional role of LHCBM4, LHCBM6 and LHCBM8 subunits, which belong to the same sub-family and share high identity (Figure 1). The biochemical and spectroscopic features of LHCBM4 and LHCBM6 subunits were first analyzed *in vitro* and their physiological function was then studied *in vivo* by a reverse genetic approach obtaining strains silencing *LHCBM4* and *LHCBM6* (L6_A and L6_B) or the *LHCBM4/6/8* (L_468) genes together. Pigment binding properties of LHCBM4 and LHCBM6 (Table 3) were comparable to those previously reported for other LHCBM proteins (Grewe *et al.*, 2014; Natali and Croce, 2015).

Refolded complexes	Chl	Chl *a*/*b*	Chl/Car	Cars	Nx	Vx	Ax	Lut	Zx
LHCBM1	14	1.41	4.1	3.4	1.5	0.28	0.03	1.54	0.034
LHCBM2	14	1.148	3.89	3.6	1.63	0.2	0.01	1.73	0.022
LHCBM4	14	1.3	3.41	4.1	2	0.24	0.012	1.81	0.026
LHCBM6	14	1.37	3.3	4.23	2.19	0.18	0.03	1.76	0.066

Chl, chlorophylls; Chl *a*/*b*, chlorophyll *a*/*b* ratio; Chl/Car, chlorophyll to carotenoid ratio, Cars, total carotenoids; Nx, neoxanthin; Vx, violaxanthin; Ax, antheraxanthin; Lut, lutein; Zx, zeaxanthin.
Chl *a*/*b* and Chl/Car ratios are absolute values.
SDs are in all cases <5% (n=3).

Table 3. *HPLC analysis of pigments content in the recombinant and reconstituted LHCBM proteins LHCBM1, LHCBM2, LHCBM4 and LHCBM6. The numbers of each pigments are expressed in picomole and normalized to 14 chlorophylls (the amount of chlorophylls putatively bound by one LHCII monomer.*

An important property was their low fluorescence yield, consistently measured for both LHCBM4 and LHCBM6 as compared to LHCBM2 (Figure 2). Since fluorescence yield is modulated by the activity of the concurrent heat dissipation channel, it can be concluded that LHCBM4 and LHCBM6 are characterized by higher quenching activity compared to LHCBM2, but comparable to LHCBM1, the LHCBM subunit with the

lowest fluorescence quantum yield (Elrad *et al.*, 2002; Grewe *et al.*, 2014; Natali and Croce, 2015). The reverse genetic experiments reported here were aimed to understand how the biochemical/biophysical properties of the individual gene products are translated into a functional role when integrated into thylakoid membranes. Analysis of selected knock-down strains showed that amiRNA silencing was effective in reducing the level of gene products *in vivo* (Figure 4). The levels of LHCBM4/6/8 subunits were reduced on a chlorophyll basis in knock-down strains, especially in the case of L_468 (Figure 3). Although the amiRNA silencing showed minor untargeted effect on other *LHCBM* genes, the overall stoichiometry of LHCII proteins per PSII was not significantly reduced in knock-down strains (Figure 4). LHCBM6 accumulation, in has been reported to be controlled by the translation repressor NAB1, which is accumulated under CO_2 deficiency, inducing an overall reduction in LHCII content and functional antenna size of PSII when cells are grown in absence of CO_2 (Berger *et al.*, 2014). The similar LHCII per PSII stoichiometry and the similar PSII antenna size observed in silencing strains in this work suggest that the translational control of NAB1is likely not limited to LHCBM6 but involves other LHCBM subunits as well. In *C. reinhardtii*, PSII supercomplexes have been reported to have a larger capacity to bind LHCII trimers compared to higher plants, their antenna moiety in supercomplexes constituted by at least six LHCII trimers in the C2S2M2N2 conformation, compared to the four LHCII trimers observed in *A. thaliana* (C2S2M2) (Drop *et al.*, 2014*a*). In addition, a pool of "extra" LHCII was identified in *C. reinhardtii*, constituting LHCII-only domains in the thylakoid membranes, possibly acting as a buffer for state transitions.

The results obtained by 2D CN-SDS-PAGE showed that LHCBM4/6/8 contribute to form monomeric and trimeric LHC bands or to PSII supercomplexes of different sizes. This evidence suggests that LHCBM4/6/8 can be part of –S, –M or -N trimers. Nevertheless, their enrichment in supercomplexes was low, and most of LHBCM4/6/8 was found in the "free LHCII" pool (Supplementary data, Figure S6). In agreement with this finding, PSII antenna size was essentially unaffected by *LHCBM4/6/8* gene silencing. LHCII trimers free in the thylakoid membrane are suggested to be bound to PSI or forming LHCII-only domains (Nagy *et al.*, 2014; Ünlü *et al.*, 2014). When wild-type and knock-down strains were forced to undergo transition to state 2, the PSII fluorescence emission was similarly reduced in wild-type and knock-down strains, while the increase of PSI fluorescence emission, detectable at 77K, was significantly smaller in

knock-down strains compared to the wild type, indicating a reduced level of LHCII-PSI interaction. On this basis we suggest that LHCBM4/6/8 are located in sub-stoichiometric amount in –S, –M or -N trimers, while the majority of these subunits are located free in the membrane, with the latter participating to state transitions, (i.e. migrating to PSI upon state 2 induction). The same conclusion can be extended to the other LHCII subunits forming heterotrimes with LHCBM4/6/8.

The down-regulation of LHCBM4/6/8 protein was correlated with a decrease in the amplitude of NPQ activity (Figure 8, Table 1, Figure S8). The high sequence identity of LHCBM4, LHCBM6 and LHCBM8 suggests that these proteins have similar functions, acting co-operatively, in the energy dissipative mechanisms. How do LHCBM4/6/8 contribute to NPQ is not clear. One possibility is that they are docking site(s) for the interaction of PSII antenna system with LHCSR3, which, owing to its short fluorescence lifetime upon lumen acidification, could act as the site for energy dissipation (Peers *et al.*, 2009; Bonente *et al.*, 2011; Liguori *et al.*, 2013; Tokutsu and Minagawa, 2013). Alternatively, it is possible that quenching sites are formed not only within LHCSR1/3 proteins but also in the interacting LHC subunits induced to switch to a dissipative conformation by the interaction with LHCSR proteins, in a mechanism similar to what was previously proposed for the PSBS-dependent quenching in higher plants (Bonente *et al.*, 2008). While the present data do not allow to distinguish between these hypotheses, the interaction between LHCSR3 and other pigment proteins appears to be very weak, at least in the fractionation conditions explored here. Indeed, the LHCSR distribution was not affected in knockdown strains, (Supplementary data, Figure S9). Thus, it is unlikely that LHCSR3 might form stable hetero-oligomers with LHCBM4/6/8. It is, however, possible that the relative abundance of high versus low fluorescence yield LHCM subunits might serve in the fine-tuning of antenna system during long-term acclimation consistent, with the recent results with LHCBM9 (Grewe *et al.*, 2014) and with the LHCII populations with different quenching properties detected *in vivo* (Tian *et al.*, 2015), rather than on the light induced short term NPQ mechanism. A role of LHCBM4/6/8 in the formation of quenched LHCII domains is also consistent with the higher level of singlet oxygen in knock-down strains compared with the wild type (Figure 9) during growth in both control and high light conditions. The level of ROS produced upon light exposure in pigment–protein antennas depends on the level of chlorophyll singlet excited states, the conversion yield into triplets, and the ROS

scavenging activity of xanthophylls (Ballottari *et al.*, 2013; Croce *et al.*, 1999*b*; Niyogi, 1999). Certainly, the reduced capacity for NPQ is likely to contribute to ROS synthesis in excess light conditions (Ferrante *et al.*, 2012). However, differences in ROS-scavenging activity cannot be excluded, especially considering the decrease of the de-epoxidation index measured in these strains (Table 2). Indeed, zeaxanthin has been involved in singlet chlorophyll excited states (Dall'Osto *et al.*, 2005), quenching of triplet chlorophyll excited states quenching (Dall'osto *et al.*, 2012) and ROS scavenging (Havaux *et al.*, 2004). Interestingly, while singlet oxygen production in high light-acclimated cells was generally lower, this was not the case in the L_468 strain, whose high light-acclimated cells produced levels of singlet oxygen comparable with cells receiving light. These results, together with the reduced LHCSR3 accumulation and reduced de-epoxidation index in the L_468 strain suggests that the reduction in level of the LHCBM4/6/8 proteins impairs the mechanisms of acclimation to high light.

We conclude that LHCBM4, LHCBM6 and LHCBM8, rather than having an essential function in photon capture, are likely to be involved in photoprotective mechanisms with a specific function within a pool of LHCII proteins free or very loosely connected to the PSII supercomplex. Beside their interest for the understanding of basic properties of light harvesting systems, these results will also be instrumental in designing domesticated strains of unicellular algae for optimal growth in photobioreactors by modulating the accumulation of specific members of the antenna system in order to improve either light harvesting, the photoprotection response or both.

References

Ahn TK, Avenson TJ, Ballottari M, Cheng YC, Niyogi KK, Bassi R, Fleming GR. 2008. Architecture of a charge-transfer state regulating light harvesting in a plant antenna protein. Science **320**, 794-797.

Allen JF, Pfannschmidt T. 2000. Balancing the two photosystems: photosynthetic electron transfer governs transcription of reaction centre genes in chloroplasts. Philosophical Transactions of the Royal Society B: Biological Sciences **355**, 1351-1359.

Allorent G, Tokutsu R, Roach T, Peers G, Cardol P, Girard-Bascou J, Seigneurin-Berny D, Petroutsos D, Kuntz M, Breyton C, Franck F, Wollman FA, Niyogi KK, Krieger-Liszkay A, Minagawa J, Finazzi G. 2013. A dual strategy to cope with high light in *Chlamydomonas reinhardtii*. The Plant Cell **25**, 545-557.

Ballottari M, Girardon J, Dall'osto L, Bassi R. 2012. Evolution and functional properties of photosystem II light harvesting complexes in eukaryotes. Biochimica et Biophysica Acta **1817**, 143-157.

Ballottari M, Mozzo M, Croce R, Morosinotto T, Bassi R. 2009. Occupancy and functional architecture of the pigment binding sites of photosystem II antenna complex Lhcb5. Journal of Biological Chemistry **284**, 8103-8113.

Ballottari M, Mozzo M, Girardon J, Hienerwadel R, Bassi R. 2013. Chlorophyll Triplet Quenching and Photoprotection in the Higher Plant Monomeric Antenna Protein Lhcb5. Journal of Physical Chemistry B **117**, 11337-11348.

Baroli I, Do AD, Yamane T, Niyogi KK. 2003. Zeaxanthin accumulation in the absence of a functional xanthophyll cycle protects *Chlamydomonas reinhardtii* from photooxidative stress. The Plant Cell **15**, 992-1008.

Benson S, Maheswaran P, Ware M, Hunter C, Horton P, Jansson S, Ruban A, Johnson M. 2015. An intact light harvesting complex I antenna system is required for complete state transitions in *Arabidopsis*. Nature Plants **1**, 15176.

Berger H, Blifernez-Klassen O, Ballottari M, Bassi R, Wobbe L, Kruse O. 2014. Integration of carbon assimilation modes with photosynthetic light capture in the green alga *Chlamydomonas reinhardtii*. Molecular Plant **7**, 1545-1559.

Betterle N, Ballottari M, Baginsky S, Bassi R. 2015. High Light-Dependent Phosphorylation of Photosystem II Inner Antenna CP29 in Monocots Is STN7 Independent and Enhances Nonphotochemical Quenching. Plant Physiology **167**, 457-471.

Bonente G, Ballottari M, Truong TB, Morosinotto T, Ahn TK, Fleming GR, Niyogi KK, Bassi R. 2011. Analysis of LhcSR3, a Protein Essential for Feedback De-Excitation in the Green Alga *Chlamydomonas reinhardtii*. Plos Biology **9** e1000577.

Bonente G, Howes BD, Caffarri S, Smulevich G, Bassi R. 2008. Interactions between the photosystem II subunit PsbS and xanthophylls studied in vivo and in vitro. Journal of Biological Chemistry **283**, 8434-8445.

Bonente G, Pippa S, Castellano S, Bassi R, Ballottari M. 2012. Acclimation of *Chlamydomonas reinhardtii* to Different Growth Irradiances. Journal of Biological Chemistry **287**, 5833–5847

Borisov AY, Il'ina MD. 1973. The fluorescence lifetime and energy migration mechanism in photosystem I of plants. Biochimica et Biophysica Acta **305**, 364–371.

Caffarri S, Croce R, Breton J, Bassi R. 2001. The major antenna complex of photosystem II has a xanthophyll binding site not involved in light harvesting. Journal of Biological Chemistry **276**, 35924–35933.

Caffarri S, Croce R, Cattivelli L, Bassi R. 2004. A look within LHCII: differential analysis of the Lhcb1-3 complexes building the major trimeric antenna complex of higher-plant photosynthesis. Biochemistry **43**, 9467-9476.

Caffarri S, Passarini F, Bassi R, Croce R. 2007. A specific binding site for neoxanthin in the monomeric antenna proteins CP26 and CP29 of Photosystem II. FEBS Letter **581**, 4704-4710.

Cardol P, Bailleul B, Rappaport F, Derelle E, Beal D, Breyton C, Bailey S, Wollman FA, Grossman A, Moreau H, Finazzi G. 2008. An original adaptation of photosynthesis in the marine green alga *Ostreococcus*. Proceedings of the National Academy of Sciences, USA **105**, 7881–7886.

Croce R, Morosinotto T, Castelletti S, Breton J, Bassi R. 2002. The Lhca antenna complexes of higher plants photosystem I. Biochimica et Biophysica Acta **1556**, 29–40.

Croce R, Remelli R, Varotto C, Breton J, Bassi R. 1999a. The neoxanthin binding site of the major light harvesting complex (LHCII) from higher plants. FEBS Letter **456**, 1-6.

Croce R, Weiss S, Bassi R. 1999b. Carotenoid-binding sites of the major light-harvesting complex II of higher plants. Journal of Biological Chemistry **274**, 29613–29623.

Dall'Osto L, Caffarri S, Bassi R. 2005. A mechanism of nonphotochemical energy dissipation, independent from PsbS, revealed by a conformational change in the antenna protein CP26. The Plant Cell **17**, 1217-1232.

Dall'Osto L, Cazzaniga S, Havaux M, Bassi R. 2010. Enhanced photoprotection by protein-bound vs free xanthophyll pools: a comparative analysis of chlorophyll b and xanthophyll biosynthesis mutants. Molecular Plant **3**, 576-593.

Dall'Osto L, Cazzaniga S, North H, Marion-Poll A, Bassi R. 2007. The *Arabidopsis* aba4-1 mutant reveals a specific function for neoxanthin in protection against photooxidative stress. The Plant Cell **19**, 1048-1064.

Dall'osto L, Holt NE, Kaligotla S, Fuciman M, Cazzaniga S, Carbonera D, Frank HA, Alric J, Bassi R. 2012. Zeaxanthin Protects Plant Photosynthesis by Modulating Chlorophyll Triplet Yield in Specific Light-harvesting Antenna Subunits. Journal of Biological Chemistry **287**, 41820-41834.

Dall'Osto L, Lico C, Alric J, Giuliano G, Havaux M, Bassi R. 2006. Lutein is needed for efficient chlorophyll triplet quenching in the major LHCII antenna complex of higher plants and effective photoprotection in vivo under strong light. BMC Plant Biology **6**, 32.

Dall'osto L, Piques M, Ronzani M, Molesini B, Alboresi A, Cazzaniga S, Bassi R. 2013. The *Arabidopsis* nox mutant lacking carotene hydroxylase activity reveals a critical role for xanthophylls in Photosystem I biogenesis. The Plant Cell **25**, 591-608.

de Bianchi S, Betterle N, Kouril R, Cazzaniga S, Boekema E, Bassi R, Dall'Osto L. 2011. *Arabidopsis* mutants deleted in the light-harvesting protein Lhcb4 have a disrupted photosystem II macrostructure and are defective in photoprotection. The Plant Cell **23**, 2659-2679.

Depege N, Bellafiore S, Rochaix JD. 2003. Role of chloroplast protein kinase Stt7 in LHCII phosphorylation and state transition in *Chlamydomonas*. Science **299**, 1572–1575.

Drop B, Webber-Birungi M, Yadav SK, Filipowicz-Szymanska A, Fusetti F, Boekema EJ, Croce R. 2014*a*. Light-harvesting complex II (LHCII) and its supramolecular organization in *Chlamydomonas reinhardtii*. Biochimica et Biophysica Acta **1837**, 63-72.

Drop B, Yadav K N S, Boekema EJ, Croce R. 2014*b*. Consequences of state transitions on the structural and functional organization of photosystem I in the green alga *Chlamydomonas reinhardtii*. The Plant Journal **78**, 181-191.

Elrad D, Niyogi KK, Grossman AR. 2002. A major light-harvesting polypeptide of photosystem II functions in thermal dissipation. The Plant Cell **14**.

Ferrante P, Ballottari M, Bonente G, Giuliano G, Bassi R. 2012. LHCBM1 and LHCBM2/7 polypeptides, components of major LHCII complex, have distinct functional roles in photosynthetic antenna system of *Chlamydomonas reinhardtii*. Journal of Biological Chemistry **287**, 16276-16288.

Finazzi G, Rappaport F, Furia A, Fleischmann M, Rochaix JD, Zito F, Forti G. 2002. Involvement of state transitions in the switch between linear and cyclic electron flow in *Chlamydomonas reinhardtii*. EMBO Reports **3**, 280-285.

Fleischmann MM, Ravanel S, Delosme R, Olive J, Zito F, Wollman FA, Rochaix JD. 1999b. Isolation and characterization of photoautotrophic mutants of *Chlamydomonas reinhardtii*

deficient in state transition. Journal of Biological Chemistry **274**, 30987-30994.

Flors C, Fryer MJ, Waring J, Reeder B, Bechtold U, Mullineaux PM, Nonell S, Wilson MT, Baker NR. 2006. Imaging the production of singlet oxygen in vivo using a new fluorescent sensor, Singlet Oxygen Sensor Green. Journal of Experimental Botany **57**, 1725-1734.

Galka P, Santabarbara S, Khuong TT, Degand H, Morsomme P, Jennings RC, Boekema EJ, Caffarri S. 2012. Functional analyses of the plant photosystem I-light-harvesting complex II supercomplex reveal that light-harvesting complex II loosely bound to photosystem II is a very efficient antenna for photosystem I in state II. The Plant Cell **24**, 2963-2978.

Giuffra E, Cugini D, Croce R, Bassi R. 1996. Reconstitution and pigment-binding properties of recombinant CP29. European Journal of Biochemistry **238**, 112-120.

Grewe S, Ballottari M, Alcocer M, D'Andrea C, Blifernez-Klassen O, Hankamer B, Mussgnug JH, Bassi R, Kruse O. 2014. Light-Harvesting Complex Protein LHCBM9 Is Critical for Photosystem II Activity and Hydrogen Production in *Chlamydomonas reinhardtii*. The Plant Cell **26**, 1598-1611.

Havaux M, Dall'osto L, Bassi R. 2007. Zeaxanthin has enhanced antioxidant capacity with respect to all other xanthophylls in *Arabidopsis* leaves and functions independent of binding to PSII antennae. Plant Physiology **145**, 1506-1520.

Havaux M, Dall'Osto L, Cuiné S, Giuliano G, Bassi R. 2004. The effect of zeaxanthin as the only xanthophyll on the structure and function of the photosynthetic apparatus in *Arabidopsis thaliana*. Journal of Biological Chemistry **279**, 13878-13888.

Havaux M, Niyogi KK. 1999. The violaxanthin cycle protects plants from photooxidative damage by more than one mechanism. Proceedings of the National Academy of Sciences, USA **96**, 8762-8767.

Havaux M, Tardy F. 1997. Thermostability and photostability of Photosystem II in leaves of the chlorina-f2 barley mutant deficient in Light-Harvesting chlorophyll a/b protein Complexes. Plant Physiology **113**, 913-923.

Hobe S, Förster R, Klingler J, Paulsen H. 1995. N-proximal sequence motif in light-harvesting chlorophyll a/b-binding protein is essential for the trimerization of light-harvesting chlorophyll a/b complex. Biochemistry **34**, 10224-10228.

Kindle KL. 1990. High-frequency nuclear transformation of *Chlamydomonas reinhardtii*. Proceedings of the National Academy of Sciences, USA **87**, 1228-1232.

Kühlbrandt W, Wang DN. 1991. Three-dimensional structure of plant light-harvesting complex determined by electron crystallography. Nature **350**, 130-134.

Kühlbrandt W, Wang DN, Fujiyoshi Y. 1994. Atomic model of plant light-harvesting complex by electron crystallography. Nature **367**, 614-621.

Lagarde D, Beuf L, Vermaas W. 2000. Increased production of zeaxanthin and other pigments by application of genetic engineering techniques to *Synechocystis* sp. strain PCC 6803. Applied and Environmental Microbiology **66**, 64-72.

Le Quiniou C, van Oort B, Drop B, van Stokkum IH, Croce R. 2015. The high efficiency of Photosystem I in the green alga *Chlamydomonas reinhardtii* is maintained after the antenna size is substantially increased by the association of Light-harvesting Complexes II. Journal of Biological Chemistry **290**, 30587-30595.

Lemeille S, Willig A, Depège-Fargeix N, Delessert C, Bassi R, Rochaix JD. 2009. Analysis of the chloroplast protein kinase Stt7 during state transitions. PLoS Biology **7**, e45.

Li Z, Ahn TK, Avenson TJ, Ballottari M, Cruz JA, Kramer DM, Bassi R, Fleming GR, Keasling JD, Niyogi KK. 2009. Lutein accumulation in the absence of zeaxanthin restores nonphotochemical quenching in the *Arabidopsis thaliana* npq1 mutant. The Plant Cell **21**, 1798-1812.

Liguori N, Roy LM, Opacic M, Durand G, Croce R. 2013. Regulation of light harvesting in the green alga *Chlamydomonas reinhardtii*: the C-terminus of LHCSR is the knob of a dimmer switch. Journal of the American Chemical Society **135**, 18339-18342.

Liu Z, Yan H, Wang K, Kuang T, Zhang J, Gui L, An X, Chang W. 2004. Crystal structure of spinach major light-harvesting complex at 2.72 A resolution. Nature **428**, 287-292.

Merchant SS, Prochnik SE, Vallon O, *et al*, 2007. The *Chlamydomonas* genome reveals the evolution of key animal and plant functions. Science **318**, 245-250.

Molnar A, Bassett A, Thuenemann E, Schwach F, Karkare S, Ossowski S, Weigel D, Baulcombe D. 2009. Highly specific gene silencing by artificial microRNAs in the unicellular alga *Chlamydomonas reinhardtii*. The Plant Journal **58**, 165-174.

Nagy G, Ünnep R, Zsiros O, Tokutsu R, Takizawa K, Porcar L, Moyet L, Petroutsos D, Garab G, Finazzi G, Minagawa J. 2014. Chloroplast remodeling during state transitions in *Chlamydomonas reinhardtii* as revealed by noninvasive techniques in vivo. Proceedings of the National Academy of Sciences, USA **111**, 5042-5047.

Natali A, Croce R. 2015. Characterization of the major light-harvesting complexes (LHCBM) of the green alga *Chlamydomonas reinhardtii*. PLoS One **10**, e0119211.

Nawrocki WJ, Santabarbara S, Mosebach L, Wollman FA, Rappaport F. 2016. State transitions redistribute rather than dissipate energy between the two photosystems in *Chlamydomonas*. Nature Plants **2**, 16031.

Nguyen AV, Thomas-Hall SR, Malnoë A, Timmins M, Mussgnug JH, Rupprecht J, Kruse O, Hankamer B, Schenk PM. 2008. Transcriptome for photobiological hydrogen production induced by sulfur deprivation in the green alga *Chlamydomonas reinhardtii*. Eukaryotic Cell **7**, 1965-1979.

Niyogi KK. 1999. Photoprotection revisited: Genetic and Molecular Approaches. Annual Review of Plant Physiology and Plant Molecular Biology **50**, 333-359.

Oey M, Ross IL, Stephens E, Steinbeck J, Wolf J, Radzun KA, Kügler J, Ringsmuth AK, Kruse O, Hankamer B. 2013. RNAi knock-down of LHCBM1, 2 and 3 increases photosynthetic H2 production efficiency of the green alga *Chlamydomonas reinhardtii*. PLoS One **8**, e61375.

Pan X, Li M, Wan T, Wang L, Jia C, Hou Z, Zhao X, Zhang J, Chang W. 2011. Structural insights into energy regulation of light-harvesting complex CP29 from spinach. Nature Structural and Molecular Biology **18**, 309-315.

Peers G, Truong TB, Ostendorf E, Busch A, Elrad D, Grossman AR, Hippler M, Niyogi KK. 2009. An ancient light-harvesting protein is critical for the regulation of algal photosynthesis. Nature **462**, 518-521.

Ruban AV, Berera R, Ilioaia C, van Stokkum IH, Kennis JT, Pascal AA, van Amerongen H, Robert B, Horton P, van Grondelle R. 2007. Identification of a mechanism of photoprotective energy dissipation in higher plants. Nature **450**, 575-578.

Schagger H, von Jagow G. 1987. Tricine-sodium dodecyl sulfate-polyacrylamide gel electrophoresis for the separation of proteins in the range from 1 to 100 kDa. Analytical Biochemistry **166**, 368-379.

Standfuss J, Terwisscha van Scheltinga AC, Lamborghini M, Kühlbrandt W. 2005. Mechanisms of photoprotection and nonphotochemical quenching in pea light-harvesting complex at 2.5 A resolution. EMBO Journal **24**, 919-928.

Takahashi H, Iwai M, Takahashi Y, Minagawa J. 2006. Identification of the mobile light-harvesting complex II polypeptides for state transitions in *Chlamydomonas reinhardtii*. Proceedings of the National Academy of Sciences, USA **103**, 477-482.

Tian L, Dinc E, Croce R. 2015. LHCII populations in different quenching states are present in the thylakoid membranes in a ratio that depends on the light conditions. Journal of Physical Chemistry Letters **6**, 2339-2344.

Tokutsu R, Minagawa J. 2013. Energy-dissipative supercomplex of photosystem II associated with LHCSR3 in *Chlamydomonas reinhardtii*. Proceedings of the National Academy of Sciences, USA **110**, 10016-10021.

Turkina MV, Kargul J, Blanco-Rivero A, Villarejo A, Barber J, Vener AV. 2006. Environmentally modulated phosphoproteome of photosynthetic membranes in the green alga *Chlamydomonas reinhardtii*. Molecular and Cellular Proteomics **5**, 1412-1425.

Ünlü C, Drop B, Croce R, van Amerongen H. 2014. State transitions in *Chlamydomonas reinhardtii* strongly modulate the functional size of photosystem II but not of photosystem I. Proceedings of the National Academy of Sciences, USA **111**, 3460–3465.

Wollman FA. 2001. State transitions reveal the dynamics and flexibility of the photosynthetic apparatus. EMBO Jurnal **20**, 3623-3630.

Xue H, Tokutsu R, Bergner SV, Scholz M, Minagawa J, Hippler M. 2015. Photosystem II subunit r is required for efficient binding of light-harvesting complex stress-related protein3 to photosystem II-light-harvesting supercomplexes in *Chlamydomonas reinhardtii*. Plant Physiology **167**, 1566-1578.

Zhao T, Wang W, Bai X, Qi Y. 2009. Gene silencing by artificial microRNAs in *Chlamydomonas*. The Plant Journal **58**, 157-164.

Supplementary data

Table S1: Nucleotide sequence of the primers used for RT-PCR analysis

Primers used for RT-PCR analysis on LHCBM1-9, RBCS2 (RIBULOSE-1,5-BISPHOSPHATE CARBOXYLASE SMALL-SUBUNIT) and CBLP (G-PROTEIN BETA SUBUNIT-LIKE POLYPEPTIDE) genes.

Gene	Forward sequence (5' -3')	Reverse sequence (5'-3')
LHCBM1	TGAGCGGTTTATTTGGGTCG	GGACCTTGCCTGCTGCAC
LHCBM2	TCGAGGCCTTCTTGACTTGAGT	CCACTTGATTCACCGGCAGT
LHCBM3	GCATTTGTTGCGTCTTTTTG	AAACGCTGCGGTTTAAAAAT
LHCBM4	TGCAGGCTTTTGTTTGCTATTG	CACACGCAACATTCGAGTCAGT
LHCBM5	GCTGATGGCAAATTATTTGGGT	GGAGATGGAAAGAAAACGCG
LHCBM6	GCAAAGGATGCCCTTGTAGT	GGAATGGGCTCTTCCCTAGT
LHCBM7	ATGTACTGGCGTGATTGAGC	AATCGCAAACCAACATACCA
LHCBM8	GCCTACGAGGATGCTGAGGAT	CACCCAGCGTTAGCCACTAGC
LHCBM9	AGGCCTTCTGGATGTACCAC	ATGGTTCTGGACACAACTGC
CBLP	CGTGGCTTTCTCGGTGGA	CGCCAATGGTGTACTTGCACT
RBCS2	CCTGCCTGGAGTTCGCTG	CCAGTAGCGGTTGTCGTAGTACAG

Table S2: Nucleotide sequence of the amiRNAs used and position on LHCBM4, LHCBM6 and LHCBM8 mRNAs.

Two different amiRNAs (LHCBM6A and LHCBM6B) were designed for silencing LHCBM6 gene while four different amiRNAs were designed for the simultaneous silencing of LHCBM4, LHCBM6 and LHCBM8 genes but just one (indicated in the Table) was effective in silencing the three selected genes. Hybridization energy between the amiRNA and its target is expressed as kcal/mole. The position of the mismatches is indicated in brackets and is relative to the reverse complement sequence of the amiRNA starting from the 5' nucleotide. The schematic position of the amiRNAs on the LHCBM mRNAs is shown in Figure S3.

Target	**amiRNA**	**amiRNA sequence**	**Position on mRNA**	**Hybridization energy**	**Mismatches**
LHCBM6	LHCBM6A	TTTGGAATGGGCTCTCCCCTA	3'UTR (1516-1536)	-41,31	1 (6)
LHCBM6	LHCBM6B	TAAGTGACCCAGGACAGGCAT	5'UTR (324-344)	-40,99	2 (7 and 21)
LHCBM4+6+8	LHCBM4+6+8	TAACTCAACGCCAGAGGTCTT	CDS (117-137 for *LHCBM4*; 543-563 for *LHCBM6*; 127-147 for *LHCBM8*)	-38.71	2 (5 and 21)

Figure S1: Fluorescence emission spectra of refolded recombinant LHCBM proteins.

Pigments connectivity on recombinant proteins refolded in vitro was evaluated by measuring the fluorescence emission spectra upon excitation of chlorophyll a (440nm), chlorophyll b (475 nm) and carotenoids (500 nm). Panel A: LHCBM1. Panel B: LHCBM2. Panel C: LHCBM4. Panel D: LHCBM6.

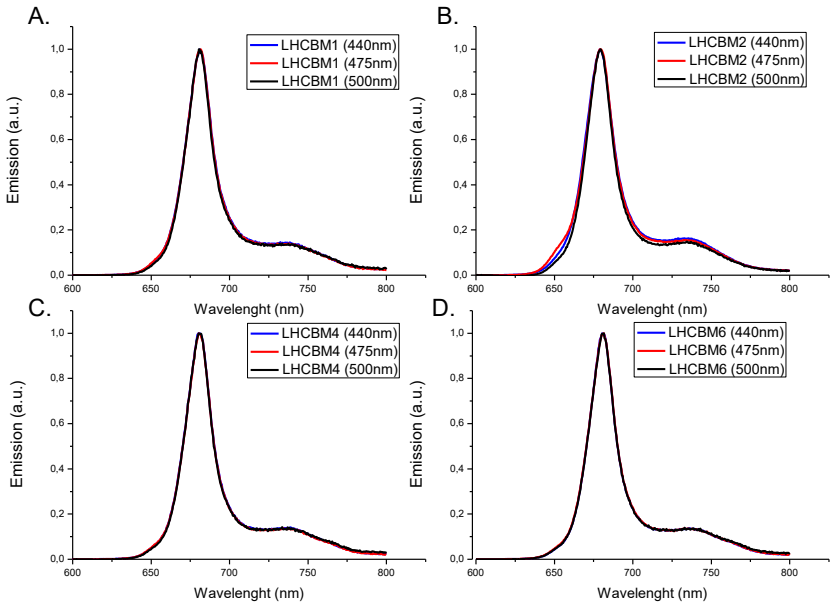

Figure S2. Evaluation of α-LHCII and α-LHCBM6 antibody cross reactivity.

α-LHCII and α-LHCBM6 antibodies were tested for their cross-reactivity against different LHCBM and CP26 and CP29 subunits. Recombinant LHCBM1, LHCBM2, LHCBM3, LHCBM4, LHCBM5, LHCBM6, LHCBM9, CP26 and CP29 apoproteins were overexpressed in E. coli and purified as inclusion bodies. 7µg of each apoproteins were loaded on SDS-PAGE gel for western blot analysis. Panel A and C reports the Red ponceau staining of filter used for immunoblotting. Panel B and D report the result of immunoblotting analysis using the antibody α-LHCII (Panel B) and α-LHCBM6 (Panel D).

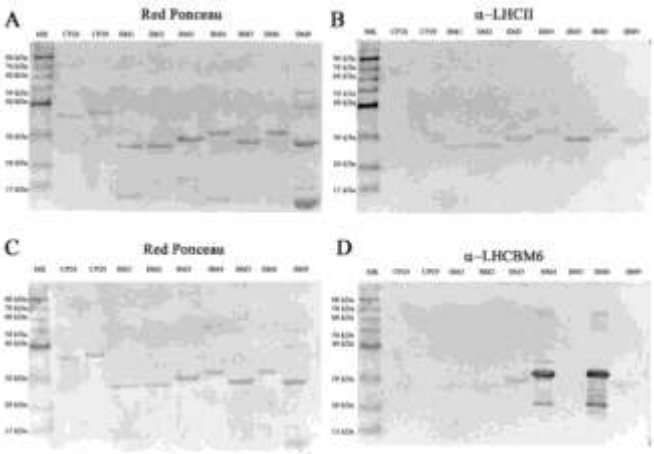

Figure S3 Determination of LHCBM4/6/8 abundance in thylakoid membrane.

The amount of LHCBM4/6/8 in thylakoid membranes was evaluated by immunoblotting reactions using the recombinant LHCBM4 or LHCBM6 proteins as reference. For comparison the same procedure was applied for LHCBM1 and total LHCII trimers using recombinant LHCBM1 and native LHCII purified from thylakoid membranes as reference. Panel A: immunoblotting reactions with the indication of the µg of chlorophylls (Chls) loaded in each lane. Panel B: amount of LHCII, LHCBM1 and LHCBM4/6/8 in thylakoid membranes expressed as the ratio between µg of Chls bound by LHC proteins per µg of Chls in thylakoid membranes. The determination of LHCBM4/6/8 amount was calculated using LHCBM4 ([a]) or LHCBM6 ([b]) as reference. Error bars indicate standard deviation (n=3).

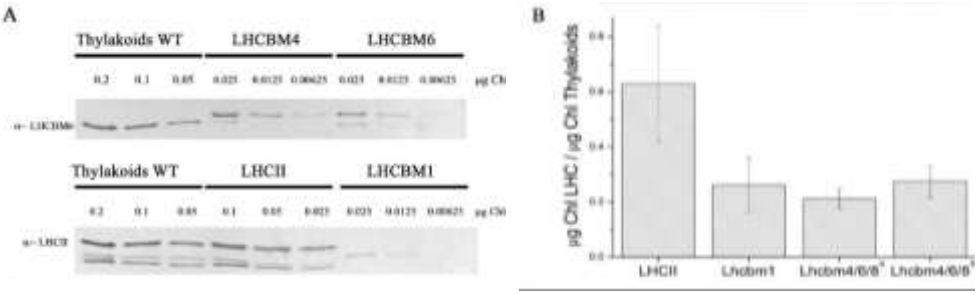

Figure S4 - Schematic maps of the constructs used.

A) Silencing cassette in the pChlamyRNA3 vector. This vector was engineered to express a 21 nucleotide silencing RNA. The PSAD promoter and terminator control the rate of amiRNA transcription. Two amiRNAs

(LCBM6A and LHCBM6B) were designed to silence LHCBM6 gene. One amiRNA (LHCBM4+6+8) of the four designed was effective in triggering silencing of LHCBM4, LHCBM6 and LHCBM8 genes. B), C) and D) Target regions of the amiRNAs on LHCBM4 (Panel B), LHCBM6 (Panel C) and LHCBM8 mRNAs (Panel D). For details on the amiRNAs sequence and features, see Table S1.

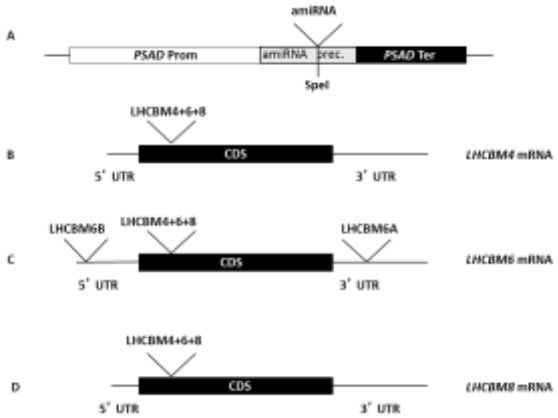

Figure S5: Determination of LHCBM mRNA level in WT and knock down strains.

mRNA level was quantified through quantitative Real Time RT-PCR on RNA extracts from cells of WT and knock down strains grown in minimal medium (HS) in control light condition. The amount of LHCBM mRNA level is expressed as a ratio with the mRNA of RBCS2 mRNA (ribulose -1, 5 - bisphosphate carboxylase/oxygenase small subunit 1 gene).

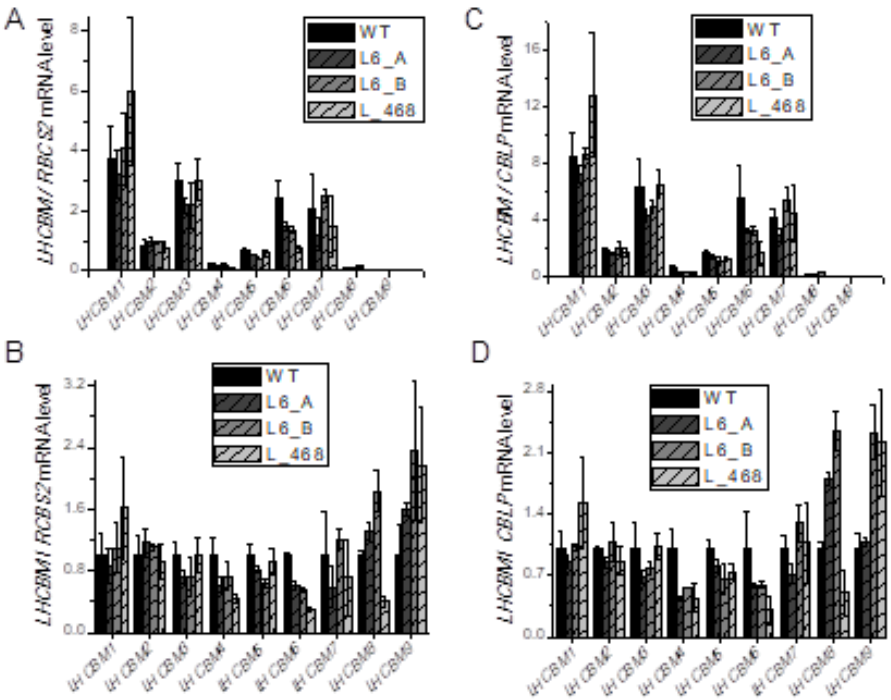

Figure S6. Chlorophylls, Photosystems and LHC distribution in 2D-PAGE.

The distribution of chlorophylls in CN-PAGE as Integrated Optical Density (IOD) is reported on the top of the figure. The distribution of immunoblot signal of PsaA, CP43, LHCII and LHCBM4/6/8 on 2D-PAGE is reported as IOD. The main composition of CN-PAGE spot is indicated on the base of immunoblot results.

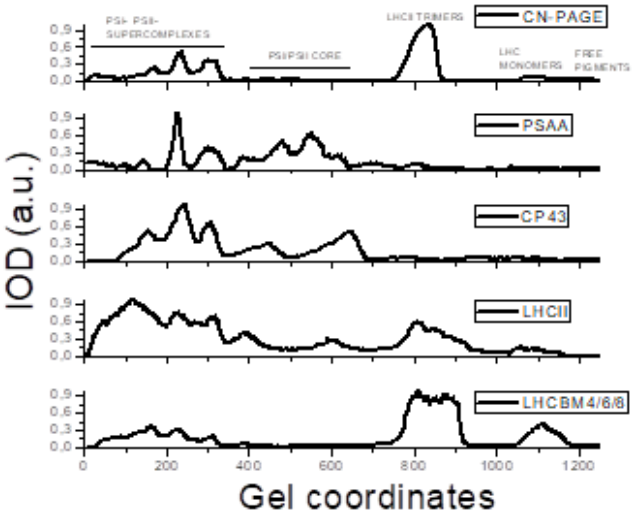

Figure S7. Fluorescence emission spectra at 77K of whole cells induced to state 1 or state 2.

C. reinhardtii cells were induced to state 1 or state 2 as described in the methods section. The 77K florescence emission in state 1 and state 2 were normalized to the 686 nm peak, related to PSII emission. The stt7 mutant was included as negative control.

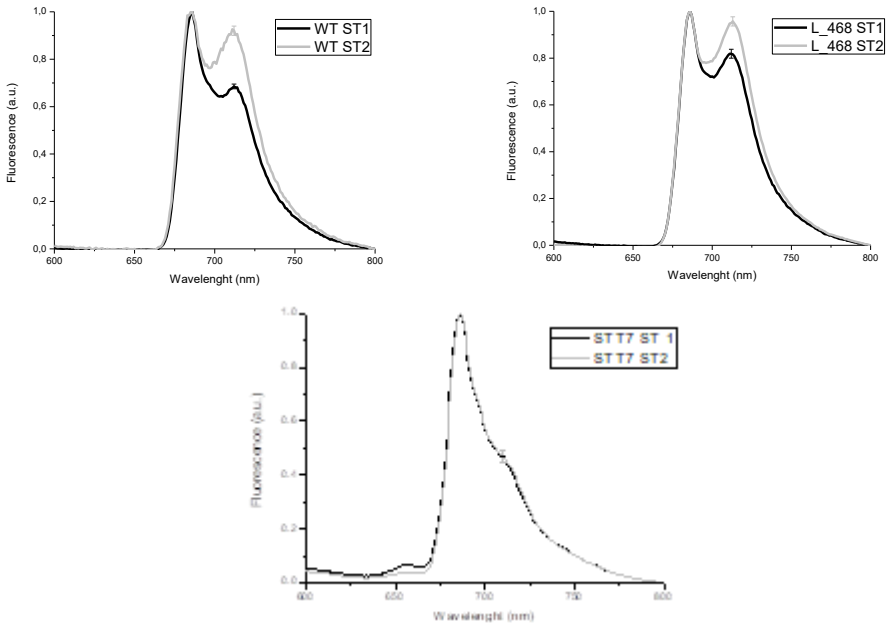

Figure S8. Correlation of NPQ values with LHCBM4/6/8, LHCBM1 or LHCSR content per PSII.

NPQ values measured for WT and silencing strains reported in Figure 8C were plotted as function of LHCBM4-6-8 (Panel A), LHCBM1 (Panel B) or LHCSR (Panel C) content per PSII calculated on the base of the western blot analysis reported in Figure 8D-E. Linear regression is reported for Panel A data, with Adjusted R^2 value of 0.84. Linear regression for data reported in Panel B or C was not successful with Adjusted R^2 values of 0.62 and -0.19 respectively.

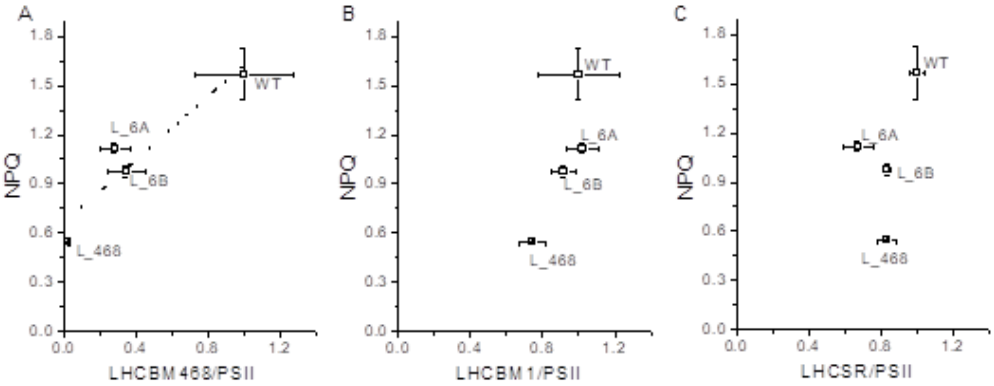

Figure S9. Analysis of the distribution of LHCBM4/6/8 and LHCSR3 protein in the thylakoids membrane by 2-D electrophoresis and immunoblotting.

Thylakoid membranes of knock-down strains acclimated to high light (400 µmol $m^{-2}s^{-1}$), were solubilized with 1% of dodecyl-maltoside (α-DM) and separated by a CN-PAGE followed by a second dimension separation by SDS-PAGE. Immunoblot detections of LHCSR (antibody α-LHCSR), LHCBM4/6/8 (antibody α-LHCBM6), PSI and PSII (antibody α-CP43) are reported.

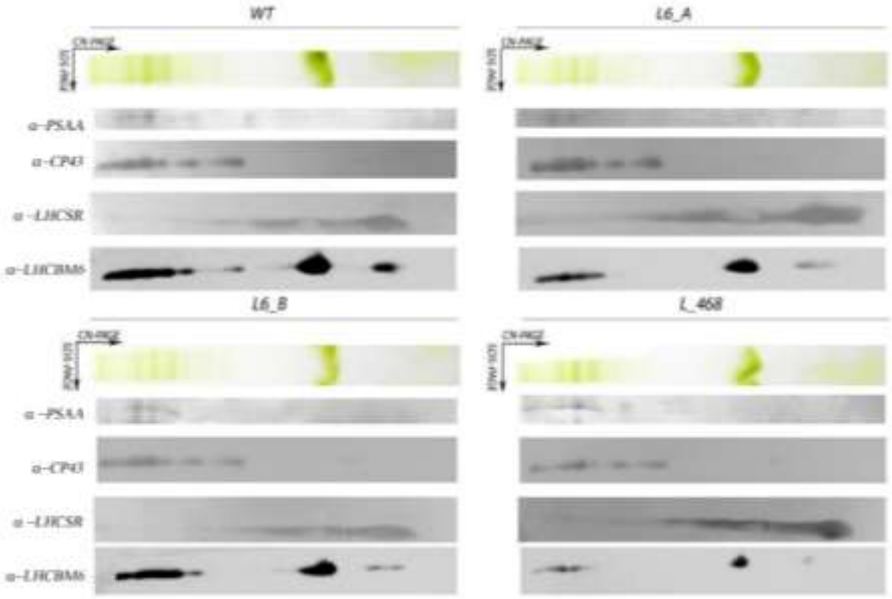

4.Chapter II

Photosynthetic adaptation to stress in commercial algae species

Section A

Chlorella vulgaris genome assembly and annotation reveal horizontal gene transfer from chloroplast to mitochondrial genomes and novel lipid biosynthetic pathways in the green lineage[3]

in this work we present the *Chlorella vulgaris 211/11P* nuclear and organelle genomes. *Chorella vulgaris* genome assembly was obtained by combining next generation sequencing and optical mapping of isolated DNA molecules. RNAseq data obtained in low or high light growth were used for genome functional annotation. Nuclear genome was assembled in 14 pseudo-molecules identifying 10746 genes with 11135 transcripts with the highest values of scaffolded genome and N50 compared to other green algal genomes. Functional annotation of nuclear, chloroplast and mitochondrial genome sequences highlighted peculiar features of *Chlorella vulgaris* previously unknown. Horizontal gene transfer from chloroplast to mitochondrial genome was observed and a single large gene encoding for a fungal/animal-like fatty-acid-synthase type I multi-subunit complex was revealed, which was not previously reported in the green lineage. Genes involved in motility and sexual reproduction were also identified. This knowledge will be useful in setting up genetic tools for biotechnological manipulation of *Chorella vulgaris* or for improving the productivity of other microalgae species.

In this work I've performed the experiments regarding the physiological characterization.

Abbreviations**:** CTAB, Cetyltrimethyl ammonium bromide; SMRT, Single-Molecule Real-Time; PFGE, Pulse-Field-Electrophoresis; SNVs, Single-Nucleotide Variants; GO, Gene Ontology; PSI/II, Photosystem I/II; NPQ, Non-Photochemical Quenching; LHC, Light Harvesting Complex;

---

[3]This section is based on the submeetted manuscript: Cecchin M, Marcolungo L, Rossato M, **Girolomoni L**, Cosentino E, Cuine S, Li-Beisson Y, Delledonne M, Ballottari M. *Chlorella vulgaris* genome assembly and annotation reveal horizontal gene transfer from chloroplast to mitochondrial genomes and novel lipid biosynthetic pathways in the green lineage.

Introduction

Photosynthetic conversion of light energy into chemical energy for CO_2 fixation is the primary process for biomass production in our planet. Photosynthetic derived products are not only the base of fossil fuels, nowadays used as the main energy sources for our society, but also potential sources of renewable biofuels. The improvement of photosynthetic biomass production is thus critical to meet the world demand for food and energy (Ort *et al.*, 2015). The improvement of photosynthetic efficiency is thus one of the major goals to increase biomass production (Ort *et al.*, 2015; Berteotti *et al.*, 2016; Kromdijk *et al.*, 2016; Kirst *et al.*, 2017). Among the organisms with the highest photosynthetic efficiency observed in real cultivation cases, microalgae scored efficiencies of 1-3%: although this is still significantly lower compared to their maximum potential of 9-11% (Walker, 2009), it highlighted the potential of microalgae for further improvement. In addition, unicellular microalgae are extremely interesting for biomass, food or biofuel production, since they can be cultivated in open ponds or in closed photobioreactors in none-arable land and in presence of waste products and wastewater-derived effluents as nutrients (Lum *et al.*, 2013). Biotechnological manipulation of microalgae in order to further boost biomass and metabolite productivity require however the availability of high-quality genomes and transcriptomes (Merchant *et al.*, 2007; Radakovits *et al.*, 2012; Vieler *et al.*, 2012; Ajjawi *et al.*, 2017; Roth *et al.*, 2017). This is especially critical considering the newly developed technology of genome editing methods (Naduthodi *et al.*, 2018). Among the many candidates of algal strains for biotechnological applications, a genus of considerable interest is *Chlorella* (Blanc *et al.*, 2010; Eckardt, 2010; Juneja *et al.*, 2016; Zuniga *et al.*, 2016; Sarayloo *et al.*, 2017; Arriola *et al.*, 2018). Several species of *Chlorella* have been proposed or used commercially over the past 40 years as a food and feed supplement for their fast growth and their high resistance to biotic and abiotic stresses (Lum *et al.*, 2013). *Chlorella vulgaris* is one of the most cultivated species at industrial level due to the high biomass yield and the possibility to grow either in autotrophic or mixotrophic conditions, in the latter case with the addition of reduced carbon source to further improve the biomass yield (Lv *et al.*, 2010; Zuniga *et al.*, 2016). The genome resources available for microalgae species in the *Chlorella* genus are however limited, with only few species having a genome available (Blanc *et al.*, 2010; Eckardt, 2010; Blanc *et al.*, 2012; Gao *et*

al., 2014; Roth *et al.*, 2017; Arriola *et al.*, 2018; Guarnieri *et al.*, 2018), leading in some cases to a different classification of the species analyzed (Darienko *et al.*, 2015). In the specific case of *C. vulgaris*, a fragmented genome of 113 scaffolds has been recently reported (Guarnieri *et al.*, 2018), which jeopardize an effective implementation of genome editing methods. Indeed, the reported *C. vulgaris* genome has been obtained only based on short-reads produced with Illumina sequencing, whose assembly is challenging and error-prone (Yoshinaga *et al.*, 2018). Moreover several questions remained unsolved, such as the presence of genes involved in sexual reproduction (Merchant *et al.*, 2007; Blanc *et al.*, 2010; Roth *et al.*, 2017) or the molecular basis for fatty acid biosynthesis (Vieler *et al.*, 2012; Alboresi *et al.*, 2016). In this work, in order to fully unravel the genetic information underlying *C. vulgaris* features, a combination of different sequencing technologies and optical mapping led to the reconstruction at nearly-chromosome level of the nuclear, chloroplast and mitochondrial genomes of *C. vulgaris* strain 211/11P as well as their functional annotation with the help of comparative RNA-seq analyses of strains grown under two most encountered conditions i.e. low light versus high light.

Materials and methods

Chlorella vulgaris cultivation

C. vulgaris (CCAP211/11P) cells were grown at 25°C in flask in the air with a white light in low (70 µmol m^{-2} s^{-1}) or high (1000 µmol m^{-2} s^{-1}) light with a 16h light 8h dark photoperiod photoautotrophically in BG-11 medium (Allen & Stanier, 1968).

Lipid, proteins and starch analysis

Considering the possession of a strong cell wall, Cells of *C. vulgaris* were first sonicated three times in a solution containing (1 ml EDTA 1 mM and acetic acid 0.15M). Sonicated cells were extracted following the method of Bligh and Dyer (BLIGH & DYER, 1959). Total lipid extracts were separated on thin layer chromatography and quantified for neutral or polar lipid content based on densitometry and the comparison to known amount of lipid standards (Siaut *et al.*, 2011). Proteins and starch content was analyzed in the harvested biomass as reported in (Cecchin *et al.*, 2018).

DNA extraction and quality control

DNA was extracted starting from 500 ml of a *C. vulgaris* liquid cultures with a cell density of $5x10^7$ cell/ml using the CTAB (Cetyltrimethyl ammonium bromide) extraction buffer. Extracted DNA was treated with 200 ug/ml RNAase A at 37°C for 20 min and subsequently purified with 1,8X AMpureXP beads (Agencourt). DNA purity and integrity were assessed at the Nanodrop 1000 spectrophotometer (Thermo Scientific) and by capillary electrophoresis on a 2200 TapeStation (Agilent Technologies), respectively. DNA quantification was performed with the Qubit dsDNA HS Assay kit (Life Technologies).

Illumina sequencing

DNA (500 ng) was fragmented by sonication using a Covaris S220 (Covaris) and DNAseq libraries were generated using the Truseq DNA kit according to manufacturer's instruction (Illumina). Library length was assessed by capillary electrophoresis on a 2200 TapeStation (Agilent Technologies) and quantified by qPCR using primers annealing on the adapter sequences. DNAseq libraries were sequenced on an Illumina HiSeq1000 platform generating 100bp paired-end reads for a total of 2.5 Gb.

PacBio sequencing

Genomic DNA (16 µg) was used for the preparation of two independent single-molecule real-time (SMRT) bell libraries according to the manufacturer's protocol (Pacific Biosciences; 20-kb template preparation using BluePippin (SageScience) size selection system with a 15-kb cut-off). Sequencing was performed at the Earlham Institute (Norwich, UK) on a PacBio RS-II platform (Pacific Biosciences, CA, USA) generating 6.4 Gb of SMRT data using PacBio P6-C4 chemistry.

BioNano Genome Mapping

High-molecular-weight DNA was extracted from the pellet of 2 L of cell culture with Optical $Density_{750}$= 5.3 corresponding approximately to a total of 3 grams. Cell wall was destroyed by grinding homogenization in liquid nitrogen. The grinded smoothie was resuspended in IrysPrep Plant Homogenization Buffer (Bionano Genomics) supplemented with 0,2% beta-mercaptoethanol and 1mM spermine-spermidine (HB+) and filtered through a 40 µm cell strainer. Nuclei were collected by centrifugation at

4500g for 20 min at 4°C. A centrifugation at 60g for 2 min at 4°C was used to remove debris, while nuclei were collected from the supernatant (3500g for 20min at 4°C). Nuclei were further purified by centrifugation over the IrysPrep Density Gradient (Bionano Genomics) at 4500g for 40 min at 4°C. Nuclei band (white layer) was collected from the gradient interphase and washed two times in HB+ and collected by centrifugation at 2500g for 20 min. Only the nuclei pellet (white band) was collected with a wide bore tip and carried on for washing after each centrifugation step. Nuclei were embedded in agarose plugs and high-molecular weight DNA was extracted as described by (Staňková *et al.*, 2016). The Mega-base size of extracted DNA was verified by Pulse-Field-Electrophoresis (PFGE). DNA (300 ng) was labeled and stained using the Nt.BspQI nicking endonuclease in combination with the –NLRS DNA labeling kit (Bionano Genomics). The nicked and labeled DNA was then loaded onto an IrysChip for imaging on the Irys system (BioNano Genomics) for a total of 3 run for 30 cycles in 1 flow cell. Molecules of <150 kb in length, label SNR < 2.75, label intensity > 0.6 and having less than 20 labels were removed. Bionano data were assembled into consensus genome maps using the BioNano Solve pipeline (v5678.6119rel) with RefAligner (v.6119).

Genome Assembly

C. vulgaris genome was assembled using FALCON (Chin *et al.*, 2016) v1.8.7. A second assembly run was performed using those 12% of PacBio subreads that did not align on the first assembly, applying more relaxed parameters. The two assemblies were merged.

PacBio subreads were aligned to the assembly using pbalign (v0.2.0.138342) and then GenomicConsensus package (v0.9.2) with Quiver algorithm was used to remove errors present in the consensus sequences. To further improve the genome quality a second polishing iteration was performed using the Illumina data, reads were aligned using BWA-MEM (0.7.15-r1140) and then we used Pilon (v1.22) to correct errors.

Hybrid assembly combining polished PacBio assembly with the Optical map was performed with the Bionano Solve Pipeline (v5678.6119rel), RefAligner (v.6119) using a merging-step P-Value of 1e-11 and a “Min alignment length and Max endoutlier” parameter of 80.

Organelle genome assembly

The Organelle genomes were assembled using Organelle_PBA pipeline (Soorni *et al.*, 2017). The sequences were then polished following the same approach used for the nuclear genome. The circularity was verified using an in-house developed script. The alignment between Falcon assembly and the organelle genomes was performed using blastn (v2.6.0). Those PacBio contig aligning to organelle genome with a similarity at least of 99% were manually removed.

RNA extraction and RNA-seq analysis

RNA was extracted from 500 ml of a *C. vulgaris* liquid cultures with a cell density of $7x10^7$ cell/ml. RNA quality and quantity were determined using a Nanodrop 2000 spectrophotometer (Thermo Scientific, Wilmington, DE) and a Bioanalyzer Chip RNA 7500 series II (Agilent, Santa Clara, CA), respectively. Directional RNA-seq library preparation was performed starting from 1 ug total RNA using the TruSeq RNA Sample Prep Kit v2 (Illumina Inc., San Diego, CA, USA) after capturing poly-adenylated transcripts. Library quality was assessed with a High Sensitivity DNA Kit on a 2200 Tape Station (Agilent, Wokingham, UK) and quantification of libraries was performed by qPCR using primers annealing on the adapter sequences. Libraries were sequenced with an Illumina NextSeq500 sequencer (Illumina Inc., San Diego, CA, USA) generating ~22 million 75bp paired-end reads per sample.

Gene annotation

Gene annotation of the nuclear genome was performed using the unsupervised RNAseq-based BRAKER1 pipeline, which takes advantage of two gene predictors: GeneMark-ET 4.32 and AUGUSTUS 3.0.3 (Specht *et al.*, 2011). Briefly, both RNA-seq data from the two different growth conditions, low light and high light, were used for the annotation. Quality of reads obtained from each sample was assessed using FastQC software (http://www.bioinformatics.babraham.ac.uk/projects/fastqc/) and reads with more than 10% of undetermined bases or more than 50 bases with a quality score <7 were discarded. Reads were then clipped from adapter sequences using Scythe software version 0.980 (https://github.com/vsbuffalo/scythe), and low-quality ends (Q score <20 on a 10-nt window) were trimmed with Sickle version 0.940 (https://github.com/vsbuffalo/sickle). The two RNAseq data above-mentioned were

merged and the alignment of reads to the assembled genome was performed using HISAT2 (https://ccb.jhu.edu/software/hisat2/index.shtml) version 2.0.1. Finally, the aligned RNA-seq reads were used as input for the BRAKER1 pipeline. Nuclear protein-coding genes were identified as beginning with a start codon (ATG) and ending with a stop codon (TAA, TGA, TAG). The quality and completeness of transcriptome was evaluated using BUSCO (Benchmarking Universal Single-Copy Orthologs, http://busco.ezlab.org/)(Simão *et al.*, 2015).

The web application GeSeq was used for the annotation of the organelle genomes with default parameters plus the tRNAscan-SE activated and selecting *Chlamydomonas reinhardtii* in the NCBI RefSeq database. Some genes were also manually curated based on RNAseq mapped reads.

Differential expression analysis

RNA-seq data were filtered as described in the previous section and aligned to the assembled reference genome with HISAT2 (v2.0.1). Differential expression analysis between the two growth conditions was conducted with DESeq2 (v 1.16.1) using the gene annotation generated.

Transcriptome functional annotation

Transcriptome functional annotation was performed by Blast2Go platform on the basis of the NCBI's RefSeq database (Conesa *et al.*, 2005). Annotated sequences were analyzed by KAAS (KEGG Automatic Annotation Server) platform to obtain KO annotation (Kanehisa & Goto, 2000; Kanehisa *et al.*, 2016; Kanehisa *et al.*, 2017). Transcripts differently expressed with KO annotation were visualized by KEGG Mapper platform, while the remaining transcripts functionally annotated were manually inspected by retrieving the function of the closest homolog gene.

Phylogenetic analysis

Phylogenetic analysis was performed by BUSCO analysis as previously reported (Waterhouse *et al.*, 2017). In particular, 111 single copy genes shared with other species which genome is available were used for protein alignment and phylogenetic tree construction. BUSCO 3.0.2 with the eukaryota_odb9 database and the genome of each species *Chlorella vulgaris, Chlorella protothecoides sp0710, Chlorella variabilis*

NC64A, Coccomyxa subellipsoidae, Chlamydomonas reinhardtii, Volvox carteri, Chromochloris zofingiensis, Arabidopsis thaliana, Micromonas pusilla CCMP1545, Ostreococcus tauri were used in order to identify the single-copy orthologous genes. Of these only those shared between the ten species were selected. For each protein a multiple alignment was performed among the species with MUSCLE 3.8.31 and then the alignments were concatenated. The tree was built using the web application Phylogeny.fr running PhyMl and TreeDyn for the construction and the visualization, respectively.

Subcellular localization prediction

Subcellular localization prediction was performed by using PredAlgo tool as previously described (Tardif *et al.*, 2012).

Data availability / Accession Numbers

The project of *C. vulgaris* genome sequencing is registered at NCBI under BioProject accession PRJNA495479. The genome assembly and transcriptome data are publicly available at NCBI under accession number xxxx and xxxx respectively. The accession numbers for the raw PacBio and Illumina reads are SRR8083355-SRR8083370.

Results

Chlorella vulgaris growth and biomass production

C. vulgaris strain 211/11P was grown photoautotrophically in low light (70 µmol m^2s^{-1}) or in high light (1000 µmol m^2s^{-1}) conditions, to evaluate its biomass productivity and composition. As shown in Figure 1, in high light the growth curves were faster compared to the low light case, reaching a higher cell density. Accordingly, the dry weight harvested when cell reached the stationary phase was higher for cells grown in high light compared to cell grown in low light. The two-fold increase in biomass accumulation observed in high light was mainly related to a strong increase in lipid accumulation. In particular, the TAG fraction of the total lipid in the cell was increased from 12% in low light to 79% in high light. Starch and protein content per cell were not significantly different in low light compared to high light, even if slightly increased in the latter.

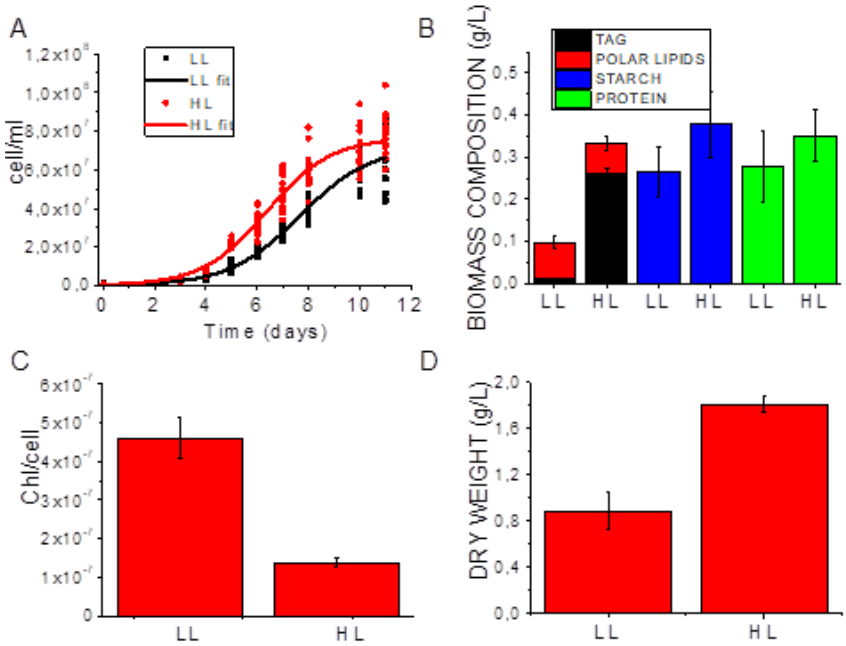

Figure 1. *Growth curves, productivity and biomass composition of Chlorella vulgaris in low light compared to high light. Panel A: growth curves of Chlorella vulgaris cells grown in low light (LL) and high light (HL) fitted by sigmoidal function. Panel B: biomass composition analysis in terms of lipids, proteins and starch. Lipid content are indicated as triacylglycerol (TAG) and polar lipids (PL). Panel C: chlorophyll (Chl) content per cell in LL and HL. Panel D: dry weight of total biomass harvested at the end of the growth curves reported in Panel A. Error bars are reported in terms of standard deviation (n=3).*

Development of a high-quality reference genome sequence of Chlorella vulgaris

Genome assembly of *C. vulgaris* strain 211/11P was obtained by integration of different genomic approaches displaying complementary features, i.e. PacBio producing long-reads, Illumina for accurate short-reads and Bionano optical mapping providing high scaffolding power. Genome sequencing analysis was conducted considering a genome of ~50Mb, as in the case of other *Chlorella* spp. High coverage (~128X) raw PacBio reads (Supplementary data, Table S1) were assembled into a draft genome assembly of 39.8Mb (Supplementary data, Table S2), consisting of 63 contigs with an average contig length of 613Kb and N50 of 1.8 Mb. In order to improve the quality of the assembled genome, Illumina paired-end reads (~50x, Supplementary data, Table S1), as well as raw PacBio reads, were aligned to the PacBio-based assembly to correct sequencing errors: 2995 single-nucleotide variants (SNVs) and 32631 small insertions and deletions (InDel) were corrected, while the remaining 81 SNV and 190 InDel account only for the

0.0007% of the reconstructed genome (Supplementary data, Table S3). The resulting polished PacBio-based contigs were anchored into a nearly chromosome-scale assembly by integrating optical mapping data (~1400X) obtained using the Bionano Genomics technology (Supplementary data, Figure S1, Table S1). As reported in Supplementary data, Table S1, the integration of Bionano data resulted into a genome assembly where 26 of the contigs obtained from PacBio data were anchored into 14 scaffolds (Figure 2) with an N50 value of 2.8Mb and the longest scaffold of 5.4Mb.

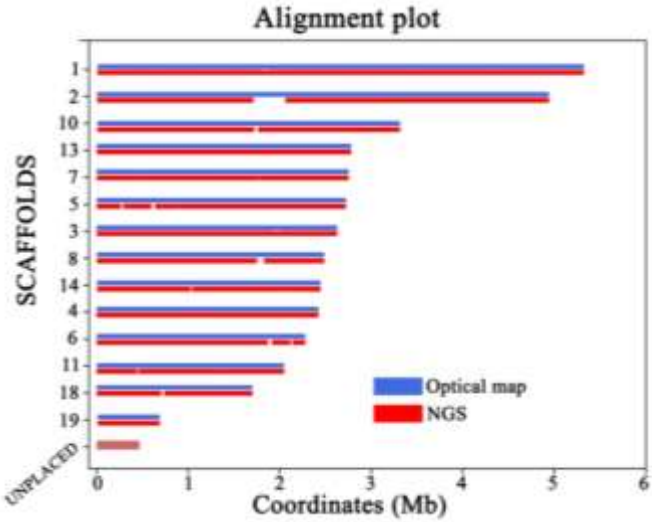

Figure 2. *Assembled Chlorella vulgaris CCAP211/11P nuclear genome. Chlorella vulgaris genome was assembled in 14 pseudo-molecules on the base of integration of next generation sequencing (NGS) and optical maps as described in the main text. The resulting gaps in the assembled genome are reported as white spaces in the NGS data. Unplaced contigs are reported representing 1.2% of the Chlorella vulgaris genome.*

These scaffolds contained 98.9% of the assembled *C. vulgaris* genome, i.e. the highest percentage as compared to other algal genomes available (Table 1), while the remaining 37 unplaced contigs counted only for the <1.11%. Eight unplaced contigs were identified by subsequent manual analysis as part of the chloroplast and the mitochondrial genomes and they were therefore removed from the nuclear genome assembly. The generated assembly represents a greater than 100-fold improvement in contiguity compared with the previously published assembly of *C. vulgaris* (Supplementary data, Table S4) and it has the highest N50 among other algal genomes of similar size as *Chromochloris zofingiensis* (Roth *et al.*, 2017) and *Chlorella variabilis* (Blanc et al., 2010) (Table 1).

	Chlorella vulgaris CCAP211/11P	*Chromochloris zofingiensis*	*Chlamydomonas reinhardtii* (v5.5)	*Chlorella variabilis* NC64A	*Nannochloropsis gaditana* B-31
Sequenced genome size	40Mbp	57 Mbp	107 Mbp	46.2 Mbp	26.3 Mbp
Genome technologies	PacBio + BioNano + Illumina	PacBio + OpGen + Illumina	Sanger + 454 + BAC + genetic map	Sanger WGS	454 + SOLiD + BAC
N° scaffold	14	19	17 chromosomes	30	21
% scaffolded genome	98.9%	95.4%	98.2%	89%	92.2%
Scaffold N50	2.8Mbp	\\	7Mbp	1.5 Mbp	1 Mbp
% G+C	61%	51%	64%	67%	54.2%
N° genes	10903	15274	17741	9791	10646
Exon average length (bp)	194	291	261	170	449
Intron average Length (bp)	207	267	269	209	178
Ave Exons Per transcript	8.12	5	8.5	7.3	2.71

Table 1. *Comparison of Chlorella vulgaris CCAP211/11P genome with other known microalgae genomes.*

Chlorella vulgaris nuclear genome annotation and phylogenetic analysis

Identification of genes present in the assembled *C. vulgaris* genome was performed by integration of RNAseq data with gene predictions tool. Directional RNAseq data obtained from *C. vulgaris* cells cultivated in low light and high light conditions were integrated into the gene annotation pipeline. Conditions of different irradiances were selected to extend the range of possible gene expressed. Genome annotation identified 10903 protein-coding genes, coding for 11262 transcripts with an average length of 3062bp and 8.12 exons per gene on average (Table 1). The number of protein-coding genes is a significantly higher compared to the previous genome presented for *C. vulgaris*, where only 7100 transcripts were predicted (Guarnieri *et al.*, 2018). The gene models predicted for *C. vulgaris* allowed to determine its codon usage (Supplementary

data, Table S5), which is similar to the codon usage of *C. reinhardtii* (Merchant *et al.*, 2007).

To further evaluate the transcriptome quality and completeness, BUSCO analysis was performed on a benchmark of 303 genes putatively found in all eukaryotes in single copy: this analysis identified complete information for 289 (95.4%) of orthologs and fragmented information for 3 (1%), while only 11 genes (3.6%) were missing, demonstrating a high completeness of the *de novo* assembled genome. Furthermore, when the mRNAseq libraries were aligned to the genome assembly, 85.58±0.32% of reads aligned uniquely (mean ± SD, n = 6) and an additional 11.81±0.37% aligned to multiple locations, indicating that the genome assembly covered nearly all coding genes.

Functional genome annotation performed by BLAST2GO analysis reported 5642 associated to Gene Ontology (GO) Terms (Figure 3).

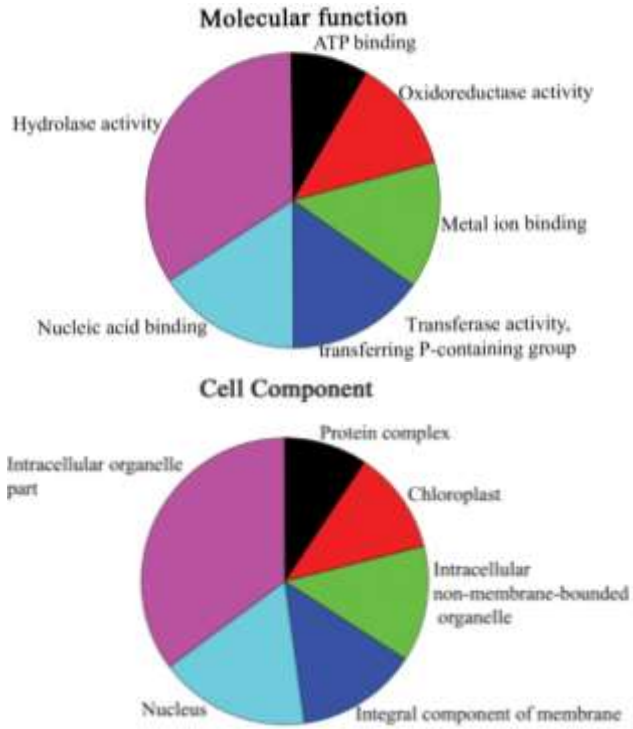

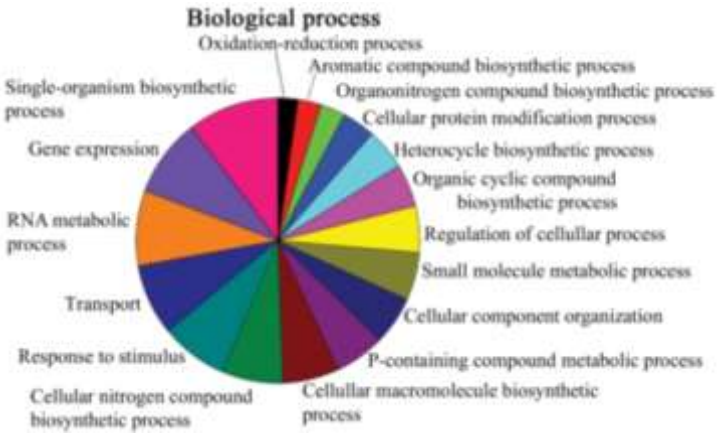

Figure 3. *Gene Ontology classification of annotated Chlorella vulgaris genes. Gene Ontology (GO) terms. Chlorella vulgaris transcripts annotated by blast2Go were functionally grouped on the basis of Gene Onthology (GO) terms cellular component (a), molecular function (b) and biological processes (c). The distribution of the different groups is reported based on the node score associated to each group considering GO term with node score higher than 1%.*

As reported in Supplementary data, Figure S2, considering the top-hit species distribution most of the *C. vulgaris* gene (~71% of the total genes) were annotated with genes from *Chorella variabilis*, followed by *Auxenochlorella prototechoides* and *Coccomyxa subellipsoidea*. Functional annotation of *C. vulgaris* genome was then exploited for the analysis of the phylogenies of the 211/11P strain. In particular, 111 single copy genes shared with other species which genome is available were used for protein alignment and phylogenetic tree construction. As reported in Supplementary data, Figure S3 *C. vulgaris* strain 211/11P resulted to be closer to other species from the *Chlorella* genus as *C. varabilis* and *C. prototechoides* (Supplementary data, Figure S3).

Chloroplast and mitochondrial genomes

Chloroplast and mitochondrial genomes were independently assembled and annotated using PacBio data. Complete (circular with no gaps or ambiguous nucleotides) chloroplast genomes of *C. vulgaris* was reconstructed using *C. reinhardtii* chloroplast genome as reference for both assembly and annotation. The chloroplast genome resulted to be 165.504bp with 127 genes encoded (Figure 4).

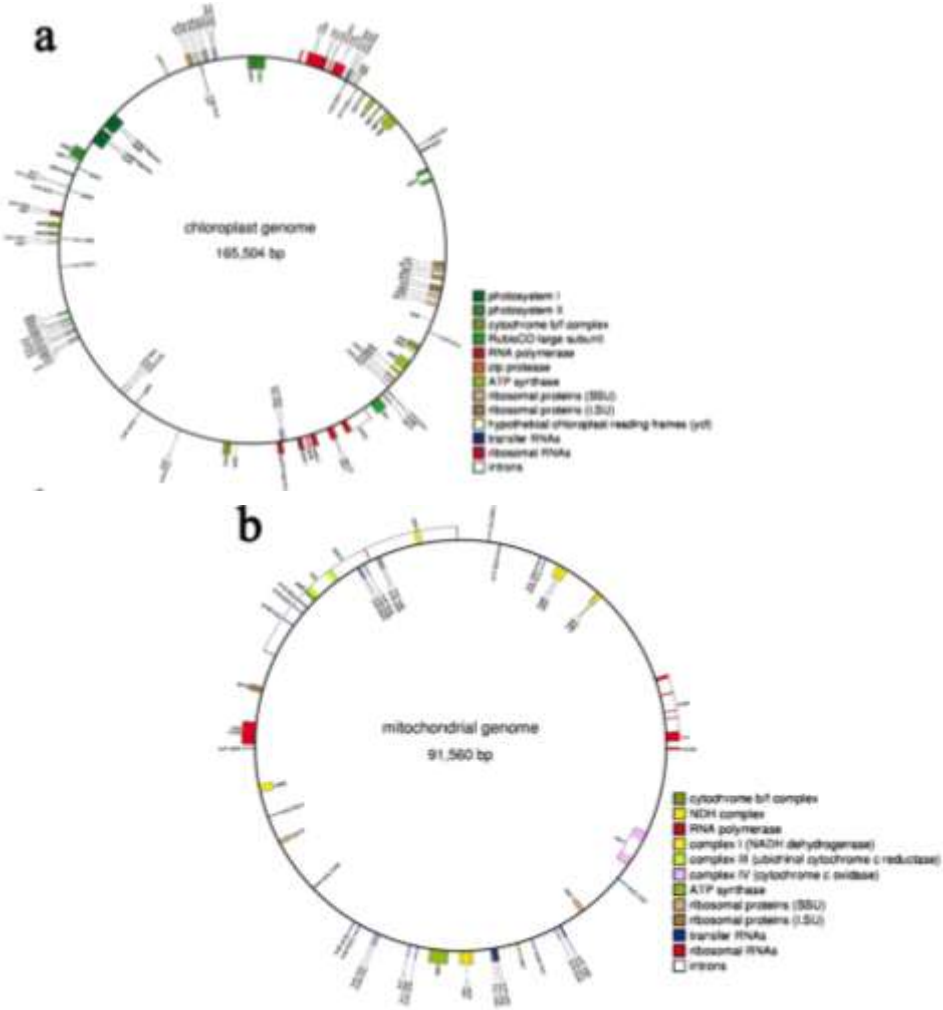

Figure 4. *Chlorella vulgaris chloroplast and mitochondrial genomes. Chloroplast (a) and mitochondrial (b) Chlorella vulgaris genomes assembled from PacBio data. Annotated genes are reported.*

The overall CG content of the chloroplast genome is 32% and the coding sequence is 3.5%. Among the genes found in the chloroplast genome 6 genes encode for rRNA, 18 for ribosomal proteins, 46 genes encode for tRNA, 7 genes are component of RNA polymerase and 2 genes encode for a translation initiation factor (*infA*) and a protein elongation factor Tu (*tufA*). Then 33 genes were identified encoding for subunits of the complexes involved in the light phase of photosynthesis (PSI, PSII, cytochrome b6f and ATP synthase) and a gene for the large subunit of RUBISCO was also identified. In the case of *psaA* and *psaB* genes a second gene was also identified in the chloroplast

genome encoding in both cases for a fragment of the PsaA or PsaB proteins. The presence of gene fragments in the *C. vulgaris* chloroplast genome remind the fragment present in higher plants mitochondrial genome encoding for subunits of NDA complex which are then trans-spliced to generate the mature transcript encoding the full-length protein (Knoop *et al.*, 1991). The role of these gene fragments needs to be further investigated by dedicated experiments. Among the other genes present in the *C. vulgaris* chloroplast genome *ycf1-4* were identified with the *ycf3* and *ycf4* involved in PSI assembly (Boudreau *et al.*, 1997). Genes involved in plastid division as minD and minE were also found in the chloroplast genome, as previously reported for other *Chlorella* species (Wakasugi *et al.*, 1997). Interestingly, three introns were identified in genes *psbA*, *rpoC2* and *rrnL3* as previously reported in the case of *C. reinhardtii* (Maul *et al.*, 2002) .

C. vulgaris mitochondrial genome was entirely reconstructed as having 91.560bp size with 52 genes encoded (Figure 4). The large size of *C. vulgaris* mitochondrial DNA is consistent with the mitochondrial genomes of other green algae *as C. zofingensis* or higher plants, but significantly larger than the mitochondrial genome of the model organism for green algae *C. reinhardtii* (Denovan-Wright *et al.*, 1998; Roth *et al.*, 2017). The increased size of *C. vulgaris* mitochondrial genome is largely due to the high level of non-coding sequences. Among the genes in the mitochondrial genome, five genes encode for rRNA and 30 for tRNA, while three genes encode for ribosomal proteins. Nine genes encoding the Complex I, and 2 genes for Complex III and IV subunits (*cob* and *cox1* respectively) were also identified together with a gene for alpha subunit of mitochondrial ATP synthase. Interestingly, some chloroplast genes as *petD* and *rpoC2* were found also in the mitochondrial genome, even if not expressed (*petD*) o with a low expression profile (*rpoC2*). This result suggests an uncommon horizontal gene transfer from chloroplast to mitochondrial genome in *Chlorophyta* which was previously reported only upon land colonization (Wang *et al.*, 2007; Gandini & Sanchez-Puerta, 2017).

Identification of genes involved in key metabolic pathways

The functional annotation of the *C. vulgaris* genome allowed for identification of genes coding for the key enzymes involved in the different metabolic pathways of the cell, such as glycolysis, gluconeogenesis, TCA and glyoxylate cycle, photosynthesis, lipid

and pigment metabolism (Supplementary data, Table S6-7). In the following sections genes involved in some critical metabolic pathways and cellular functions are described in detail.

Photosynthesis

All genes encoding subunits of the membrane complexes or soluble electron carriers involved in the light phase of photosynthesis are present in the *C. vulgaris* nuclear or chloroplast genomes (Supplementary data, Table S6). Genes encoding for PSII core subunits were identified in the chloroplast and nuclear genome, in agreement with previous data reported for *A. thaliana* and *C. reinhardtii* (Daniell *et al.*, 2016). Only in the case of *psbX* gene, no homologous gene could be found in *C. vulgaris* genome. PSBX subunit has been reported previously in higher plants and in some algae: even if antisense genotypes on this subunit in *A. thaliana* or knockout mutants in cyanobacteria were characterized by a 30-40% reduction of PSII accumulation, no growth phenotype was reported, suggesting this subunit is not essential for PSII assembly and function (Shi *et al.*, 2012).

In the case of PSI complex, all the core subunit could be identified with the exception of PsaM and PsaX: PsaM has been previously reported in cyanobacteria, in some green algae, mosses and gymnosperms but not angiosperms, while PsaX has only been found in cyanobacteria (Scheller *et al.*, 2001). Different genes were identified in *C. vulgaris* genome encoding for Light Harvesting Complexes (LHC), the pigment binding antenna proteins bound to the periphery of Photosystems devoted to light harvesting and photoprotection . While both LHCII and LHCI type complexes could be identified, being bound to PSII and PSI respectively, no gene coding for a LHCB6 (CP24) like protein was found, supporting that this PSII antenna proteins appeared only in land plant, in agreement with previous finding (Kouřil *et al.*, 2016).

Interestingly both the LHC-like subunits PSBS and LHCSR were found in *C. vulgaris* encoded by single genes: these subunits are involved in the photoprotective mechanism known as Non-photochemical Quenching (NPQ), where a significant portion of the excitation energy absorbed by photosystems is thermally dissipated confirmatory experiments. Protein subunits reported in *C. reinhardtii* to be involved in alternative chloroplast electron transport pathway as PGR1, PGR5 and NDH, involved in cyclic electron flow and PTOX involved in chlororespiration (Rumeau *et al.*, 2007) are present

in the *C. vulgaris* genome but not differently expressed in low light or in high light. (Li *et al.*, 2000; Peers *et al.*, 2009). Differently from *C. reinhardtii*, where LHCSR subunits are strongly overexpressed in high light (Peers *et al.*, 2009), LHCSR in *C. vulgaris* is constitutively expressed either in low light or high light grown cells. Also, in the case of PSBS *C. vulgaris* behaves differently compared to *C. reinhardtii*, since in the latter PSBS is transiently overexpressed in UV or high light condition (Allorent *et al.*, 2016; Correa-Galvis *et al.*, 2016; Tibiletti *et al.*, 2016), while in *C. vulgaris* the *psbs* gene is always expressed but upregulated in high light, as in the case of *A. thaliana* (Ballottari *et al.*, 2007). These results suggest a different regulation of NPQ in *C. vulgaris* compared to *C. reinhardtii*, even if the potential role of LHCSR and PSBS in NPQ induction in the former require additional

In the case of enzymes involved in the dark phase of photosynthesis and carbon fixation, all the different subunits previously reported to be involved in this pathway have been identified (Supplementary data, Table S6). Interestingly according to KEGG Mapper tool, all the enzymes required for a C4-like carbon fixation pathway are present in the *C. vulgaris* genome (Supplementary data, Figure S4), with the key enzyme involved in carbon fixation in C4 compounds, phosphoenolpyruvate carboxylase (PPC), encoded by two genes, g3928 and g4635, being predicted in the cytosol and in the mitochondria respectively. These two isoforms of PPC might have a role in oxaloacetate formation in the anaplerotic reactions, or for gluoconeogenesis or as alternative carbon fixation to RUBISCO, as previously suggested in the case of *C. sorokiniana* (Cecchin *et al.*, 2018).

Carotenoid biosynthesis

Carotenoid biosynthetic genes were identified in the *C. vulgaris* genome and reported in Supplementary data, Table S6. Each of the genes involved in carotene and xanthophyll biosynthesis was found in single copy and most of them overexpressed in high light, in agreement with the increased carotenoid content per cell identified in this condition. Interestingly a gene coding for neoxanthin synthase could be identified, catalyzing the synthesis of neoxanthin from violaxanthin (Dall'Osto *et al.*, 2007), while this enzyme has not been identified yet in the model organism for green algae *C. reinhardtii*. Differently, in the *C. vulgaris* genome no gene coding for a beta-carotene ketolase (BKT) was identified. This is the key enzyme together with a hydroxylase (CRTZ) for astaxanthin biosynthesis from beta-carotene or zeaxanthin in different algal species known to

accumulate astaxanthin as *Haematococcus pluvialis* or *C. zofingensis* (Zhong *et al.*, 2011). While CTRZ is present in *C. vulgaris*, the absence of BKT in *C. vulgaris* explains the absence of astaxanthin in this organism and suggests for a possible biotechnological manipulation of this species to induce the accumulation of this carotenoid with a high value on the market.

Lipid biosynthesis

De novo fatty acid biosynthesis occurs in plant cells mainly in the chloroplast catalyzed by Fatty Acid Synthase type II (FAS2) multi-subunit complex, while animals and fungi possess FAS type I complexes (FAS1) located in the cytosol which appear as large multi-enzyme complexes on one or two large polypeptide chains (Alboresi *et al.*, 2016). *C. vulgaris* genes involved in lipid metabolism are reported in Supplementary data, Table S7. All genes encoding key enzymes required for fatty acid biosynthesis were identified in *C. vulgaris* genome, with subunits of acetyl-CoA carboxylase being encoded by the nuclear or chloroplast genome. Intriguingly, in addition to genes coding for FAS type II subunits, a single large gene encoding for FAS type I multisubunit complex was also identified (g276). The gene is 55Kbp and contains all the different protein domains required for fatty acid biosynthesis (Figure 5).

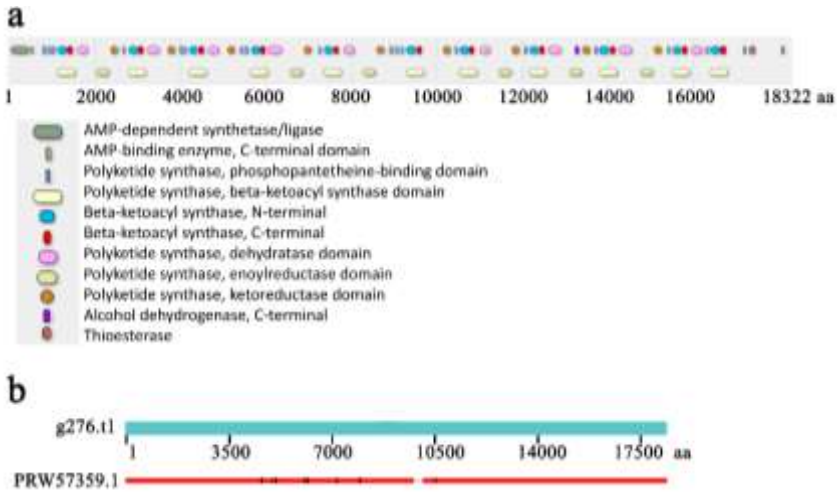

Figure 5*. Schematic organization of the FAS1 gene identified in Chlorella vulgaris. Different catalytic domains encoded in the Chlorella vulgaris gene g276.t1 are reported in Panel a. Gene size is 55Kbp and it contains all the different domains required for fatty acid biosynthesis. Panel b: schematic alignment of Chlorella vulgaris gene g276.t1 and Chlorella sorokiniana gene PRW57359.1.*

The occurrence of FAS1-like complexes in algal cell have already been suggested in the oleaginous species *Nannochloropsis oceanica* and *Nannochloropsis gaditana* (Vieler *et al.*, 2012; Alboresi *et al.*, 2016), but not yet in the green lineage. BLAST search of *C. vulgaris* g276 gene for other putative FAS1-like multi-domain gene gave only one positive result with a gene from *C. sorokiniana* which displays similar size and features (Figure 5). This result demonstrates the presence in *C. vulgaris* and possibly also in *C. sorokiniana* of dual fatty acid biosynthetic pathways, one which is the plant-like fatty acid biosynthetic pathway in the chloroplast and the second one peculiar of fungal and animal cells located in the cytosol.

Consistent with the increased lipid accumulation observed in *C. vulgaris* grown in high light conditions, the transcriptions of the genes coding for enzymes involved in lipid metabolism were altered: despite no changes in genes involved in polar membrane lipid synthesis and TAG assembly, genes encoding enzymes involved in earlier steps of de novo fatty acid synthesis, the formation of G3P and TAG packaging were upregulated in high light (Supplementary data, Table S7). Among the highly upregulated genes is a gene coding acetyl-CoA synthetase (ACS). ACS is involved in the pyruvate dehydrogenase bypass pathway, by which acetyl-CoA is produced by glycolytic pyruvate through the intermediates acetaldehyde and acetate (Lin & Oliver, 2008). The importance of ACS enzymes in lipid biosynthesis in plant cells has been demonstrated in *A. thaliana*, where mutations on *acs* genes caused a strong reduction in plant fitness (Lin & Oliver, 2008). Two genes coding for ACS enzymes were identified in *C. vulgaris*, g2176 and g2145, the former being predicted in the cytosol, while the latter in the chloroplast: only the gene encoding the cytosolic ACS was upregulated in high light, suggesting an upregulation of cytoplasmic biosynthesis of fatty acids in high light as previously reported in the case of *N. gaditana* (Alboresi *et al.*, 2016).

High light adaptation caused the increased accumulation of several plastid (PLAP/fibrillin) lipid associated proteins: these subunits have been reported to be involved in the formation of lipid droplets observed in cells accumulating neutral lipids or carotenoids (Youssef *et al.*, 2010), which are both strongly increased in high light in *C. vulgaris.* Increased lipid accumulation in *C. vulgaris* in high light can thus be related to increased precursor production (acetyl-CoA) by ACS in the cytosol for FAS1 enzymatic complex and increased stabilization of lipids produced in the chloroplast by interaction with PLAP/fibrillin subunits.

Identification of genes involved in meiosis and motility

C. vulgaris strains has been usually described as non-motile and asexual. To go deeper into details, genes previously reported to be associated to meiosis event and motility were searched in *the C. vulgaris* genome. As reported in Supplementary data, Table S6 the main genes involved in meiosis (Malik *et al.*, 2007) are present and transcribed in *C. vulgaris* genome, as previously reported for other green algae as *C. zofingensis* (Roth *et al.*, 2017) or *C. variabilis NC64A* (Blanc *et al.*, 2010) where sexual reproduction is cryptic and not well defined. This result suggests a possible sexual reproductive stage also in *C. vulgaris* with gamete formation. In agreement with these finding a gene in the *C. vulgaris* genome encoding for gametolysin was found (g3347), together with a gene encoding for a protein containing a domain with putative CGS1/HAP2 function, which is essential for cell fusion (Blanc *et al.*, 2010; Wong & Johnson, 2010) (Supplementary data, Figure S5). The genes involved in motility were then investigated looking for genes present in the CiliaCut list, a group of genes identified in *C. reinhardtii* involved in formation of sensory or motility cilia and flagella (Merchant *et al.*, 2007). Among the 195 genes in the CiliaCut list 114 genes were identified also in *C. vulgaris (*58.4%). In particular, 78.2% of the genes in the CiliaCut present in the diatom *Thalassiosira pseudonana* are present also in *C. vulgaris* (Supplementary data, Table S8): 84.2% of the *T. pseudonana* genes in the MotileCut (genes in the CiliaCut involved in motile flagella functions) are present also in *C. vulgaris.* This result suggests that *C. vulgaris* might be able to form gametes with motile flagella as previously observed for *T. pseudonana* during gametogenesis (Moore *et al.*, 2017).

Discussion

Integration of highly-accurate next generation sequencing data (Illumina) with third generation long-read sequencing (PacBio) and next-generation mapping (Bionano Genomics) allowed to obtain the assembled genome of *C. vulgaris* in 14 scaffolds with a relatively good N50 of 2.8Mb, with a 100-fold improvement compared to the recently released *C. vulgaris* genome (Guarnieri *et al.*, 2018) (Supplementary data, Table S4). We can speculate that the 14 pseudo-molecules reconstructed may represent the chromosomes of *C. vulgaris*, with 98.9% of scaffolded genome, a much higher percentage compared to all other available genomes of green algae (Table 1). The *C. vulgaris* genome size of 40Mbp is consistent with that of other members of the *Chlorella*

genus or closed related species (Table 1). The GC content of the *C. vulgaris* genome is similar compared to *C. variabilis* or *C. reinhardtii*, but higher compared to *C. zofingensis*. The integration of RNAseq data allowed to obtain a detailed functional annotation of the assembled *C. vulgaris* genome, revealing a number of transcripts and proteins consistent with the data reported for *C. variabilis*, but almost halved compared to *C. reinhardtii* or *C. zofingesis*, revealing a strong variability in the green lineage. For comparison, in the case of the microalga *Nannochloropsis gadiatana* (Heterokonta) with a much smaller genome (23Mbp) a similar protein number compared to *C. vulgaris* was observed. Interestingly, exon and intron average length and the number of exons per transcript were similar compared to another member of the *Chlorella* genus, *Chlorella varibilis NC64A*, but smaller compared to *C. reinhardtii* or *C. zofingensis* (Table 1).

The results obtained by genome assembly and functional annotation revealed the presence of some peculiar features in *C. vulgaris*. In particular evidences for horizontal transfer from chloroplast to the mitochondria could be found in the organelle genomes as in the case of genes *petD* and *rpoC2*, while usually the opposite was found in the *Chlorophyta* (Smith, 2014). Chloroplast gene or gene fragments was indeed previously observed only in mitochondria of higher plants, attributing the earlier event of plastid to mitochondria horizontal gene transfer to the common ancestor of extant angiosperms and gymnosperms: the analysis of *C. vulgaris* genome demonstrate that this horizontal gene transfer can found also in some *Chlorophyta*, but not in the model organism for green algae *C. reinhardtii* (Wang *et al.*, 2007). The possible functions of plastid gene in mitochondrial genome is still not clear, being usually not expressed (Wang *et al.*, 2007). In the case of *C. vulgaris*, the plastid gene *rpoC2* found in the mitochondrial genome presented a low expression profile: this gene encodes for a RNA polymerase beta subunit (Shimada *et al.*, 1990), but further experiments are required in order to investigate its possible role in mitochondrial gene expression.

The analysis of *C. vulgaris* genome revealed several features in common with higher plants, but different from the model organism for green algae, *C. reinhardtii*, as for instance mitochondrial genome size. Considering the genes involved in photoprotection and regulation of light use efficiency a mixed situation compared to higher plants and other green algae was found in *C. vulgaris*: *psbs* and *lhcsr* genes were found being expressed even in low light, with only the former upregulated in high light. LHCSR subunits have been reported to be critical for the regulation of the photosynthetic

efficiency and photoprotection in microalgae, being overexpressed in high light, while PSBS has a similar function and regulation in higher plants, but it has been reported to be only transiently expressed in *C. reinhardtii*: in *C. vulgaris lhcsr* gene is similarly expressed in low and high light, while *psbs* gene is constitutively expressed and upregulated in high light, adding further evidences about the strongly debated role of PSBS protein also in green algae and not only in higher plants. Finally, in the *C. vulgaris* genome a cytosolic fatty acid synthase (FAS) with common traits compared to animal or fungal FAS type I was found. This gene has not been observed yet in the green lineage, revealing a potential additional pathway in parallel to the chloroplast pathway for fatty acid biosynthesis.

In conclusion, the assembly and functional annotation of *C. vulgaris* genome allowed the identification of potential targets for the biotechnological manipulation of this organism, for its exploitation for biomass and high value products or for transferring peculiar *C. vulgaris* properties to other species.

References

Ajjawi I, Verruto J, Aqui M, Soriaga L, Coppersmith J, Kwok K, Peach L, Orchard E, Kalb R, Xu W, et al. 2017. Lipid production in *Nannochloropsis gaditana* is doubled by decreasing expression of a single transcriptional regulator. Nature Biotechnology **35**(7): 647-+.

Alboresi A, Perin G, Vitulo N, Diretto G, Block M, Jouhet J, Meneghesso A, Valle G, Giuliano G, Maréchal E, et al. 2016. Light Remodels Lipid Biosynthesis in *Nannochloropsis gaditana* by Modulating Carbon Partitioning between Organelles. Plant Physiology **171**(4): 2468-2482.

Allen MM, Stanier RY. 1968. Growth and division of some unicellular blue-green algae. Journal of General Microbiology **51**(2): 199-202.

Allorent G, Lefebvre-Legendre L, Chappuis R, Kuntz M, Truong TB, Niyogi KK, Ulm R, Goldschmidt-Clermont M. 2016. UV-B photoreceptor-mediated protection of the photosynthetic machinery in *Chlamydomonas reinhardtii*. Proceedings of the National Academy of Sciences, USA **113**(51): 14864-14869.

Arriola M, Velmurugan N, Zhang Y, Plunkett M, Hondzo H, Barney B. 2018. Genome sequences of *Chlorella sorokiniana* UTEX 1602 and *Micractinium conductrix* SAG 241.80: implications to maltose excretion by a green alga. The Plant Journal **93**(3): 566-586.

Ballottari M, Dall'Osto L, Morosinotto T, Bassi R. 2007. Contrasting behavior of higher plant photosystem I and II antenna systems during acclimation. The Journal of Biological Chemistry **282**(12): 8947-8958.

Berteotti S, Ballottari M, Bassi R. 2016. Increased biomass productivity in green algae by tuning non-photochemical quenching. Scientific Reports **6**: 21339.

Blanc G, Agarkova I, Grimwood J, Kuo A, Brueggeman A, Dunigan DD, Gurnon J, Ladunga I, Lindquist E, Lucas S, et al. 2012. The genome of the polar eukaryotic microalga *Coccomyxa subellipsoidea* reveals traits of cold adaptation. Genome Biology **13**(5): R39.

Blanc G, Duncan G, Agarkova I, Borodovsky M, Gurnon J, Kuo A, Lindquist E, Lucas S, Pangilinan J, Polle J, et al. 2010. The *Chlorella variabilis* NC64A genome reveals adaptation to photosymbiosis, coevolution with viruses, and cryptic sex. Plant Cell **22**(9): 2943-2955.

Bligh EG, Dyer WJ. 1959. A rapid method of total lipid extraction and purification. Canadian journal of biochemistry and physiology **37**(8): 911-917.

Boudreau E, Takahashi Y, Lemieux C, Turmel M, Rochaix JD. 1997. The chloroplast ycf3 and ycf4 open reading frames of *Chlamydomonas reinhardtii* are required for the accumulation of the photosystem I complex. The EMBO Journal **16**(20): 6095-6104.

Cecchin M, Benfatto S, Griggio F, Mori A, Cazzaniga S, Vitulo N, Delledonne M, Ballottari M. 2018. Molecular basis of autotrophic vs mixotrophic growth in *Chlorella sorokiniana*. Scientific Reports **8**(1): 6465.

Chin CS, Peluso P, Sedlazeck FJ, Nattestad M, Concepcion GT, Clum A, Dunn C, O'Malley R, Figueroa-Balderas R, Morales-Cruz A, et al. 2016. Phased diploid genome assembly

with single-molecule real-time sequencing. Nature Methods **13**(12): 1050-1054.

Conesa A, Gotz S, Garcia-Gomez J, Terol J, Talon M, Robles M. 2005. Blast2GO: a universal tool for annotation, visualization and analysis in functional genomics research. Bioinformatics **21**(18): 3674-3676.

Correa-Galvis V, Redekop P, Guan K, Griess A, Truong TB, Wakao S, Niyogi KK, Jahns P. 2016. Photosystem II Subunit PsbS Is Involved in the Induction of LHCSR Protein-dependent Energy Dissipation in *Chlamydomonas reinhardtii*. The Journal of Biological Chemistry **291**(33): 17478-17487.

Dall'Osto L, Cazzaniga S, North H, Marion-Poll A, Bassi R. 2007. The Arabidopsis aba4-1 mutant reveals a specific function for neoxanthin in protection against photooxidative stress. Plant Cell **19**(3): 1048-1064.

Daniell H, Lin CS, Yu M, Chang WJ. 2016. Chloroplast genomes: diversity, evolution, and applications in genetic engineering. Genome Biology **17**(1): 134.

Darienko T, Gustavs L, Eggert A, Wolf W, Pröschold T. 2015. Evaluating the species boundaries of green microalgae (Coccomyxa, Trebouxiophyceae, Chlorophyta) using integrative taxonomy and dna barcoding with further implications for the species identification in environmental samples. PLoS One **10**(6): e0127838.

Denovan-Wright EM, Nedelcu AM, Lee RW. 1998. Complete sequence of the mitochondrial DNA of *Chlamydomonas eugametos*. Plant Molecular Biology **36**(2): 285-295.

Eckardt N. 2010. The *Chlorella* Genome: Big Surprises from a Small Package. Plant Cell **22**(9): 2924-2924.

Gandini CL, Sanchez-Puerta MV. 2017. Foreign plastid sequences in plant mitochondria are frequently acquired via mitochondrion-to-mitochondrion horizontal transfer. Scientific Reports **7**: 43402.

Gao C, Wang Y, Shen Y, Yan D, He X, Dai J, Wu Q. 2014. Oil accumulation mechanisms of the oleaginous microalga *Chlorella protothecoides* revealed through its genome, transcriptomes, and proteomes. BMC Genomics **15**: 582.

Guarnieri MT, Levering J, Henard CA, Boore JL, Betenbaugh MJ, Zengler K, Knoshaug EP. 2018. Genome sequence of the oleaginous green alga, *Chlorella vulgaris* UTEX 395. Frontiers in Bioengineering and Biotechnology **6**: 37.

Juneja A, Chaplen F, Murthy G. 2016. Genome scale metabolic reconstruction of *Chlorella variabilis* for exploring its metabolic potential for biofuels. Bioresource Technology **213**: 103-110.

Kanehisa M, Furumichi M, Tanabe M, Sato Y, Morishima K. 2017. KEGG: new perspectives on genomes, pathways, diseases and drugs. Nucleic Acids Research **45**(D1): D353-D361.

Kanehisa M, Goto S. 2000. KEGG: kyoto encyclopedia of genes and genomes. Nucleic Acids Research **28**(1): 27-30.

Kanehisa M, Sato Y, Kawashima M, Furumichi M, Tanabe M. 2016. KEGG as a reference resource for gene and protein annotation. Nucleic Acids Research **44**(D1): D457-462.

Kirst H, Gabilly ST, Niyogi KK, Lemaux PG, Melis A. 2017. Photosynthetic antenna engineering to improve crop yields. Planta **245**(5): 1009-1020.

Knoop V, Schuster W, Wissinger B, Brennicke A. 1991. Trans splicing integrates an exon of 22 nucleotides into the nad5 mRNA in higher plant mitochondria. The EMBO Journal **10**(11): 3483-3493.

Kouřil R, Nosek L, Bartoš J, Boekema EJ, Ilík P. 2016. Evolutionary loss of light-harvesting proteins Lhcb6 and Lhcb3 in major land plant groups--break-up of current dogma. New Phytologist **210**(3): 808-814.

Kromdijk J, Głowacka K, Leonelli L, Gabilly ST, Iwai M, Niyogi KK, Long SP. 2016. Improving photosynthesis and crop productivity by accelerating recovery from photoprotection. Science **354**(6314): 857-861.

Li XP, Björkman O, Shih C, Grossman AR, Rosenquist M, Jansson S, Niyogi KK. 2000. A pigment-binding protein essential for regulation of photosynthetic light harvesting. Nature **403**(6768): 391-395.

Lin M, Oliver DJ. 2008. The role of acetyl-coenzyme a synthetase in Arabidopsis. Planta Physiology **147**(4): 1822-1829.

Lum KK, Kim J, Lei XG. 2013. Dual potential of microalgae as a sustainable biofuel feedstock and animal feed. Journal of Animal Science and Biotechnology **4**(1): 53.

Lv JM, Cheng LH, Xu XH, Zhang L, Chen HL. 2010. Enhanced lipid production of *Chlorella vulgaris* by adjustment of cultivation conditions. Bioresour Technology **101**(17): 6797-6804.

Malik SB, Pightling AW, Stefaniak LM, Schurko AM, Logsdon JM. 2007. An expanded inventory of conserved meiotic genes provides evidence for sex in *Trichomonas vaginalis*. PLoS One **3**(8): e2879.

Maul JE, Lilly JW, Cui L, dePamphilis CW, Miller W, Harris EH, Stern DB. 2002. The *Chlamydomonas reinhardtii* plastid chromosome: islands of genes in a sea of repeats. Plant Cell **14**(11): 2659-2679.

Merchant SS, Prochnik SE, Vallon O, Harris EH, Karpowicz SJ, Witman GB, Terry A, Salamov A, Fritz-Laylin LK, Maréchal-Drouard L, et al. 2007. The *Chlamydomonas* genome reveals the evolution of key animal and plant functions. Science **318**(5848): 245-250.

Moore ER, Bullington BS, Weisberg AJ, Jiang Y, Chang J, Halsey KH. 2017. Morphological and transcriptomic evidence for ammonium induction of sexual reproduction in *Thalassiosira pseudonana* and other centric diatoms. PLoS One **12**(7): e0181098.

Naduthodi MIS, Barbosa MJ, van der Oost J. 2018. Progress of CRISPR-Cas based genome editing in photosynthetic microbes. Biotechnol Journal.

Ort DR, Merchant SS, Alric J, Barkan A, Blankenship RE, Bock R, Croce R, Hanson MR, Hibberd JM, Long SP, et al. 2015. Redesigning photosynthesis to sustainably meet global food and bioenergy demand. Proceedings of the National Academy of Sciences USA **112**(28): 8529-8536.

Peers G, Truong TB, Ostendorf E, Busch A, Elrad D, Grossman AR, Hippler M, Niyogi KK. 2009. An ancient light-harvesting protein is critical for the regulation of algal photosynthesis. Nature **462**(7272): 518-521.

Radakovits R, Jinkerson RE, Fuerstenberg SI, Tae H, Settlage RE, Boore JL, Posewitz MC. 2012. Draft genome sequence and genetic transformation of the oleaginous alga *Nannochloropis gaditana*. Nature Communication **3**: 686.

Roth MS, Cokus SJ, Gallaher SD, Walter A, Lopez D, Erickson E, Endelman B, Westcott D, Larabell CA, Merchant SS, et al. 2017. Chromosome-level genome assembly and transcriptome of the green alga *Chromochloris zofingiensis* illuminates astaxanthin production. Proceedings of the National Academy of Sciences USA **114**(21): E4296-E4305.

Rumeau D, Peltier G, Cournac L. 2007. Chlororespiration and cyclic electron flow around PSI during photosynthesis and plant stress response. Plant, Cell & Environment **30**(9): 1041-1051.

Sarayloo E, Tardu M, Unlu Y, Simsek S, Cevahir G, Erkey C, Kavakli I. 2017. Understanding lipid metabolism in high-lipid-producing *Chlorella vulgaris* mutants at the genome-wide level. Algal Research-Biomass Biofuels and Bioproducts **28**: 244-252.

Scheller HV, Jensen PE, Haldrup A, Lunde C, Knoetzel J. 2001. Role of subunits in eukaryotic Photosystem I. Biochimica et Biophysica Acta **1507**(1-3): 41-60.

Shi LX, Hall M, Funk C, Schröder WP. 2012. Photosystem II, a growing complex: updates on newly discovered components and low molecular mass proteins. Biochimica et Biophysica Acta **1817**(1): 13-25.

Shimada H, Fukuta M, Ishikawa M, Sugiura M. 1990. Rice chloroplast RNA polymerase genes: the absence of an intron in rpoC1 and the presence of an extra sequence in rpoC2. Molecular Genetics and Genomics **221**(3): 395-402.

Siaut M, Cuiné S, Cagnon C, Fessler B, Nguyen M, Carrier P, Beyly A, Beisson F, Triantaphylidès C, Li-Beisson Y, et al. 2011. Oil accumulation in the model green alga *Chlamydomonas reinhardtii*: characterization, variability between common laboratory strains and relationship with starch reserves. BMC Biotechnology **11**: 7.

Simão FA, Waterhouse RM, Ioannidis P, Kriventseva EV, Zdobnov EM. 2015. BUSCO: assessing genome assembly and annotation completeness with single-copy orthologs. Bioinformatics **31**(19): 3210-3212.

Smith DR. 2014. Mitochondrion-to-plastid DNA transfer: it happens. New Phytologist **202**(3): 736-738.

Soorni A, Haak D, Zaitlin D, Bombarely A. 2017. Organelle_PBA, a pipeline for assembling chloroplast and mitochondrial genomes from PacBio DNA sequencing data. *B*MC Genomics **18**(1): 49.

Specht M, Stanke M, Terashima M, Naumann-Busch B, Janssen I, Höhner R, Hom EF, Liang C, Hippler M. 2011. Concerted action of the new Genomic Peptide Finder and AUGUSTUS allows for automated proteogenomic annotation of the *Chlamydomonas reinhardtii* genome. Proteomics **11**(9): 1814-1823.

Staňková H, Hastie AR, Chan S, Vrána J, Tulpová Z, Kubaláková M, Visendi P, Hayashi S, Luo M, Batley J, et al. 2016. BioNano genome mapping of individual chromosomes supports physical mapping and sequence assembly in complex plant genomes. Planta Biotechnology Journal **14**(7): 1523-1531.

Tardif M, Atteia A, Specht M, Cogne G, Rolland N, Brugière S, Hippler M, Ferro M, Bruley C, Peltier G, et al. 2012. PredAlgo: a new subcellular localization prediction tool dedicated to green algae. Molecular Biology and Evolution **29**(12): 3625-3639.

Tibiletti T, Auroy P, Peltier G, Caffarri S. 2016. *Chlamydomonas reinhardtii* PsbS protein is functional and accumulates rapidly and transiently under high light. Planta Physiologist **171**(4): 2717-2730.

Vieler A, Wu G, Tsai CH, Bullard B, Cornish AJ, Harvey C, Reca IB, Thornburg C, Achawanantakun R, Buehl CJ, et al. 2012. Genome, functional gene annotation, and nuclear transformation of the heterokont oleaginous alga *Nannochloropsis oceanica* CCMP1779. PLoS Genetics **8**(11): e1003064.

Wakasugi T, Nagai T, Kapoor M, Sugita M, Ito M, Ito S, Tsudzuki J, Nakashima K, Tsudzuki T, Suzuki Y, et al. 1997. Complete nucleotide sequence of the chloroplast genome from the green alga *Chlorella vulgaris*: The existence of genes possibly involved in chloroplast division. Proceedings of the National Academy of Sciences USA **94**(11): 5967-5972.

Walker D. 2009. Biofuels, facts, fantasy, and feasibility. *Journal of Applied Phycology* **21**(5): 509-517.

Wang D, Wu YW, Shih AC, Wu CS, Wang YN, Chaw SM. 2007. Transfer of chloroplast genomic DNA to mitochondrial genome occurred at least 300 MYA. Molecular Biology and Evolution **24**(9): 2040-2048.

Waterhouse RM, Seppey M, Simão FA, Manni M, Ioannidis P, Klioutchnikov G, Kriventseva EV, Zdobnov EM. 2017. BUSCO applications from quality assessments to gene prediction and phylogenomics. Molecular Biology and Evolution **35**(3): 543–548.

Wong JL, Johnson MA. 2010. Is HAP2-GCS1 an ancestral gamete fusogen? Trends in Cell Biology **20**(3): 134-141.

Yoshinaga Y, Daum C, He G, O'Malley R. 2018. Genome Sequencing. Methods in Molecular Biology **1775**: 37-52.

Youssef A, Laizet Y, Block MA, Maréchal E, Alcaraz JP, Larson TR, Pontier D, Gaffé J, Kuntz M. 2010. Plant lipid-associated fibrillin proteins condition jasmonate production under photosynthetic stress. Plant Journal **61**(3): 436-445.

Zhong YJ, Huang JC, Liu J, Li Y, Jiang Y, Xu ZF, Sandmann G, Chen F. 2011. Functional characterization of various algal carotenoid ketolases reveals that ketolating zeaxanthin efficiently is essential for high production of astaxanthin in transgenic Arabidopsis. Journal of Experimental Botany **62**(10): 3659-3669.

Zuniga C, Li C, Huelsman T, Levering J, Zielinski D, McConnell B, Long C, Knoshaug E, Guarnieri M, Antoniewicz M, et al. 2016. Genome-scale metabolic model for the green alga *Chlorella vulgaris* UTEX 395 accurately predicts phenotypes under autotrophic, heterotrophic, and mixotrophic growth conditions. Planta Physiology **172**(1): 589-602.

Supplementary data

Table S1 Summary of raw PacBio and Illumina sequencing data and Bionano mapping data

	PacBio	Illumina	Bionano
Number of bases (Gb)	6.4	2.5	69.0
Number of reads	1,113,721	25,428,036	566,536
Genome Coverage	128X	50X	1380X
Mean Read lenght (bp)	5,784	100	121,810
N50 (in bp)	8,757	100	191,600

Table S2 Chlorella vulgaris Genome Assembly statistics

	Falcon assembly*	Bionano Consensus Genome Map	Hybrid Assembly	Hybrid Assembly + Unplaced	Unplaced	Chloroplast	Mitochondrion	Hybrid Assembly + Unplaced without Organelle Contamination
Total assembly length (bp)	39,785,701	171,505	39,740,717	40,466,139	468,358	165,504	91,583	40,180,792
Number of sequences	62	255	14	51	35	1	1	43
Sequences average length (bp)	641,704	673,000	2,838,622	793,453	13,381	165,504	91,583	934,437
Sequence N50 (bp)	1,800,706	1,049,000	2,825,136	2,825,136	21,914	165,504	91,583	2,825,136
Sequence L50	8	54	6	6	5	1	1	6
Sequence N90 (bp)	795,186	346,446	2,150,204	2,150,204	6,639	165,504	91,583	2,150,204
Sequence L90	19	160	12	12	19	1	1	12
Largest Sequence (bp)	5,417,522	5,015,440	5,422,624	5,422,624	128,459	165,504	91,583	5,422,624
Smallest Sequence (bp)	416	50,112	795,975	416	416	165,504	91,583	416
% GC Content	61.6	//	60.2	60.0	59.4	31.7	29.8	60.0
Number of Gap	0	//	12	12	0	0	0	12
Total Gap length (bp)	0	//	634,943	634,943	0	0	0	634,943

Table S3. Single nucleotide variants (SNV) and insertion-deletion (InDel) in the Chlorella vulgaris assembled genome before and after correction with Illumina and PacBio data

	PacBio	**PacBio+Illumina**
SNV	3076	81
InDel	32821	190
TOTAL	35897	271
% GENOME	0.09%	0.0007%

Table S4. Comparison of Chlorella vulgaris genomes reported in Guarnieri et al 2018 and that generated in the present work

	Chlorella vulgaris NCBI	*Chlorella Vulgaris* 211/11P
Total sequence length	37,342,230	40,437,856
Total assembly gap length	40,625	634,943
Gaps between scaffolds	0	0
Number of scaffolds	3,600	14
Scaffold N50	27,824	2,825,136
Scaffold L50	358	6
Number of contigs	4,754	45
Contig N50	20,333	1,802,178
Contig L50	501	8
Total number of chromosomes and plasmids	0	0 chr 2 plasmid
Number of component sequences (WGS or clone)	3,600	43

Table S5. Codon usage in Chlorella vulgaris.

The codon usage table gives for each codon: i. Sequence of the codon. ii. The encoded amino acid. iii. The proportion of usage of the codon among its redundant set, i.e. the set of codons which code for this codon's amino acid. iv. The expected number of codons, given the input sequence(s), per 1000 bases. v. The observed number of codons in the input sequences.

```
#Codon AA Fraction Frequency
Number
GCA    A     0.253    37.206
219120
GCC    A     0.299    44.031
259312
GCG    A     0.257    37.744
222285
GCT    A     0.191    28.126
165643
TGC    C     0.807    13.076
77007
TGT    C     0.193     3.132
18448
GAC    D     0.673    30.175
177711
GAT    D     0.327    14.646
86253
GAA    E     0.174     9.821
57841
GAG    E     0.826    46.536
274064
TTC    F     0.574    15.009
88392
TTT    F     0.426    11.137
65592
GGA    G     0.101     8.659
50998
GGC    G     0.579    49.753
293009
GGG    G     0.194    16.684
98255
GGT    G     0.126    10.870
64018
CAC    H     0.757    17.008
100166
```

CAT	H	0.243	5.454	32123
ATA	I	0.120	3.013	17743
ATC	I	0.610	15.291	90055
ATT	I	0.270	6.762	39822
AAA	K	0.144	4.609	27143
AAG	K	0.856	27.343	161029
CTA	L	0.030	3.019	17777
CTC	L	0.149	14.949	88040
CTG	L	0.636	63.856	376067
CTT	L	0.072	7.198	42392
TTA	L	0.008	0.852	5017
TTG	L	0.104	10.452	61556
ATG	M	1.000	19.628	115598
AAC	N	0.784	16.095	94787
AAT	N	0.216	4.424	26056
CCA	P	0.210	13.228	77906
CCC	P	0.322	20.337	119770
CCG	P	0.265	16.701	98356
CCT	P	0.204	12.849	75669
CAA	Q	0.149	9.126	53746
CAG	Q	0.851	51.994	306208
AGA	R	0.036	2.264	13336
AGG	R	0.133	8.447	49746
CGA	R	0.096	6.071	35754
CGC	R	0.383	24.222	142651
CGG	R	0.260	16.441	96828
CGT	R	0.092	5.836	34368
AGC	S	0.431	31.268	184148
AGT	S	0.068	4.947	29137
TCA	S	0.105	7.604	44785
TCC	S	0.169	12.228	72014
TCG	S	0.127	9.212	54252
TCT	S	0.101	7.292	42943
ACA	T	0.220	10.108	59529
ACC	T	0.392	18.005	106035
ACG	T	0.232	10.661	62786
ACT	T	0.156	7.150	42107
GTA	V	0.052	3.318	19543
GTC	V	0.201	12.871	75804
GTG	V	0.635	40.676	239551
GTT	V	0.112	7.183	42301
TGG	W	1.000	13.320	78445
TAC	Y	0.754	13.708	80730
TAT	Y	0.246	4.481	26391
TAA	*	0.086	0.164	964
TAG	*	0.210	0.398	2346
TGA	*	0.703	1.331	7840

Table S6. Identification of key genes involved in different metabolic pathway in Chlorella vulgaris

Photosystem II

Description	Abbreviations	Gene name in *C. vulgaris*	Description Blast2go	C_v LL_1	C_v LL_2	C_v LL_3	C_v HL_1	C_v HL_2	C_v HL_3	baseMean	log2 Fold Change	lfcSE	stat	pvalue	padj
Photosystem II D1	psbA	psbA-chl.t1		17,8	16	26,77	33,30	22,24	20,56	563,05	0,32	0,20	1,58	0,11	0,17
Photosystem II CP47	psbB	psbB-chl.t1		4,16	5,82	7,89	7,00	4,76	5,37	205,04	-0,08	0,23	-0,33	0,74	0,81
Photosystem II CP43	psbC	psbC-chl.t1		4,11	3,77	10,09	12,74	8,66	8,48	257,23	0,73	0,50	1,47	0,14	0,21
Photosystem II D2	psbD	psbD-chl.t1		5,75	5,77	15,87	43,10	22,55	28,65	499,96	1,78	0,56	3,19	0,00	0,00
Photosystem II Cytochrome b559 Subunit E	psbE	psbE-chl.t1		6,40	8,36	8,03	5,81	4,81	6,87	36,88	-0,41	0,34	-1,22	0,22	0,31
Photosystem II Cytochrome b559 Subunit F	psbF	psbF-chl.t1		1,84	0,60	5,17	1,62	2,33	0,96	5,14	-0,62	0,96	-0,65	0,52	0,61
Photosystem II Subunit H	psbH	psbH-chl.t1		1,83	1,86	2,63	3,33	2,40	3,59	14,56	0,51	0,53	0,98	0,33	0,43
Photosystem II Subunit I	psbI	psbI-chl.t1		0,49	0,64	0,43	0,00	0,83	0,51	1,12	-0,04	1,80	-0,02	0,98	0,99
Photosystem II Subunit L	psbL	psbL-chl.t1		0,42	1,63	3,96	1,46	0,42	0,00	3,58	-1,80	1,25	-1,43	0,15	0,22
Oxygen Evolving Subunit O	psbO	g2581.t1	Oxygen-evolving enhancer chloroplastic	972,99	1301,63	1150,30	473,55	488,39	494,07	16928,77	-1,23	0,10	-12,53	0,00	0,00
Oxygen Evolving Subunit P	psbP	g3781.t1	Oxygen-evolving enhancer chloroplastic	605,72	738,39	720,62	369,56	392,26	396,02	9376,69	-0,83	0,09	-9,67	0,00	0,00
		g8738.t1	psbP chloroplastic	104,69	116,48	105,48	133,12	124,58	121,90	1841,03	0,22	0,08	2,71	0,01	0,01
Photosystem II Subunit S	psbS	g6210.t1	photosystem II 22 kDa chloroplastic	253,17	297,23	235,32	979,50	841,58	843,07	10319,11	1,76	0,10	17,74	0,00	0,00
Photosystem II Subunit 27	psb27	g5143.t1	Photosystem II repair PSB27-chloroplastic	70,30	73,36	71,92	67,12	70,18	74,71	890,83	-0,02	0,09	-0,27	0,79	0,85
Photosystem II Subunit 28	psb28	g5974.t1	Photosystem II reaction center psb28 chloroplastic	103,57	105,78	114,30	321,65	293,72	278,85	2097,82	1,46	0,09	17,10	0,00	0,00
Photosystem II Subunit J	psbJ	psbJ-chl.t1		1,71	3,91	5,54	6,01	2,31	3,11	9,99	-0,04	0,69	-0,05	0,96	0,97
Photosystem II Subunit K	psbK	psbK-chl.t1		1,93	0,51	3,68	1,81	0,52	0,80	4,52	-1,12	1,02	-1,09	0,27	0,37
Photosystem II Subunit M	psbM	psbM-chl.t1		0,51	0,66	0,00	1,19	0,69	2,11	1,92	1,81	1,59	1,14	0,25	0,34
Oxygen Evolving Subunit Q	psbQ	g10583.t1	oxygen-evolving enhancer chloroplast precursor	373,38	320,25	488,97	211,39	251,79	258,19	4587,10	-0,71	0,14	-5,26	0,00	0,00
Photosystem II Subunit R	psbR	g259.t1	Photosystem II 10 kDa chloroplastic	3745,67	4544,51	3886,01	5654,21	4710,74	4888,70	45971,83	0,33	0,10	3,39	0,00	0,00
Photosystem II Subunit T	psbT	psbT-chl.t1		5,07	3,98	11,41	10,12	5,31	4,75	15,14	-0,08	0,58	-0,14	0,88	0,92
Photosystem II Subunit W	psbW	g588.t1	photosystem II reaction center W chloroplastic-like	595,14	658,87	625,30	395,52	418,23	445,91	4310,99	-0,58	0,08	-7,65	0,00	0,00
Photosystem II Subunit Y	psbY	g7534.t1	photosystem II	89,82	85,40	108,18	48,91	54,31	58,62	1813,68	-0,81	0,11	-7,47	0,00	0,00
Photosystem II Subunit Z	psbZ	psbZ-chl.t1		0,27	0,00	0,23	0,95	0,37	0,00	1,27	1,27	1,91	0,66	0,51	0,60

Photosystem I

Description	Abbreviations	Gene name in *C. vulgaris*	Description Blast2go	C_vLL_1	C_vLL_2	C_vLL_3	C_vHL_1	C_vHL_2	C_vHL_3	baseMean	Log2 Fold Change	lfcSE	stat	pvalue	padj
Photosystem I Subunit A	psaA	psaA-chl.t1		0,56	0,56	1,66	3,49	1,78	1,98	87,85	1,35	0,39	3,43	0,00	0,00
		psaA-fragment-chl.t1		0	0	0	0	0	0	0	NA	NA	NA	NA	NA
Photosystem I Subunit B	psaB	psaB-chl.t1		0,38	0,61	1,78	2,10	1,16	1,26	62,31	0,69	0,46	1,51	0,13	0,20
		psaB-fragment-chl.t1		0	0	0	0	0	0	0	NA	NA	NA	NA	NA
Photosystem I Subunit C	psaC	psaC-chl.t1		1,39	1,81	2,74	2,09	2,01	2,47	11,93	0,12	0,57	0,21	0,84	0,88
Photosystem I Subunit D	psaD	g7512.t1	Photosystem I reaction center subunit chloroplastic	708,8	755,94	843,55	333,43	363,35	387,15	7580,5	-1,09	0,09	-12,46	0,00	0,00
Photosystem I Subunit E	psaE	g3953.t1	Photosystem I reaction center subunit IV chloroplastic	394,2	449,76	409,81	80,01	105,73	108,65	1783,9	-2,08	0,11	-18,36	0,00	0,00
Photosystem I Subunit F	psaF	g6041.t1	Photosystem I reaction center subunit chloroplastic-like	630,7	687,94	681,61	310,75	299,95	304,82	7975,1	-1,13	0,06	-17,56	0,00	0,00
Photosystem I Subunit G	psaG	g5915.t1	Photosystem I reaction center subunit chloroplastic-like	310,8	340,07	376,12	125,24	140,82	148,21	2180,8	-1,31	0,10	-13,46	0,00	0,00
Photosystem I Subunit H	psaH	g2296.t1	Photosystem I reaction center subunit chloroplastic	191,6	144,07	215,49	77,44	99,48	91,61	1144,8	-1,03	0,14	-7,21	0,00	0,00
Photosystem I Subunit K	psaK	g5227.t1	Photosystem I reaction center subunit XI	464,8	471,56	539,48	212,47	243,84	269,84	5023,2	-1,02	0,10	-10,31	0,00	0,00
Photosystem I Subunit L	psaL	g9278.t1	Photosystem I reaction center subunit chloroplastic	314,2	377,46	332,43	114,12	120,21	134,98	2432,7	-1,47	0,10	-15,29	0,00	0,00
Photosystem I Subunit N	psaN	g1880.t1	Photosystem I reaction center subunit chloroplastic-like	335,4	358,60	395,04	121,53	145,70	160,67	2401,2	-1,35	0,11	-12,49	0,00	0,00
Photosystem I Subunit O	psaO	g9054.t1	Photosystem I subunit O	546,0	612,92	601,19	289,84	306,41	329,22	4094,6	-0,93	0,08	-11,70	0,00	0,00
Photosystem I Subunit I	psaI	psaI-chl.t1		1,32	1,15	1,90	3,60	0,74	0,00	3,75	-0,11	1,17	-0,09	0,93	0,95
Photosystem I Subunit J	psaJ	psaJ-chl.t1		2,32	1,01	4,01	6,35	3,92	2,81	9,98	0,77	0,69	1,12	0,26	0,35

Cytochromebuf

Description	Abbreviations	Gene name in *C. vulgaris*	Description Blast2go	C_v LL_1	C_v LL_2	C_v LL_3	C_v HL_1	C_v HL_2	C_v HL_3	baseMean	Log2 Fold Change	lfcSE	stat	pvalue	padj
Apocytochrome f	petA	petA-chl.t1		5,43	4,66	5,18	2,72	2,62	1,82	74,94	-1,08	0,25	-4,39	0,00	0,00
Cytochrome b_6	petB	petB-chl.t1		2,18	1,57	2,53	1,97	2,51	1,52	40,94	0,62	0,34	1,80	0,07	0,11
Cytochrome b_6-f complex iron-sulfur subunit	petC	g6949.t1	cytochrome b6-f complex iron-sulfur chloroplastic-like	376,96	380,93	416,05	512,21	569,93	571,95	6879,17	0,49	0,08	6,55	0,00	0,00
Cytochrome b_6-f complex subunit 4	petD	petD-chl.t1		1,21	0,79	1,48	2,06	2,18	2,52	20,87	1,09	0,46	2,38	0,02	0,03
Cytochrome b_6-f complex subunit 5	petG	petG-chl.t1		1,71	3,91	3,69	1,50	1,01	0,44	5,43	-1,66	0,89	-1,85	0,06	0,10
Subunit of the chloroplast cytochrome b6f complex	petN	g8264.t1	cytochrome b6 f complex subunit VIII (chloroplast)	143,75	108,15	154,01	123,77	145,65	155,12	985,86	0,06	0,14	0,47	0,64	0,72

Photosynthetic electron transport

Description	Abbreviations	Gene name in *C. vulgaris*	Description Blast2go	C_v LL_1	C_v LL_2	C_v LL_3	C_v HL_1	C_v HL_2	C_v HL_3	baseMean	Log2 Fold Change	lfcSE	stat	pvalue	padj
Plastocyanin	petE	g4717.t1	chloroplast precursor	543,06	515,57	504,93	490,72	529,39	554,17	5577,09	-0,08	0,08	-0,82	0,41	0,51
Ferredoxin	petF	g807.t1	chloroplast precursor	81,97	92,11	80,26	113,54	108,39	109,92	1835,28	0,39	0,08	4,75	0,00	0,00
		g334.t1	root R-B1	54,43	46,11	58,09	95,40	96,48	96,67	1020,08	0,86	0,10	8,63	0,00	0,00
		g4942.t1	chloroplast precursor	687,94	777,93	829,69	436,62	510,08	583,00	5713,43	-0,58	0,11	-5,25	0,00	0,00
		g7026.t1	root R-B2	21,80	23,68	25,38	41,21	44,00	41,29	335,38	0,84	0,13	6,66	0,00	0,00
Ferredoxin-NADP+ reductase	petH	g6815.t1	ferredoxin--NADP root isozyme chloroplastic	146,46	155,91	150,15	152,44	143,58	142,32	9342,07	-0,05	0,06	-0,75	0,46	0,56
Cytochrome c6	petJ	g4007.t2	cytochrome c6	6924,94	8105,36	6552,38	6134,8	5308,71	5293,60	85179,52	-0,35	0,10	-3,57	0,00	0,00

F-type chloroplastic ATPase

Description	Abbreviations	Gene name in *C. vulgaris*	Description Blast2go	C_v LL_1	C_v LL_2	C_v LL_3	C_v HL_1	C_v HL_2	C_v HL_3	baseMean	Log2 Fold Change	lfcSE	stat	pvalue	padj
CF_0 subunit A	atpI	atpI-chl.t1		2,57	2,92	2,11	2,30	1,53	1,06	34,86	-0,64	0,37	-1,75	0,08	0,13
CF_0 subunit B	atpF	atpF-chl.t1		1,01	1,59	1,75	2,14	1,58	2,11	9,49	0,39	0,64	0,61	0,54	0,64
CF_0 subunit B'	atpG	g5146.t1	ATP synthase subunit b chloroplastic	155,82	128,81	185,74	116,17	144,00	152,14	2136,85	-0,19	0,13	-1,42	0,16	0,23
CF_0 subunit C	atpH	atpH-chl.t1		1,57	1,28	1,15	3,44	1,19	2,01	10,49	0,60	0,66	0,90	0,37	0,46
CF_1 subunit alfa	atpA	atpA-chl.t1		0,52	0,76	1,04	1,21	1,00	1,14	33,10	0,51	0,37	1,38	0,17	0,24
CF_1 subunit beta	atpB	atpB-chl.t1		1,04	0,92	1,14	2,57	1,09	1,44	46,01	0,67	0,37	1,82	0,07	0,11
CF_1 subunit gamma	atpC	g222.t1	ATP synthase gamma chain chloroplastic-like	169,81	186,09	187,63	127,68	120,66	128,46	3804,96	-0,54	0,07	-7,54	0,00	0,00
CF_1 subunit delta	atpD	g6994.t1	ATP synthase delta chloroplastic	142,92	158,91	156,83	101,30	105,14	104,28	1982,76	-0,57	0,08	-7,54	0,00	0,00
CF_1 subunit epsilon	atpE	atpE-chl.t1		0,49	0,80	1,06	0,58	0,58	0,64	6,39	-0,40	0,77	-0,53	0,60	0,69

Antennae protein KEGG

Description	Abbreviations	Gene name in *C. vulgaris*	Description Blast2go	C_v LL_1	C_v LL_2	C_v LL_3	C_v HL_1	C_v HL_2	C_v HL_3	baseMean	Log2 Fold Change	lfcSE	stat	pvalue	padj
Light-Harvesting Complex I	LHCA1	g472.t1	chlorophyll a-b binding chloroplastic-like isoform X1	848,63	859,01	1006,11	105,51	128,32	155,12	7946,84	-2,80	0,12	-22,78	0,00	0,00
Light-Harvesting Complex I	LHCA2	g471.t1	Chlorophyll a-b binding chloroplastic	327,35	320,65	419,74	30,27	41,90	46,56	3700,84	-3,17	0,14	-22,15	0,00	0,00
Light-Harvesting Complex I	LHCA3	g8185.t1	Chlorophyll a-b binding chloroplastic	446,27	532,40	547,70	46,88	61,79	68,40	5491,77	-3,11	0,13	-24,76	0,00	0,00
Light-Harvesting Complex I	LHCA4	g1028.t1	Chlorophyll a-b binding chloroplastic	922,03	1144,33	986,28	316,85	315,83	320,35	11681,4	-1,67	0,09	-19,28	0,00	0,00
		g3933.t1	chlorophyll a-b binding chloroplastic-like	736,38	880,87	820,43	236,19	252,16	264,06	9839,12	-1,70	0,08	-20,30	0,00	0,00
		g5969.t1	chlorophyll a-b binding chloroplastic	345,61	409,17	455,38	13,98	20,65	22,89	3939,38	-4,39	0,15	-30,17	0,00	0,00
Light-Harvesting Complex I	LHCA5	g8434.t1	Chlorophyll a-b binding chloroplastic	490,62	591,64	533,27	61,84	72,32	73,43	4625,72	-2,96	0,10	-30,96	0,00	0,00
Light-Harvesting Complex II	LHCB1	g1760.t1	Chlorophyll a-b binding of LHCII type chloroplastic	263,06	314,20	331,51	4,21	4,92	5,12	2621,28	-5,98	0,13	-45,90	0,00	0,00
		g1761.t1	chlorophyll a-b binding chloroplastic	2920,20	3224,76	3572,81	159,75	209,01	228,20	29892,5	-4,02	0,12	-33,45	0,00	0,00
		g2614.t1	chlorophyll a b-binding	1393,53	1623,95	1769,17	122,30	160,63	165,46	15415,1	-3,41	0,12	-28,75	0,00	0,00
Light-Harvesting Complex II	LHCB2	g6051.t1	chlorophyll a-b binding chloroplastic	1515,36	1789,83	1770,32	1,92	6,24	8,38	15911,1	-8,26	0,50	-16,54	0,00	0,00
Light-Harvesting Complex II	LHCB3	g1760.t1	Chlorophyll a-b binding of LHCII type chloroplastic	263,06	314,20	331,51	4,21	4,92	5,12	2621,28	-5,98	0,13	-45,90	0,00	0,00
		g1761.t1	chlorophyll a-b binding chloroplastic	2920,20	3224,76	3572,81	159,75	209,01	228,20	29892,5	-4,02	0,12	-33,45	0,00	0,00
CP29	LHCB4	g9593.t1	chlorophyll a-b binding chloroplastic-like	556,91	525,32	698,07	233,33	281,79	297,07	8810,63	-1,13	0,12	-9,60	0,00	0,00
CP26	LHCB5	g506.t1	Chlorophyll a-b binding chloroplastic	296,33	326,34	355,72	197,07	207,83	211,83	5421,02	-0,67	0,08	-8,10	0,00	0,00
Light-Harvesting Complex II	LHCB7	g6543.t1	chlorophyll a-b binding of LHCII type 1	33,49	31,62	33,48	34,21	35,83	38,44	889,29	0,14	0,09	1,52	0,13	0,19
		g6543.t2	chlorophyll a-b binding of LHCII type 1												
		g6543.t3	chlorophyll a-b binding of LHCII type 1												

Chlorophyll metabolism

Description	Abbreviations	Gene name in C. vulgaris	Description Blast2go	C_v LL_1	C_v LL_2	C_v LL_3	C_v HL_1	C_v HL_2	C_v HL_3	baseMean	Log2 Fold Change	lfcSE	stat	pvalue	padj
Protochlorophyllide Reductase	por	g2548.t1	protochlorophyllide reductase	169,1	201,7	181,9	152,8	151,3	153,67	4823,43	-0,27	0,08	-3,45	0,00	0,00
Coproporphyrinogen III Oxidase	CPOX	g2205.t1	coproporphyrinogen III oxidase	13,59	13,71	13,65	12,07	11,85	13,66	297,05	-0,13	0,13	-1,01	0,31	0,41
		g10315.t1	oxygen-dependent coproporphyrinogen-III chloroplastic	94,56	104,8	105,0	115,5	116,1	108,32	2805,23	0,16	0,08	2,12	0,03	0,06
Protoporphyrinogen/Coproporphyrinogen III Oxidase	PPOX	g7074.t1	Protoporphyrinogen oxidase chloroplastic	64,83	72,84	60,91	62,76	61,76	61,76	2405,45	-0,09	0,08	-1,09	0,28	0,37
Uroporphyrinogen Decarboxylase	hemE	g552.t1	Uroporphyrinogen decarboxylase chloroplastic	32,31	33,39	34,77	45,81	44,11	44,97	1073,82	0,42	0,08	5,18	0,00	0,00
		g1569.t1	uroporphyrinogen decarboxylase	9,28	7,92	12,07	11,55	15,59	14,60	329,76	0,51	0,17	2,95	0,00	0,01
		g8174.t1	Uroporphyrinogen decarboxylase chloroplastic	106,4	120,35	114,46	144,1	130,7	132,46	3415,35	0,25	0,08	3,28	0,00	0,00
Porphobilinogen Synthase	hemB	g2181.t1	delta-aminolevulinic acid dehydratase chloroplastic-like	70,24	79,60	80,72	115,1	110,4	112,02	2618,61	0,55	0,08	7,01	0,00	0,00
Uroporphyrinogen-III Synthase	hemD	g7177.t1	uroporphyrinogen-III chloroplastic	17,92	22,83	21,38	30,68	29,53	30,90	586,71	0,55	0,11	4,89	0,00	0,00
		g7177.t2	uroporphyrinogen-III chloroplastic												
Hydroxymethylbilane Synthase	hemC	g4163.t1	Porphobilinogen chloroplastic	43,92	50,41	49,57	30,17	31,07	32,16	983,21	-0,62	0,09	-6,79	0,00	0,00
Magnesium Chelatase Subunit H	chlH	g2717.t1	magnesium-chelatase subunit chloroplastic	83,39	102,86	101,41	147,5	138,2	122,49	11363,1	0,51	0,10	5,08	0,00	0,00
		g2054.t1	magnesium chelatase subunit H	72,79	78,84	66,91	185,9	171,3	152,91	12977,3	1,22	0,09	13,40	0,00	0,00
Magnesium Chelatase Subunit D	chlD	g1236.t1	magnesium-chelatase subunit chloroplastic	38,14	45,92	44,96	64,52	58,38	59,78	2775,22	0,50	0,09	5,57	0,00	0,00
Magnesium Chelatase Subunit I	chlI	g2785.t1	magnesium chelatase subunit of protochlorophyllide reductase (chloroplast)	42,87	42,58	43,78	47,14	48,62	50,13	1325,63	0,17	0,08	2,30	0,02	0,04
Magnesium-Protoporphyrin O-Methyltransferase	bchM	g2528.t1	magnesium protoporphyrin IX chloroplastic-like	55,06	63,89	55,74	63,07	61,64	64,49	1452,67	0,12	0,09	1,35	0,18	0,25
Magnesium-Protoporphyrin IX Monomethyl Ester (Oxidative) Cyclase	CRD1	g8510.t1	magnesium-protoporphyrin IX monomethyl ester [oxidative] chloroplastic	313,5	364,0	340,62	312,2	288,28	298,79	8904,78	-0,18	0,08	-2,37	0,02	0,03
Light-Independent Protochlorophyllide Reductase Subunit L	chlL	chlL-chl.t1		1,21	1,03	1,30	1,06	0,45	0,69	17,96	-0,77	0,50	-1,55	0,12	0,18
Light-Independent Protochlorophyllide Reductase Subunit N	chlN	chlN-chl.t1		0,28	0,78	0,65	0,84	0,28	0,49	15,82	-0,14	0,59	-0,23	0,82	0,87
Light-Independent Protochlorophyllide Reductase Subunit B	chlB	chlB-chl.t1		0,10	0,00	0,25	0,11	0,06	0,10	3,68	-0,43	1,13	-0,38	0,71	0,78
Chlorophyll/Bacteriochlorophyll a Synthase	chlG	g2937.t1	chlorophyll chloroplastic	63,30	68,52	66,02	76,04	73,08	73,31	1979,00	0,17	0,07	2,38	0,02	0,03
Chlorophyllide a Oxygenase	CAO	g5283.t1	chlorophyllide a chloroplastic	16,03	13,39	17,37	14,65	19,38	19,36	834,98	0,19	0,13	1,43	0,15	0,22
		g9069.t1	chlorophyllide a chloroplastic	45,59	46,17	50,13	9,96	10,10	11,16	1140,32	-2,19	0,09	-23,83	0,00	0,00
Chlorophyll(ide) b Reductase	NOL	g3259.t1	chlorophyll(ide) b reductase chloroplastic	36,33	34,31	40,64	38,67	38,99	37,26	853,04	0,04	0,10	0,46	0,64	0,73
		g312.t1	probable chlorophyll(ide) b reductase chloroplastic	31,00	27,38	29,13	64,25	60,20	61,36	1224,76	1,08	0,09	12,69	0,00	0,00
		g9809.t1	chlorophyll(ide) b reductase chloroplastic isoform X1	61,27	56,08	55,18	65,52	65,47	68,57	1433,42	0,21	0,08	2,60	0,01	0,02
7-Hydroxymethyl Chlorophyll a Reductase	HCAR	g9788.t1	7-hydroxymethyl chlorophyll a chloroplastic	41,75	43,64	38,15	62,70	61,06	57,51	1670,91	0,56	0,08	6,65	0,00	0,00
Divinyl Chlorophyllide a 8-Vinyl-Reductase	DVR	g6701.t1	divinyl chlorophyllide a 8-vinyl-chloroplastic	24,57	27,10	26,92	13,40	14,70	15,14	602,61	-0,86	0,10	-8,33	0,00	0,00
Magnesium Dechelatase	SGR	g6672	STAY-GREEN chloroplastic-like	18,35	15,11	22,85	27,37	37,00	33,77	830,46	0,80	0,15	5,25	0,00	0,00
Chlorophyllase 1	Chlase	g5337	chlorophyllase 1	47,90	39,85	47,74	53,02	57,19	54,72	4917,03	0,28	0,09	3,27	0,00	0,00
		g6657	chlorophyllase 1	14,92	16,09	15,85	17,34	18,35	18,86	596,01	0,22	0,10	2,25	0,02	0,04
Pheophorbide a Oxygenase	PAO	g3716	pheophorbide a oxygenase	15,94	13,64	15,75	36,02	37,52	38,32	1081,16	1,30	0,09	14,16	0,00	0,00

Carotenoid biosynthesis

Description	Abbreviations	Gene name in *C. vulgaris*	Description Blast2go	C_v LL_1	C_v LL_2	C_v LL_3	C_v HL_1	C_v HL_2	C_v HL_3	baseMean	Log2 Fold Change	lfcSE	stat	pvalue	padj
Zeta-Carotene Desaturase	ZDS	g9775.t1	Zeta-carotene chloroplastic chromoplastic	23,79	26,51	23,23	87,92	78,82	75,92	2139,18	1,71	0,09	18,37	0,00	0,00
15-Cis-Phytoene Synthase	crtB	g2543.t1	phytoene synthase chloroplastic	77,65	84,46	74,25	103,41	94,25	95,69	2340,07	0,30	0,08	3,70	0,00	0,00
15-Cis-Phytoene Desaturase	PDS	g6600.t1	15-cis-phytoene chloroplastic chromoplastic	79,39	88,98	77,98	221,30	196,65	191,68	5479,34	1,31	0,08	15,46	0,00	0,00
Lycopene Beta-Cyclase	lcyB	g1330.t1	lycopene beta chloroplastic chromoplastic	34,65	33,12	33,92	73,41	67,46	68,27	1946,29	1,04	0,08	13,83	0,00	0,00
Lycopene Epsilon-Cyclase	lcyE	g5897.t1	lycopene epsilon chloroplastic	11,83	12,61	14,23	10,38	10,50	9,82	422,21	-0,33	0,12	-2,81	0,00	0,01
Prolycopene Isomerase	crtISO	g10585.t1	carotene isomerase	15,78	18,90	16,08	39,50	35,26	32,57	1115,05	1,08	0,11	10,09	0,00	0,00
Carotene Epsilon-Monooxygenase	LUT1	g2969.t1	carotene epsilon-chloroplastic	45,80	54,55	47,10	69,27	62,46	64,96	2299,02	0,42	0,09	4,67	0,00	0,00
Zeaxanthin Epoxidase	ZEP	g9297.t1	Zeaxanthin chloroplastic	87,16	89,77	96,06	52,24	53,29	56,27	3274,07	-0,76	0,07	-10,45	0,00	0,00
		g7598.t1	monooxygenase	26,68	30,30	26,63	41,02	42,71	42,94	856,61	0,60	0,09	6,51	0,00	0,00
Violaxanthin De-Epoxidase	VDE	g7391.t1	Violaxanthin de-chloroplastic	143,23	151,60	131,07	328,10	262,40	270,87	6951,76	1,02	0,10	10,36	0,00	0,00
Zeta-Carotene Isomerase	Z-ISO	g10591.t1	15-cis-zeta-carotene chloroplastic	101,56	114,79	102,05	136,55	116,28	105,39	4827,36	0,17	0,10	1,68	0,09	0,14
Beta-Carotene 3-Hydroxylase	crtZ	g8453.t1	beta-carotene 3-hydroxylase chloroplastic-like	17,12	20,47	22,40	49,61	42,87	43,02	714,42	1,17	0,12	9,68	0,00	0,00
Beta-Ring Hydroxylase	LUT5	g5535.t1	LUTEIN DEFICIENT chloroplastic	32,81	33,77	32,48	54,21	46,24	46,39	1343,59	1,91	0,10	19,46	0,00	0,00
Neoxanthin Synthase	NXS	g5367.t1	ABA DEFICIENT chloroplastic-like isoform X3	7,57	5,94	5,82	4,14	4,58	4,64	73,42	-0,53	0,24	-2,20	0,03	0,05

Alternative pathways

Description	Abbreviations	Gene name in *C. vulgaris*	Description Blast2go	C_v LL_1	C_v LL_2	C_v LL_3	C_v HL_1	C_v HL_2	C_v HL_3	baseMean	Log2 Fold Change	lfcSE	stat	pvalue	padj
Plastid alternative oxidase	PTOX1	g6516.t1	Ubiquinol oxidase chloroplastic chromoplastic	48,24	52,95	46,27	58,65	53,97	54,48	1779,32	0,18	0,08	2,17	0,03	0,05
	PTOX2	g6516.t1	Ubiquinol oxidase chloroplastic chromoplastic	48,24	52,95	46,27	58,65	53,97	54,48	1779,32	0,18	0,08	2,17	0,03	0,05
Alternative oxidase	AOX1	g4347.t1	alternative mitochondrial-like	143,82	159,86	160,32	281,39	272,32	266,93	5442,38	0,82	0,07	11,66	0,00	0,00
	AOX2	g4347.t1	alternative mitochondrial-like	143,82	159,86	160,32	281,39	272,32	266,93	5442,38	0,82	0,07	11,66	0,00	0,00
Thylakoid transmembrane protein involved in cyclic electron flow	PGRL1	g7642.t1	PGR5 chloroplastic	90,19	96,11	88,27	136,33	121,31	124,58	4837,29	0,48	0,07	6,39	0,00	0,00
Proton gradient regulation protein	PGR5	g4605.t1	PROTON GRADIENT REGULATION chloroplastic	65,45	60,50	60,42	100,99	82,33	89,81	721,94	0,54	0,11	5,02	0,00	0,00
Type-II calcium-dependant NADH dehydrogenase	NDA2	g1441.t1	external alternative NAD(P)H-ubiquinone oxidoreductase mitochondrial-like	65,29	71,05	58,01	54,80	49,15	49,58	2481,95	-0,34	0,09	-3,67	0,00	0,00
		g8388.t1	external alternative NAD(P)H-ubiquinone oxidoreductase mitochondrial	12,07	12,82	14,41	9,96	11,35	11,84	820,41	-0,24	0,11	-2,27	0,02	0,04

NPQ

Description	Abbreviations	Gene name in *C. vulgaris*	Description Blast2go	C_v LL_1	C_v LL_2	C_v LL_3	C_v HL_1	C_v HL_2	C_v HL_3	baseMean	Log2 Fold Change	lfcSE	stat	pvalue	padj
Photosystem II Subunit S	PSBS	g6210.t1	photosystem II 22 kDa chloroplastic	253,17	297,23	235,32	979,50	841,58	843,07	10319,11	1,76	0,10	17,74	0,00	0,00
Light-Harvesting Complex Stress Response	LHCSR	g8851new		167,23	162,89	169,93	185,03	170,12	184,83	3149,99	0,13	0,06	2,09	0,04	0,06

Rubisco

Description	Abbreviation	Gene name in *C. vulgaris*	Description Blast2go	C_v LL_1	C_v LL_2	C_v LL_3	C_v HL_1	C_v HL_2	C_v HL_3	baseMean	Log2 Fold Change	lfcSE	stat	pvalue	padj
Rubisco large subunit		rbcL-chl.t1		24,77	34,54	52,09	28,72	18,08	22,49	890,22	-0,43	0,16	-2,47	0,01	0,03
Rubisco activase	RCA1	g10592.t1	Ribulose bisphosphate carboxylase oxygenase chloroplastic	189,96	172,19	170,18	198,53	181,59	183,46	14010,96	0,14	0,06	2,27	0,02	0,04
		g10040.t1	Ribulose bisphosphate carboxylase oxygenase chloroplastic	144,40	155,50	142,95	107,29	98,85	102,84	1681,89	-0,52	0,07	-7,19	0,00	0,00
Rubisco activase-like protein	RCA2	g8580.t1	ribulose bisphosphate carboxylase oxygenase chloroplastic	30,80	34,82	28,34	43,51	42,94	46,07	1238,36	0,48	0,09	5,10	0,00	0,00
Ribulose-1,5-bisphosphate carboxylase/oxygenase small subunit 1, chloroplast precursor	RBCS1	g10103.t1	ribulose-bisphosphate carboxylase small chain	429,44	434,41	402,51	216,19	222,98	244,80	4296,09	-0,99	0,08	-11,79	0,00	0,00
Ribulose-1,5-bisphosphate carboxylase/oxygenase small subunit 2	RBCS2	g10102.t1	ribulose-bisphosphate carboxylase small chain	1109,31	1424,22	1523,88	783,93	881,32	911,58	14395,42	-0,72	0,08	-8,61	0,00	0,00
Rubisco large subunit N-methyltransferase	RBCMT3	g7063.t1	fructose-bisphosphate aldolase-lysine N- chloroplastic	22,36	21,08	19,88	39,32	42,70	40,42	1065,86	0,95	0,09	10,71	0,00	0,00

	Oxidative phosphorylation															
Description	Abbreviations	Gene name in *C. vulgaris*	Description Blast2go	C_v LL_1	C_v LL_2	C_v LL_3	C_v HL_1	C_v HL_2	C_v HL_3	baseMean	Log2Fold Change	lfcSE	stat	pvalue	padj
NADH-ubiquinone oxidoreductase subunit 1	ND1	nad1-mt													
NADH-ubiquinone oxidoreductase subunit 2	ND2	nd1/f-mt.t1		0,77	0,79	0,89	0,50	0,38	0,36	7,67	-1,22	0,70	-1,74	0,08	0,13
NADH-ubiquinone oxidoreductase subunit 4	ND4	nad4-mt.t1		0,00	0,32	0,00	0,00	0,32	0,00	0,69	-0,89	2,83	-0,31	0,75	0,82
NADH-ubiquinone oxidoreductase subunit 5	ND5	nd1/f-mt.t1		0,00	0,51	0,10	0,14	0,00	0,13	1,08	-0,80	2,09	-0,38	0,70	0,78
		nad5-mt.t1		0,21	0,19	0,32	0,25	0,10	0,07	2,50	-0,38	1,22	-0,31	0,75	0,82
NADH dehydrogenase (ubiquinone) Fe-S protein 1	NDUFS1	g687.t1	NADH dehydrogenase [ubiquinone] iron-sulfur mitochondrial	98,14	85,55	91,37	100,72	104,08	104,65	4891,59	0,21	0,06	3,37	0,00	0,00
NADH dehydrogenase (ubiquinone) Fe-S protein 2	NDUFS2	nd1/f-mt.t1		0,26	0,50	0,11	0,75	0,56	0,13	3,42	0,81	1,14	0,71	0,48	0,57
NADH dehydrogenase (ubiquinone) Fe-S protein 3	NDUFS3	nd3-mt.t1		0,81	0,53	1,75	0,48	0,34	0,84	2,12	-1,30	1,40	-0,93	0,35	0,45
NADH dehydrogenase (ubiquinone) Fe-S protein 4	NDUFS4	g1728.t1	NADH dehydrogenase [ubiquinone] iron-sulfur mitochondrial	177,08	162,98	180,12	185,99	184,35	191,17	2801,56	0,11	0,07	1,46	0,15	0,21
NADH dehydrogenase (ubiquinone) Fe-S protein 5	NDUFS5	g4687.t1	NADH dehydrogenase [ubiquinone] iron-sulfur 5-B-like	211,49	261,45	208,47	170,42	143,66	166,75	1682,18	-0,51	0,11	-4,40	0,00	0,00
NADH dehydrogenase (ubiquinone) Fe-S protein 6	NDUFS6	g1385.t1	NADH dehydrogenase [ubiquinone] iron-sulfur mitochondrial-like	177,18	188,58	195,87	147,54	145,95	148,99	1714,53	-0,34	0,08	-4,51	0,00	0,00
NADH dehydrogenase (ubiquinone) Fe-S protein 7	NDUFS7	g835.t1	NADH dehydrogenase [ubiquinone] iron-sulfur mitochondrial-like	307,60	362,54	345,05	461,15	431,03	437,03	3721,89	0,31	0,07	4,55	0,00	0,00
NADH dehydrogenase (ubiquinone) Fe-S protein 8	NDUFS8	g4625.t1	NADH dehydrogenase [ubiquinone] iron-sulfur 8-mitochondrial	181,26	193,61	189,55	219,10	191,04	198,16	3338,29	0,11	0,08	1,45	0,15	0,23
NADH dehydrogenase (ubiquinone) flavoprotein 1	NDUFV1	g4435.t1	NADH dehydrogenase [ubiquinone] flavo mitochondrial	219,45	233,88	207,82	385,48	340,71	326,33	9191,29	0,67	0,08	7,87	0,00	0,00
		g10721.t1	NADH dehydrogenase [ubiquinone] flavo mitochondrial	32,37	34,69	29,28	99,64	100,30	121,56	653,19	2,03	0,44	4,66	0,00	0,00
NADH dehydrogenase (ubiquinone) flavoprotein 2	NDUFV2	g923.t1	NADH dehydrogenase [ubiquinone] flavo mitochondrial	152,83	166,05	148,40	182,57	160,94	163,16	3355,33	0,12	0,08	1,43	0,15	0,22
NADH dehydrogenase (ubiquinone) 1 alpha subcomplex subunit 2	NDUFA2	g6666.t1	NADH dehydrogenase [ubiquinone] 1 alpha subcomplex subunit 2-like	226,41	246,03	198,64	208,21	166,53	176,75	1522,53	-0,29	0,11	-2,57	0,01	0,02
NADH ubiquinone oxidoreductase 18 kDa subunit	NDUFA3	g6612.t1	probable NADH dehydrogenase [ubiquinone] 1 alpha subcomplex subunit mitochondrial	64,55	68,62	72,88	61,71	64,41	64,84	748,53	-0,11	0,09	-1,16	0,24	0,33
NADH dehydrogenase (ubiquinone) 1 alpha subcomplex subunit 6	NDUFA6	g4620.t1	NADH dehydrogenase [ubiquinone] 1 alpha subcomplex subunit 6	121,54	142,32	124,67	92,65	92,07	99,88	1035,74	-0,49	0,09	-5,38	0,00	0,00
NADH dehydrogenase (ubiquinone) 1 alpha subcomplex subunit 8	NDUFA8	g742.t1	NADH dehydrogenase [ubiquinone] 1 alpha subcomplex subunit 8-B-like	204,37	255,17	209,61	128,45	122,54	123,24	1284,17	-0,83	0,10	-8,16	0,00	0,00
NADH dehydrogenase (ubiquinone) 1 alpha subcomplex subunit 9	NDUFA9	g1558.t1	NADH dehydrogenase [ubiquinone] 1 alpha subcomplex subunit mitochondrial	41,45	47,51	64,55	58,85	61,43	62,88	1076,06	0,01	0,12	0,11	0,91	0,94
NADH dehydrogenase (ubiquinone) 1 alpha/beta subcomplex 1	NDUFAB1	g1590.t1	hypothetical protein CHLNCDRAFT_140343	366,14	188,48	170,80	153,14	152,10	158,64	5457,62	-0,18	0,07	-2,50	0,01	0,02
NADH dehydrogenase (ubiquinone) 1 beta subcomplex subunit 3	NDUFB3	g9426.t1	probable mitochondrial ribosome release factor	26,73	33,53	25,38	28,38	19,06	28,13	334,67	-0,52	0,14	-3,73	0,00	0,00

NADH dehydrogenase (ubiquinone) 1 beta subcomplex subunit 7	NDUFB7	g5028.t1	NADH-ubiquinone oxidoreductase B18 subunit family	150,25	160,31	140,56	120,76	109,09	117,56	734,22	-0,38	0,10	-3,85	0,00	0,00
NADH dehydrogenase (ubiquinone) 1 beta subcomplex subunit 9	NDUFB9	g5339.t1	NADH dehydrogenase [ubiquinone] 1 beta subcomplex subunit 9	285,66	346,88	282,33	237,85	204,98	228,43	1993,23	-0,85	0,10	-4,39	0,00	0,00
NADH dehydrogenase (ubiquinone) 1 beta subcomplex subunit 10	NDUFB10	g2196.t1	NADH dehydrogenase [ubiquinone] 1 beta subcomplex subunit 10-A-like	614,11	583,77	599,28	506,58	544,56	548,65	4303,80	-0,09	0,07	-1,32	0,19	0,28
NADH dehydrogenase (ubiquinone) 1 alpha subcomplex subunit 12	NDUFA12	g8177.t1	probable NADH dehydrogenase [ubiquinone] 1 alpha subcomplex subunit 12	163,68	185,37	158,76	144,92	136,28	132,37	1597,80	-0,30	0,09	-3,36	0,00	0,00
NADH dehydrogenase (ubiquinone) 1 alpha subcomplex subunit 13	NDUFA13	g5574.t1	NADH dehydrogenase [ubiquinone] 1 alpha subcomplex subunit 13-B	214,52	217,66	232,62	187,20	185,48	180,52	2032,98	-0,27	0,07	-3,67	0,00	0,00
succinate dehydrogenase (ubiquinone) flavoprotein subunit	SDHA	g699.t1	Succinate dehydrogenase [ubiquinone] flavo subunit mitochondrial	96,28	89,83	97,84	184,01	160,07	161,59	5858,14	0,83	0,07	12,05	0,00	0,00
succinate dehydrogenase (ubiquinone) iron-sulfur subunit	SDHB	g280.t1	Succinate dehydrogenase [ubiquinone] iron-sulfur mitochondrial	170,41	192,53	165,93	349,21	335,57	308,44	4845,83	0,88	0,08	10,53	0,00	0,00
Succinate dehydrogenase subunit b560	SDHC, SDHD	g10434.t1	succinate dehydrogenase subunit b560	324,02	393,52	332,51	355,48	317,28	328,18	4251,32	-0,07	0,09	-0,74	0,46	0,58
succinate dehydrogenase (ubiquinone) membrane anchor subunit	SDHD, SDH4	g10349.t1	Succinate dehydrogenase [ubiquinone] cytochrome b small mitochondrial	333,93	336,28	333,97	335,13	301,28	317,76	2596,98	-0,04	0,07	-0,59	0,56	0,65
ubiquinol-cytochrome c reductase iron-sulfur subunit	UQCRFS1	g1831.t1	cytochrome b-c1 complex subunit Rieske- mitochondrial-like	369,37	391,17	356,13	302,88	283,41	287,89	6163,58	-0,35	0,07	-5,24	0,00	0,00
ubiquinol-cytochrome c reductase cytochrome b subunit	CYTB	cob-mat.t1		0,22	0,14	0,38	0,19	0,11	0,23	6,39	-0,59	0,94	-0,62	0,53	0,63
ubiquinol-cytochrome c reductase cytochrome c1 subunit	CYC1	g10722.t1	cytochrome c1- heme mitochondrial	27,87	46,07	45,15	36,66	55,96	58,98	422,17	0,35	0,21	1,72	0,08	0,13
		g6434.t1	Cytochrome c1- heme mitochondrial	243,06	269,47	239,28	298,36	283,33	280,29	5530,63	0,21	0,07	2,93	0,00	0,01
ubiquinol-cytochrome c reductase subunit 6	QCR6	g6828.t1	cytochrome b-c1 complex subunit 6-like	338,90	375,78	339,13	220,34	235,13	261,19	1444,03	-0,55	0,09	-5,93	0,00	0,00
ubiquinol-cytochrome c reductase subunit 7	QCR7	g3568.t1	cytochrome b-c1 complex subunit 7-2	314,83	328,13	328,54	267,04	259,48	264,42	2572,87	-0,29	0,07	-4,38	0,00	0,00
cytochrome c oxidase subunit 1	COX1	cox1-mat.t1		0,79	0,61	1,05	0,96	0,97	1,19	31,54	0,10	0,40	0,25	0,80	0,88
cytochrome c oxidase subunit 6b	COX6B	g6206.t1	cytochrome c oxidase subunit 6b-1-like	1,76	2,30	2,29	3,25	3,40	2,23	22,86	0,50	0,42	1,19	0,23	0,32
heme o synthase	COX10	g7575.t1	Protoheme IX mitochondrial	15,15	14,23	15,95	15,79	18,24	17,85	556,63	0,20	0,31	1,82	0,07	0,11
cytochrome c oxidase assembly protein subunit 11	COX11	g1904.t1	cytochrome c oxidase assembly mitochondrial	35,05	42,71	32,16	64,08	65,88	63,45	801,41	0,82	0,11	7,29	0,00	0,00
cytochrome c oxidase assembly protein subunit 15	COX15	g7499.t1	cytochrome c oxidase assembly COX15	12,64	9,84	12,05	32,02	35,72	33,99	851,65	1,56	0,11	14,15	0,00	0,00
Cytochrome c oxidase assembly protein subunit 17	COX17	g983.t1	cytochrome c oxidase copper chaperone 1	22,44	28,23	24,38	28,08	33,21	43,80	229,08	0,54	0,18	3,06	0,00	0,00
F-type H+-transporting ATPase subunit alpha	ATPaF1A	atpA-mat.t1		0,53	0,40	0,59	0,58	0,32	0,36	11,87	-0,32	0,54	-0,60	0,55	0,64
F-type H+-transporting ATPase subunit beta	ATPaF1B	g1519.t1	ATP synthase subunit mitochondrial	417,33	459,39	420,45	311,66	277,78	274,06	13152,12	-0,59	0,08	-7,09	0,00	0,00
F-type H+-transporting ATPase subunit delta	ATPaF1D	g5613.t1	ATP synthase subunit delta mitochondrial-like	258,25	268,10	283,33	191,78	177,07	192,70	3403,57	-0,58	0,08	-7,25	0,00	0,00
F-type H+-transporting ATPase subunit epsilon	ATPaF1E	g6778.t1	ATP synthase subunit mitochondrial	623,14	700,87	620,06	672,04	597,68	607,69	3425,28	-0,05	0,08	-0,61	0,54	0,64
F-type H+-transporting ATPase subunit gamma	ATPaF1G	g6547.t1	ATP synthase subunit mitochondrial	249,68	251,14	268,52	187,41	189,64	192,11	5125,34	-0,44	0,06	-6,86	0,00	0,00
F-type H+-transporting ATPase subunit O	ATPaF0O	g578.t1	ATP synthase subunit mitochondrial	434,78	490,13	418,84	327,80	292,71	287,61	5739,75	-0,57	0,09	-6,61	0,00	0,00
F-type H+-transporting ATPase subunit d	ATPaF0D	g865.t1	ATP synthase subunit mitochondrial-like	280,71	299,87	284,35	228,81	233,12	238,70	3352,72	-0,30	0,07	-4,62	0,00	0,00
F-type H+-transporting ATPase subunit g	ATPaFG	g8168.t1	hydrogen-transporting ATP synthesis mechanism	161,60	157,66	168,03	102,06	105,55	106,59	1186,08	-0,63	0,08	-7,98	0,00	0,00

Chloroplast division

Description	Abbreviations	Gene name in *C. vulgaris*	Description Blast2go	C_v LL_1	C_v LL_2	C_v LL_3	C_v HL_1	C_v HL_2	C_v HL_3	Base Mean	Log2 Fold Change	lfcSE	stat	pvalue	padj
Chloroplast division site-determinant MinE	MINE1	g6808.t1	cell division topological specificity factor chloroplastic-like	62,47	67,68	64,86	37,64	32,99	34,01	751,80	-0,90	0,10	-9,34	0,00	0,00
Chloroplast septum site-determining protein	minD1	minD.t1													

Glycolysis

Description	Abbreviations	Gene name in *C. vulgaris*	Description Blast2go	C_v LL_1	C_v LL_2	C_v LL_3	C_v HL_1	C_v HL_2	C_v HL_3	Base Mean	Log2 Fold Change	lfcSE	stat	pvalue	padj
Glyceraldehyde 3-phosphate dehydrogenase	GAPDH	g223.t1	major facilitator transporter	0,11	0,17	0,21	0,11	0,10	0,10	8,10	-0,09	0,08	-1,01	0,31	0,41
		g8925.t1	type I glyceraldehyde-3-phosphate dehydrogenase	1573,64	1803,44	1553,16	1102,34	929,36	988,40	31275,77	-0,71	0,09	-8,07	0,00	0,00
		g3524.t1	glyceraldehyde-3-phosphate dehydrogenase chloroplastic-like	83,54	92,90	86,05	55,38	46,71	50,87	1900,29	-0,78	0,09	-8,79	0,00	0,00
Hexokinase	HK	g1762.t1	hexokinase-2-like isoform X2	9,06	9,18	9,73	12,00	12,43	12,94	737,65	0,42	0,09	4,54	0,00	0,00
Glucokinase	glk	g5259.t1	glucokinase	98,49	103,64	91,79	76,00	73,75	78,00	2139,00	-0,57	0,08	-4,78	0,00	0,00
6-phosphofructokinase 1	pfkA	g362.t1	phosphofructokinase family	364,70	380,15	344,58	335,38	289,32	284,01	11418,66	-0,26	0,08	-3,18	0,00	0,00
		g3278.t1	phosphofructokinase family	0,19	0,00	0,08	0,17	0,19	0,30	3,69	1,20	1,10	1,09	0,28	0,37
		g3998.t1	phosphofructokinase family	72,59	89,32	73,48	48,73	44,75	49,01	2383,68	-0,72	0,10	-7,48	0,00	0,00
		g3998.t2	phosphofructokinase family												
		g5910.t1	phosphofructokinase family	257,37	285,35	239,93	237,97	205,32	206,30	8451,34	-0,27	0,09	-3,01	0,00	0,01
Pyruvate kinase	PK	g2308.t1	Pyruvate kinase	23,38	26,23	22,90	18,70	18,03	17,83	1082,61	-0,41	0,09	-4,61	0,00	0,00
		g2878.t1	Pyruvate kinase	13,32	15,53	14,44	13,89	16,62	15,56	1099,29	0,10	0,10	0,95	0,34	0,44
		g6475.t1	plastidial pyruvate kinase 2-like	85,04	92,50	85,64	75,92	70,54	70,94	3445,53	-0,28	0,07	-3,87	0,00	0,00
		g2889.t1	pyruvate kinase	68,60	80,31	71,84	55,28	47,37	48,45	2947,23	-0,55	0,09	-6,02	0,00	0,00
		g6026.t1	Pyruvate kinase isozyme chloroplastic	60,86	50,25	68,05	62,17	66,98	72,19	5765,86	0,17	0,11	1,55	0,12	0,18
		g7944.t1	Pyruvate cytosolic isozyme	34,39	38,73	36,13	39,82	34,33	35,02	1311,71	0,00	0,09	-0,04	0,97	0,98
Diphosphate-dependent phosphofructokinase	pfp	g6649.t1	pyrophosphate--fructose 6-phosphate 1-phosphotransferase subunit beta	109,25	123,08	123,93	73,84	73,67	72,89	3899,42	-0,69	0,07	-9,38	0,00	0,00
		g6650.t1	pyrophosphate--fructose 6-phosphate 1-phosphotransferase subunit beta-like	49,00	60,57	56,96	46,24	42,16	37,76	1705,14	-0,38	0,10	-3,65	0,00	0,00
Phosphoglycerate kinase	PGK	g3225.t1	Phosphoglycerate cytosolic	338,01	348,23	324,41	252,07	222,04	216,39	7998,93	-0,55	0,08	-7,11	0,00	0,00
		g3661.t1	Phosphoglycerate chloroplastic	66,66	81,24	76,79	22,74	25,14	24,27	1603,04	-1,63	0,10	-16,93	0,00	0,00
Fructose-bisphosphate aldolase, class I	ALDO	g1374.t1	fructose-bisphosphate aldolase cytoplasmic isozyme	45,15	53,17	47,54	63,11	54,67	56,43	1493,76	0,26	0,09	2,69	0,01	0,01
		g10705.t1	fructose-bisphosphate aldolase cytoplasmic isozyme	38,55	43,96	47,12	42,93	58,43	48,13	1302,69	0,21	0,12	1,70	0,09	0,14
		g2570.t1	probable fructose-bisphosphate aldolase chloroplastic	856,60	934,45	926,46	680,73	701,25	691,09	21129,03	-0,39	0,06	-6,31	0,00	0,00
		g9790.t1	fructose-bisphosphate cytoplasmic isozyme 1	350,41	424,86	354,16	122,29	118,04	129,98	6283,80	-1,61	0,09	-17,87	0,00	0,00
Enolase	ENO	g9540.t1	enolase	397,08	433,63	412,97	242,83	211,26	223,36	12007,03	-0,88	0,07	-11,80	0,00	0,00
Aldose 1-epimerase	galM	g5349.t1	Aldose 1-epimerase	99,79	110,92	95,94	121,21	111,24	111,64	2650,84	0,17	0,08	2,03	0,04	0,07
Glucose-6-phosphate 1-epimerase		g3815.t1	glucose-6-phosphate 1-epimerase	56,13	60,34	61,11	69,31	80,62	81,51	1375,77	0,38	0,09	4,17	0,00	0,00
		g10611.t1	glucose-6-phosphate 1-epimerase	80,00	76,51	80,05	70,02	66,92	66,41	1822,72	-0,22	0,07	-3,08	0,00	0,00
		g3967.t1	glucose-6-phosphate 1-epimerase	38,49	42,18	38,44	25,77	28,85	28,05	824,30	-0,52	0,09	-5,50	0,00	0,00
Triosephosphate isomerase (TIM)	TPI	g9016.t1	triosephosphate cytosolic-like	405,55	450,43	404,45	241,67	219,87	226,60	5737,75	-0,87	0,07	-11,72	0,00	0,00
		g4561.t1	triosephosphate chloroplastic	32,87	37,47	35,46	17,65	20,03	20,24	546,91	-0,86	0,11	-7,88	0,00	0,00
Glucose-6-phosphate isomerase	GPI	g4329.t1	Glucose-6-phosphate cytosolic	43,49	50,43	46,33	41,76	40,50	39,24	2000,48	-0,21	0,08	-2,54	0,01	0,02
		g4329.t2	Glucose-6-phosphate cytosolic												
		g3314.t1	glucose-6-phosphate cytosolic	27,98	26,87	27,35	19,93	20,56	20,04	900,13	-0,44	0,08	-5,37	0,00	0,00
Phosphoglucomutase	pgm	g1983.t1	chloroplastic	187,15	197,22	186,10	155,41	140,97	138,14	7251,96	-0,39	0,07	-5,55	0,00	0,00
Fructose-1,6-bisphosphatase I	FBP	g8765.t1	Fructose-1,6- chloroplastic	99,55	114,78	105,24	96,52	88,93	94,94	2939,76	-0,19	0,08	-2,38	0,02	0,03
		g8895.t1	fructose-1,6- cytosolic-like	67,67	80,56	68,73	37,42	32,55	34,65	1295,04	-1,06	0,10	-10,58	0,00	0,00

2,3-bisphosphoglycerate-independent phosphoglycerate mutase	gpmI	g8973.t1	2,3-bisphosphoglycerate-independent phosphoglycerate mutase	347,22	420,18	356,35	390,30	343,27	344,85	14224,87	-0,06	0,09	-0,65	0,51	0,61
		g8966.t1	2,3-bisphosphoglycerate-independent phosphoglycerate mutase	34,47	39,74	33,12	52,76	48,92	49,63	1785,13	0,50	0,09	5,54	0,00	0,00
Probable phosphoglycerate mutase	gpmB	g4905.t1	bifunctional RNase H acid phosphatase	19,92	20,89	21,32	25,00	29,06	28,54	549,14	0,42	0,11	3,86	0,00	0,00
		g7532.t1	phosphoglycerate mutase 4	8,84	5,66	8,04	9,35	10,54	10,52	173,19	0,43	0,19	2,29	0,02	0,04
Phosphoglucomutase / phosphopentomutase	PGM2	g629.t1	phosphoglucomutase-2	8,14	8,93	7,71	9,12	8,47	7,79	787,47	0,04	0,10	0,36	0,72	0,79

TCA + glyoxylate

Description	Abbreviations	Gene name in *C. vulgaris*	Description Blast2go	C_v LL_1	C_v LL_2	C_v LL_3	C_v HL_1	C_v HL_2	C_v HL_3	Base Mean	Log2 Fold Change	lfcSE	stat	pvalue	padj
Malate Dehydrogenase	mdh	g1635.t1	Malate glyoxysomal	109,87	105,70	113,72	124,29	120,04	125,21	2822,37	0,16	0,07	2,43	0,02	0,03
Malate Dehydrogenase	MDH1	g9160.t1	malate dehydrogenase	160,20	173,77	160,06	146,72	135,16	135,71	3490,71	-0,24	0,07	-3,35	0,00	0,00
Malate Dehydrogenase	MDH2	g4174.t1	malate mitochondrial	323,57	301,47	356,54	244,45	259,20	261,57	7014,06	-0,36	0,08	-4,56	0,00	0,00
		g5770.t1	malate chloroplastic-like	92,53	109,24	92,38	78,60	74,01	75,48	2236,69	-0,37	0,09	-4,18	0,00	0,00
Isocitrate Dehydrogenase (Nad+)	IDH3	g2872.t1	isocitrate dehydrogenase [NAD] catalytic subunit mitochondrial-like	62,72	72,25	63,66	50,57	44,12	43,03	1456,34	-0,53	0,10	-5,50	0,00	0,00
Isocitrate Dehydrogenase	IDH1	g3593.t1	isocitrate NADP-dependent	146,24	170,87	153,99	164,96	146,89	150,49	4932,30	-0,03	0,08	-0,33	0,74	0,80
Pyruvate Dehydrogenase E1 Component Alpha Subunit	PDHA	g4311.t1	Pyruvate dehydrogenase E1 component subunit mitochondrial	168,84	180,05	165,84	123,01	123,15	121,19	4127,03	-0,49	0,07	-7,46	0,00	0,00
		g9488.t1	pyruvate dehydrogenase E1 component subunit alpha- chloroplastic-like	266,92	289,50	264,42	224,22	205,09	211,02	7329,66	-0,36	0,07	-5,13	0,00	0,00
Pyruvate Dehydrogenase E1 Component Beta Subunit	PDHB	g1705.t1	pyruvate dehydrogenase E1 component subunit beta- mitochondrial-like	146,55	166,07	144,37	96,76	91,57	92,50	3057,02	-0,70	0,08	-8,88	0,00	0,00
		g7465.t1	pyruvate dehydrogenase E1 component subunit beta- chloroplastic-like	89,59	92,38	90,82	71,34	69,03	66,55	2093,73	-0,40	0,07	-5,73	0,00	0,00
2-Oxoglutarate Dehydrogenase E1 Component	OGDH	g2760.t1	2-oxoglutarate mitochondrial-like	146,00	151,14	140,57	187,76	165,32	161,29	11435,59	0,23	0,08	3,02	0,00	0,01
Succinate Dehydrogenase (Ubiquinone) Flavoprotein Subunit	SDHA	g499.t1	Succinate dehydrogenase [ubiquinone] flavo subunit mitochondrial	96,28	95,83	97,84	184,01	160,07	163,59	5858,14	0,83	0,07	12,05	0,00	0,00
Succinate Dehydrogenase (Ubiquinone) Iron-Sulfur Subunit	SDHB	g280.t1	Succinate dehydrogenase [ubiquinone] iron-sulfur mitochondrial	170,41	192,53	165,93	349,21	315,57	309,44	4845,83	0,88	0,08	10,53	0,00	0,00
Dihydrolipoamide Dehydrogenase	DLD	g2561.t1	Dihydrolipoyl dehydrogenase mitochondrial	251,15	277,11	245,02	220,99	192,70	186,20	7863,10	-0,37	0,09	-4,27	0,00	0,00
		g1708.t1	Dihydrolipoyl dehydrogenase	86,35	87,58	92,42	66,08	67,83	68,04	3139,46	-0,40	0,07	-6,05	0,00	0,00
Pyruvate Dehydrogenase E2 Component (Dihydrolipoamide Acetyltransferase)	DLAT	g3442.t1	dihydrolipoyllysine-residue acetyltransferase component of pyruvate dehydrogenase mitochondrial	37,60	37,87	38,73	31,33	30,61	30,33	1545,25	-0,31	0,07	-4,30	0,00	0,00
		g5680.t1	dihydrolipoyllysine-residue acetyltransferase component 1 of pyruvate dehydrogenase mitochondrial isoform X1	24,58	25,28	25,85	16,27	13,02	13,42	711,19	-0,84	0,11	-7,66	0,00	0,00

2-Oxoglutarate Dehydrogenase E2 Component (Dihydrolipoamide Succinyltransferase)	DLST	g7147.t1	dihydrolipoylysine-residue acetyltransferase component 5 of pyruvate dehydrogenase chloroplastic-like	32,64	37,87	35,28	19,47	17,23	18,22	922,08	-0,95	0,10	-9,75	0,00	0,00
Phosphoenolpyruvate Carboxykinase (Atp)	E4.1.1.49	g6027.t1	dihydrolipoylysine-residue succinyltransferase component of 2-oxoglutarate dehydrogenase complex mitochondrial-like isoform X1	121,61	125,00	114,05	106,57	93,34	100,23	3583,99	-0,27	0,08	-3,43	0,00	0,00
		g5175.t1	phosphoenolpyruvate carboxykinase [ATP]-like	29,52	33,47	28,19	26,93	25,00	26,24	1255,55	-0,22	0,09	-2,41	0,02	0,03
Isocitrate Lyase	aceA	g5714.t1	phosphoenolpyruvate carboxykinase [ATP]-like	302,52	427,99	378,99	486,59	378,47	384,07	18524,35	0,06	0,10	0,57	0,57	0,66
Malate Synthase	aceB, glcB	g5128.t1	malate synthase A	61,26	54,87	49,36	361,00	286,84	284,51	7078,73	2,49	0,11	22,56	0,00	0,00
		g5577.t1	malate synthase A	98,57	98,80	98,62	125,01	121,83	119,58	4268,65	0,32	0,06	5,23	0,00	0,00
Citrate Synthase	CS	g870.t1	citrate glyoxysomal	110,23	110,05	108,24	110,18	93,23	99,73	3757,78	-0,12	0,08	-1,48	0,14	0,20
		g1304.t1	citrate (Si)-synthase	119,58	127,02	103,77	107,35	298,91	294,25	11517,49	1,50	0,12	12,63	0,00	0,00
		g8948.t1	citrate mitochondrial	72,11	80,98	75,05	48,36	44,70	45,25	1983,22	-0,72	0,08	-9,12	0,00	0,00
Atp Citrate (Pro-S)-Lyase	ACLY	g7302.t1	ATP-citrate synthase beta chain 1	167,15	194,78	163,86	146,04	124,55	129,40	6745,13	-0,39	0,09	-4,30	0,00	0,00
		g1158.t1	ATP-citrate synthase alpha chain 1	93,04	99,95	88,34	124,52	105,06	106,46	3089,80	0,26	0,09	2,84	0,00	0,01
Fumarate Hydratase, Class Ii	E4.2.1.2B	g6213.t1	fumarate mitochondrial isoform X1	86,53	93,57	87,93	78,40	74,87	78,32	2849,27	-0,21	0,07	-2,94	0,00	0,01
Aconitate Hydratase	ACO	g1559.t1	Aconitate mitochondrial	249,18	248,56	253,77	187,48	167,09	160,19	11672,36	-0,55	0,07	-7,38	0,00	0,00
Succinyl-Coa Synthetase Alpha Subunit	LSC1	g1523.t1	succinyl- ligase [ADP-forming] subunit alpha-mitochondrial	55,66	62,11	60,04	55,75	50,71	48,88	1287,30	-0,20	0,09	-2,22	0,03	0,05
Succinyl-Coa Synthetase Beta Subunit	LSC2	g1427.t1	Succinyl- ligase [ADP-forming] subunit mitochondrial	225,77	260,60	211,32	175,52	154,39	151,73	5737,45	-0,53	0,10	-5,62	0,00	0,00
Pyruvate Carboxylase	PC	g6158.t1	biotin carboxylase chloroplastic	153,81	162,50	164,69	124,84	123,89	124,73	5550,15	-0,37	0,06	-5,95	0,00	0,00

Carbon fixation metabolism

Description	Abbreviations	Gene name in C. vulgaris	Description Blast2go	C_v LL_1	C_v LL_2	C_v LL_3	C_v HL_1	C_v HL_2	C_v HL_3	Base Mean	Log2 Fold Change	lfcSE	stat	pvalue	padj
Malate Dehydrogenase	mdh	g1635.t1	Malate glyoxysomal	109,87	105,70	113,72	124,29	120,04	125,21	2822,37	0,16	0,07	2,43	0,02	0,03
Malate Dehydrogenase	MDH1	g9160.t1	malate dehydrogenase	160,20	173,77	180,06	146,72	135,16	135,71	3490,71	-0,24	0,07	-3,35	0,00	0,00
Malate Dehydrogenase	MDH2	g4174.t1	malate mitochondrial	323,57	301,47	356,54	244,45	259,20	261,57	7014,06	-0,36	0,08	-4,56	0,00	0,00
		g5770.t1	malate chloroplastic-like	92,53	109,24	92,56	78,60	74,01	75,48	2236,69	-0,37	0,09	-4,18	0,00	0,00
Malate Dehydrogenase (Oxaloacetate-Decarboxylating)(NADP+)	E1.1.1.40	g412.t1	NADP-dependent malic enzyme	24,60	22,94	24,59	34,22	30,46	30,98	1031,07	0,40	0,09	4,49	0,00	0,00
		g6340.t1	NADP-dependent malic enzyme	23,55	23,39	26,41	23,89	26,07	26,97	1070,64	0,07	0,09	0,77	0,44	0,54
Malate Dehydrogenase (NADP+)	E1.1.1.82	g5791.t1	Malate dehydrogenase [NADP] chloroplastic	581,29	555,91	605,23	407,44	405,81	413,62	14962,86	-0,51	0,06	-8,42	0,00	0,00
Glyceraldehyde 3-Phosphate Dehydrogenase	GAPDH	g223.t1	major facilitator transporter	0,11	0,17	0,23	0,11	0,10	0,10	8,10	-0,69	0,68	-1,01	0,31	0,41
		g8925.t1	type I glyceraldehyde-3-phosphate dehydrogenase	1573,64	1805,44	1553,16	1102,34	929,36	988,40	31275,77	-0,71	0,09	-8,07	0,00	0,00
		g3524.t1	glyceraldehyde-3-phosphate dehydrogenase chloroplastic-like	83,54	92,90	86,05	55,38	46,71	50,87	1900,29	-0,78	0,09	-8,79	0,00	0,00
Transketolase	E2.2.1.1	g621.t1	chloroplastic	195,30	205,68	207,01	124,14	129,89	132,93	8337,58	-0,65	0,06	-10,41	0,00	0,00
Alanine Transaminase	GPT	g5785.t1	alanine aminotransferase 2	188,59	208,38	180,64	400,02	329,31	330,50	9795,75	0,88	0,09	9,29	0,00	0,00
Phosphoribulokinase	PRK	g7999.t1	chloroplastic-like	101,17	129,46	110,59	84,66	84,40	86,38	2833,27	-0,42	0,09	-4,80	0,00	0,00
Phosphoglycerate Kinase	PGK	g3225.t1	Phosphoglycerate cytosolic	318,01	348,23	324,41	252,07	222,04	216,39	7998,93	-0,55	0,08	-7,11	0,00	0,00
		g3661.t1	Phosphoglycerate chloroplastic	66,66	81,24	76,79	22,74	25,14	24,27	1603,04	-1,63	0,10	-16,93	0,00	0,00
Pyruvate, Orthophosphate Dikinase	ppdK	g5044.t1	phosphate chloroplastic	229,24	221,51	216,32	441,26	398,13	398,02	20703,91	0,89	0,07	11,16	0,00	0,00
Sedoheptulose-Bisphosphatase	E3.1.3.37	g5810.t1	Sedoheptulose-1,7-chloroplastic	170,64	174,97	172,49	110,41	113,93	109,70	3838,17	-0,63	0,06	-10,30	0,00	0,00
		g1164.t1	Sedoheptulose-1,7-chloroplastic	9,05	10,38	11,56	11,32	11,70	13,07	252,17	0,22	0,15	1,46	0,15	0,21
Phosphoenolpyruvate Carboxylase	ppc	g3928.t1	phosphoenolpyruvate carboxylase 2	167,00	203,49	159,94	113,50	100,10	95,43	9467,62	-0,78	0,10	-7,56	0,00	0,00
		g4635.t1	phosphoenolpyruvate carboxylase 4	55,98	51,08	61,35	51,02	49,78	49,99	4205,56	-0,16	0,08	-2,00	0,05	0,08
Ribulose-Bisphosphate Carboxylase Large Chain	rbcL	rbcL-chl.t1		24,77	34,54	32,09	28,72	18,08	22,49	890,22	-0,41	0,16	-2,47	0,01	0,03

Ribulose-Bisphosphate Carboxylase Small Chain	rbcS	g10102.t1	ribulose-bisphosphate carboxylase small chain	1309,31	1424,22	1523,98	783,03	881,32	911,58	14395,42	-0,72	0,08	-8,61	0,00	0,00
		g10103.t1	ribulose-bisphosphate carboxylase small chain	420,44	433,41	492,51	216,19	222,98	244,80	4296,09	-0,99	0,08	-11,79	0,00	0,00
Phosphoenolpyruvate Carboxykinase (ATP)	EC 4.1.1.4	g5175.t1	phosphoenolpyruvate carboxykinase [ATP]-like	29,52	33,47	28,19	26,93	25,00	26,24	1255,55	-0,22	0,09	-2,41	0,02	0,03
		g5714.t1	phosphoenolpyruvate carboxykinase [ATP]-like	382,52	427,99	378,99	486,59	378,47	384,07	18524,35	0,06	0,10	0,57	0,57	0,60
Fructose-Bisphosphate Aldolase, Class I	ALDO	g1374.t1	fructose-bisphosphate aldolase cytoplasmic isozyme	45,15	53,17	47,54	61,11	54,67	56,43	1403,76	0,26	0,09	2,60	0,01	0,01
		g10705.t1	fructose-bisphosphate aldolase cytoplasmic isozyme	38,55	43,96	47,12	42,93	58,43	48,13	1302,69	0,21	0,12	1,70	0,09	0,14
		g2570.t1	probable fructose-bisphosphate aldolase chloroplastic	856,00	934,45	926,46	680,73	701,25	691,09	21329,03	-0,39	0,06	-6,31	0,00	0,00
		g9790.t1	fructose-bisphosphate cytoplasmic isozyme 1	350,41	424,86	354,16	122,29	118,04	120,98	6281,80	-1,61	0,09	-17,87	0,00	0,00
Ribulose-Phosphate 3-Epimerase	rpe	g678.t1	carbohydrate kinase	16,15	13,03	18,20	16,21	18,86	18,82	920,27	0,39	0,13	1,48	0,14	0,20
		g6497.t1	ribulose-phosphate 3-chloroplastic	280,06	315,67	282,18	266,02	282,40	259,09	5222,83	-0,37	0,07	-2,49	0,01	0,02
Triosephosphate Isomerase (TIM)	TPI	g9036.t1	triosephosphate cytosolic-like	405,55	450,43	404,45	241,67	219,87	226,60	5737,75	-0,87	0,07	-11,72	0,00	0,00
		g8563.t1	triosephosphate chloroplastic	32,87	37,67	35,46	17,65	20,03	20,24	546,91	-0,86	0,11	-7,88	0,00	0,00
Ribose 5-Phosphate Isomerase A	rpiA	g6358.t1	probable ribose-5-phosphate isomerase chloroplastic	9,33	12,19	11,84	2,56	2,87	3,81	136,35	-1,86	0,21	-8,87	0,00	0,00
		g10579.t1	probable ribose-5-phosphate isomerase chloroplastic	18,91	17,78	16,30	21,71	21,87	23,36	746,63	0,34	0,10	3,44	0,00	0,00
Fructose-1,6-Bisphosphatase I	FBP	g8745.t1	Fructose-1,6- chloroplastic	99,55	114,78	105,24	96,52	88,93	94,04	2939,76	-0,39	0,08	-2,38	0,02	0,03
		g6895.t1	fructose-1,6- cytosolic-like	67,67	80,56	68,73	37,42	32,55	34,65	1295,04	-1,66	0,10	-10,58	0,00	0,00
Glyceraldehyde-3-Phosphate Dehydrogenase (NADP+) (Phosphorylating)	GAPA	g9980.t1	Glyceraldehyde-3-phosphate dehydrogenase chloroplastic	363,81	384,45	417,32	491,86	463,07	473,98	12289,01	0,29	0,07	4,10	0,00	0,00
Glutamate--Glyoxylate Aminotransferase	GGAT	g7537.t1	glutamate--glyoxylate aminotransferase 2	280,61	275,74	291,10	316,62	283,64	280,00	11341,13	0,05	0,07	0,77	0,44	0,54
Aspartate Aminotransferase, Mitochondrial	GOT2	g1363.t1	aspartate cytoplasmic	321,39	355,30	298,71	293,22	244,65	243,98	8303,59	-0,32	0,10	-3,34	0,00	0,00
Aspartate Aminotransferase, Cytoplasmic	GOT1	g1363.t1	aspartate cytoplasmic	321,39	355,30	298,71	293,22	244,65	243,98	8303,59	-0,32	0,10	-3,34	0,00	0,00
Malate Dehydrogenase (Decarboxylating)		g6021.t1	NAD-dependent malic enzyme 59 kDa mitochondrial-like	17,38	20,45	18,00	11,34	11,18	11,09	464,14	-0,73	0,10	-7,16	0,00	0,00

Meiosis

Description	Abbreviations	Gene name in *C. reinhardtii*	Description Blast2go	C_vs LL_1	C_vs LL_2	C_vs LL_3	C_vs HL_1	C_vs HL_2	C_vs HL_3	Base Mean	Log2 Fold Change	lfcSE	stat	pvalue	padj
Rad51-like protein	DMC1*	g289.t1	meiotic recombination DMC1 homolog	0,29	0,44	0,29	0,11	0,54	0,40	8,13	0,14	0,74	0,19	0,85	0,90
DNA-binding HORMA family protein	HOP1*	g2065.t1	HORMA domain-containing 1	0,47	0,69	0,71	0,90	1,38	1,59	56,90	1,06	0,37	2,89	0,00	0,01
Predicted protein	HOP2*	g1434.t1	homologous-pairing 2 homolog	4,58	4,30	3,96	0,14	0,70	0,37	37,63	-3,02	0,40	-7,47	0,00	0,00
Predicted protein	MER3*	g6016.t1	probable ATP-dependent DNA helicase HFM1	35,73	34,46	38,27	27,90	28,57	28,62	2730,30	-0,35	0,07	-4,93	0,00	0,00
OAJ-like protein, partial	MND1*	g5361.t1	meiotic nuclear division 1 homolog	36,02	41,66	32,93	27,96	29,20	31,62	510,52	-0,31	0,12	-2,60	0,01	0,02
Predicted protein, partial	MSH4*	g5446.t1	DNA mismatch repair MSH4	0,17	0,12	0,16	0,35	0,39	0,33	15,41	1,24	0,52	2,40	0,02	0,03
Gametolysin	mmp1	g5347.t1	expressed protein	0,00	0,00	0,00	0,03	0,06	0,03	0,99	3,25	2,17	1,50	0,13	0,20
Gamete-specific protein	HAP2	g3658.t1	male gamete fusion factor	38,22	40,40	35,87	47,38	43,59	45,08	3121,41	0,25	0,08	2,94	0,00	0,01
* Blanc et al. Plant Cell. (2010)															

Table S7. Identification of key genes involved in lipid biosynthesis and degradation in Chlorella vulgaris.

Carbon sources for de novo fatty acid synthesis

Description	Abbreviations	Gene name in *C. vulgaris*	Description Blast2go	C_v LL_1	C_v LL_2	C_v LL_3	C_v HL_1	C_v HL_2	C_v HL_3	Base Mean	Log2 Fold Change	lfcSE	stat	pvalue	padj
Acetyl CoA Synthase	ACS1	g2176.t1	acetyl-coenzyme A chloroplastic glyoxysomal-like	202,70	215,02	184,43	651,01	522,13	528,42	17749,76	1,50	0,10	15,21	0,00	0,00
	ACS2	g2145.t1	acetyl-coenzyme A chloroplastic glyoxysomal isoform X1	54,86	56,08	54,20	84,48	74,00	71,37	1264,04	0,48	0,08	5,83	0,00	0,00
Biotin Acetyl-CoA Ligase	BPL	g4888.t1	biotin-- ligase 2-like	19,90	16,29	19,35	18,69	20,03	19,30	496,18	0,06	0,11	0,54	0,59	0,68
	KAS3	g2168.t1	3-oxoacyl-[acyl-carrier-] mitochondrial	31,27	23,11	28,81	31,24	32,52	31,68	954,25	0,20	0,11	1,73	0,08	0,13

Fatty acid activation

Description	Abbreviations	Gene name in *C. vulgaris*	Description Blast2go	C_v LL_1	C_v LL_2	C_v LL_3	C_v HL_1	C_v HL_2	C_v HL_3	Base Mean	Log2 Fold Change	lfcSE	stat	pvalue	padj
Acyl carrier protein thioesterase	FAT	g250.t1	oleoyl-acyl carrier thioesterase chloroplastic-like	86,34	83,91	88,18	67,31	64,70	68,39	1917,14	-0,37	0,07	-5,20	0,00	0,00
Long-chain acyl-CoA synthetase	LCS1	g5564.t1	long chain acyl- synthetase 4-like	375,20	397,22	395,82	270,74	261,29	261,65	15184,65	-0,56	0,06	-9,57	0,00	0,00
	LCS2	g7010.t1	long chain acyl- synthetase 4	230,04	262,75	224,12	272,26	230,72	236,77	11155,46	0,05	0,09	0,50	0,62	0,70
Acetyl-CoA Acyltransferase Thiolase	ATO2	g3807.t1	acetyl- cytosolic 1 isoform X2	36,61	34,54	37,41	35,78	41,42	42,41	1250,81	0,14	0,09	1,52	0,13	0,19

Fatty acid biosynthesis

Description	Abbreviations	Gene name in *C. vulgaris*	Description Blast2go	C_v LL_1	C_v LL_2	C_v LL_3	C_v HL_1	C_v HL_2	C_v HL_3	Base Mean	Log2 Fold Change	lfcSE	stat	pvalue	padj
Acetyl-CoA carboxylase components															
α-Carboxyltransferase (ACCase complex)	ACX1 (a-CT)	g4387.t1	acetyl-coenzyme A carboxylase carboxyl transferase subunit chloroplastic	279,57	282,2	291,43	221,3	217,54	232,03	9366,70	-0,35	0,06	-5,77	0,00	0,00
β-Carboxyltransferase (ACCase complex)	BCX1 (b-CT)	g2036.t1	Propionyl- carboxylase beta mitochondrial	114,42	123,7	112,66	130,4	128,86	126,89	4752,04	0,14	0,07	2,10	0,04	0,06
		accD-chl.t1		0,56	0,73	0,27	1,30	0,75	0,90	13,78	0,94	0,58	1,61	0,11	0,16
Acetyl-CoA biotin carboxyl carrier protein (ACCase complex)	BCC1	g6763.t1	biotin carboxyl carrier of acetyl- chloroplastic-like	331,86	352,6	336,62	303,2	277,14	309,53	5182,21	-0,20	0,07	-2,81	0,00	0,01
	BCC2	g2297.t1	Biotin carboxyl carrier of acetyl- carboxylase	194,48	223,9	207,42	150,3	149,21	148,87	3333,53	-0,48	0,07	-6,46	0,00	0,00
Biotin carboxylase (ACCase complex)	BCR1	g6158.t1	biotin carboxylase chloroplastic	153,81	162,5	164,69	124,8	123,89	124,73	5559,15	-0,37	0,06	-5,95	0,00	0,00
Acyl-carrier protein (ACCase complex)	ACP1	g1590.t1	hypothetical protein CHLNCDRAFT_140343	166,14	188,4	170,80	153,1	152,10	158,64	5457,62	-0,18	0,07	-2,50	0,01	0,02
	ACP2	g6087.t1	acyl carrier chloroplastic-like	158,00	141,3	187,26	95,87	115,44	123,78	1099,75	-0,54	0,13	-4,27	0,00	0,00
Malonyl-CoA: ACP transacylase	MCT1	g6284.t1	malonyl -acyl carrier transacylase-like	7,98	6,64	9,36	19,42	21,36	22,13	351,95	1,38	0,14	9,62	0,00	0,00
	MCT2	g8816.t1	malonyl -acyl carrier transacylase	4,31	4,58	4,14	1,46	1,64	2,07	115,73	-1,34	0,20	-6,61	0,00	0,00
Fatty acid synthase Type II															
3-Ketoacyl-CoA-synthase (type II FAS complex)	KAS1	g2568.t1	3-oxoacyl-[acyl-carrier-] synthase chloroplastic	227,53	256,9	234,45	165,2	152,10	153,91	6427,49	-0,61	0,07	-8,26	0,00	0,00
	KAS2	g7735.t1	3-oxoacyl-[acyl-carrier-] synthase chloroplastic	78,34	88,93	74,16	57,69	51,25	52,73	2223,76	-0,58	0,09	-6,34	0,00	0,00
	KAS3	g7770.t1	3-oxoacyl-ACP synthase	9,36	12,04	10,88	4,17	4,28	5,06	184,97	-1,26	0,17	-7,36	0,00	0,00
3-ketoacyl-CoA synthase (Beta-Ketoacyl Synthase in articolo chromoclorie)(type II FAS complex)	KCS4	g4315.t2	3-ketoacyl- synthase 1-like												
3-Hydroxyacyl-ACP dehydratase (type II FAS complex)	HAD1	g823.t1	3-hydroxyacyl-[acyl-carrier-] dehydratase -like	63,43	66,77	61,69	17,45	18,97	19,22	584,82	-1,78	0,10	-17,12	0,00	0,00
Beta-Hydroxyacyl ACP Dehydrase/Dehydratase (type II FAS complex)	FABZ	g823.t1	3-hydroxyacyl-[acyl-carrier-] dehydratase -like	63,43	66,77	61,69	17,45	18,97	19,22	584,82	-1,78	0,10	-17,12	0,00	0,00
3-Oxoacy-[acyl carrier protein] reductase (type II FAS complex)	KAR1	g7446.t1	3-oxoacyl-[acyl-carrier-] reductase 4-like	42,40	49,26	48,92	13,03	13,54	13,58	633,17	-1,80	0,11	-16,69	0,00	0,00
Enoyl-[acyl carrier protein] reductase (type II FAS complex)	ENR1	g5675.t1	enoyl-[acyl-carrier-] reductase [NADH] chloroplastic-like	44,34	47,73	46,31	19,61	19,50	21,43	852,00	-1,20	0,09	-13,10	0,00	0,00
Homomeric ACCase 1, predicted to be mitochondria	ACC1	g3400.t1	acetyl- carboxylase 1-like	12,92	11,82	12,90	10,12	10,61	9,42	1931,36	-0,32	0,08	-3,92	0,00	0,00
Fatty acid synthase Type II															
Type I polyketide synthase	Type I fatty acid synthase component	g276.t1	Polyketide synthase	2,03	2,01	1,92	2,94	2,99	2,64	3096,09	0,53	0,08	6,87	0,00	0,00
Polyketide synthase	Type I fatty acid synthase component	g10371.t1	non-ribosomal peptide synthetase	8,52	10,74	9,97	1,20	1,41	1,39	2805,03	-2,86	0,10	-27,31	0,00	0,00

Galactolipid synthesis

Description	Abbreviations	Gene name in *C. vulgaris*	Description Blast2go	C_v LL_1	C_v LL_2	C_v LL_3	C_v HL_1	C_v HL_2	C_v HL_3	Base Mean	Log2 Fold Change	lfcSE	stat	pvalue	padj
Monogalactosyldiacylglycerol synthase	MGD	g8394.t1	probable monogalactosyldiacylglycerol chloroplastic	23,23	24,37	24,01	26,21	24,53	24,15	1236,23	0,06	0,08	0,79	0,43	0,52
Digalactosyldiacylglycerol synthase	DGD	g707.t1	digalactosyldiacylglycerol synthase chloroplastic-like	98,60	98,48	98,76	87,46	79,85	84,29	5294,72	-0,24	0,06	-3,86	0,00	0,00

Fatty acid desaturations

Description	Abbreviations	Gene name in *C. vulgaris*	Description Blast2go	C_v LL_1	C_v LL_2	C_v LL_3	C_v HL_1	C_v HL_2	C_v HL_3	Base Mean	Log2 Fold Change	lfcSE	stat	pvalue	padj
Plastid acyl-ACP desaturase, D-9 stearate desaturase	SAD	g8797.t1	Acyl-[acyl-carrier-] desaturase chloroplastic	180,22	174,8	173,87	206,8	183,51	184,43	6101,86	0,12	0,07	1,66	0,10	0,15
w-6 fatty acid desaturase, D-12	FAD2	g7807.t1	omega-6 fatty acid endoplasmic reticulum isozyme 2-like	60,41	60,84	58,82	54,51	52,61	53,04	4205,41	-0,17	0,06	-2,79	0,01	0,01
D-3 palmitate desaturase	FAD4	g3706.t1	fatty acid desaturase chloroplastic-like	79,02	71,75	71,04	307,3	275,26	279,54	3964,57	1,95	0,08	24,86	0,00	0,00
MGDG-specific palmitate D-7 desaturase	FAD5	g6064.t1	palmitoyl-monogalactosyldiacylglycerol delta-7 chloroplastic-like	68,02	73,27	75,95	123,8	110,76	111,03	2699,17	0,67	0,08	8,26	0,00	0,00
	FAD5 like	g3144.t1	palmitoyl-monogalactosyldiacylglycerol delta-7 chloroplastic-like	24,03	25,34	21,99	29,30	29,82	28,96	1412,06	0,31	0,08	3,70	0,00	0,00
w-6 fatty acid desaturase	FAD6	g2544.t1	serine threonine-phosphatase 2A 65 kDa regulatory subunit A beta isoform-like	186,77	204,4	180,16	287,6	258,50	253,13	16191,77	0,48	0,08	6,18	0,00	0,00
Chloroplast glycerolipid w-3 fatty acid desaturase	FAD7	g2075.t1	omega-3 fatty acid chloroplastic	72,89	88,95	73,17	226,3	198,76	188,09	4135,87	1,38	0,10	13,64	0,00	0,00

From glycerol to DAG

Description	Abbreviations	Gene name in *C. vulgaris*	Description Blast2go	C_v LL_1	C_v LL_2	C_v LL_3	C_v HL_1	C_v HL_2	C_v HL_3	Base Mean	Log2 Fold Change	lfcSE	stat	pvalue	padj
Glycerol-3-Phosphate Dehydrogenase	GPD1	g7166.t1	glycerol-3-phosphate dehydrogenase [NAD(+)] chloroplastic	48,60	51,25	45,78	54,61	46,72	48,25	1924,01	0,04	0,09	0,42	0,68	0,76
	GPD2	g7879.t1	glycerol-3-phosphate dehydrogenase [NAD(+)]	43,05	50,51	41,10	313,1	411,59	410,17	9575,24	3,08	0,12	26,65	0,00	0,00
Glycerol-3-phosphate O-acyltransferase	GPAT1	g3072.t1	Glycerol-3-phosphate chloroplastic	46,20	48,78	46,59	45,87	48,88	47,59	1688,53	0,01	0,07	0,15	0,88	0,92
	GPAT2	g4271.t1	glycerol-3-phosphate acyltransferase 3-like	45,88	57,23	49,66	40,12	40,39	42,84	1381,89	-0,31	0,10	-3,16	0,00	0,00
1-Acyl-sn-glycerol-3-phosphate acyltransferase	LPAT1	g2639.t1	1-acyl-sn-glycerol-3-phosphate acyltransferase chloroplastic-like isoform X1	147,18	165,3	129,10	138,3	115,65	116,43	2069,81	-0,25	0,11	-2,33	0,02	0,04
	LPAT2	g397.t1	lysophospholipid acyltransferase LPEAT1-like isoform X1	61,98	66,29	60,05	82,32	74,86	79,85	1623,79	0,33	0,08	4,08	0,00	0,00
Phosphatidate phosphatase	PAP1	g920.t1	lipid phosphate phosphatase	36,04	36,28	31,54	22,12	22,36	25,43	663,40	-0,57	0,11	-5,32	0,00	0,00
	PAP2	g4622.t1	lipid phosphate phosphatase delta	9,42	9,04	10,14	8,99	9,79	8,78	326,73	-0,05	0,13	-0,39	0,70	0,77
Diacylglycerol Kinase	KDG1	g10111.t1	diacylglycerol kinase theta isoform X5	5,31	4,85	5,17	5,06	6,16	6,34	373,18	0,20	0,13	1,55	0,12	0,18
	KDG2	g7314.t1	sphingosine kinase ( )	19,01	18,46	19,87	15,00	17,81	16,82	662,37	-0,20	0,10	-1,95	0,05	0,08
	KDG3	g3849.t1	diacylglycerol kinase 7-like	6,74	8,45	7,50	5,57	5,94	5,99	278,30	-0,37	0,14	-2,67	0,01	0,02

DGTS synthesis

Description	Abbreviations	Gene name in *C. vulgaris*	Description Blast2go	C_v LL_1	C_v LL_2	C_v LL_3	C_v HL_1	C_v HL_2	C_v HL_3	Base Mean	Log2 Fold Change	lfcSE	stat	pvalue	padj
S-adenosylmethionine synthetase	SAS1	g328.t1	S-adenosylmethionine synthase 1	158,12	152,9	157,04	79,70	72,95	72,81	10570,14	-1,06	0,06	-16,40	0,00	0,00
Diacylglyceryl-N,'N,'N'-trimethylhomoserine synthase	BTA1	g5289.t1	diacylglyceryl-N,N,N-trimethylhomoserine synthesis	0,09	0,12	0,10	0,03	0,01	0,02	3,04	-2,65	1,28	-2,08	0,04	0,07

Phospholipid synthesis

Description	Abbreviations	Gene name in *C. vulgaris*	Description Blast2go	C_v LL_1	C_v LL_2	C_v LL_3	C_v HL_1	C_v HL_2	C_v HL_3	Base Mean	Log2 Fold Change	lfcSE	stat	pvalue	padj
Mitochondrial half-size ABC transporter (PtdGro synthesis)	CDS1	g9210.t1	ATP-binding cassette sub-family B member mitochondrial	71,77	80,57	68,60	77,63	68,71	67,49	4407,35	-0,05	0,09	-0,54	0,59	0,68
		g1846.t1	ATP-binding cassette sub-family B member mitochondrial	21,52	18,26	25,28	22,30	28,19	27,54	1520,41	0,26	0,13	2,05	0,04	0,07
Phosphatidylglycerolphosphate synthase (PtdGro synthesis)	PGPS1	g6789.t1	CDP-diacylglycerol--glycerol-3-phosphate 3-phosphatidyltransferase	73,68	67,71	65,13	78,39	70,78	72,81	1326,57	0,10	0,09	1,16	0,24	0,33
Phosphatidylglycerolphosphate synthase (PtdGro synthesis)	PGPS2	g2699.t1	cardiolipin synthase (CMP-forming) mitochondrial	6,55	5,16	7,35	6,88	7,08	7,65	180,80	0,17	0,17	0,98	0,33	0,42
Phosphatidylglycerolphosphate synthase (PtdGro synthesis)	PGPS3	g5080.t1	CDP-diacylglycerol--glycerol-3-phosphate 3-phosphatidyltransferase 2-like	15,00	15,91	13,31	10,38	10,71	12,08	259,37	-0,41	0,14	-2,92	0,00	0,01
myo-Inositol-1-phosphate synthase (PtdIns synthesis)	INO1	g3350.t1	inositol-3-phosphate synthase	260,53	273,4	256,39	222,6	194,94	190,90	8270,77	-0,38	0,08	-4,87	0,00	0,00
Phosphatidylinositol synthase (PtdIns synthesis)	PIS1	g5807.t1	probable CDP-diacylglycerol--inositol 3-phosphatidyltransferase 2	18,17	21,13	21,78	13,68	14,61	14,68	305,15	-0,50	0,13	-3,83	0,00	0,00
Serine decarboxylase (PtdEtn synthesis)	SDC1	g2092.t1	serine decarboxylase-like	404,74	428,5	390,71	339,0	285,95	288,42	11816,35	-0,42	0,08	-5,06	0,00	0,00
Phosphatidate cytidylyltransferase	PCT1	g3043.t1	phosphatidate cytidylyltransferase-like	35,96	41,49	35,17	33,35	30,86	30,96	1148,79	-0,24	0,09	-2,58	0,01	0,02
Phosphatidate cytidylyltransferase	PCT2	g7626.t1	Phosphatidate cytidylyltransferase	88,92	85,76	80,69	100,7	86,05	90,90	2605,98	0,12	0,08	1,41	0,16	0,23
CDP-ethanolamine synthase	ECT1	g4386.t1	ethanolamine-phosphate cytidylyltransferase-like	83,92	80,04	78,66	63,65	58,52	59,17	2148,73	-0,42	0,07	-5,79	0,00	0,00
Ethanolamine kinase (PtdEtn synthesis)	ETK1	g2105.t1	probable choline kinase 1 isoform X2	20,86	22,28	20,12	15,08	15,59	15,88	534,19	-0,44	0,10	-4,30	0,00	0,00
Lysophosphatidylcholine acyltransferase	LPCAT1	g6734.t1	lysophospholipid acyltransferase 1-like	57,62	67,38	55,50	68,50	57,50	59,07	2103,81	0,04	0,10	0,35	0,73	0,79

Sulfolipid synthesis

Description	Abbreviations	Gene name in *C. vulgaris*	Description Blast2go	C_v LL_1	C_v LL_2	C_v LL_3	C_v HL_1	C_v HL_2	C_v HL_3	Base Mean	Log2 Fold Change	lfcSE	stat	pvalue	padj
UDP-glucose pyrophosphorylase	UGP3	g6264.t1	nucleotide-diphospho-sugar transferase	17,50	12,77	17,83	11,99	13,22	13,03	984,79	-0,33	0,13	-2,63	0,01	0,02
UDP-sulfoquinovose synthase	SQD1	g9859.t1	UDP-sulfoquinovose chloroplastic	114,11	127,9	101,94	97,18	83,60	82,97	3352,54	-0,38	0,10	-3,80	0,00	0,00
	SQD2	g4144.t1	sulfoquinovosyl transferase SQD2-like	52,88	50,83	49,38	43,72	42,75	41,75	1669,82	-0,26	0,07	-3,48	0,00	0,00

TAG synthesis

Description	Abbreviations	Gene name in *C. vulgaris*	Description Blast2go	C_v LL_1	C_v LL_2	C_v LL_3	C_v HL_1	C_v HL_2	C_v HL_3	Base Mean	Log2 Fold Change	lfcSE	stat	pvalue	padj
Diacylglycerol acyltransferase, DGAT Type 1	DGAT1	g2077.t1	diacylglycerol O-acyltransferase 1-like	78,76	76,02	74,88	71,63	67,00	66,50	3694,14	-0,16	0,07	-2,45	0,01	0,03
Diacylglycerol acyltransferase, DGAT Type 2	DGTT1	g8780.t1	diacylglycerol O-acyltransferase 2B	9,87	11,72	10,38	8,57	10,34	11,55	276,13	-0,06	0,15	-0,42	0,68	0,76
	DGTT2	g561.t1	diacylglycerol O-	34,53	33,86	31,59	36,58	39,58	40,39	1691,03	0,22	0,08	2,79	0,01	0,01
	DGTT3	g4840.t1	Diacylglycerol O-acyltransferase 2	25,44	33,43	28,33	36,39	33,01	35,63	757,45	0,28	0,11	2,50	0,01	0,02

Lipid droplet proteins

Description	Abbreviations	Gene name in *C. vulgaris*	Description Blast2go	C_v LL_1	C_v LL_2	C_v LL_3	C_v HL_1	C_v HL_2	C_v HL_3	Base Mean	Log2 Fold Change	lfcSE	stat	pvalue	padj
Plastid-lipid associated protein PAP/fibrillin family protein	PLP1 (PLAP1)	g10612.t1	probable plastid-lipid-associated chloroplastic isoform X2	8,56	8,21	9,90	12,26	13,38	13,68	642,76	0,56	0,11	5,12	0,00	0,00
	PLAP2	g555.t1	probable plastid-lipid-associated chloroplastic	50,35	55,34	44,47	228,18	184,53	186,13	1560,41	2,00	0,11	17,49	0,00	0,00
	PLAP3	g2051.t1	probable plastid-lipid-associated 11	62,61	72,53	60,20	64,24	61,46	62,68	991,44	-0,05	0,10	-0,52	0,60	0,69
	PLAP4	g3511.t1	probable plastid-lipid-associated chloroplastic	53,00	47,32	52,33	44,06	49,59	52,49	1251,88	-0,06	0,09	-0,66	0,51	0,60
	PLAP5	g6559.t1	probable plastid-lipid-associated chloroplastic isoform X1	9,87	8,32	10,70	22,78	22,89	24,02	526,63	1,26	0,12	10,78	0,00	0,00
	PLAP7	g2013.t1	plastid-lipid-associated chloroplastic-like	18,43	18,70	23,61	40,34	43,10	41,87	803,38	1,04	0,11	9,20	0,00	0,00
	PLAP9	g216.t1	probable plastid-lipid-associated chloroplastic	142,89	149,12	136,79	305,54	280,11	270,94	11055,68	1,00	0,07	13,87	0,00	0,00
	PLAP10	g2013.t1	plastid-lipid-associated chloroplastic-like	18,43	18,70	23,61	40,34	43,10	41,87	803,38	1,04	0,11	9,20	0,00	0,00
	PLAP11	g8445.t1	plastid fibrillin 3	58,85	56,41	61,27	55,47	61,36	64,32	720,19	0,04	0,10	0,38	0,70	0,77
Calcosin	CLO	g8245.t1	calcosin domain containing	814,55	1022,46	819,82	1229,69	1181,40	1290,67	19315,58	0,48	0,09	5,05	0,00	0,00
		g8244.t1	peroxygenase 2-like	70,90	94,37	73,99	19,04	17,80	20,85	971,19	-2,06	0,13	-16,33	0,00	0,00

Lipid trafficking

Description	Abbreviations	Gene name in *C. vulgaris*	Description Blast2go	C_v LL_1	C_v LL_2	C_v LL_3	C_v HL_1	C_v HL_2	C_v HL_3	Base Mean	Log2 Fold Change	lfcSE	stat	pvalue	padj
ER-to-plastid lipid import (TGD complex)															
Lipid transfer machine permease (TGD complex)	TGD1	g8972.t1	TRIGALACTOSYLDIACYLGLYCEROL chloroplastic-like	30,19	31,21	28,81	30,51	29,15	30,09	1248,33	-0,01	0,08	-0,10	0,92	0,95
Permease-like component of an ABC transporter (TGD complex)	TGD2	g3884.t1	TRIGALACTOSYLDIACYLGLYCEROL chloroplastic	125,71	144,12	125,23	98,03	99,29	99,23	2930,00	-0,41	0,08	-5,25	0,00	0,00
Putative ABC transport system ATP-binding protein (TGD complex)	TGD3	g4737.t1	TRIGALACTOSYLDIACYLGLYCEROL chloroplastic	38,51	37,45	37,04	51,07	47,27	47,93	1234,17	0,37	0,08	4,64	0,00	0,00
Vesicle inducing protein in plastids 1	VIP1	g1461.t1	membrane-associated 30 kDa chloroplastic-like isoform X2	299,81	316,82	296,86	438,45	387,59	383,67	7611,14	0,40	0,08	5,38	0,00	0,00
P-type ATPase; putative phospholipid-transporting ATPase	ALA1	g7650.t1	probable phospholipid-transporting ATPase IM isoform X4	48,33	48,42	45,72	44,15	38,44	36,45	4373,76	-0,26	0,08	-3,07	0,00	0,00

Lipases

Description	Abbreviations	Gene name in *C. vulgaris*	Description Blast2go	C_v LL_1	C_v LL_2	C_v LL_3	C_v HL_1	C_v HL_2	C_v HL_3	Base Mean	Log2 Fold Change	lfcSE	stat	pvalue	padj
Galactolipid lipase	PGD1	g5667.t1	alpha beta-hydrolase	68,47	59,72	73,58	94,88	96,48	94,81	8876,29	0,50	0,08	6,06	0,00	0,00
DAG lipase	LIP1	g9452.t1	Sn1-specific diacylglycerol lipase alpha	39,33	34,74	37,42	44,59	40,10	40,20	2762,01	0,16	0,08	2,00	0,05	0,08
Triacylglycerol Lipase	SDP1	g7100.t1	triacylglycerol lipase SDP1	100,97	94,97	105,75	101,92	102,98	105,85	5096,55	0,04	0,07	0,62	0,54	0,63
	LIP2	g1996.t1	Lysosomal acid lipase cholesteryl ester hydrolase	5,65	5,79	6,01	8,19	9,84	10,16	560,60	0,70	0,12	6,01	0,00	0,00
	LIP3	g8617.t1	lysosomal acid lipase cholesteryl ester hydrolase	53,27	56,51	60,84	65,63	65,31	62,69	1992,57	0,18	0,08	2,31	0,02	0,04
a/b Hydrolase: soluble epoxide hydrolase	Hydrolase	g9929.t1	epoxide hydrolase	34,02	35,66	38,21	22,10	23,51	23,51	756,16	-0,64	0,09	-6,77	0,00	0,00

Fatty acid β-oxidation pathway

Description	Abbreviations	Gene name in *C. vulgaris*	Description Blast2go	C_v LL_1	C_v LL_2	C_v LL_3	C_v HL_1	C_v HL_2	C_v HL_3	Base Mean	Log2 Fold Change	lfcSE	stat	pvalue	padj
Peroxisomal long-chain acyl-CoA transporter, ABC superfamily	CTS	g633.t1	ATP-binding cassette sub-family D member 3	63,65	68,34	64,34	92,27	86,67	87,27	3838,42	0,44	0,07	6,50	0,00	0,00
Long-chain acyl-CoA synthetase	LCS3	g4991.t1	Long chain acyl-synthetase peroxisomal	161,93	170,19	145,63	172,82	144,00	150,96	7692,36	-0,03	0,09	-0,34	0,73	0,80
Acyl-CoA oxidase	ACX1	g1724.t1	peroxisomal acyl-coenzyme A oxidase 1-like	82,19	72,67	87,70	158,20	146,97	149,40	5639,09	0,90	0,08	10,92	0,00	0,00
	ACX2	g2045.t1	acyl-coenzyme A oxidase peroxisomal	69,16	66,55	65,89	103,48	91,60	91,77	3860,01	0,51	0,08	6,74	0,00	0,00
	ACX3	g5124.t1	acyl- oxidase	74,26	74,65	72,85	116,68	100,97	103,93	3971,33	0,53	0,08	7,00	0,00	0,00
	ACX4	g1927.t1	Acyl-coenzyme A oxidase peroxisomal	148,46	132,93	153,33	290,53	288,40	282,50	6969,49	0,99	0,07	13,61	0,00	0,00
3-Hydroxyacyl-CoA dehydrogenase	ECH1	g3993.t1	Glyoxysomal fatty acid beta-oxidation multifunctional MFP-a	222,93	242,20	220,76	258,40	216,54	219,40	11582,28	0,02	0,09	0,20	0,84	0,89
	ECH2														
Enoyl-CoA hydratase/isomerase	DCI1	g5241.t1	enoyl- hydratase	16,18	13,11	16,80	18,91	19,04	19,96	338,90	0,32	0,13	2,44	0,01	0,03
	ECH1	g7740.t1	Enoyl- delta isomerase mitochondrial	119,77	134,48	108,98	103,62	94,40	96,20	2096,60	-0,30	0,09	-3,26	0,00	0,00
	ECH2	g2958.t1	Hydroxyacyl-thioester dehydratase type mitochondrial	25,94	28,59	31,43	9,93	11,81	12,85	258,18	-1,31	0,15	-8,66	0,00	0,00
	ECHD	g8015.t1	1,4-dihydroxy-2-naphthoyl- peroxisomal-like	33,38	29,28	31,85	57,29	59,11	59,79	1077,52	0,90	0,09	10,36	0,00	0,00
3-Oxoacyl CoA thiolase/acetyl-CoA acyltransferase 1 (ATO1)	ATO1 (KAT1/KAT2/PKT1)	g2206.t1	3-ketoacyl- thiolase peroxisomal	238,38	212,27	227,04	336,51	322,52	319,17	8942,42	0,53	0,07	7,77	0,00	0,00
Peroxisomal 2,4-dienoyl-CoA reductase	RED	g9594.t1	peroxisomal 2,4-dienoyl-reductase-like	62,15	56,90	69,40	65,32	65,16	70,62	1369,24	0,09	0,09	0,95	0,34	0,44
3-Hydroxyisobutyryl-CoA hydrolase	HIBCH	g5912.t1	3-hydroxyisobutyryl-mitochondrial-like	66,14	60,10	63,91	91,65	87,63	84,52	1988,23	0,41	0,07	5,45	0,00	0,00

Regulatory proteins and transcription factors

Description	Abbreviations	Gene name in *C. vulgaris*	Description Blast2go	C_v LL_1	C_v LL_2	C_v LL_3	C_v HL_1	C_v HL_2	C_v HL_3	Base Mean	Log2 Fold Change	lfcSE	stat	pvalue	padj
Putative nitrogen specific regulator/DNA-binding protein	NRR1	g3553.t1	squamosa promoter binding	37,62	36,30	45,77	31,73	35,99	35,31	3167,40	-0,22	0,10	-2,15	0,03	0,06
Compromised hydrolysis of triacylglycerols 7	CHT7	g6968.t1	tomin TSO1-like CXC 5	10,93	11,05	13,58	6,08	6,13	6,10	400,65	-0,96	0,13	-7,49	0,00	0,00

Table S8. Identification of genes involved in flagella and cilia formation in Chlorella vulgaris according to the CiliaCut list

JGI v3 protein ID	Protein family (cluster) ID	Chlamy-domonas gene name	JGI *Chlamydomonas* browser defline	Manual annotation of molecular function	*Chlorella* gene name
Proteins in CiliaCut, but neither CentricCut nor MotileCut					
185788	5709716	UNC119	Signal transduction protein	Trafficking	
126758	5711323	BBS2		No data	
182299	5709609	BBS5	Similar to Bardet-Biedl syndrome 5	No data	
190054	5709103	BBS7	Similar to Bardet-Biedl syndrome 7	No data	
140113	5706980	BBS8	Tetratricopeptide repeat protein 8 (Bardet-Biedl syndrome 8) similarity	Protein-protein interraction	
101137	5709290	BBS9	Bardet-Biedl syndrome 9	No data	
130394	5708472	D1bLIC	Cytoplasmic dynein 1b light intermediate chain (homologue of mammalian D2LIC/LIC3), the retrograde motor for intraflagellar transport.	Flagellar transport	
195385	5709351	FAP118	(FBB1) In the flagellar basal body proteome as FBB1	Protein-protein interraction	g8575.t1
81760	5709994	DYF13	(FBB2) Homologous to protein required for ciliogenesis in C. elegans.	Protein-protein interraction	
189076	5706101	FAP47		No data	
126867	5710863	FAP60		Protein-protein interraction	
143468	5706244	FAP66		Protein-protein interraction	g1356.t1
195877	5708672	FAP9	Ortholog RABL5 in human, member of the Ras superfamily of GTPases but the GTP-specificity motif abrogated (ATPase?).	GTP-Binding	
192205	5705047	IFT140	Intraflagellar transport particle protein IFT140	Flagellar transport	
183240	5708965	IFT172	Intraflagellar transport protein 172	Flagellar transport	
182072	5705822	IFT20	Intraflagellar transport particle protein 20	Flagellar transport	
24171	5709540	IFT80	Intraflagellar transport particle protein 80	Flagellar transport	g8575.t1
98915	5709897	FBB17		Protein metabolism	g4638.t1
194946	5710084	PTP1	Putative Protein Tyrosine Phosphatase 1; Dephosphorylates phosphotyrosine residues	Signaling	
102300	5706231	SSA1		Signaling	g4307.t1
172866	5709515	SSA10	Similar to copper type II, ascorbate-dependent monooxygenase , similar to dopamine beta-monooxygenase	Metabolism	g9475.t1
118345	5708916	SSA11		Microtubule Regulation and Metabolism	g2896.t1, g2896.t2
150669	5706961	SSA2		Protein metabolism	g4638.t1
150480	5709110	SSA3	Contains an engulfement and cell motility, ELM, domain (IPR006816) found in a number of eukaryotic proteins involved in the cytoskeletal rearrangements required for phagocytosis of apoptotic cells and cell motility.	Unclear	
107835	5709188	SSA4		No data	
176942	5709323	SSA5		Signaling	g3257.t1
176788	5709889	SSA6		No data	g5745.t1
180447	5709065	SSA7		Protein-protein interraction	g7184.t1
95290	5709079	SSA8		Metabolism	g6020.t1
172167	5707709	SSA9		RNA metabolism	g9427.t1
24475	5705258		(ARL6a , BBS3B) Most similar to mammalian ARL6, causative gene for Bardet-Biedl syndrome 3, member of the ARF/Sar1 GTPase family. The C. elegans ARL6 undergoes intraflagellar transport. Two ARL6 paralogs in Chlamydomonas (see ARL6b).	GTP-Binding	g9427.t1

JGI v3 protein ID	Protein family (cluster) ID	Chlamy-domonas gene name	JGI *Chlamydomonas* browser defline	Manual annotation of *Chlorella* gene molecular function	name
Proteins in MotileCut but not CentricCut					
188195	5710277	BLD2	Epsilon tubulin (TUE) [gi:20514387, PMID: 12429830]	Flagellar Structure	g4405.t1
130324	5710955	DHC2	Dynein heavy chain 2 (putative flagellar inner arm dynein heavy chain)	Flagellar Structure	g4263.t1
134599	5705986	DHC6	Dynein heavy chain 6 (putative flagellar inner arm dynein heavy chain)	Flagellar Structure	g4263.t1
188180	5710541	FAP111		Protein-protein interaction	g735.t1
195529	5710730	ARLP1	(ARL13) Expressed Protein. ARF-like 13, a member of the ARF/Sar1 family of Ras-like GTPases. C. elegans ortholog specifically expressed in flagellated cells	GTP-Binding	g9427.t1
21780	5711546	ARM1	contains armadillo (Arm) repeat	Protein-protein interaction	
134605	5711269	CDJ2		Chaperone	g2530.t1
93765	5708783	FAP240		No data	
145396	5707456	FAP251		Protein-protein interaction	
154904	5706505	FAP263		No data	
193355	5710580	FAP43		Protein-protein interaction	g7727.t1
149708	5705337	FAP44		Protein-protein interaction	
141109	5710324	FAP46		No data	
177591	5706388	FAP50		Protein-protein interaction	g1973.t1
194338	5709355	FAP57	Hypothetical protein contains WD40 repeats	Protein-protein interaction	g7727.t1
189109	5706889	FAP59		No data	g6903.t1
144011	5705309	FAP61	(FAP61)	No data	
188246	5710879	FAP69		Protein-protein interaction	
167096	5706093	FAP74		No data	
142494	5709113	FAP75	Flagellar Associated P-Loop Containing Protein	No data	
188960	5710498	FAP81		Unclear	
190653	5706159	FAP94		No data	
191232	5711862	EGL12	exostosin-like glycosyltransferase	Metabolism	g3877.t1
190937	5710532	FBB5		No data	
105624	5708696	FBB9		No data	g6884.t1
196807	5711862	ELG34	exostosin-like glycosyltransferase	Metabolism	g3877.t1
179158	5710249	FAD5b	Fatty acid desaturase like, similar to Arabidopsis putative FAD5	Membrane synthesis/differentiatio n	g6064.t1
153533	5710249	FAD5C		Membrane synthesis/differentiatio n	g6064.t1
122385	5710249	FAD5D		Membrane synthesis/differentiatio n	g6064.t1
146448	5711707	FAP122		Signaling	
172483	5711560	FAP134		Protein-protein interaction	g735.t1
186414	5709707	KLP1	Kinesin-like protein 1; kinesin associated with one of the central pair microtubules of the flagellar axoneme	Flagellar Structure	g2002.t1
189194	5711344	FAP146		No data	
190077	5709733	FAP155		Protein-protein interaction	g8930.t1
187854	5710441	FAP161		No data	
192295	5706575	FAP184		No data	g4863.t1
119090	5709342	FAP198	Presence of a cyt-b5 -like domain in the N terminal part of the protein	Unclear	
116240	5709840	HY3	(HYD3) Similar to mouse hydrocephaly protein hydin HY3	Unclear	
169142	5705315	MOT1		Protein-protein interaction	g6459.t1
165974	5710024	MOT10		Membrane Protein	
126569	5710065	MOT11		Microtubule Regulation and Metabolism	g2896.t2
121332	5711016	MOT12		No data	
94516	5710642	MOT13		DNA Binding	g383.t1
43319	5705234	MOT14		Unclear	g9137.t1
141685	5710115	MOT15		Signaling	
193672	5710456	MOT16		Unclear	g9425.t1

192915	5711490	MOT17		Signaling	
177575	5708309	MOT18		RNA metabolism	g4356.t1
173947	5710187	MOT19		Membrane Protein	g10444.t1
169983	5710231	MOT2		Unclear	
192150	5709694	MOT20		Membrane Protein	g1329.t1
135100	5709694	MOT21	putative phosphate/phosphoenolpyruvate translocator protein	Membrane Protein	g1329.t1
177375	5709293	MOT22		Signaling	
173608	5710430	MOT23		Signaling	g5953.t1
184899	5710794	MOT24		Flagellar Structure	g3201.t1
192442	5711802	MOT25		Unclear	
117499	5709647	MOT26		No data	
168675	5707372	MOT27		No data	g8710.t1
177784	5705352	MOT28		No data	
181739	5709937	MOT29		No data	
148926	5705281	MOT3		No data	g240.t1
179771	5709937	MOT30		No data	
151105	5710089	MOT31		Protein-protein interaction	
109243	5710241	MOT32		No data	
106614	5710241	MOT33		No data	
107462	5710241	MOT34		No data	
191879	5710410	MOT35		No data	
180607	5710673	MOT36		No data	
146778	5711548	MOT37		Protein-protein interaction	
151348	5711741	MOT38		No data	
173581	5710018	MOT39		Protein turnover	g4608.t1
176821	5706137	MOT4		Unclear	
189500	5710403	MOT40		No data	
142470	5710516	MOT41	This gene is in the location of Probe 2 used in PMID: 11805055.	No data	
152883	5705024	MOT42		Protein turnover	g4673.t1
173632	5707289	MOT5	Alanine rich novel protein	No data	
103782	5706246	PF16	Central pair associated protein	Flagellar Structure	g4663.t1
101210	5710416	PF20	WD-repeat containing protein PF20 of the central pair of the flagella. Associates with the intermicrotubule bridge.	Flagellar Structure	g7644.t1
112249	5710479	POC1	Found in basal body proteome [PMID: 15964273].	Protein-protein interaction	g7644.t1
13542	5710242	POC11	Found in basal body proteome as POC11 [PMID: 15964273].	No data	g5018.t1
6466	5710586	POC18	Found in basal body proteome [PMID: 15964273]	Protein-protein interaction	
138046	5710963	RSP3	Flagellar radial spoke protein 3 (RSP3), axonemal A-kinase anchoring protein KAP [PMID: 11309423; PMID: 16571668; PMID: 16267272; GI:134041]. Gene originally termed PF14 [PMID: 7204490; PMID: 2745550; PMID: 2377611]	Flagellar Structure	
182960	5711716	RSP9	Flagellar radial spoke protein 9; A subunit in the radial spoke head; Gene originally termed pf17 [PMID: 7204490, PMID: 16507594; GI:83284713]	Flagellar Structure	
102649	5708715	MOT6		Signaling	
146683	5708925	MOT7		No data	
194218	5709378	MOT8		No data	
194403	5709602	MOT9		No data	
195517	5710628	RAB23		GTP-Binding	g323.t1
171647	5706202	RTN1		No data	
140873	5711553	SMP10	(PRP1) Predicted snRNP core protein; SMP10 name replaces previous PRP1 name	RNA metabolism	g729.t1
138013	5709708	SPEF1		Unclear	g9425.t1
150732	5710991	SSMT	SET domain-containing methyltransferase; catalyzes methylation of the N-terminal alpha-amino group of the processed form of RuBisCO small subunit prior to holoenzyme assembly	Protein-protein interaction	g1005.t1
150998	5711866	TEX9	(FBB15)	No data	g6017.t1
136082	5711457	UNI3	Delta tubulin (TUD)[gi:7441381] Required for assembly of the basal body/centriole and localizes to the basal body	Flagellar Structure	g5454.t1
130542	5709131	VFL3		Flagellar Structure	g6293.t1

JGI v3 protein ID	Protein family (cluster) ID	Chlamydomonas gene name	JGI *Chlamydomonas* browser defline	Manual annotation of molecular function	*Chlorella* gene name
			Proteins in both CentricCut and MotileCut		
186669	5707578	DLC1	Flagellar outer dynein arm light chain 1	Flagellar Structure	g2003.t1
186878	5705821	FAP100		No data	g2128.t1
182403	5709730	C1	RNA-binding protein with three KH domains and a protein-protein interaction domain (WW) at the C-terminus Subunit of the circadian RNA-binding protein CHLAMY 1 (Zhao et al., Euk. Cell, in press)	RNA metabolism	g225.t1
132143	5710434	CTO59	(FBB5) Similar to C21orf59 (CTO59)	No data	
106450	5709417	FAP250		No data	g1271.t1
144241	5710529	FAP264		Protein-protein interaction	g8930.t1
196793	5708194	FAP45	Identified in Chlamydomonas basal body proteome as BUG28 [Keller et al., 2005; PMID: 15964273]. Weakly similar to nasopharyngeal epithelium-specific protein 1	No data	g1897.t1
121413	5709547	FAP73		No data	g1567.t1
160148	5705956	FBB11		No data	g8371.t1
169559	5709521	FBB15		Signalling	g8804.t1
115671	5706503	ECH1		Membrane synthesis/differentiation	g7740.t1
189445	5711409	FAP147		Unclear	
129193	5709938	FAP156	Expressed Protein. Rab-type GTPase distantly related to Rab-like proteins from mammals.	GTP-Binding	g323.t1
135463	5705051	FBB4		Signalling	
129295	5708315	KIF6		Trafficking	g2002.t1
192170	5706578	MB02	Move backward only mutant defective in the production of the ciliary waveform. Mbo2p is a novel coiled-coil protein.	Protein-protein interaction	g7837.t1
145799	5711409	MOT43		Unclear	g2576.t1
142227	5708384	MOT44		Membrane Protein	g5944.t1
175396	5711057	MOT45		No data	
195180	5706594	MOT46		RNA metabolism	g5942.t1
107408	5707103	MOT47		Protein-protein interaction	g7956.t1
143267	5710023	MOT48		No data	g2883.t1
116664	5709999	MOT49		Protein-protein interaction	g2319.t1
132719	5709873	ODA1	Flagellar outer dynein arm-docking complex subunit 2 (ODA-DC 2)	Flagellar Structure	g10008.t1
24252	5709882	ODA4	Flagellar outer dynein arm heavy chain beta	Flagellar Structure	g4263.t1
188612	5709886	ODA6	Flagellar outer dynein arm intermediate chain 2, IC2, ODA-IC2, IC69, IC70	Flagellar Structure	g411.t1
151144	5706167	PF2	Component of dynein regulatory complex (DRC) of flagellar axoneme; has similarity to mammalian growth-arrest specific gene product (Gas11/Gas8), trypanin related, PMID: 10969087 PMID: 11864997	Flagellar Structure	g6831.t1
107386	5706608	MOT50		Protein metabolism	g8160.t1
168908	5708554	MOT51		Unclear	g1989.t1
192763	5709569	MOT52		Microtubule Regulation and Metabolism	
149002	5710454	MOT53		Protein-protein interaction	g8107.t1
77703	5708336	RIB43a	Coiled-coil protein associated with protoflament ribbons of flagellar microtubules (PMID 10637302).	Flagellar Structure	
126286	5709885	Rib72	novel component of the ribbon compartment of flagellar microtubules.	Flagellar Structure	g2089.t1
188421	5710529	MOT54		Protein-protein interaction	g8930.t1
180221	5708949	NDK7	(BUG5) in basal body proteome as BUG5 [PMID: 15964273].	Metabolism	g1611.t1
137793	5710049	NKRN1	(FAP106)	Signalling	g8371.t1
192441	5705837	RABL2A	Expressed Protein. Distantly similar to a class of Rab-like proteins from mammals.	GTP-Binding	g2407.t1
3686	5705975	RJL1	Expressed Protein. Member of the RJL family in the Ras superfamily of GTPases (Nepomuceno-Silva et al. 2004, Gene 327:221-32)	GTP-Binding	g323.t1

JGI v3 protein ID	Protein family (cluster) ID	Chlamy-domonas gene name	JGI *Chlamydomonas* browser defline	Manual annotation of molecular function	*Chlorella* gene name
Proteins in CentricCut but not MotileCut					
128761	5708192	ARLC2	(ARL3) Expressed Protein. Similar to the ARLC-type GTPases., ARF-like 3, a member of the ARF/Sar1 GTPase family. Experimental evidence and presence only in organisms with flagella suggest a function in the flagellum/basal body.	Microtubule Regulation and Metabolism	g8394.t1
3897	5709171	DPY30	(FBB12) Desc Chromatin modifying protein complex member, identified by mutations in C. elegans defective in male sensory behavior.	Protein-protein interaction	
132451	5709415	IDA4	Flagellar inner arm dynein light chain p28	Flagellar Structure	
24116	5709496	BLD1	(IFT52) Intraflagellar transport protein IFT52(Curr Biol. 2001. 11(20):1591-4. The C. elegans homologue is osm-6.	Flagellar transport	g6899.t1
136521	5708482	IFT74/72	Intraflagellar transport particle protein 74/72	Flagellar transport	
160948	5706569	IRK1	putative inward rectifier K+ channel TC# 1.A.2	Membrane Protein	g5473.t1
182554	5707722	KAP	Kinesin-associated protein; probable non-motor subunit of kinesin-II, the anterograde motor for intraflagellar transport.	Flagellar transport	g1456.t1
131284	5708587	DIP13	Similar to Sjogren's syndrome nuclear autoantigen 1.	Microtubule Regulation and Metabolism	g2295.t1
147682	5706286	PP11		No data	
195496	5709491	SSA12		Unclear	g1814.t1
127720	5706974	SSA13		Signalling	g5006.t1
171688	5709575	SSA14	Some similarities with flavoprotein monooxygenases	Metabolism	g1188.t1
191923	5709909	SSA15		Protein-protein interaction	g3672.t1
192430	5709753	SSA16		Signalling	
169222	5706998	SSA17		Protein-protein interaction	
111541	5707143	SSA18		RNA metabolism	
185392	5709600	FAP116	Similar to Microtubule Interacting TNF Receptor-Associated Factor 3 Interacting Protein 1	Trafficking	g5061.t1
147671	5705982	SSA19		Protein metabolism	g1168.t1
143218	5709875	SSA20		Protein metabolism	g4383.t1
128801	5711212	TPR5	(FAP259) Desc TPR protein with similarity to human FLJ30990. similar to dyf-1 (C. elegans)	Protein-protein interaction	g5033.t1
192420	5705900	FAP22	Similar to D. rerio cystic kidney disease gene qilin	No data	g6809.t1
100760	5710578	FAP267		Microtubule Regulation and Metabolism	g2896.t1
108954	5709902	FAP32		No data	g9202.t1
128114	5706542	FAP52	(BUG14) in basal body proteome as BUG14 [PMID: 15964273].	Protein-protein interaction	g1897.t1
98642	5710979	IFT57	Intraflagellar transport particle protein 57	Flagellar transport	g7571.t1
138649	5707942	IFT81	Desc Intraflagellar Transport Protein 81	Flagellar transport	
24421	5705296	IFT88	Intraflagellar transport particle protein 88	Flagellar transport	g3783.t1
130473	5709311	MKS1	Ortholog of the human Meckel Syndrome 1 gene	No data	
32880	5708502	NPH4	Found in basal body proteome as POC10 [PMID: 15964273]. Mammalian homolog is NPHP-4, also known as nephroretinin, gene mutated in Senior-Loken syndrome.	No data	g6915.t1
129433	5710308	ODA9	Flagellar outer dynein arm intermediate chain 1, IC1, ODA-IC1, IC78	Flagellar Structure	g2869.t1
97201	5705256	PACRG1	(BUG21) in basal body proteome as BUG21 [PMID: 15964273]. Homologous to mammalian PACRG parkin co-regulated gene.	No data	g2856.t1

Figure S1. Example of Optical mapping-based scaffolding of Chlorella genome

PacBio contigs are colored in blue, while map assembly in green; vertical lines represent the recognition sites of Nt.BspQI. Figure S2 Distribution of Chlorella vulgaris gene annotation results.

Figure S2. Distribution of Chlorella vulgaris gene annotation results

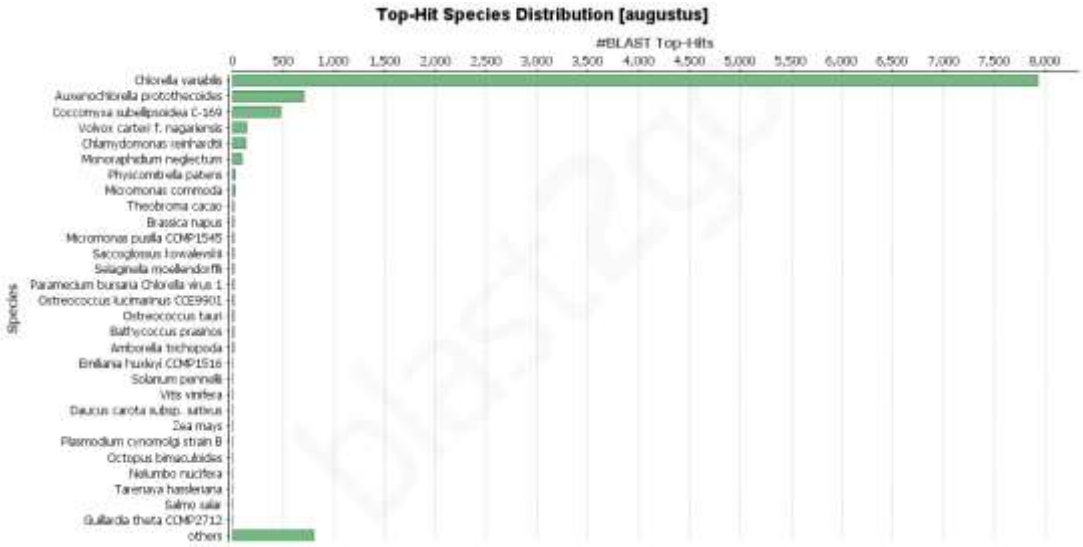

Figure S3 Phylogenetic analysis of Chlorella vulgaris strain 211/11

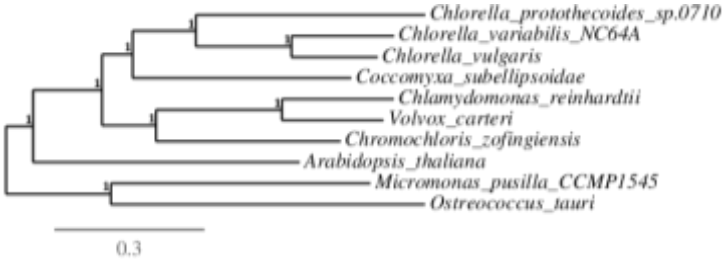

Figure S4 Carbon fixation pathway in Chlorella vulgaris identified by KEGG Mapper

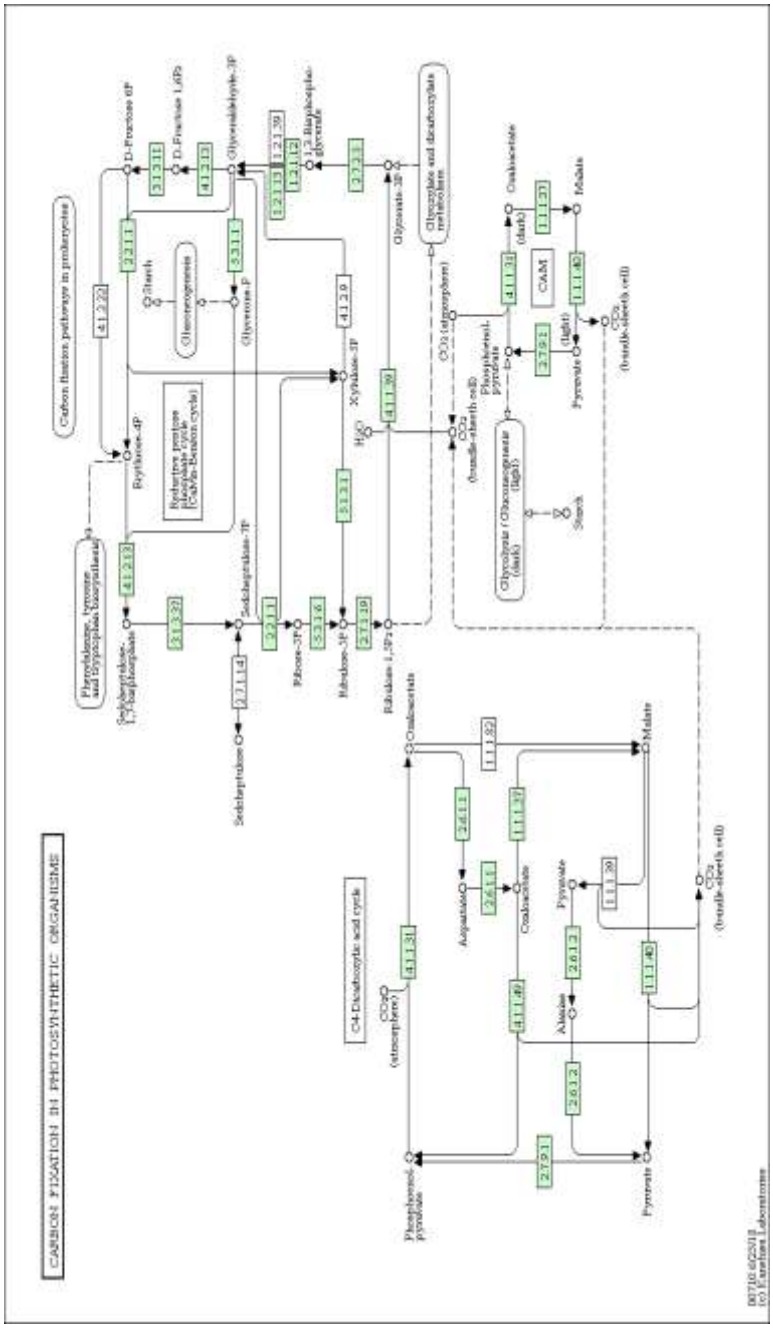

Figure S5 Alignment of Chlorella vulgaris g3658 gene product with HAP2 from Chamydomonas reinhardtii

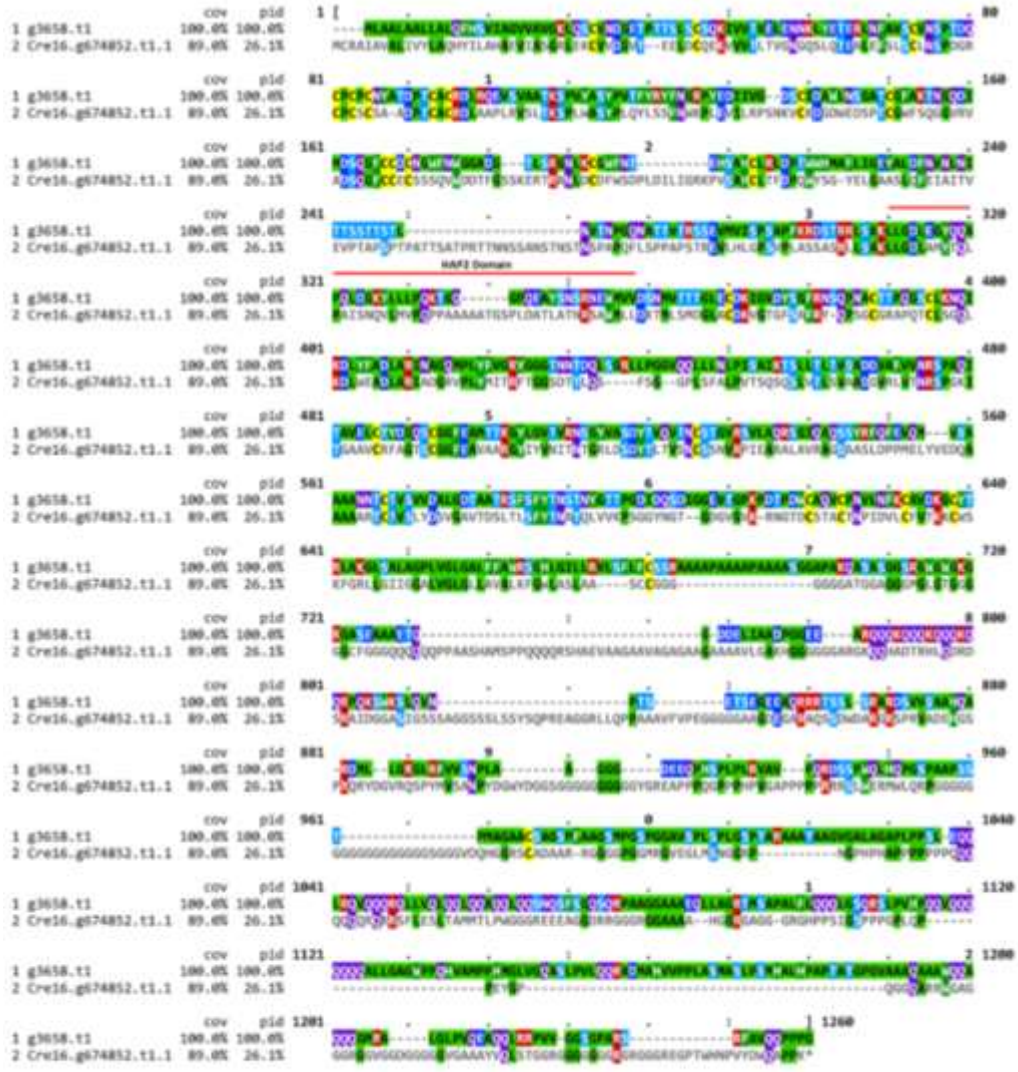

Section B

Identification of a plant-like Violaxanthin De-Epoxidase enzyme in the green alga *Chlorella vulgaris* reveals evolutionary divergency of photoprotective mechanisms in the green lineage[4]

Xanthophyll cycle is a photoprotective metabolic process by which in stress conditions violaxanthin is de-epoxidated to zeaxanthin. The enzyme responsible for violaxanthin de-epoxidation is not conserved among higher plants and green algae. In this work we focused on the identification and characterization of a plant-like violaxanthin de-epoxidase (VDE) enzyme in one of the most used green alga for industrial cultivation, *Chlorella vulgaris*. In particular, by local alignment and homology modelling algorithms, we successfully reconstructed a model structure for *C. vulgaris* VDE identifying almost all the key residues previously reported being important for its activity in higher plant VDE. The catalytic activity of this enzyme was thus investigated *in vitro* upon heterologous expression in *E. coli*, and *in vivo* in *C. vulgaris* by using the VDE inhibitor DTT (DL-Dithiothreitol). The results obtained demonstrate the existence of plant-like xanthophyll cycle activation and function in *C. vulgaris*, differently from other *Chlorophyta*. The results obtained demonstrate a divergence during evolution in the molecular mechanism and function of xanthophyll cycle.

In this work I've performed all the experiments excluding the phylogenetic tree construction and the prediction of the protein model 3D structure.

Abbreviations**:** PSI/II, Photosystem I/II; NPQ, Non-Photochemical Quenching; LHC, Light Harvesting Complex; VDE, Violaxanthin De-Epoxidase; DTT, DL-Dithiothreitol; ROS, Reactive Oxygen Species; DI, de-epoxidation index.

---

[4]This section is based on the manuscript: **Girolomoni L**, Bellamoli F, Morosinotto T, Cazzaniga S, Ballottari M. Identification of a plant-like Violaxanthin De-Epoxidase enzyme in the green alga *Chlorella vulgaris* reveals evolutionary divergency of photoprotective mechanisms in the green lineage

Introduction

Photosynthetic organisms use the Photosynthetic Active Radiation (PAR) for their metabolic processes but irradiance undergo rapid or seasonal changes during season. Depending on the growth conditions, light may be a limit or even a stressor when the products of light phase, ATP and NADPH, are not fully consumed by the Calvin-Benson Cycle. The impaired regeneration of NADP and ADP by carbon fixation reactions indeed causes a saturation of the photosynthetic electron transport chain reducing the photochemical quenching of the excitation energy absorbed by Photosystems: this event increases the population of chlorophyll singlet excited states increasing the probability of energy transfer to oxygen forming the high toxic reactive oxygen species (ROS) (Havaux and Niyogi, 1999). Long term exposure to relative high light induces several acclimation responses in photosynthetic organisms as changing in the amount and quality of pigments, pigment binding and stress-related proteins or molecules, which are only partially conserved among the different species (Havaux and Niyogi, 1999; Ballottari *et al.*, 2007; Bonente *et al.*, 2012). On a mid-short term scale higher plants usually respond to the sun-tracking with specific movements of leaves and chloroplasts thus changing orientation and light interception to properly balance light absorption (Li *et al.*, 2009), while the main short term mechanism activated for photoprotection is Non-Photochemical Quenching (NPQ) by which chlorophylls singlet excited states are dissipated into heat (Demmig-Adams and Adams, 1992). NPQ is composed by three different components, distinguishable by their kinetics. The fastest component activated upon illumination is the pH- or energy-dependent component, called qE (Horton *et al.*, 1996) (Muller, 2001). The mid-range component is qT, related to the phenomenon of the state transition, where some antenna proteins of Photosystem II (PSII), called Light Harvesting Complexes II (LHCII), moves in a minute scale to Photosystem I (PSI) in order to balance the excitation among the two Photosystems (Wollman, 2001). The last component of NPQ is related to the photoinhibition of photosynthesis and/or zeaxanthin accumulation by xanthophyll cycle activation and is called qI (Dall'Osto *et al.*, 2005) or qZ (Nilkens *et al.*, 2010). In higher plants the xanthophyll cycle is induced by luminal acidification triggered by the Violaxanthin De-Epoxidase enzyme (VDE) which is responsible of violaxanthin conversion into zeaxanthin across two consequential de-epoxidation steps forming antheraxanthin as intermediate. Zeaxanthin is involved in

singlet and triplet chlorophyll excited states quenching and scavenging of reactive oxygen species (Betterle *et al.*, 2010; Nilkens *et al.*, 2010; Dall'Osto *et al.*, 2012; Ballottari *et al.*, 2014; Xu *et al.*, 2015; Rockholm & Yamamoto, 1996). VDE is a nuclear encoded protein activated by lumenal acidification upon transmembrane proton gradient formation, which is the consequence of photosynthetic light phase saturation (Gilmore and Yamamoto, 1993) and for its activity requires ascorbate to reduce the epoxy group with the consequent water production (A., Richmond; H., 2013). Previous studies reveal that the VDE activity is inhibited by dithiothreitol (DTT) which reduces one or more di-sulphide bonds formed by cysteine residues (Yamamoto and Kamite, 1972). The proteins sequence of the VDE from *A. thaliana* contains three main domains: a cysteine rich region (13,5% of the residues of this region are cysteines), a catalytic site and a glutamate rich region (Simionato *et al.*, 2015). Site directed mutagenesis experiments showed that in the catalytic domain the residues essential for the VDE activity are the Asp177 and the Tyr198 while the amino acids important for the structural organization are the Asp114, Arg138, His121 and the Tyr214 (Saga *et al.*, 2010). The pH dependent activity was also proved by substituting the protonatable residues with aliphatic amino acids (Fufezan *et al.*, 2012). In microalgae, the role of xanthophyll cycle seems to be not homogeneous: in the model green alga *Chlamydomonas reinhardtii* zeaxanthin accumulation has been reported to important for ROS scavenging but its role in NPQ induction is still controversial (Niyogi *et al.*, 1997; Bonente *et al.*, 2011; Quaas *et al.*, 2015). Differently a partial zeaxanthin-dependent NPQ has been reported in some green algae (Quaas *et al.*, 2015), in brown algae (García-Mendoza and Colombo-Pallotta, 2007) or in eustigmatophytes (Chukhutsina *et al.*, 2017). In the case of *C. reinhardtii* the catalytic violaxanthin de-epoxidation activity has been recently attributed to an enzyme not related to the plant-VDE, called CVDE, which is related to a lycopene cyclase from photosynthetic bacteria (Li *et al.*, 2016). This observation led to the hypothesis that green algae and plants evolved a different violaxanthin de-epoxidase enzymes with implication on their regulation and functions (Li *et al.*, 2016). In this work the effect of zeaxanthin in NPQ induction and the molecular details of enzyme responsible for its accumulation were fully investigated *in vivo* and *in vitro* in one of the most promising green algae for industrial cultivation, *Chorella vulgaris.*

Materials and Methods

Strains and culture conditions

C. vulgaris (CCAP211/11P) cells were grown at 25°C in flask with a white light in low (60 µE m^{-2} s^{-1}) and high (450 µE m^{-2} s^{-1}) light with a 16h light 8h dark photoperiod in BG-11 medium (Allen and Stanier, 1968).

In vitro de-epoxidation on thylakoids

C. vulgaris and *C. reinhardtii* thylakoids were obtained by destroying cells with glass beads directly in the de-epoxidation buffer (40mM MES pH 5.1, 330mM sorbitol, 5mM $MgCl_2$, 10mM NaCl 20mM ascorbate and BSA 0,5%). In the case of spinach, leaves were grinded in 0.4M NaCL,5mM $MgCl_2$, 20mM Tricine/KOH pH 7.8 and 0.5% BSA, filtered through a 10µm filter, centrifuged at 10.000g and then resuspended in the in the de-epoxidation buffer. De-epoxidation reaction was then performed at 20°C for 4 hours. Pigment were then extracted using acetone 80% and analyzed by HPLC.

VDE identification and phylogenetic analysis

Putative VDE genes were searched in the assembled *C. vulgaris* genome by BLAST search using *A. thaliana* VDE1 (AT1G08550) as query and *C. vulgaris* translated genome as database. Sequences carry a VDE lipocalin domain was retrieved from InterPro (IPR010788). Sequence alignment was obtained by MAFFD (version 7.394) software. The phylogenetic tree graphic was rendered with MEGA (Hall, 2013).

NPQ measurements

NPQ was measured using a Dual PAM-101 (Waltz, Effeltrich, Germany). Cells were pre-treated for 2 min with far-red light-emitting diode (LED) before NPQ analysis and during dark recovery. A 5000 µE m^{-2} s^{-1} saturation light was used while actinic lights used were reported in the results section.

Pigment analysis

Pigment were extracted using dimethyl sulphoxide (DMSO) and analysed by HPLC as described in (Lagarde *et al.*, 2000) .

VDE expression and purification

The plasmid expressing mature VDE of *A. thaliana* was kindly provide by Prof. Morosinotto (Saga *et al.*, 2010). The *vde* gene identifications was based on a local blast on the genome of *C. vulgaris* strain 211/11P aligned with *A. thaliana* VDE annotated protein sequence (At1G08550.1) presents in Phytozome V12.1 (https://phytozome.jgi.doe.gov/pz/portal.html). Total RNA from *C. vulgaris* was extracted from cell grown in high light using the Direct-zol™. RNA Miniprep Plus kit (Zymo Research). Transcript sequence was amplified from cDNA using specific primers designed on transcript g7391 (Supplementary Table 1). Mature VDE coding sequence was cloned into pET28 expression vector removing the initial 28 amino acids putative signal peptide for the chloroplast. The signal peptide was calculated using ChloroP 1.1 tool. VDE was expressed in *Escherchia coli* Origami™ 2(DE3) (Novagen) by inducing cells with 1mM isopropyl β-D-1-thiogalactopyranoside for 5 h at 37°C and purified as described in Saga *et al.*, 2010.

VDE activity assay and HPLC

VDE activity was tested by adding pure violaxanthin as substrate in a de-epoxidation buffer as described in Saga *et al.*, 2010. In particular, the de-epoxidation buffer was composed by MES at pH 5.1, and 60mM ascorbate and 9µM MGDG. Violaxanthin de-epoxidation was monitored by changes in absorption spectra in the 480-520 nm region and by HPLC analysis.

SDS-PAGE and western blotting

Total protein extracts were loaded into SDS-PAGE 12% gels as described in Laemmli, 1970. Western blot analysis was performed using antibody for *A. thaliana* VDE (Ballottari *et al.*, 2007).

Results

In vitro de-epoxidation

*Possib*le violaxanthin de-epoxidaton activity in *C. vulgaris* was studied *in vitro* in isolated thylakoids. *C. vulgaris*, spinach and *C. reinhardtii* thylakoids were exposed at pH 5.1 in presence of 20mM ascorbate as reducing agent to activate VDE enzyme. The

VDE inhibitor DTT (DL-Dithiothreitol) was also tested for its possible inhibitory activity (Figure 1).

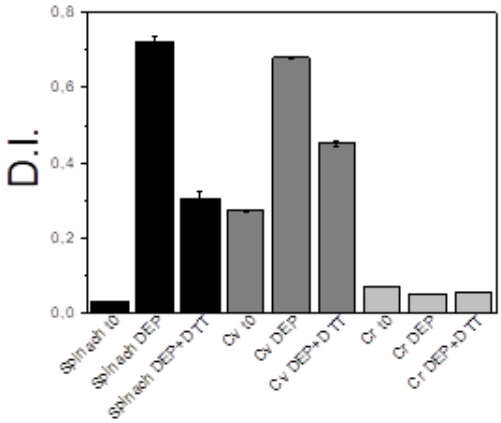

Figure 1 *In vitro de-epoxidation of thylakoid membranes. De-epoxidation index (D.I.) of thylakoids isolated from spinach, C. vulgaris (Cv) and C. reinhardtii (Cr) before (t0) or after (DEP) 4 hours at pH 5.1 in presence of ascorbate in order to induce violaxanthin de-epoxidation. De-epoxidation index obtained in in presence of VDE inhibitor DTT is also reported*

After 4 hours of reaction, pigments were extracted from thylakoids and analysed by HPLC demonstrating for both spinach and *C. vulgaris* a clear *in vitro* de-epoxidation of violaxanthin with zeaxanthin accumulation and a specific inhibitory activity of DTT. Differently, in the case of *C. reinhardtii* no violaxanthin de-epoxidation was observed in these conditions, in agreement with previous observation in this species (Li *et al.*, 2016).

Sequences analysis and protein activity of VDE in C. vulgaris

C. vulgaris 211/11P strain genomic and transcriptomic data were used to mine a possible VDE gene. From blast2go functional annotation of the genome data gene g7391 was annotated as VDE gene. This gene g7391 resulted overexpressed in high light and also the protein accumulation is increased in this condition (Supplementary data, Figure S1). Protein sequence encoded by *C. vulgaris* g7391 was thus analysed with InterPro scan (https://www.ebi.ac.uk/interpro/search/sequence-search), which attributed a VDE lipocalin domain. Multiple alignment, with different VDE sequences was thus performed to study its conservation among evolution. The multiple alignment obtained (Figure 2) show high similarity of *C. vulgaris* VDE with the other VDE sequences analysed, in particular for the catalytic domains. Differently, the CVDE protein of *C. reinhardtii* is divergent from other VDE sequences (Supplementary data, Figure 2) as previously reported (Li *et al.*, 2016). In the case of *C. vulgaris* VDE its N- terminal domain is cysteine enriched with 10 Cys residues which represent 12,9% of this domain, a conserved feature compared to VDE sequence from all the organisms analysed. The

multiple alignment also reveals the conservation in *C. vulgaris* of the key residues for catalytic activity (Asp177 and Tyr198) previously reported in the case of higher plants (Saga *et al.*, 2010). Residues important for the structural organization, Asp114, His121, Arg138 and Tyr214 are conserved in all the VDE sequences reported in Figure 2, while some variations can be observed in the case of residues involved pH dependent activation of the enzyme with only Asp 114 being conserved also in all the sequences analysed, except for *P. tricornutum*. In particular, Asp96 and Asp98 are conserved only in higher plants, while Asp206 is conserved only in land plants: in the case His168 this residue is conserved in higher plats, mosses and diatoms but not in the green algae *C. vulgaris* and *C. variabilis*, where it is substituted with a lysine (Figure 2). These results open the question about a possible pH independent activation of suggest a possible different pH dependency of *C. vulgaris* VDE enzyme compared to VDE enzymes from higher plants.

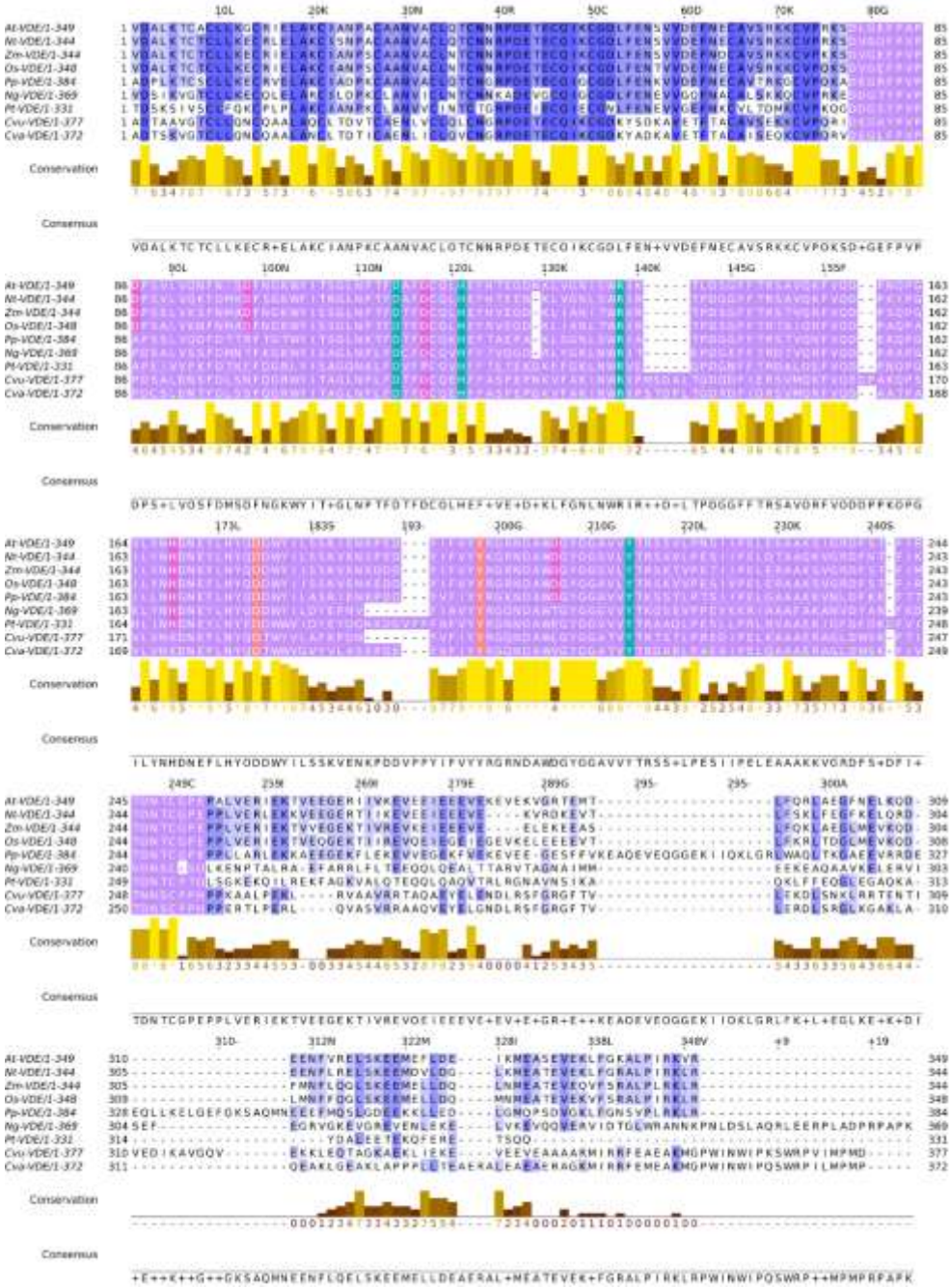

Figure 2 *Multiple alignment of VDE enzyme sequences. The domains organization is divided in three main parts. The first part is the cysteine rich region, the violet part is the lipocalin domain and the last part the glutamic rich region. In the lipocalin domain are evidenced the residues important for the catalytic activity (orange), for the structure organization (green) and for pH sensitivity (purple). At: Arabidopsis thaliana; Nt:*

Nicotiana tabacum; Zm: Zea mays; Os: Oryza sativa; Pp: Physcomitrella patens; Ng: Nannochlopsis gaditana; Pt: Phaeodactylum tricornutum; Cvu: Chlorella vulgaris; Cva: Chlorella variabilis.

On the base of *C. vulgaris* homology with *A. thaliana* VDE, a model structure for the putative catalytic domain of C. vulgaris VDE was built (Figure 3). The structure of lipocalin catalytic domain of *A. thaliana* VDE has been indeed previously reported (Arnoux *et al.*, 2009). The model structure obtained for *C. vulgaris* was almost overlapping with *A. thaliana* VDE catalytic domain, showing the typical lipocalin fold with an eight-stranded antiparallel β-barrel.

Figure 3 *Chlorella vulgaris VDE 3D model structure. Homology model of the VDE lipocalin domain was obtained by ITASSER tool upon alignment with the deposited structure of A. thaliana VDE catalytic domain. A. thaliana VDE catalytic domain structure is reported in cyan, while the model structure for C. vulgaris VDE is reported in green*.

cDNA of *C. vulgaris* putative VDE gene was cloned in expression vector and overexpressed in *E. coli* as previously reported (Saga *et al.*, 2010). Recombinant VDE was then purified from the soluble fraction of lysate bacterial cells though affinity column (Supplementary data, Figure S2). Purified recombinant VDE protein was then used for evaluating its catalytic activity in presence of violaxanthin setting the reaction conditions at pH 5.1 in presence of ascorbate. Recombinant VDE protein form *A. thaliana* was also tested as positive control (Saga *et al.*, 2010). Figure 4 reports changes in absorption spectrum due to violaxanthin de-epoxidation during *C. vulgaris* VDE *in vitro* assay: this is consistent with violaxanthin de-epoxidation catalysed by *C. vulgaris* VDE since zeaxanthin is indeed red-shifted compared to violaxanthin. Zeaxanthin accumulation was then confirmed by HPLC analysis (Figure 4B). Similar results were obtained in presence of *A. thaliana* VDE.

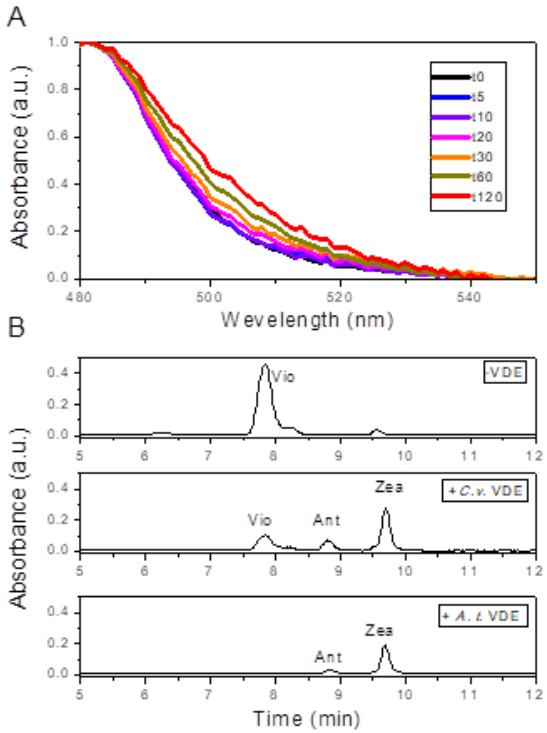

Figure 4 *In vitro violaxanthin de-epoxidation assasy. VDE activity of recombinant C. vulgaris was evaluated in vitro measuring changes in carotenoid absorption spectrum due to violaxanthin conversion to zeaxanthin (A). Chromatogram related to HPLC pigment analysis before and after VDE in vitro assay (B). A. thaliana VDE (A.t. VDE) was also tested as positive control.*

Phylogenetic distribution of VDE

To investigate the distribution of VDE among different photosynthetic organism, a phylogenetic tree of putative VDE enzymes was then assembled. Protein sequences with VDE lipocalin domain identified by InterPro Scan was used to assemble a phylogenetic tree with C. *vulgaris* VDE. As reported in Figure 5 VDE enzymes from eudicots and monocots clustered together, followed by a cluster with mosses, liverworts and club-mosses. In the case of Chlorophyta a separate cluster could be drawn, with VDE enzymes being identified in some green algae, among which the VDE enzyme found in *C. vulgaris*, clustering close to VDE enzyme found in *Chlorella variabilis, Auxenochlorella prototechoides, Monoraphydium neglectum and Lobopshera incisa,* among others. Interestingly, no VDE enzymes could be found in green algae as *Chlorella sorokiniana, Chromochlorosis zofingensis, Vovox carterii* or *C. reinhardtii* indicating a divergency of VDE during evolution even among *Chlorophyta*. Interestingly, a separate group of VDE-like protein cold be found grouping sequences from organisms which plastids originated by a secondary symbiosis as diatoms, brown

algae, *Eustigmatophyceae* as *Nannochloropsis sp*. and photosynthetic *Alveolata* as *Chromera velia*. A separate and more divergent group be found including lipocalin from higher plants, with no VDE function reported and a more divergent group including different organisms from diatoms, to *Eustigmatophyceae* and *Alveolata*. Interestingly, in the latter group enzymes with de-epoxidation activity as diadinoxanthin exposidase could be found, which have a different catalytic activity compared to VDE (Lavaud *et al.*, 2012).

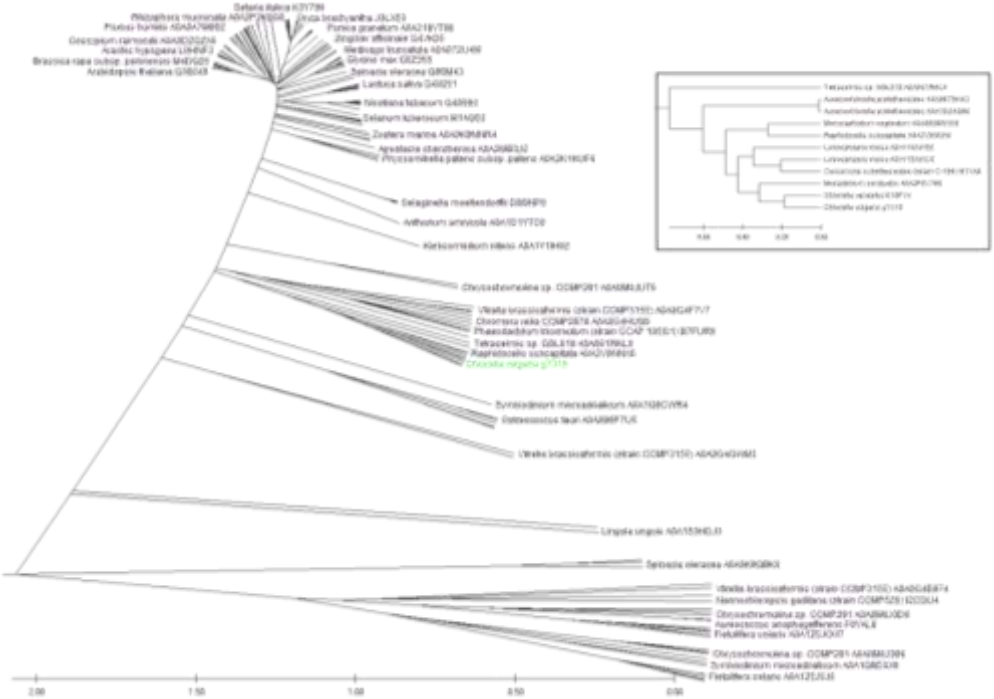

Figure 5 *Phylogenetic tree of VDE-like proteins. Phylogenetic tree was obtained by multiple alignment of protein sequences carrying a VDE lipocalin domain identified by InterPro (IPR010788). The units of branch length are residues substitution per site divided by the length of the sequence. Subtree reported in the inset refers to the Chlorophyte group.*

Kinetics of zeaxanthin accumulation and relaxation

To properly investigate the role *in vivo* of zeaxanthin in *C. vulgaris* the kinetics of xanthophyll cycle activation and relaxation was investigated. *C. vulgaris* cells, grown in low and high light, were thus exposed in presence or absence of the VDE inhibitor DTT to 2000 µmol photons m^{-2} s^{-1} for 5’ or 20’ followed by 5’ or 20’ of dark recovery.

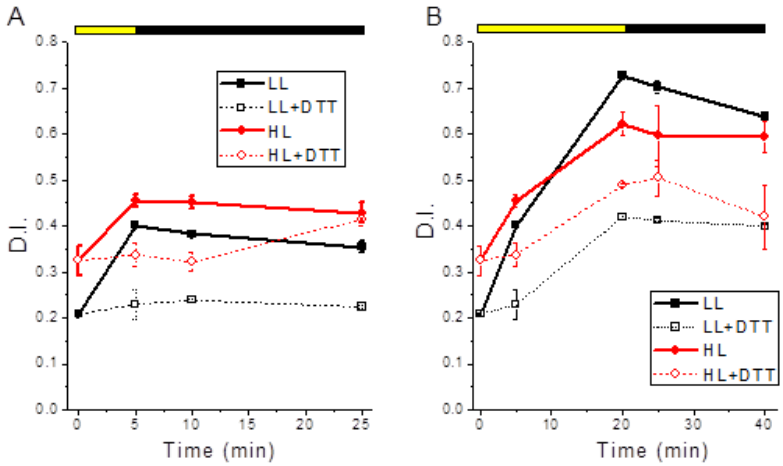

Figure 6 *HPLC analysis from cells acclimated in low light and high light in presence or not of DTT (1mM). A) De-epoxidation index of cells treated for 5' with 2000 µmol photons m^{-2} s^{-1} followed with 20' of dark recovery. B) De-epoxidation index of cells treated for 20' with 2000 µmol photons m^{-2} s^{-1} followed with 20' of dark recovery. Standard deviations are reported as error bars (n=3).*

As reported in the Figure 6 zeaxanthin accumulation and the de-epoxidation index increased upon light exposure, and then decreased only partially during the dark recovery. DTT treatments reduce the zeaxanthin accumulation, confirming its inhibitory effect on zeaxanthin synthesis even in whole cells.

Role of xanthophyll cycle in NPQ induction in C. vulgaris

In order to elucidate the possible role of xanthophyll cycle in NPQ induction in *C. vulgaris*, cells were grown in low light 50 µmol photons m^{-2} s^{-1} or high light 450µmol photons m^{-2} s^{-1} condition for 7 days. NPQ induction curves were then measured at different actinic lights (from 200 µmol photons m^{-2} s^{-1} to 2500 µmol photons m^{-2} s^{-1}) (Figure 7).

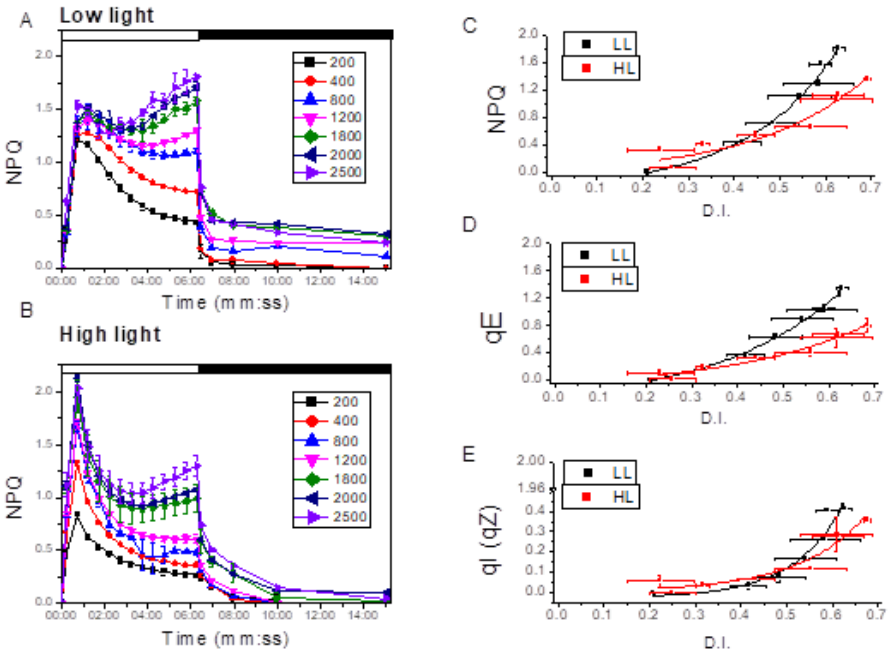

Figure 7 *NPQ kinetics and their correlation with zeaxanthin accumulation. Panel A/B: NPQ traces measured were collected on cell grown in low light (A) or high light (B) by using an actinic light of 200, 400, 800, 1200, 1800, 2000 and 2500 µmol photons m^{-2} s^{-1}. Panel C/D/E: correlation of de-epoxidation index with NPQ measured at the end of the actinic light exposure (C), qE measured as the NPQ component decaying in one minute in the dark (D), and qI(qZ) measured the residual NPQ component after 10 minutes of dark relaxation (E). Standard deviations are reported as error bars (n=3).*

In the case of cells grown in low light, NPQ traces measured with actinic lights up to 1200 µmol photons m^{-2} s^{-1} were characterized by a transient peak followed by a decay even if the actinic light was still turned on. Similar kinetics were observed in the case of cells grown in HL even if treated with 2500µmol photons m^{-2} s^{-1} as actinic light. Only in the case of cells grown in low light, when the actinic light intensities were increased to 1800-2500µmol photons m^{-2} s^{-1}, a continuous rise of NPQ was observed (Figure 7A). The decrease of NPQ values even during treatment with actinic light was likely related to the activation of the Calvin-Benson cycle which are activated by the reduced thioredoxin in a minute scale chain (Michelet *et al.*, 2013) leading to NADPH consumption and regeneration of $NADP^+$, the final electron acceptor in the light phase of photosynthesis. High levels of $NADP^+$ relax the photosynthetic apparatus decreasing the NPQ induction. Cells grown in high light were thus more adapted in managing high light intensities compared to cells grown in low light. Xanthophyll cycle activation during the

NPQ measurement was then investigated by pigment analysis of *C. vulgaris* cells before (T0) or after the light treatment at the different light intensities. As shown in Supplementary data, Figure S3 increasing the light intensities caused higher levels of zeaxanthin accumulation. as previously reported in higher plants (Rees *et al.*, 1989) (Eskling *et al.*, 1997). When cells were treated with relatively low actinic light cells grown in low light were characterized by a higher de-epoxidation index compared to the cells grown in high light, while no major differences were noticeable at high actinic lights. The possible relation between NPQ induction ad zeaxanthin accumulation was thus investigated plotting the NPQ values measured at the end of the actinic light treatment and its components qE and qI (or qZ) as a function of the de-epoxidation index measured. As reported in Figure 6 an exponential correlation was found between NPQ, qE or qI with de-epoxidation index. These results demonstrate that zeaxanthin accumulation is not the only actor responsible for NPQ induction in *C. vulgaris*, but especially at higher light intensities some other components determine the extent of NPQ, qE or qI observed. The higher NPQ, qE and qI (qZ) values observed in low light cells observed at similar de-epoxidation further indicates the additional role of other factors in NPQ induction apart from xanthophyll cycle activation. The specific role of zeaxanthin in NPQ induction was thus studied by measuring NPQ upon a double cycle of illumination interrupted by 5 minutes of dark: in this way zeaxanthin accumulation is induced in the first cycle and its potential role in NPQ can be highlighted in the second cycle due to the long timing required for zeaxanthin epoxidation (Figure 8). This experiment was performed in both low light and high light grown cells in presence or absence of DTT. As reported in Figure 7 in both low light and high light grown cells the presence of DTT caused a partial decrease of NPQ during both the first and second cycle of actinic light illumination, thus suggesting a partial zeaxanthin dependency for NPQ induction.

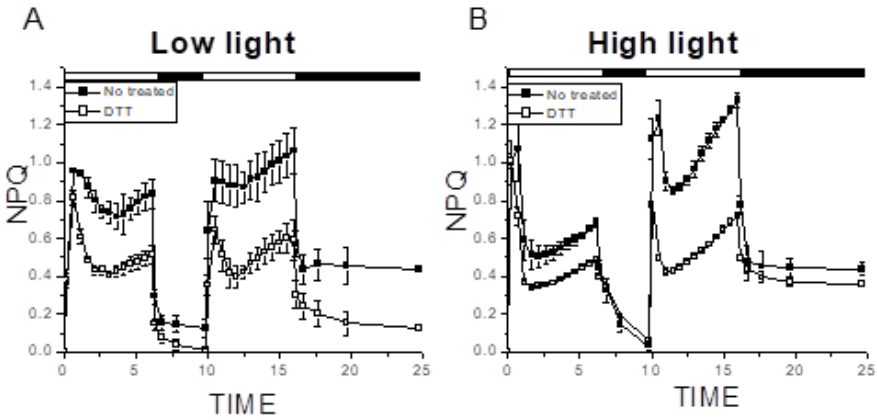

Figure 7 *Effect of DTT on NPQ kinetics. In the graphics A) and B) double cycle of NPQ induction of cells acclimated in low and high light are reported. For these measurements were used an actinic light of 2000µmol photons* m^{-2} s^{-1} *and a saturating light of 4000µmol photons* m^{-2} s^{-1}*. Standard deviations are reported as error bars (n=3)*

Consistently, during the second illumination cycle the NPQ measured was higher compared to the NPQ measured in the first cycle and the inhibitory effect given by the presence of DTT was even stronger compared to the first cycle, with a significant reduction in the level of NPQ in both low and high light acclimated cells. Interestingly both in low light and high light grown cells the presence of DTT caused a decrease of qE and qI (or qZ) components of NPQ, suggesting a partial role of zeaxanthin in both fast and long relaxing components of NPQ. Zeaxanthin accumulation upon high light exposure and requires minutes, while its kinetic of zeaxanthin epoxidation are much longer (Figure 5). According to this finding, the initial NPQ induction in the first 1-2 minutes of illumination in the first cycle was essentially independent from zeaxanthin accumulation, while the second phase of NPQ and the second cycle was more affected by DTT addition. When the same experiment was performed in the case of *C. reinhardtii* any evident effect of DTT was measured (Supplemental data Figure S4).

Discussion

In this work the identification of a plant-like VDE enzyme is reported in *C vulgaris*, and the relationship of its activity with between the photoprotective mechanism NPQ is presented. *C. vulgaris* is one of the leading microalgae at industrial level due to the high growth rate and resistance to biotic and abiotic stresses (Liang *et al.*, 2009).

Photoprotective mechanisms as NPQ have been reported as key targets for biotechnological manipulation of photosynthetic organisms assuring on one side enough photoprotection and on the other higher photosynthetic efficiency (Berteotti *et al.*, 2016; Kromdijk *et al.*, 2016). Zeaxanthin has been associated with different photoprotective functions, from singlet and triplet chlorophyll excited quenching to ROS scavenging in both higher plants and green algae (Havaux and Niyogi, 1999; Baroli *et al.*, 2000; Dall'Osto *et al.*, 2012). However, the identification of CVDE, the gene product responsible for violaxanthin de-epoxidation in *C. reinhardtii*, revealed a divergency in the evolution in the green lineage of the enzyme carrying the VDE catalytic activity, being this enzyme not homologous to the VDE of *A. thaliana*, but more similar to a lycopene cyclase (Li *et al.*, 2016). Moreover, CVDE is in the stromal side of thylakoid membranes and it is not activated by lumen acidification. In this work a violaxanthin de-epoxidase catalytic activity inducible at low pH was found in *C. vulgaris*, which lead by *C. vulgaris* genome mining to identify a conserved plant-like VDE enzyme in this member of the Chlorophyta group. Phylogenetic distribution of VDE sequences reveals indeed that VDE sequences are widely distributed in higher and lower plants, while in unicellular algae, only in some green algae a plant-like VDE sequences could be found. *C. vulgaris* VDE was revealed having a high level of identity compared to *A. thaliana* VDE with the conservation of all the key residues involved in protein structure and catalytic activity (Figure 2). Only in the case of residues involved to protein activation by protonation a partial conservation was found in *C. vulgaris* VDE compared to VDE from higher plants. It is interesting to note that plant-like VDE enzyme could be found in other green algae as *Chlorella variabilis* but not in other green algae as *C. sorokiniana* or *C. zofingesis.* In the latter in particular a CVDE-like enzyme was rather identified (Roth *et al.*, 2017). The divergency between CVDE and VDE despite a similar catalytic activity demonstrate the plasticity of the carotenoid biosynthetic pathway and divergent evolution of the key enzyme involved likely driven by their specific functions and interaction with the environment. In higher plants the photoprotective NPQ mechanism depends on the interaction of an LHC-like protein called PSBS with other LHC proteins (Li *et al.*, 2002). Xanthophyll cycle activation has an important, though not crucial, role in higher plants in the induction of NPQ as observed in *npq1* and *npq2* mutants in *A. thaliana*, lacking VDE and zeaxanthin epoxidase (ZE) respectively, which show reduced NPQ phenotypes compared to WT but not zeroed (Havaux and Niyogi, 1999).

Differently, in the case of *Physcomitrella patens* VDE activity has been reported to be essential for NPQ induction (Pinnola *et al.*, 2013). In microalgae, the role of zeaxanthin in the NPQ process is still unclear and highly species-specific (Quaas *et al.*, 2015). In *C. reinhardtii*, mutants that are unable to accumulate zeaxanthin show an induction of NPQ similar to the WT (Niyogi *et al.*, 1997), thus demonstrating zeaxanthin does not have a specific role in NPQ in that organism (Supplemental data, Figure S4). In *Phaeodactylum triconornutum* strains with a reduces level of diatoxanthin reflects lower induction od NPQ (Lavaud *et al.*, 2012). The role of zeaxanthin was also studied in the stramenophile *Phaeomonas* sp. where NPQ level is correlated with its accumulation and is already active at dark (Berne *et al.*, 2018). In this work an exponential correlation between the induction of NPQ and zeaxanthin accumulation was found in *C. vulgaris*: this result demonstrates that additional components are contributing to NPQ induction, especially at higher actinic lights. Pigment binding proteins involved in quenching as PSBS, LHCSR or other LHCII protein present indeed protonatable sites (Walters *et al.*, 1996; Li *et al.*, 2004; Liguori *et al.*, 2013; Ballottari *et al.*, 2016) that could be responsible for the modulation of the extent of NPQ at different actinic light independently from the contribution of zeaxanthin. By the way, the presence of DTT reduces the ability of cells to accumulate zeaxanthin and reduces the level of induced NPQ, demonstrating a partial role of zeaxanthin in NPQ induction in *C. vulgaris*. Moreover, when two cycles of illumination and dark recovery was applied to *C. vulgaris*, the induction of NPQ was observed to be greater in the second cycle, where zeaxanthin was accumulated during a first cycle of illumination. The whole of these findings thus demonstrates the partial role of zeaxanthin in inducing NPQ as in the cases of higher plants (Supplemental data, Figure S5). However, it is not possible to fully determine whether zeaxanthin is essential or not for the NPQ process, as even in the presence of DTT, zeaxanthin synthesis is only partially inhibited. It is interesting to note that the similar relationship between NPQ and zeaxanthin and the similar characteristics of the VDE enzyme in higher plants and *C. vulgaris* may be correlated with the capacity of this algae to form biofilms on land surface. In the case of *C. reinhardtii*, showing an almost zeaxanthin independent NPQ and a CVDE enzyme for xanthophyll cycle induction, this species cold be found mainly in planktonic form, with a relatively limited risk of sudden changes in irradiance. Differently *C. vulgaris*, where a plant-like VDE and plant-like correlation of NPQ and xanthophyll cycle has been found, is mainly present in biofilms which increases the risk

of being exposed to rapid light changes, as in the case of lower or higher plants (Quaas *et al.*, 2015). In these conditions the cells of *C. vulgaris* are exposed to environmental changes in a manner like the higher plants. It is therefore possible to speculate that *C. vulgaris* has evolved photoprotective mechanisms that have proved to be successful in the case of higher plants in which zeaxanthin has a central role.

Bibliography

A., Richmond; H. Q. 2013. *Handbook of Microalgal Culture*.

Allen MM, Stanier RY. 1968. Selective isolation of blue-green algae from water and soil. Journal of General Microbiology **51**, 203–209.

Arnoux P, Morosinotto T, Saga G, Bassi R, Pignol D. 2009. A structural basis for the pH-Dependent xanthophyll cycle in *Arabidopsis thaliana*; The Plant Cell **21**, 2036 LP-2044.

Ballottari M, Alcocer MJP, D'Andrea C, Viola D, Ahn TK, Petrozza A, Polli D, Fleming GR, Cerullo G, Bassi R. 2014. Regulation of Photosystem I light harvesting by zeaxanthin. Proceedings of the National Academy of Sciences **111**, E2431–E2438.

Ballottari M, Dall'Osto L, Morosinotto T, Bassi R. 2007. Contrasting behavior of higher plant photosystem I and II antenna systems during acclimation. Journal of Biological Chemistry **282**, 8947–8958.

Ballottari M, Truong TB, Re De E, Erickson E, Stella GR, Fleming GR, Bassi R, Niyogi KK. 2016. Identification of pH-sensing sites in the light harvesting complex stress-related 3 protein essential for triggering non-photochemical quenching in *Chlamydomonas reinhardtii*. Journal of Biological Chemistry **291**, 7334–7346.

Baroli I, Niyogi KK, Barber J, Heifetz P. 2000. Molecular genetics of xanthophyll-dependent photoprotection in green algae and plants. Philosophical Transactions of the Royal Society B: Biological Sciences **355**, 1385–1394.

Berne N, Fabryova T, Istaz B, Cardol P, Bailleul B. 2018. The peculiar NPQ regulation in the stramenopile *Phaeomonas* sp. challenges the xanthophyll cycle dogma. Biochimica et Biophysica Acta - Bioenergetics **1859**, 491–500.

Berteotti S, Ballottari M, Bassi R. 2016. Increased biomass productivity in green algae by tuning non-photochemical quenching. Scientific reports **6**, 21339.

Betterle N, Ballottari M, Hienerwadel R, Dall'Osto L, Bassi R. 2010. Dynamics of zeaxanthin binding to the photosystem II monomeric antenna protein Lhcb6 (CP24) and modulation of its photoprotection properties. Archives of Biochemistry and Biophysics **504**, 67–77.

Bonente G, Ballottari M, Truong TB, Morosinotto T, Ahn TK, Fleming GR, Niyogi KK, Bassi R. 2011. Analysis of LHcSR3, a protein essential for feedback de-excitation in the green alga *Chlamydomonas reinhardtii*. PLoS Biology **9**.

Bonente G, Pippa S, Castellano S, Bassi R, Ballottari M. 2012. Acclimation of *Chlamydomonas reinhardtii* to different growth irradiances. Journal of Biological Chemistry **287**, 5833–5847.

Chukhutsina VU, Fristedt R, Morosinotto T, Croce R. 2017. Photoprotection strategies of the alga *Nannochloropsis gaditana*. Biochimica et Biophysica Acta - Bioenergetics **1858**, 544–552.

Dall'Osto L, Caffarri S, Bassi R. 2005. A mechanism of nonphotochemical energy dissipation, independent from PsbS, revealed by a conformational change in the antenna protein CP26. The Plant cell **17**, 1217–1232.

Dall'Osto L, Holt NE, Kaligotla S, Fuciman M, Cazzaniga S, Carbonera D, Frank HA, Alric J, Bassi R. 2012. Zeaxanthin protects plant photosynthesis by modulating chlorophyll triplet yield in specific light-harvesting antenna subunits. Journal of Biological Chemistry **287**, 41820–41834.

Demmig-Adams B, Adams WW. 1992. Responses of plants to high light stress. Annu. Rev. Plant Physiol. Plant Mol. Biol. **43**, 599–626.

Eskling M, Arvidsson P-O, Akerlund H-E. 1997. The xanthophyll cycle, its regulation and components. Physiologia Plantarum **100**, 806–816.

Fufezan C, Simionato D, Morosinotto T. 2012. Identification of key residues for pH dependent activation of violaxanthin de-epoxidase from *Arabidopsis thaliana*. PLoS ONE **7**, 1–10.

García-Mendoza E, Colombo-Pallotta MF. 2007. The giant kelp *Macrocystis pyrifera* presents a different nonphotochemical quenching control than higher plants. New Phytologist **173**, 526–536.

Gilmore AM, Yamamoto HY. 1993. Linear models relating xanthophylls and lumen acidity to non-photochemical fluorescence quenching. Evidence that antheraxanthin explains zeaxanthin-independent quenching. Photosynthesis Research **35**, 67–78.

Hall BG. 2013. Building phylogenetic trees from molecular data with MEGA. Molecular Biology and Evolution **30**, 1229–1235.

Havaux M, Niyogi KK. 1999. The violaxanthin cycle protects plants from photooxidative damage by more than one mechanism. Proceedings of the National Academy of Sciences **96**, 8762–8767.

Horton P, Ruban A V., Walters RG. 1996. Regulation of Light Harvesting in green plants. Annual Review of Plant Physiology and Plant Molecular Biology **47**, 655–684.

Kromdijk J, Głowacka K, Leonelli L, Gabilly ST, Iwai M, Niyogi KK, Long SP. 2016. Improving photosynthesis and crop productivity by accelerating recovery from photoprotection.

Science **354**, 857 LP-861.

Laemmli UK. 1970. Cleavage of structural proteins during the assembly of the head of bacteriophage T4. Nature **227**, 680.

Lagarde D, Beuf L, Vermaas W. 2000. Increased production of zeaxanthin and other pigments by application of genetic engineering techniques to *Synechocystis* sp. strain PCC 6803. Applied and environmental microbiology **66**, 64–72.

Lavaud J, Materna AC, Sturm S, Vugrinec S, Kroth PG. 2012. Silencing of the violaxanthin de-epoxidase gene in the diatom *Phaeodactylum tricornutum* reduces diatoxanthin synthesis and non-photochemical quenching. PLoS ONE **7**.

Li X-P, Gilmore AM, Caffarri S, Bassi R, Golan T, Kramer D, Niyogi KK. 2004. Regulation of photosynthetic light harvesting involves intrathylakoid lumen pH sensing by the PsbS protein. Journal of Biological Chemistry.

Li X-P, Muller-Moule P, Gilmore AM, Niyogi KK. 2002. PsbS-dependent enhancement of feedback de-excitation protects photosystem II from photoinhibition. Proceedings of the National Academy of Sciences **99**, 15222–15227.

Li Z, Peers G, Dent RM, Bai Y, Yang SY, Apel W, Leonelli L, Niyogi KK. 2016. Evolution of an atypical de-epoxidase for photoprotection in the green lineage. Nature Plants **2**, 1–6.

Li Z, Wakao S, Fischer BB, Niyogi KK. 2009. Sensing and Responding to Excess Light. Annual Review of Plant Biology **60**, 239–260.

Liang Y, Sarkany N, Cui Y. 2009. Biomass and lipid productivities of *Chlorella vulgaris* under autotrophic, heterotrophic and mixotrophic growth conditions. Biotechnology Letters **31**, 1043–1049.

Liguori N, Roy LM, Opacic M, Durand G, Croce R. 2013. Regulation of Light Harvesting in the green alga *Chlamydomonas reinhardtii*: The C-Terminus of LHCSR is the knob of a dimmer switch. Journal of the American Chemical Society **135**, 18339–18342.

Michelet L, Zaffagnini M, Morisse S, *et al.* 2013. Redox regulation of the Calvin–Benson cycle: something old, something new. Frontiers in Plant Science **4**, 1–21.

Muller P. 2001. Non-Photochemical Quenching. A response to excess light energy. Plant Physiology **125**, 1558–1566.

Nilkens M, Kress E, Lambrev P, Miloslavina Y, Müller M, Holzwarth AR, Jahns P. 2010. Identification of a slowly inducible zeaxanthin-dependent component of non-photochemical quenching of chlorophyll fluorescence generated under steady-state conditions in *Arabidopsis*. Biochimica et Biophysica Acta - Bioenergetics **1797**, 466–475.

Niyogi KK, Bjorkman O, Grossman AR. 1997. *Chlamydomonas* xanthophyll cycle mutants identified by Video Imaging of chlorophyll fluorescence quenching. the Plant Cell **9**, 1369–1380.

Pinnola A, Dall'Osto L, Gerotto C, Morosinotto T, Bassi R, Alboresi A. 2013. Zeaxanthin binds to Light-Harvesting Complex Stress-Related Protein to enhance Nonphotochemical Quenching in *Physcomitrella patens*. The Plant Cell **25**, 3519–3534.

Quaas T, Berteotti S, Ballottari M, Flieger K, Bassi R, Wilhelm C, Goss R. 2015. Non-photochemical quenching and xanthophyll cycle activities in six green algal species suggest mechanistic differences in the process of excess energy dissipation. Journal of Plant Physiology **172**, 92–103.

Rees D, Young A, Noctor G, Britton G, Horton P. 1989. Enhancement of the ΔpH-dependent dissipation of excitation energy in spinach chloroplasts by light-activation: correlation with the synthesis of zeaxanthin. FEBS Letters **256**, 85–90.

Rockholm DC, Yamamoto HY. 1996. Violaxanthin De-Epoxidase. , 697–703.

Roth MS, Cokus SJ, Gallaher SD, *et al.* 2017. Chromosome-level genome assembly and transcriptome of the green alga *Chromochloris zofingiensis* illuminates astaxanthin production. Proceedings of the National Academy of Sciences of the United States of America **114**, E4296–E4305.

Saga G, Giorgetti A, Fufezan C, Giacometti GM, Bassi R, Morosinotto T. 2010. Mutation analysis of violaxanthin de-epoxidase identifies substrate-binding sites and residues involved in catalysis. Journal of Biological Chemistry **285**, 23763–23770.

Simionato D, Basso S, Zaffagnini M, Lana T, Marzotto F, Trost P, Morosinotto T. 2015. Protein redox regulation in the thylakoid lumen: The importance of disulfide bonds for violaxanthin de-epoxidase. FEBS Letters **589**, 919–923.

Walters RG, Ruban a V, Horton P. 1996. Identification of proton-active residues in a higher plant light-harvesting complex. Proceedings of the National Academy of Sciences of the United States of America **93**, 14204–14209.

Wollman Â. 2001. State transitions reveal the dynamics and fexibility of the photosynthetic apparatus. The EMBO Journal **20**, 3623–3630.

Xu P, Tian L, Kloz M, Croce R. 2015. Molecular insights into Zeaxanthin-dependent quenching in higher plants. Scientific Reports **5**, 1–10.

Yamamoto HY, Kamite L. 1972. The effects of dithiothreitol on violaxanthin de-epoxidation and absorbance changes in the 500-nm region. Biochimica et Biophysica Acta (BBA) - Bioenergetics **267**, 538–54

Supplementary data

Table S1 Primers used for Vde transcript amplification from cDNA and vde gene and transcript sequences.

Forward sequence (5' -3')	Reverse sequence (5'-3')
ATATAAAGCTTATGGCAGCTGCAGCACGC	ATATACTCGAGATCCATGGGCATGATGACTG

VDE sequences *VDE transcript and protein sequences. Signal peptide is underlined*.

>g7391.t1_protein

MQASRCTAAAVPAAPATNLPRCRRRVVRAAAARRPAASQQQRDADRQQEAQQPQQLGLTPLQKVA
TGAAGLLASAVLLTAPGSALAADTAAVGTCLLQNCQAALAQCLTDVTCAENLVCLQLCNGRPDETE
CQIKCGDKYSDKAVETFTACAVSEKKCVPQRIDEDAYPVPPDSALDNSFDLSNFQGRWYITAGLNPLF
DTFDCQEHFFASPEPNKVFAKINWRIPMSDALTGDQDFIERSVMQKFVQEDPAKQPSVLVNKDNEFLN
YQDTWYVLAFKPDNYVFIYYRGQNDAWLGYGGATVYTRTSTLPREDIPELKAAAERAGLDWSKFTI
TNNSCPPHPPKAALPEKLRVAAVRRTAQAEYELENDLRSFGRGFTVLEKDLSNKLRRTENTIVEDIKA
VGQVEKKLEQTAGKAEKLIEKEVEEVEAAAARMIRRFEAEAKMGPWINWIPKSWRPVIMPMD

>g7391.t1_transcript

ATGCAGGCCTCGAGGTGCACCGCAGCAGCCGTGCCAGCAGCCCCCGCCACAAACCTCCCGAGGT
GCCGCCGGCGTGTGGTGCGGGCAGCTGCAGCACGCCGCCCAGCCGCGTCTCAACAACAGCGCGA
TGCAGATAGGCAGCAGGAGGCACAACAGCCGCAGCAGCTGGGCCTGACCCCACTGCAGAAGGTG
GCAACTGGTGCGGCAGGCCTGCTAGCCTCTGCGGTCCTCCTCACGGCGCCTGGCTCAGCATTGGC
GGCAGACACTGCGGCTGTGGGCACGTGCCTGCTGCAAAACTGTCAAGCTGCGCTGGCCCAGTGCC
TCACAGACGTCACCTGCGCGGAGAACCTGGTGTGCCTGCAGCTGTGCAACGGCCGCCCAGACGA
GACTGAGTGCCAGATCAAGTGTGGTGACAAGTATTCCGACAAGGCGGTGGAGACGTTCACTGCCT
GCGCAGTCAGCGAGAAGAAGTGTGTCCCGCAGCGAATTGACGAGGATGCCTACCCCGTGCCACC
AGACAGTGCACTTGACAACAGCTTCGATTTGTCGAACTTCCAGGGCCGCTGGTACATCACTGCTG
GGCTAAACCCACTGTTCGACACATTCGACTGCCAGGAGCATTTCTTTGCCAGCCCGGAACCAAAC
AAGGTGTTTGCCAAGATCAACTGGCGGATTCCCATGTCAGACGCTCTGACTGGGGATCAGGACTT
CATTGAGCGGTCTGTGATGCAGAAGTTTGTGCAGGAGGACCCTGCCAAGCAGCCTTCTGTCCTAG
TGAACAAGGACAACGAATTTTTGAACTACCAAGACACTTGGTATGTGCTAGCTTTCAAGCCTGAC
AACTACGTCTTCATCTACTATCGAGGCCAGAATGATGCGTGGCTGGGCTACGGCGGCGCTACTGT
TTACACACGCACCTCGACCCTGCCTCGTGAGGACATTCCGGAGCTTAAGGCTGCAGCAGAGCGTG
CGGGACTGGACTGGTCCAAGTTCACCATCACCAACAACAGCTGCCCACCTCACCCGCCCAAGGCA
GCCCTGCCCGAGAAGCTGCGGGTGGCTGCGGTGCGCCGTACTGCCCAGGCTGAATATGAGCTTGA
GAACGATCTGCGCTCCTTTGGCCGAGGCTTCACCGTGCTAGAGAAGGATCTGTCAAATAAGCTGC
GCCGCACTGAGAACACGATTGTGGAGGACATCAAGGCTGTGGGGCAGGTCGAAAAGAAGCTGGA
GCAGACGGCGGGCAAGGCAGAGAAGCTCATTGAGAAGGAGGTAGAAGAGGTGGAGGCAGCTGC
GGCCCGCATGATTCGGCGCTTTGAGGCAGAGGCAAAGATGGGACCCTGGATCAACTGGATTCCC
AAGAGCTGGCGGCCAGTCATCATGCCCATGGATTGA

Figure S1. Determination of VDE protein accumulation in low light and high light grown cells.

The amount of VDE was evaluated by immunoblotting reactions. Protein level was normalized to chlorophylls and PSAa amount Panel A-B: Amount of VDE expressed as ratio between µg of Chls or PSAa amount. Panel C: immunoblotting reactions with the indication of the µg of chlorophylls (Chls) loaded in each lane.

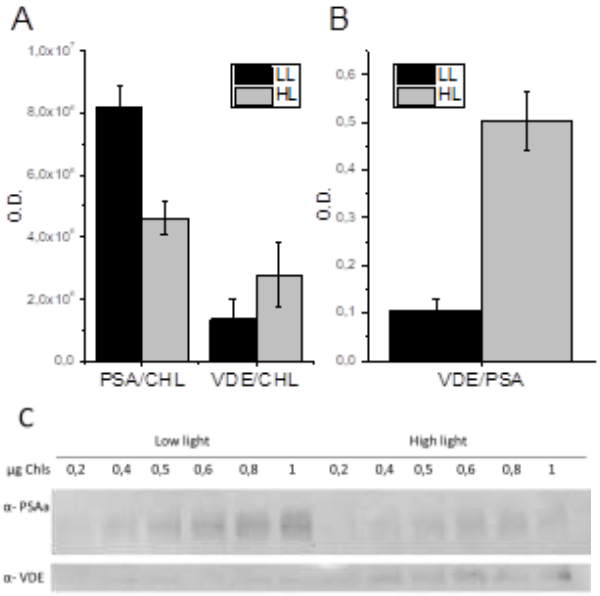

Figure S2. Phylogenetic tree obtained with the protein sequences aligned in Figure.2.

The units of branch length are residues substitution per site divided by the length of the sequence.

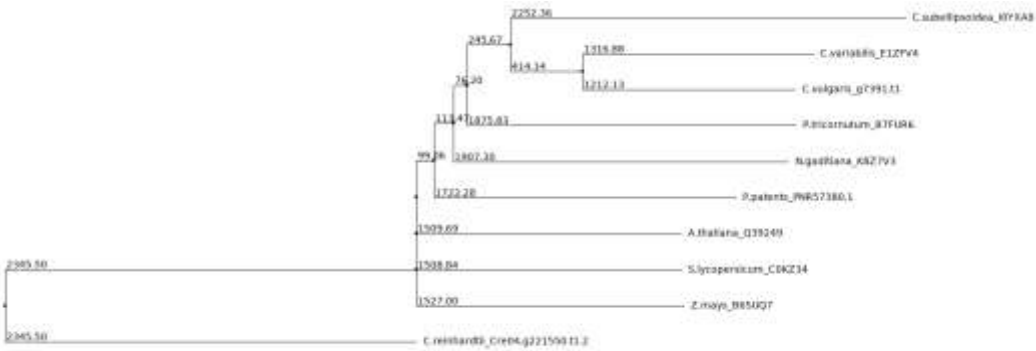

Figure S3. HPLC analysis of cells grown in low and high light adapted at dark for 30 minutes (T0) or treated for 6 minutes with actinic lights (200, 400, 800, 1200, 1800, 2000 and 2500 µmol photons m^{-2} s^{-1}). *A) Chl a/b ratio and B) Chl/Car ratio C) the de-epoxidation index and D) Zea/Car ratio. The increase in Chl a/b and Chl/Car ratios in high light grown cells is consistent with the high light acclimation response observed in higher plants.*

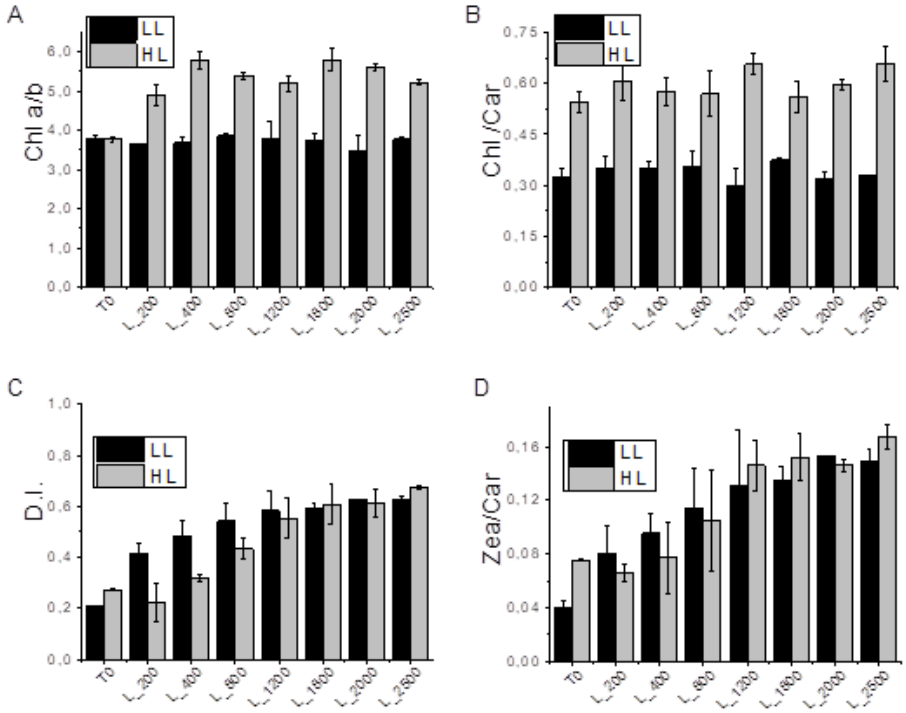

Figure S4. Effect of DTT on NPQ kinetics of Chlamydomonas reinhardtii.

In the graphics A) and B) double cycle of NPQ induction of C. reinhardtii cells acclimated to high light are reported. High light acclimated cells were used for this experiment since in C. reinhardtii high light acclimation is required for NPQ induction. An actinic light of 2000µmol photons m^{-2} s^{-1} and a saturating light of 4000µmol photons m^{-2} s^{-1} was applied for this measurement. Standard deviations are reported as error bars (n=3)

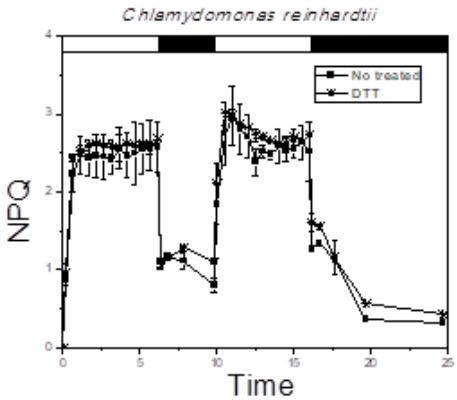

Figure S5. NPQ kinetics of Arabidopsis thaliana in presence or absence of zeaxanthin.

NPQ induction of A. thlaliana WT, npq1 and WT in presence of DTT are reported. npq1 is mutant on vde gene in A. thaliana. An actinic light of 1200µmol photons m^{-2} s^{-1} and a saturating light of 4000µmol photons m^{-2} s^{-1} was applied for this measurement. Standard deviations are reported as error bars (n=3).

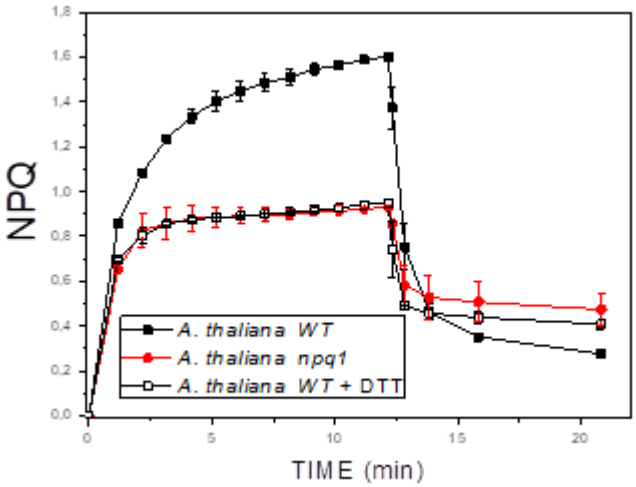

Section C

Photosynthetic response to nitrogen starvation and high light in *Haematococcus pluvialis*[5]

In the green alga *Haematococcus pluvialis* astaxanthin biosynthesis is induced by high irradiances and/or nitrogen starvation. The aim of this work was to investigate their influence on the photosynthetic properties of *H. pluvialis* cultures. The results reported here demonstrate that nitrogen starvation inhibits chlorophyll biosynthesis and favors chlorophyll b degradation, chlororespiration and cyclic electron transport, while cells grown in high light are characterized by a higher destabilization of PSII. The combination of high light and nitrogen deprivation induced the highest astaxanthin production and also the fastest photoprotective response which cooperatively prevented Photosystem II from the damage observed in high light stress and nitrogen supplemented medium. In these conditions inhibition of astaxanthin accumulation leads to a reduced cell size but does not induce a higher photosensitivity of photosynthetic machinery.

In this work I've performed the experiments regarding the photosynthetic characterization.

Abbreviations: PSI, Photosystem I; PSII, Photosystem II; PTOX, Plastid Terminal Oxidase; ROS, Reactive Oxygen Species; DPA, diphenylamine; DMSO, dimethyl sulphoxide; DCMU, 3-(3,4-dichlorophenyl)-1,1-dimethylurea; PG, n-propyl gallate; Chl a, b, chlorophyll a, b; NPQ, non-photochemical quenching; PQ, Plastoquinone, pmf, proton motive force.

[5]This section is based on the published article: Scibilla L, **Girolomoni L**, Berteotti S, Alboresi A, Ballottari M; Photosynthetic response to nitrogen starvation and high light in *Haematococcus pluvialis*, *Algal Research*, Volume 12, November 2015, Pages 170–181.

Introduction

The freshwater green microalga *Haematococcus pluvialis* is well known for its ability to synthetize and store a large amount of the carotenoid astaxanthin under stress conditions (Boussiba, 2000; Aflalo *et al.*, 2007; Lemoine and Schoefs, 2010). Astaxanthin is a high value carotenoid used in aquaculture and poultry farming as pigmentation agent (Lorenz and Cysewski, 2000; Higuera-Ciapara *et al.*, 2006). Furthermore, due to its strong antioxidant properties, natural astaxanthin is used in nutraceutical and pharmaceutical application to prevent free-radical associated diseases (Guerin *et al.*, 2003; Yuan *et al.*, 2011; Ambati *et al.*, 2014). In the last decade *H. pluvialis* has become the main commercial source of natural astaxanthin, and much research has been done to determine best conditions for growth and carotenoid accumulation (Aflalo *et al.*, 2007; Li *et al.*, 2011; Zhang *et al.*, 2014; Wan *et al.*, 2014*a*,*b*). Astaxanthin biosynthesis occurs at the level of the endoplasmic reticulum using a precursor produced in the chloroplast then exported to the cytosol (Collins *et al.*, 2011; Chen *et al.*, 2015). Astaxanthin production in *H. pluvialis* is also accompanied by esterification of this molecule with fatty acids (Chen *et al.*, 2015). It has been demonstrated that *H. pluvialis* synthetizes and accumulates astaxanthin when exposed to various environmental stresses, such as high light (Kobayashi *et al.*, 1992), nutrient deprivation (Kobayashi *et al.*, 1992; Boussiba *et al.*, 1999; Aflalo *et al.*, 2007), high salinity (Harker and Young, 1995) or high temperature (Tjahjono *et al.*, 1994; Giannelli *et al.*, 2015), and that astaxanthin biosynthesis has multiple roles protecting cells against oxidative stress (Li *et al.*, 2008) even though the photoprotective role of this carotenoid in *H. pluvialis* is still under debate (Fan *et al.*, 1998; Wang *et al.*, 2003). While *H. pluvialis* carotenogenesis has been widely investigated (Boussiba, 2000; Li *et al.*, 2010; Gao *et al.*, 2013; Recht *et al.*, 2014; Chen *et al.*, 2015; Choi *et al.*, 2015) less research has been conducted on the photosynthetic processes occurring in this species, and apparently conflicting results are present in literature: some authors reported an increase of photosynthetic activity during astaxanthin accumulation while others reported a decline (Zlotnik (Shmerler) *et al.*, 1993; Tan *et al.*, 1995; Qiu and Li, 2006; Wang *et al.*, 2014; Gu *et al.*, 2014) or no significant variations (Gu *et al.*, 2013). These contrasting results mainly derive from the misleading direct relationship between the photosynthetic data obtained and astaxanthin accumulation, without considering the type of stress at which cells were exposed. The

condition for astaxanthin production as high light stress (Boussiba *et al.*, 1999; Wang *et al.*, 2003, 2014; Qiu and Li, 2006; Gu *et al.*, 2014) nitrogen starvation (Zlotnik (Shmerler) *et al.*, 1993), culture aging (Chen *et al.*, 2012; Gu *et al.*, 2013), high light combined with nitrogen (Hagen *et al.*, 2000; Recht *et al.*, 2014) or phosphorus (Tan *et al.*, 1995) starvation indeed have strong and different impacts on photosynthesis: interpreting photosynthetic results as a direct consequence of the kind of stress used, and considering astaxanthin accumulation only as an additional effect caused by stressing could clarify contrasting results present in literature.

Light energy conversion into biomass occurs in the chloroplast of eukaryotic photosynthetic organisms, where pigment binding protein complexes called Photosystems I and II (PSI and PSII) absorb light and use the excitation energy to transfer electrons from water to $NADP^+$ forming NADPH: this process is coupled with proton translocation into the lumen, forming a proton transmembrane gradient which is used to produce ATP by ATP synthase. ATP and NADPH are then used to fix inorganic CO_2. PSI and PSII activities are strongly influenced by the light intensity available and by the metabolic state of the cell, since the formation and consumption of ATP and NADPH is linked with light energy conversion and cell metabolic demands. In addition, the chloroplastic light dependent electron transport chain can be perturbed by reducing power exchange with the mitochondria or by the onset of alternative electron flow pathways within the chloroplast such as cyclic electron transport or chlororespiration (Xue *et al.*, 1996; Cardol *et al.*, 2009). In particular during cyclic electron transport across PSI electrons transported by PSI are recycled in order to pump protons in the lumen to sustain ATP production, while during chlororespiration plastoquinones pool is oxidized by a Plastid Terminal Oxidase (PTOX) enzyme (Arnon *et al.*, 1981; Bennoun, 1982; Garab *et al.*, 1989). PTOX activity has been previously reported to prevent electron transport chain saturation (Niyogi, 2000), but at same time its activity has been reported to be crucial for carotenogenesis, being involved with redox reaction of phytoene desaturase and/or ζ-carotene desaturase (Shahbazi *et al.*, 2007; Li *et al.*, 2010). The presence of two genes *PTOX1* and *PTOX2* coding for a plastid terminal oxidase have been reported in the genome of *H. pluvialis* (Li *et al.*, 2008) and the dependence of carotenogenesis on PTOX activity has been proposed (Li *et al.*, 2008, 2010; Wang *et al.*, 2009). Investigation of PTOX activity modulating photosynthetic performance is thus essential in order to elucidate *H. pluvialis* photosynthetic response to different stress

condition. In this work astaxanthin accumulation was induced in *H. pluvialis* cells, using nitrogen starvation and high light as single or combined stressors in order to elucidate the stress specific photosynthetic responses. In addition, the astaxanthin specific role(s) during stress exposure was investigated by the addition of diphenylamine, an astaxanthin synthesis inhibitor (Harker and Young, 1995).

Materials and methods

Strain and culture conditions

Haematococcus pluvialis strain K-0084 was obtained from Scandinavian Culture Collection of Algae & Protozoa. Stock cultures were maintained at 10 µmol photons m^{-2} s^{-1} on agarized BG-11 medium (Rippka *et al.*, 1979) with 1 g L^{-1} of Na-acetate at 22 °C. Liquid cultures were grown photoautotrophically at 40 µmol photons m^{-2} s^{-1} on BG-11 medium at 22 °C in homemade 50 mL photobioreactors. Culture mixing was provided by bubbling filtered (0,2 µm) air. Different stressing conditions were applied to cell cultures in their exponential phase (approximately 5×10^5 cells ml^{-1}). Cells were harvested by centrifugation, washed twice with sterile water and suspended in BG-11 medium either supplemented or not by nitrogen at a cell density of $1\cdot10^5$ cells ml^{-1}. The cultures were exposed for 10 days to a 16:8 hours light:dark cycle at 40 (control light) and 400 (high light) µmol photons m^{-2} s^{-1}, in order to obtain four different conditions of cultivation: control light with nitrogen (CL), control light without nitrogen (CL-N), high light with nitrogen (HL) and high light without nitrogen (HL-N). 17.65 mM of sodium nitrate was used as nitrogen source. When specified, astaxanthin synthesis inhibitor diphenylamine (DPA) was added at the final concentration of 120 µM (Harker and Young, 1995). Each experiment was repeated at least in two independent treatments with three biological replicates for each sample.

Cell concentration and pigment analysis

Cell concentrations (cells mL^{-1}) were determined using a Neubauer improved counting chamber under a light microscope. For pigment extraction, 750 µL of culture were centrifuged and cell pellets were treated by dimethyl sulphoxide (DMSO) preheated at 70 °C for 10 min (Zhekisheva *et al.*, 2002). The extraction was repeated until the pellet was colorless. DMSO extracts were diluted in acetone and water, in order to obtain a

final mixture of acetone:water:DMSO 80:15:5 v/v. Chlorophyll and carotenoid content was determined by HPLC analysis (Ferrante *et al.*, 2012).

PSII quantum yield and Non-Photochemical Quenching

For each sample 200 µL of culture were transferred in a 96 well culture plate and cells were dark-adapted for at least 30 minutes at room temperature. Chlorophyll a fluorescence was measured by imaging with a closed fluorometer, FluorCam FC 800MF (Photon Systems Instruments, Czech Republic) with a saturating red light at 4500 µmol photons m^{-2} s^{-1} and an actinic red light at 550 µmol photons m^{-2} s^{-1}. Actinic light was applied for 10 minutes, followed by 10 minutes of dark recovery. PSII quantum yield (*Fv/Fm*) and Non-Photochemical Quenching (*NPQ*) were calculated, respectively, as $(Fm-F_0)/F_0$ and $(Fm-Fm')/Fm'$ (Bilger and Björkman, 1990).

Photosynthetic O_2 evolution and consumption

O_2 consumption and evolution were measured respectively in dark and at different red actinic light intensities (25, 70, 140, 286, 560, 1200 µmol photons m^{-2} s^{-1}) in a Clark-type oxygen electrode (Hansatech) on whole cells at 25 °C under vigorous stirring. Cells were concentrated with a low-speed centrifugation (1000 rpm for one minute) at $5 \cdot 10^5$ cell·ml^{-1} and resuspended in fresh medium. For cyclic electron transport activation analysis a group of samples, was treated by 2 mM n-propyl gallate (PG) by adding it before O_2 evolution measurements to inhibit PTOX enzymatic activity (Josse *et al.*, 2000).

PSII antenna size

PSII functional antenna size was estimated following the kinetics of PSII fluorescence emission of cells treated with 10 µM 3-(3,4-dichlorophenyl)-1,1-dimethylurea (DCMU) considering that PSII antenna size is inversely proportional to the time required for reaching 2⁄3 of the maximum fluorescence emission (de Bianchi *et al.*, 2008).

SDS-PAGE analysis and immunoblot

Total protein extracts were obtained as described in (Steinbrenner and Sandmann, 2006). Total protein concentration was measured by bicinchoninic acid (BCA) assay. SDS-

PAGE and immunoblots against LHCII were performed as previously reported (Bonente *et al.*, 2012).

P700 activity

PSI reaction center activity was monitored as transient decrease of 705 nm absorption as previously described using a JTS 10-LED pump-probe spectrometer (Bio-Logic SAS, Claix, France) (Bonente *et al.*, 2012).

Electrochromic shift

The extent of the light-driven proton fluxes across thylakoid membranes was determined by measurements of the electrochromic shift (ECS) at a wavelength of 520 nm as previously described (Bailleul *et al.*, 2010). In particular samples were measured using a JTS 10-LED pump-probe spectrometer (Bio-Logic SAS, Claix, France) in the presence of 15% Ficoll, in order to prevent cell sedimentation during the measurement. The sample was adapted to a light intensity of 35 µmol photons m^{-2} s^{-1} for 8 min before the measurement. After the adaptation, the sample was measured at a light intensity of 940 µmol photons m^{-2} s^{-1} for 20 s, followed by a 60 s dark adaptation.

Fluorescence curve for PTOX effect analysis

PTOX activity was monitored following the kinetic of fluorescence emission of cells either in the presence or absence of 2 mM n-propylgallate during the exposure to the following protocol of illumination: 1 min of dark, 5 min of actinic light, 5 min of dark and 1 min of far red light. Actinic light was set at the same intensity used for cell growth (Joet *et al.*, 2002).

Results

Effects of high irradiance and nitrogen starvation on growth

To assess the effects of high light and nitrogen starvation on *Haematococcus pluvialis* growth, cells at early exponential phase were exposed to two different light intensities: 40 µmol photons m^{-1} s^{-1} either with nitrogen (CL) or in nitrogen deficiency (CL-N), or to a light intensity of 400 µmol photons m^{-1} s^{-1} again with nitrogen (HL) or in nitrogen deficiency (HL-N). Preliminary experiments demonstrated that the latter was the

condition with the highest astaxanthin accumulation in agreement with previous results (Aflalo *et al.*, 2007), therefore an additional condition was investigated adding diphenylamine (DPA), an inhibitor of astaxanthin biosynthesis, to HL-N cells (HL-N+DPA). Five different cultivation conditions were thus investigated: CL, CL-N, HL, HL-N, HL-N+DPA. Cell concentration was monitored for 10 days as reported in Figure 1A.

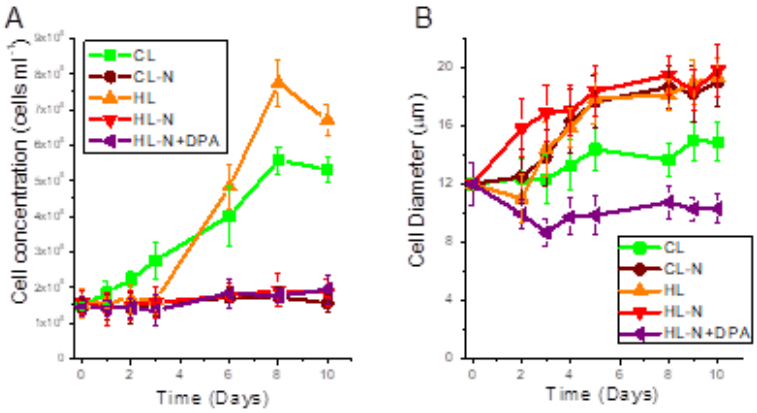

Figure 1. *Growth curve and cell diameter of Haematococcus pluvialis exposed to different light intensities and nitrogen content. (A) Growth curves of H. pluvialis exposed to control light (40 µmol photons m^{-1} s^{-1}) with (CL, green) and without (CL-N, brown) nitrogen and high light (400 µmol photons m^{-1} s^{-1}) with (HL, orange) and without nitrogen in presence (HL-N+DPA, purple) or absence (HL-N, red) of diphenylamine. (B) Variation of cell diameter during growth. Reported data are the average of six biological replicates, standard deviations are indicated.*

In CL, cell concentration continuously increased and achieved the maximum cell density ($5.58 \cdot 10^5$ cells·ml^{-1}) eight days after the inoculum while in HL cell density started to increase only after three days of adaptation to the new stress conditions of excessive irradiation. In HL and CL, the highest cell concentration was achieved after eight days of cultivation, with HL cells being more concentrated than CL cells. As expected, in nitrogen deficiency (CL-N, HL-N and HL-N+DPA) cell division was blocked likely due to inhibition of cell replication by the lack of nutrients: this is a common feature already observed in several algae species (Borowitzka *et al.*, 1991; Berges *et al.*, 1996; Hockin *et al.*, 2012; Cakmak *et al.*, 2012; Dong *et al.*, 2013). Cell diameter variations upon exposure to the different growth conditions are reported in Figure 1B. As previously reported (Kakizono *et al.*, 1992; Kobayashi *et al.*, 2001; Wang *et al.*, 2004) cell diameter strongly increased from 12 µm to almost 20 µm in samples exposed to nitrogen

deprivation, while smaller cell diameter (14 µm) was observed in CL cells at the end of the experiment. Differently in the first three days a decrease of cell diameter to 10 µm was evident in HL-N+DPA (Figure 1; Supplementary data, Figure S1).

Effects of high irradiance and nitrogen starvation on chlorophyll content

Chlorophyll content on a volumetric (µg chl ml^{-1}) or cellular base (pg chl $cell^{-1}$) and Chl a/b ratio were analyzed daily to verify high light and nitrogen starvation effects on chlorophyll synthesis and modulation. CL and HL growth conditions were the only cases in which chlorophyll content increased on a volumetric base (Figure 2).

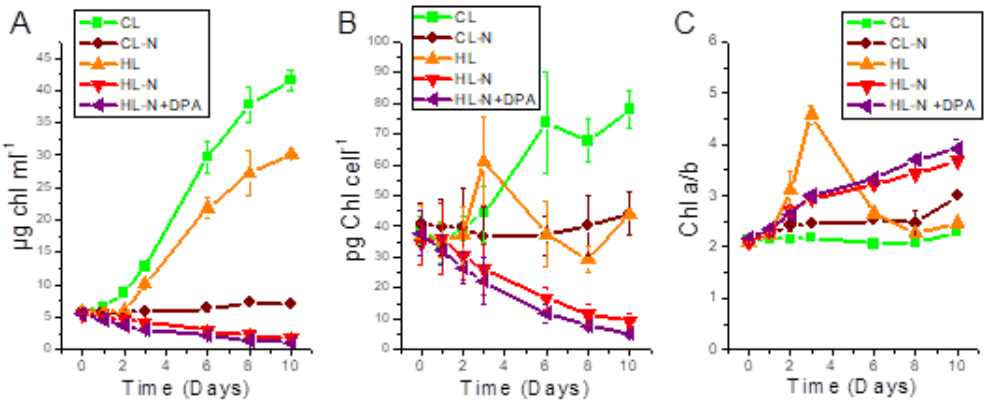

Figure 2. *Changes in chlorophyll content during exposure at different stress conditions. (A) Volumetric chlorophyll content expressed as µg chl per ml of culture. (B) Cellular chlorophyll content expressed as pg chl per cell. (C) Chlorophyll a/b ratio. Green squares: cells in control light (40 µmol photons m^{-1} s^{-1}) with nitrogen, CL; brown circles: cells in control light without nitrogen, CL-N; orange triangles: cells grown in high light (400 µmol photons m^{-1} s^{-1}) with nitrogen, HL; red triangles: cells grown in high light without nitrogen, HL-N; purple triangles: cells grown in high light without nitrogen in presence of diphenylamine; HL-N+DPA. Reported data are the average of six biological replicates, standard deviations are indicated.*

In CL, chlorophyll content per cell increased from 37.60 to 78.06 pg chl·$cell^{-1}$ (Figure 2A) while Chl a/b ratio remained stable at ~2.15 (Figure 2C). Conversely in HL both chlorophyll content per cell and Chl a/b ratio transiently increased in the first three days of stress exposure, returning then to values similar to the starting ones (29.14 pg chl·$cell^{-1}$ and 2.4 respectively). Interestingly after two days of exposure to HL, a transient increase of chlorophyll content per cell was observed, likely due to a dephasing of cell duplication and chlorophyll biosynthesis. As expected only in presence of nitrogen there was a net chlorophyll synthesis (Figure 2B): when nitrate was not added to the cultures,

the volumetric chlorophyll content remained stable in CL-N and decreased in HL-N from 37.60 to 5.06 pg chl·cell^{-1}. In both cases increased Chl a/b ratio could be observed, more evident in HL-N (from 2.15 to 3.70 in HL-N and 2.16 to 2.99 in CL-N): in these conditions increase Chl a/b ratio was due to a preferential degradation of chlorophyll b during stress exposure, even if chlorophyll a was also degraded. The presence of DPA did not significantly change either the chlorophyll per cell content or the Chl a/b ratios compared to HL-N cells (Figure 2).

Effects of high irradiance and nitrogen starvation on carotenoid content

Daily content changes on the carotenoids content throughout cultivation period are reported in Figure 3.

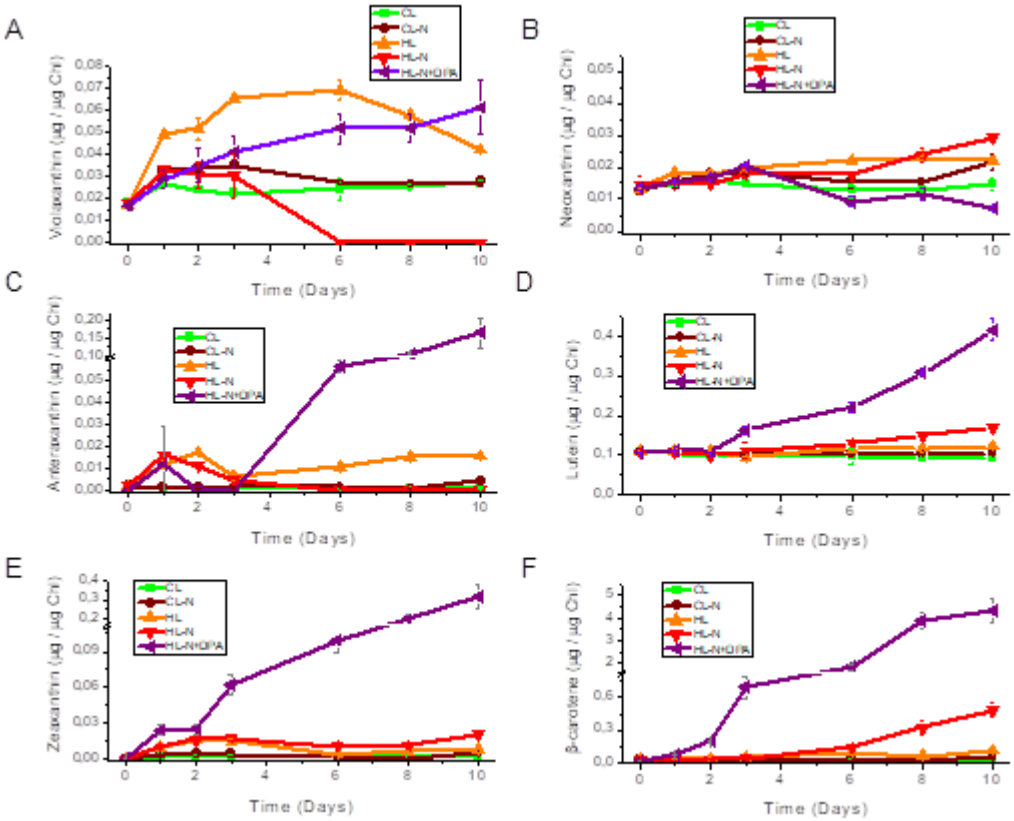

Figure 3. *Changes in carotenoid contents during stress exposure. Carotenoids were extracted with DMSO, and the extraction was repeated until obtain a colorless pellet. Carotenoids content was analyzed by HPLC, and expressed on per chlorophyll basis. (A) Violaxanthin (B) Anteraxanthin (C) Zeaxanthin (D) Neoxanthin (E) Lutein (F) β-carotene. Green squares: cells in control light (40 µmol photons m^{-1} s^{-1}) with nitrogen, CL; brown circles: cells in control light without nitrogen, CL-N; orange triangles: cells grown in high light (400*

µmol photons m^{-1} s^{-1}) with nitrogen, HL; red triangles: cells grown in high light without nitrogen, HL-N; purple triangles: cells grown in high light without nitrogen in presence of diphenylamine; HL-N+DPA. Reported data are the average of six biological replicates, standard deviations are indicated.

In control light the content of major carotenoids remains stable for all the time points of the kinetic. During the first 3 days in HL and HL-N, a rapid accumulation of de-epoxidized xanthophylls as anteraxanthin and zeaxanthin was observed due to the activation of the xanthophyll cycle. In HL and HL-N xanthophyll cycle activation followed a biphasic kinetic, with a later additional increase of de-epoxidated carotenoids upon acclimation. Interestingly while zeaxanthin resulted to be the main de-epoxidated carotenoid in HL-N cells, HL conditions lead to preferential anteraxanthin accumulation. Similarly to zeaxanthin, also lutein, neoxanthin and β-carotene content increased in HL-N condition suggesting a general accumulation of carotenoid in response to excess light. As shown in Figure 4, in all stress conditions (CL-N, HL, HL-N) astaxanthin accumulation was induced and the most effective condition for astaxanthin production was HL-N with 306.63 µg·ml^{-1}, compared to 200.53 µg·ml^{-1} in HL and 97.08 µg·ml^{-1} in CL-N.

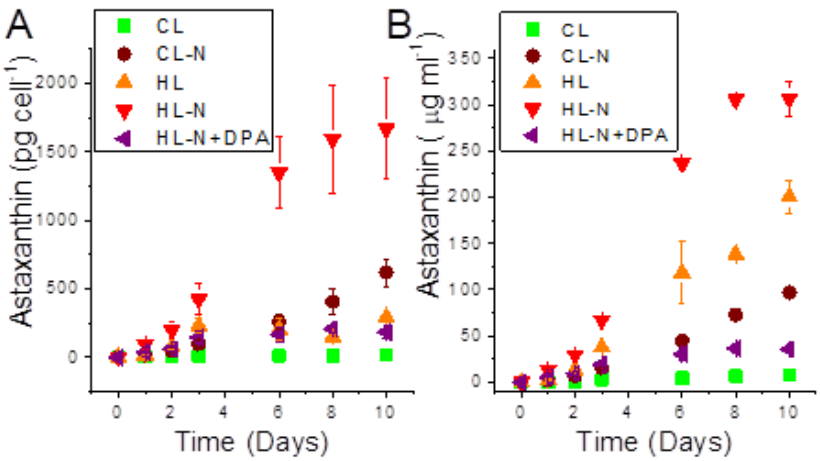

Figure 4. *Kinetics of astaxanthin accumulation during stress exposure. Astaxanthin was extracted with DMSO, and the extraction was repeated until obtain a colorless pellet. Content was analyzed By HPLC. (A) Cellular astaxanthin content, as pg of astaxanthin per cell. (B Volumetric astaxanthin content, as mg of astaxanthin per ml of culture). Green squares: cells in control light (40 µmol photons m^{-1} s^{-1}) with nitrogen, CL; brown circles: cells in control light without nitrogen, CL-N; orange triangles: cells grown in high light (400 µmol photons m^{-1} s^{-1}) with nitrogen, HL; red triangles: cells grown in high light without nitrogen, HL-N; purple triangles: cells grown in high light without nitrogen in presence of diphenylamine; HL-N+DPA. Reported data are the average of six biological replicates, standard deviations are indicated.*

As previously reported (Harker and Young, 1995) addition of DPA to HL-N cells resulted into a significant inhibition of astaxanthin of about ten times compared to HL-N. At the same time in HL-N+DPA the strong accumulation of other carotenoids as β-carotene, lutein and zeaxanthin was observed indicating that DPA treatment affected specifically astaxanthin biosynthesis.

Effects of high irradiance and nitrogen starvation on PSII quantum yield, Non Photochemical Quenching and PSII photosensitivity

PSII quantum yield (Fv/Fm) and non-photochemical quenching (NPQ) were analyzed in the different growth conditions to evaluate changes in the performance of the photosynthetic apparatus (Figure 5A).

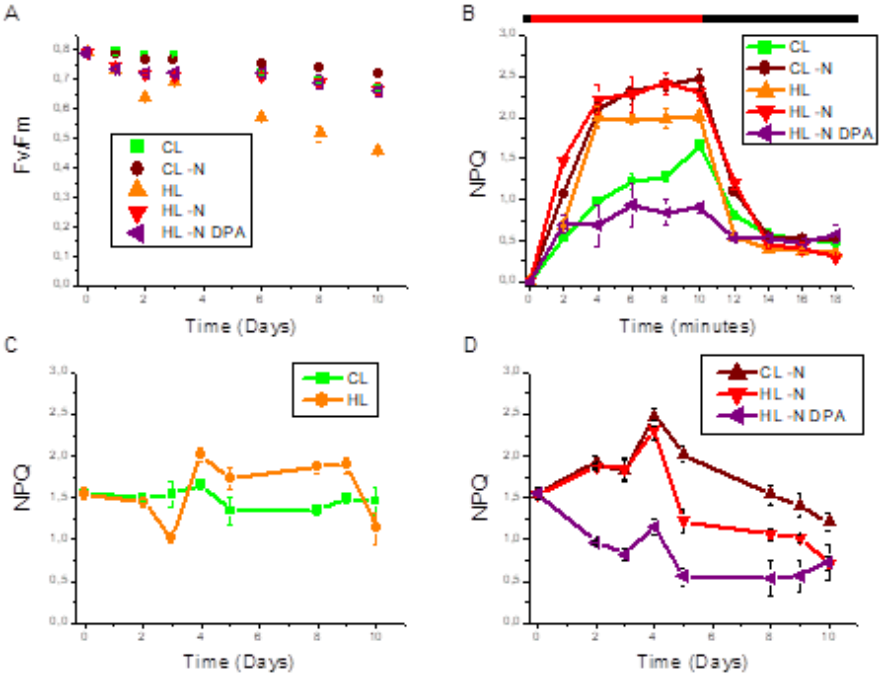

Figure 5. *Variation of photosynthetic efficiency and non photochemical quenching during stress exposure.* ***(A)*** *Photosynthetic efficiency measured as PSII quantum yield (Fv/Fm) in dark-adapted cells.* ***(B)*** *Non Photochemical Quenching (NPQ) kinetics measured on cells grown for 4 days at the different stressing conditions. (C, D) NPQ maximum value measured at the different days of growth. Green squares: cells in control light (40 µmol photons m^{-1} s^{-1}) with nitrogen, CL; brown circles: cells in control light without nitrogen, CL-N; orange triangles: cells grown in high light (400 µmol photons m^{-1} s^{-1}) with nitrogen, HL; red triangles: cells grown in high light without nitrogen, HL-N; purple triangles: cells grown in high light without nitrogen*

in presence of diphenylamine; HL-N+DPA. Reported data are the average of six biological replicates, standard deviations are indicated.

Fv/Fm generally decreased from the initial value of 0.8 to 0.66 with two exceptions: CL-N cells, where the Fv/Fm remained above 0.72, and HL cells in which Fv/Fm decreased to 0.42. No significant differences were evident comparing HL-N and HL-N+DPA cells. NPQ induced in the different growth conditions is reported in Figure 5B-D. In all the different growth conditions *H. pluvialis* showed a significant light dependent NPQ induction (Figure 5B). NPQ maximum values were quite stable at around 1.5 in CL cells, while upon stress exposure more variable maximum NPQ values were measured (Figure 5C-D). In HL NPQ in the first days drops from 1.5 to 1 and then rises in one day until 2 remaining quite stable until day 10 when it drops again to ~1. In CL-N and HL-N cells NPQ immediately increases reaching after four days the maximum value of ~2.4 followed by a decrease to 1.2 and 0.7 respectively. These results indicate that in HL the photosynthetic apparatus is strongly perturbed and three days are necessary in order to properly activate the photoprotective NPQ response, while depletion of nitrogen in HL-N and CL-N accelerate the activation of photoprotective mechanism in the first days of stress exposure. Interestingly HL-N+DPA cells showed decreased of NPQ to 0.5 which remained quite stable until the end of the experiment. This result suggests that the accumulation of carotenoid in the chloroplast in HL-N+DPA cells (Figure 4) reduces the capacity of NPQ induction. The effect of adaptation to the different growth conditions on the photostability of PSII was then investigating exposing the cells at the sixth day of growth to strong white light (2000 µmol photons $m^{-2}s^{-}1$) following the decay of Fv/Fm (Figure 6). As reported in Figure 6A, cells grown in CL were the most susceptible to PSII damage and loss of Fv/Fm, followed by HL cells. Cells grown in nitrogen starvation were instead the conditions with the lower photosensitivity, with the best photoprotection appearing in HL-N and HL-N+DPA. In order to evaluate if these different photoprotective behavior was influenced by astaxanthin or carotenoid direct absorption of the blue region of the white light spectrum used for, we repeated the experiments using a red light (1000 µmol photons $m^{-2}s^{-1}$). The results reported in Figure 6B demonstrate that the lower photosensitivity of HL-N and HL-N+DPA is maintained, while little differences are noticeable among CL, HL and CL-N. This result

demonstrates that overall carotenoid accumulation rather than specific astaxanthin biosynthesis is necessary to increase PSII photoprotection.

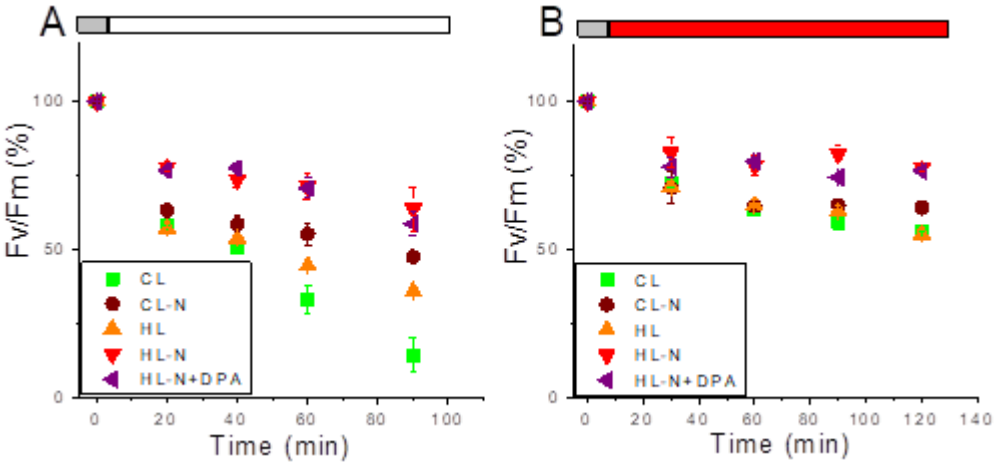

Figure 6. *Photosystem II photoinhibition. Photosystem II photoinhibition was measured following the decrease of Fv/Fm upon exposure to white light (2000 µmol $m^{-2}s^{-1}$, A) or red light (1000 µmol $m^{-2}s^{-1}$, B). Green squares: cells in control light (40 µmol photons m^{-1} s^{-1}) with nitrogen, CL; brown circles: cells in control light without nitrogen, CL-N; orange triangles: cells grown in high light (400 µmol photons m^{-1} s^{-1}) with nitrogen, HL; red triangles: cells grown in high light without nitrogen, HL-N; purple triangles: cells grown in high light without nitrogen in presence of diphenylamine; HL-N+DPA. Reported data are the average of six biological replicates, error bars are indicated.*

Effects of high irradiance and nitrogen starvation on PSII functional antenna size

PSII functional antenna size was measured after eight days of cultivation in order to establish the influence of growth conditions on PSII-LHCII supercomplexes assembly and light harvesting efficiency. PSII functional antenna size were determined by measuring the kinetics of fluorescence emission of PSII in dark-adapted cells treated with DCMU (Figure 7): in limiting light conditions the rate of fluorescence induction is inversely proportional to the functional antenna size of PSII. Figure 7 shows the kinetics of fluorescence emission (A) and the estimated PSII functional antenna size (B). In HL without nitrogen the antenna size of PSII was reduced by half compared to the other conditions, in agreement with the increase of Chl a/b ratio observed in these conditions. This effect was not influenced by DPA addition suggesting that astaxanthin synthesis is not directly responsible of the reduction in PSII functional antenna size observed in HL-N.

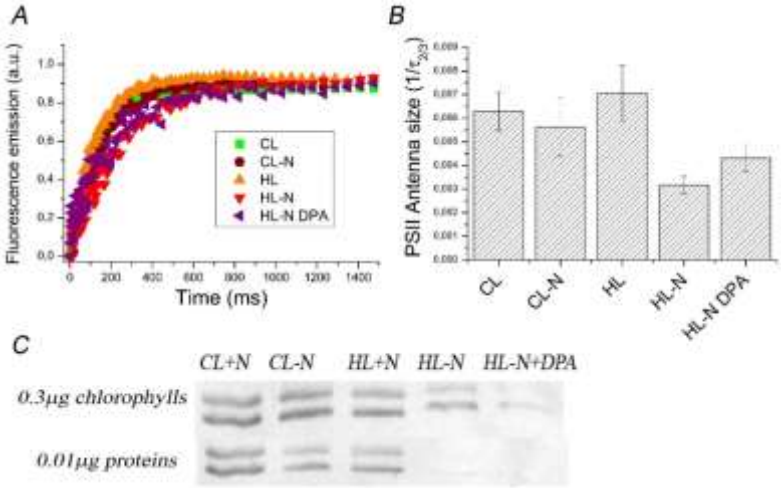

Figure 7. *PSII functional antenna size and LHCII immunoblot. (A) Fluorescence emission kinetics of photosystem II of cell dark-adapted and treated with DCMU are shown. Green squares: cells in control light (40 µmol photons m^{-1} s^{-1}) with nitrogen, CL; brown circles: cells in control light without nitrogen, CL-N; orange triangles: cells grown in high light (400 µmol photons m^{-1} s^{-1}) with nitrogen, HL; red triangles: cells grown in high light without nitrogen, HL-N; purple triangles: cells grown in high light without nitrogen in presence of diphenylamine; HL-N+DPA. (B) The estimated PSII antenna size is reported as the reciprocal number of the time required for reaching 2/3 of the fluorescence maximum emission. (C) Immunoblots on total protein extracts with specific antibodies for LHCII. Different samples were loaded on SDS-PAGE gel on the base of chlorophyll content or protein content, as indicated. Reported data are the average of six biological replicates, standard deviations are indicated.*

Effects of high irradiance and nitrogen starvation on oxygen consumption and evolution

O_2 consumption and evolution at increasing light intensities were measured in order to assess how photo-oxidative stress affects the photosynthetic activity of *H. pluvialis* cells. O_2 measurements were performed after eight days of cultivation in stressing conditions, when astaxanthin synthesis was already induced in HL-N, HL and CL-N. In order to prevent sunscreen effect by astaxanthin reducing the actual irradiance of the cells, red light (λ>600 nm) was used to measure the light-driven O_2 production in the different growth conditions. As reported in Figure 8A, photosynthetic oxygen production was reduced on a cell basis in CL-N and HL-N compared to CL and HL respectively, with the highest production rate in CL. However on a chlorophyll basis, nitrogen starvation (CL-N and HL-N) promotes an increase of oxygen production rate compared to condition in which nitrogen was supplemented: in particular P_{max} appeared higher in HL-

N and CL-N compared to HL and CL (Figure 8B). Interestingly the block of astaxanthin synthesis by DPA addition resulted in a slight increase of P_{max} compared to HL-N on a chlorophyll basis. Dark respiration rate (Figure 8C) was higher in all stress condition (HL, HL-N, CL-N and HL-N+DPA) compared to CL.

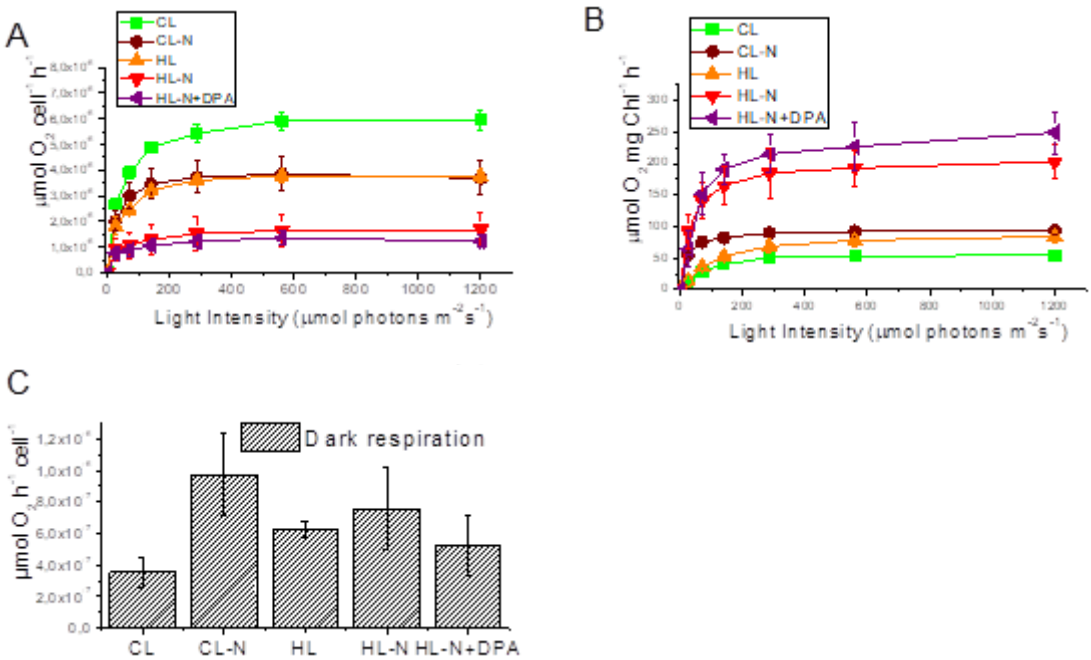

Figure 8. *Oxygen evolution and consumption. O_2 production and consumption were evaluated in cells adapted for 8 days at different stress conditions. (A,B) Light dependent oxygen evolution, on a cell basis (A) or on chlorophyll basis (B) evaluated using red filtered light to avoid astaxanthin sunscreen effects. Green squares: cells in control light (40 µmol photons m^{-1} s^{-1}) with nitrogen, CL; brown circles: cells in control light without nitrogen, CL-N; orange triangles: cells grown in high light (400 µmol photons m^{-1} s^{-1}) with nitrogen, HL; red triangles: cells grown in high light without nitrogen, HL-N; purple triangles: cells grown in high light without nitrogen in presence of diphenylamine; HL-N+DPA. (C) Respiration rate, on cell basis, analyzed in dark adapted cells. Reported data are the average of six biological replicates, standard deviations are indicated.*

Cyclic electron transport activation in stressing conditions

Cyclic electron transport around Photosystem I is an alternative electron transport pathway that has been reported to be induced in different photosynthetic organisms in order to balance ATP and NADPH production, or when linear electron transport from PSII is somehow impaired (Rumeau *et al.*, 2007; Alric, 2010). In order to evaluate the influence of the stressing conditions herein investigated on cyclic electron transport, the

kinetics of PSI reduction in the dark were investigated in DCMU treated cells after illumination with an actinic light of 940 µmol photons $m^{-2}s^{-1}$. In case of cyclic electron transport activation, it has been reported that the first phase of Photosystem I re-reduction in the dark occurs faster. As reported in Figure 9 the kinetics of re-reduction in the dark of PSI after illumination are clearly faster in nitrogen starvation, especially in the case of HL-N and HL-N+DPA. These results suggest that *H. pluvialis* in nitrogen starvation activates cyclic electron transport to a higher extent compared to CL and HL conditions.

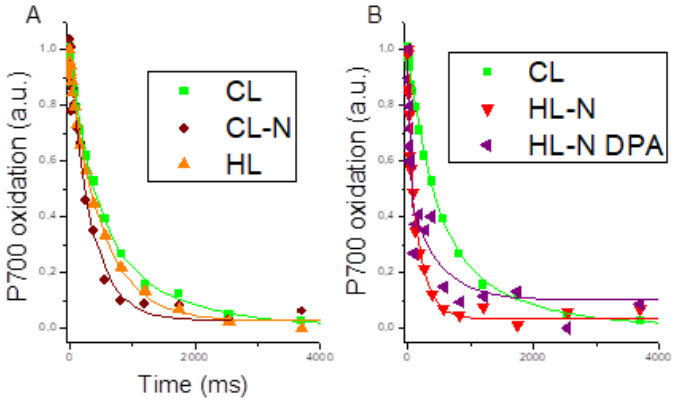

Figure 9. *P700 reduction kinetics in the dark. Dark adapted cells were treated with DCMU and exposed to actinic light (940 µmol photons m-2s-1) for 30 seconds: P700 re-reduction in the dark was followed measuring the difference absorption at 700 nm in the ms time-range. Green squares: cells in control light (40 µmol photons m-1 s-1) with nitrogen, CL; brown circles: cells in control light without nitrogen, CL-N; orange triangles: cells grown in high light (400 µmol photons m-1 s-1) with nitrogen, HL; red triangles: cells grown in high light without nitrogen, HL-N; purple triangles: cells grown in high light without nitrogen in presence of diphenylamine; HL-N+DPA. Experimental values were fitted with exponential decay curves (straight lines). Reported data are the average of six biological replicates, standard deviations are indicated.*

PTOX activity in stressed cells

Astaxanthin synthesis has been associated to activation of plastidial oxidase PTOX (Li *et al.*, 2008, 2010; Wang *et al.*, 2009). PTOX activation is correlated to chlororespiration induction which oxidizes PQ pool and can be measured following the PSII fluorescence kinetics in the seconds range. In order to evaluate the activation of PTOX and chlororespiration in the different growth conditions PSII fluorescence kinetics were measured in presence or absence of the PTOX inhibitor n-propylgallate (PG). Treated and untreated cells were exposed to the following illumination steps: 1 min of dark, 5

min of actinic light at the same irradiance used for cultivation, 5 min of dark and 1 min of far red light. As shown in Figure 10 inhibition of PTOX activity leads to an increase in fluorescence during light treatment in CL+PG and even higher in CL-N+PG compared to CL and CL-N respectively, indicating that plastoquinone pools in presence of PG was in average more reduced.

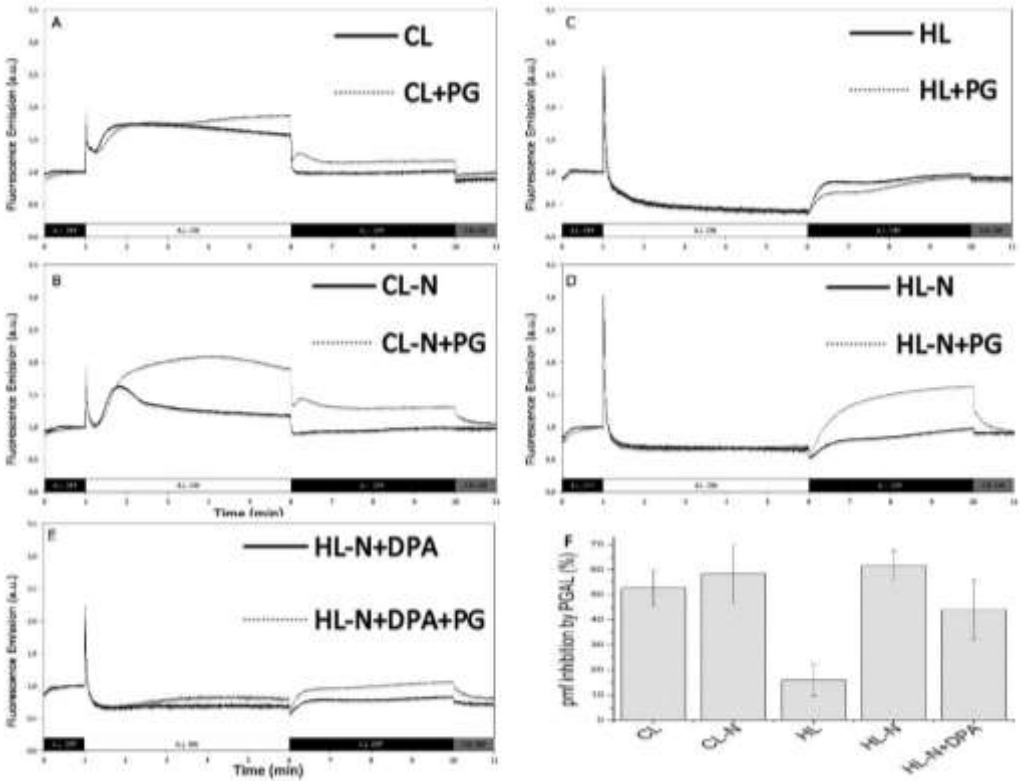

Figure 10. *Evaluation of PTOX activity effects in stressed cells. (A-E) Kinetics of fluorescence emission of cells adapted for 8 days at different stress condition in presence or not of the potx inhibitor n-propylgallate (PG), during the following protocol of illumination: 1min dark, 5 min red filtered actinic light at the cultivation intensity (A-B 40 µmol photons m^{-2} s^{-1}; C-E 400 µmol photons m^{-2} s^{-1}), 5 min dark and 1 min far red light.* ***(F)*** *PTOX inhibition influence on proton motive force. Proton motive force (pmf) was determined by electrochromic shift measurement at 520nm. Data reported were calculated as $(pmf-pmf_{PGAL})/pmf * 100$, where pmf is the total pmf while pmf_{PGAL} is the pmf measured upon addition of propyl gallate to inhibit PTOX. Reported data are the average of six biological replicates, standard deviations are indicated.*

When light was switched off the transient fluorescence rise in the dark was observed in both CL and CL-N when treated with PG: this dark transient florescence rise has been previously reported when PTOX activity was low or absent (Joet *et al.*, 2002). Moreover

the fluorescence signal remained higher in CL-N in the second dark period, indicating again a more reduced state when PTOX was inhibited. Upon far red illumination, CL, CL+PG and CL-N+PG fluorescence signal was significantly reduced, indicating a full oxidation of the plastoquinone pool, while in CL-N the far red illumination has almost no effect, likely due to the PTOX activity in plastoquinones oxidation. These results demonstrate that plastoquinones in CL-N are mainly oxidized by PTOX, which is more active compared to CL, in agreement with the activation of astaxanthin biosynthesis in this condition. In HL, the inhibition of PTOX activity doesn't produce a significant effect, while in HL-N, PG addition leads to an increase in fluorescence during dark period, indicating an important effects of PTOX on relaxing PQ redirecting electrons to carotenogenesis. The inhibition of astaxanthin synthesis with DPA results in a lower increase of fluorescence in the dark, indicating a lower activity of PTOX compared to HL-N. In order to confirm these results, the influence of PTOX activity on lumen acidification *in vivo* was investigated by measuring the light dependent electrochromic shift (ECS) of carotenoid absorption. This method has been reported to be reliable in order to monitor the proton motive force (pmf) induced by light absorption, following the changes in carotenoid absorption induced by thylakoid membrane polarization (Bailleul *et al.*, 2010). In this experiment ECS was measured in cells treated with an actinic light of 940 µmol $m^{-2}s^{-1}$ in presence or absence of PGAL in order to inhibit PTOX activity. PTOX dependent plastoquinones oxidation indeed is expected to increase pmf, increasing proton transport in the lumen. As reported in Figure 10F the addition of PGAL induced a decrease of pmf observed in absence of PGAL in all the samples analyzed, but with a minor effect in HL cells. This result is consistent with a reduced activation of PTOX in HL compared to other conditions.

Discussion

In this study, the effects of nitrogen starvation and high light stress on the photosynthetic properties of *Haematococcus pluvialis* cells were analyzed. The results reported here demonstrate that nitrogen starvation promotes astaxanthin biosynthesis and accumulation in *H. pluvialis* cells exposed to nitrogen starvation both under medium or high irradiance (CL-N and HL-N) (Figure 4) in agreement with previous results (Zlotnik (Shmerler) *et al.*, 1993; Boussiba *et al.*, 1999; Hagen *et al.*, 2000). Nitrogen starvation has been already reported to be a strong stressing condition in microalgae impairing both

chlorophyll and protein biosynthesis: algal cells grown in the absence of nitrogen generally redirect their metabolism accumulating lipids and carotenoids favoring respiration over photosynthesis (Berges *et al.*, 1996; Cakmak *et al.*, 2012; Schmollinger *et al.*, 2014). In the case of *H. pluvialis* it has been recently reported that the combination of nitrogen starvation and high light leads to starch degradation, accumulation of monomeric or oligomeric carbohydrates and fatty acids, and increased activity of the tricarboxylic acid cycle (Boussiba and Vonshak, 1991; Recht *et al.*, 2014). Our results show that nitrogen starvation in *H. pluvialis* inhibits cell division (Figure 1), as previously reported for other microalgal species (Cakmak *et al.*, 2012; Zhu *et al.*, 2014) and somehow change the composition of photosynthetic membranes continuously increasing the Chl a/b ratio in both CL-N and HL-N (Figure 2). This is the result of a combined inhibition of chlorophyll biosynthesis due to nitrogen deprivation and preferential degradation of chlorophyll b, suggesting that antenna proteins of PSII are more destabilized in nitrogen starvation. This is confirmed especially in HL-N, where LHCII accumulation and the PSII functional antenna size are dramatically reduced compared to HL, while in CL-N the reduction is less evident compared to CL (Figure 7). Dark respiration was clearly increased in nitrogen starvation, confirming a redirection of metabolism favoring mitochondrial respiration: photosynthetic oxygen production was indeed reduced on a cell basis, as a consequence of reduction of chlorophyll amount per cell content in HL-N and CL-N compared to HL and CL respectively. However, in nitrogen starvation *H. pluvialis* cells remain photosynthetically active as evidenced by the high PSII quantum yield (Fv/Fm higher than 0.65) observed even after 10 days of stress, and by the increase of maximal oxygen production rate calculated on a chlorophyll basis (Figure 5A; Figure 8B). The latter result is in contrast with what has been observed, in a similar stress condition, by Zlotnik (Shmerler) *et al.* (1993), who reported a reduction of maximal photosynthetic rate. These conflicting results are related to the use of red actinic light in the experiment reported at Figure 8 while in Zlotnik (Shmerler) *et al.* (1993) a white light was used for oxygen evolution measurement, which is partially absorbed by astaxanthin accumulated in the cells, thus reducing the light energy available for photochemistry. In fact the use of red light during oxygen evolution measurement prevents the light screening function of astaxanthin accumulated in starved nitrogen cultures (Wang *et al.*, 2003). The results reported here show an increased Pmax in nitrogen starvation compared to cells grown in the presence of a

nitrogen source (Figure 8B). This increase in Pmax could be related to the reduced chlorophyll per cell content observed in CL-N and HL-N compared to CL and HL: insertion mutants obtained in *Chlamydomonas reinhardtii* and *Chlorella sorokiniana* with a reduced Chl/cell ratio indeed have been reported to increase their Pmax compared to the respective WT strains (Formighieri *et al.*, 2013; Cazzaniga *et al.*, 2014). Non photochemical quenching is also affected by nitrogen starvation; in particular NPQ is significantly higher in CL-N and HL-N at the beginning of the stress treatment, when the accumulation of astaxanthin becomes relevant, even if at the end of treatment the NPQ level is similar.

High light treatment by itself is reported in the literature as one of the most effective stressor inducing astaxanthin accumulation in *Haematococcus pluvialis* cells (Wang *et al.*, 2003; Qiu and Li, 2006; Li *et al.*, 2010). Indeed as reported in Figure 4 cells grown in HL and HL-N accumulated much more astaxanthin compared to cells grown in other growth conditions on a volume basis, with the highest astaxanthin production in HL-N. The high volumetric production of astaxanthin however is mainly dependent on the higher cell density in HL compared to HL-N and CL-N: on a cell basis indeed HL-N is the condition with the highest astaxanthin production followed by CL-N. Xanthophyll cycle is also rapidly activated when *H. pluvialis* cells were exposed to high light (HL and HL-N) as indicated by the increase of anteraxanthin and zeaxanthin in the first two days of stress exposure (Figure 3B,C) as generally reported for microalgae (Torzillo *et al.*, 2005; Qiu and Li, 2006; Bonente *et al.*, 2012; La Rocca *et al.*, 2014) and for *H. pluvialis* specifically (Gu *et al.*, 2014). Anyway, differently form the work of Gu and coworkers, we exposed cells to high light for more than 48 hours, observing a peculiar biphasic modulation of the xanthophyll cycle in HL and HL-N, with a later further increase of de-epoxidated carotenoid after the rapid activation in the first two days. Zeaxanthin accumulation is a strong photoprotective mechanism in photosynthetic organisms (Havaux and Niyogi, 1999; Dall'Osto *et al.*, 2012; Pinnola *et al.*, 2013) and its rapid accumulation in HL and HL-N suggests that this carotenoid has a photoprotective role also in *H. pluvialis.* Interestingly anteraxanthin and zeaxanthin are respectively the main de-epoxidated xanthophyll in HL and HL-N respectively, suggesting that only in HL-N the activation of photoprotective mechanisms is complete. It should also be considered that zeaxanthin is one of the precursors of astaxanthin biosynthesis, linking its accumulation in HL-N with astaxanthin accumulation. Cells

exposed at 400 µmol photons m^{-1} s^{-1} (HL) need three days of adaptation before re-starting cellular division. In these three days NPQ dramatically declines and Chl a/b ratio transiently increases, while in the following days cells seem to be adapted: NPQ and Chl a/b ratio return to ~2 and ~2.65. The transient increase in Chl a/b ratio indicated that chlorophyll b binding antenna proteins are an early target of photoinhibition in HL, while photosystem core complexes are more stable or somehow regenerated through D1 protein repair cycle. PSII antenna proteins are also the most likely site of NPQ in *H. pluvialis*, as recently demonstrated for *Chlamydomonas reinhardtii* in the case of LHCSR3 and LHCBM1 subunits (Elrad, 2002; Peers *et al.*, 2009; Bonente *et al.*, 2011). Wang and coworkers reported that upon exposure to high irradiances D1 protein repair cycle is rapidly induced until the amount of astaxanthin accumulated is sufficient to shield the light directed to photosystems (Wang *et al.*, 2003). Moreover a rapid degradation of PSII core subunits has been recently reported upon exposure to HL stress of motile cells, but not in the case of palmella cells (Wang *et al.*, 2014). The data reported in Figure 3 and Figure 5 are in accordance with these results, indeed the PSII quantum yield declines in HL of 20% in the first two days, while in the case of HL-N, where astaxanthin is more rapidly accumulated, Fv/Fm remains stable. Moreover HL-N cell showed a constant increase of Chl a/b ratio and the rapid increase in NPQ induction. The higher destabilization of PSII in HL compared to HL-N, which was expected to be as the most stressing growth condition, is confirmed by the higher O_2 evolution curve in HL-N compared to HL on a chlorophyll basis reported at Figure 8. These results suggest that nitrogen starvation boosts the stress response in *H. pluvialis*, inducing the cells to quickly counteract the photo-oxidative stress induced by the exposure to high irradiance. In our experiment high light combined with nitrogen starvation (HL-N) is the most effective condition to induce astaxanthin production in *H. pluvialis* cells, in accordance with previous report (Aflalo *et al.*, 2007). Volumetric and cellular astaxanthin content increase similarly and continuously throughout stress exposure, achieving respectively 306 mg ml^{-1} and 1665 pg $cell^{-1}$. The accumulation of astaxanthin is very fast and after only one day of stress exposure a content of 94.46 pg $cell^{-1}$ was achieved. It is worth noting that HL-N is the only growth condition in which a significant reduction of PSII functional antenna size and LHCII content per chlorophyll was observed. PSII antenna size reduction, the rapid NPQ increase in the first days of stress, and the faster and higher astaxanthin accumulation observed in HL-N produce a more photoprotected state,

reducing the amount of light absorbed by photosystems and preventing photosynthetic efficiency decrease. It's known that DPA inhibits astaxanthin synthesis, blocking the oxidation of the β-ionone ring made by β-carotene oxygenase, and promoting β-carotene accumulation in the cytoplasm (Harker and Young, 1995; Fan *et al.*, 1995; Schoefs *et al.*, 2001; Grünewald and Hagen, 2001). Treatment of *H. pluvialis* cells with DPA during stress exposure can help to elucidate the physiological effects related with astaxanthin accumulation. As expected, the inhibition of astaxanthin biosynthesis in HL-N, the most effective condition to induce astaxanthin accumulation, promotes an increase of its biosynthetic intermediates as β-carotene and enhances the accumulation of lutein, zeaxanthin, anteraxanthin and violaxanthin, redirecting β-carotene towards hydroxylation pathway. The inhibition of astaxanthin biosynthesis however did not significantly change the photostability of PSII in *H. pluvialis*: the results reported in Figure 6 indeed demonstrate that HL-N and HL-N+DPA (with or without astaxanthin accumulation respectively) were similarly photoinhibited upon exposure to strong white or red light. In both cases the accumulation of carotenoids (astaxanthin or other carotenes and xanthophylls) indeed confer an increased resistance to white light exposure in cells with higher carotenoid content per chlorophylls (HL-N≈HL-N+DPA>CL-N>HL>CL), likely due to carotenoid absorption of the bluest wavelengths of the stressing light, even if a specific role for astaxanthin was not evident. The screen effect of carotenoids was not the only photoprotective mechanisms induced in HL-N and HL-N+DPA cells, since the exposure to red light, which cannot be absorbed by carotenoids, still produced a more pronounced photoinhibition in CL, CL-N and HL cells compared to HL-N and HL-N+DPA. Carotenoid increased in the chloroplast upon DPA treatment produces as a side effect a decrease of NPQ during the experiment: accumulation of carotenoids in the chloroplast likely switches the chloroplastic photoprotective mechanisms from chlorophyll singlets excited state quenching (NPQ) to chlorophyll triplets excited states quenching or ROS scavenging, being both mechanisms strongly influenced by carotenoid quantity and quality (Ballottari *et al.*, 2013). The increased carotenoid content in HL-N and HL-N+DPA is likely the reason for their enhanced photostability (Figure 6), together with the modification of photosynthetic apparatus discussed above. The reduction of cell diameter in HL-N+DPA cells (Figure 1) clearly indicate that the impairment of astaxanthin biosynthesis affect cell growth and biomass accumulation, even if the photoprotective function of astaxanthin is directed to

the photosynthetic apparatus (Figure 6). The localization of astaxanthin outside the chloroplast clearly suggests that the photoprotective role of this carotenoid is mainly directed to the nucleus to prevent DNA modification by UV exposure or excessive ROS formation in the cytoplasm. Additional future experiments are required in order to fully prove our hypothesis, as the evaluation of DNA modifications induced upon UV exposure and/or the measurement of oxidation level of cytoplasmic proteins vs. chloroplastic proteins in HL-N vs. HL-N+DPA cells. By the way our results are consistent with the observations of Fan and coworkers which suggested that astaxanthin accumulation is a consequence of activation of photoprotection process rather than being the main photoprotective actor (Fan *et al.*, 1998).

Astaxanthin biosynthesis has been previously reported to be modulated by PTOX activity (Li *et al.*, 2008, 2010; Wang *et al.*, 2009), the results reported here are partially in agreement with this finding, observing that a strong induction of PTOX activity is evident in nitrogen starvation (CL-N and HL-N). The most surprising result obtained is the apparent lack of effects on PQ reduction state upon PTOX inactivation in cells grown in HL (Figure 10), where astaxanthin biosynthesis is fully induced (Figure 4). The apparently low chlororespiration activity in HL is confirmed by the similar proton motive force observed in HL in presence or absence of PGAL, inhibiting PTOX (Figure 10). This result is on the same line with the transcriptional analysis conducted by Li and coworkers (Li *et al.*, 2010) on *H. pluvialis* cells grown at high irradiances, where the overexpression of *ptox2* gene was observed only transiently upon exposure to high light: likely, acclimation to HL activate other adaptive mechanisms that balance the excitation pressure on Photosystems, reducing the need for chlororespiration, as for example an increase electron demand from PSI. In particular it has been reported by Gu and coworker that HL exposure in *H. pluvialis* did not significantly reduce the electron transport rate (ETR) from PSII to PSI and an increase of PSI/PSII ratio was observed (Wang *et al.*, 2014); similarly in *C. reinhardtii* it has been reported that HL acclimation induced an increased PSI/PSII ratio and an increased linear electron transport. Differently, in HL-N we observed a clear induction of cyclic electron transport across PSI. A similar effect was also evident in CL-N, even if to less extent. The activation of chlororespiration in nitrogen starvation reduces the electrons availability for PSI, thus inducing the activation of alternative electron transport pathway. Even if an active PTOX cannot be fully excluded in HL, it is possible to claim that PTOX activity is

strongly required upon nitrogen starvation, where cell division and chloroplast metabolism are partially blocked and NADPH demand is reduced, likely leading to a more difficult oxidation of the plastoquinones pool. In this context a strong PTOX activity and cyclic electron transport activation provide the channels through which both fueling the carotenoid biosynthetic enzymes astaxanthin production and oxidizing the PQ pool alleviating the excitation pressure on PSII.

In conclusion, the results reported in this work demonstrate that the photosynthetic properties of *H. pluvialis* are differentially modulated in response to nitrogen starvation and high light. In particular nitrogen starvation inhibits chlorophyll biosynthesis, promotes chlorophyll b degradation, PTOX activity, cyclic electron transport and favors respiration over photosynthesis, while high light mainly activates xanthophyll cycle and carotenogenesis. The combined exposure of *H. pluvialis* to high light and nitrogen starvation strongly induce a more rapid acclimation of photosynthetic apparatus to stress with a significant reduction of functional PSII antenna size and increase astaxanthin production, improving the resistance of cells to photo-oxidation. From an applicative point of view, a correct balance between biomass accumulation and proper exposure to high light and nitrogen starvation seems to be essential for efficient astaxanthin production in *H. pluvialis*.

Bibliography

Aflalo C, Meshulam Y, Zarka A, Boussiba S. 2007. On the relative efficiency of two- vs. one-stage production of astaxanthin by the green alga *Haematococcus pluvialis*. Biotechnology and bioengineering **98**, 300–305.

Alric J. 2010. Cyclic electron flow around photosystem I in unicellular green algae. Photosynthesis research **106**, 47–56.

Ambati RR, Moi PS, Ravi S, Aswathanarayana RG. 2014. Astaxanthin: Sources, extraction, stability, biological activities and its commercial applications - A review. Marine Drugs **12**, 128–152.

Arnon DI, Tsujimoto HY, Tang GM. 1981. Proton transport in photooxidation of water: A new perspective on photosynthesis. Proceedings of the National Academy of Sciences of the United States of America **78**, 2942–2946.

Bailleul B, Cardol P, Breyton C, Finazzi G. 2010. Electrochromism: a useful probe to study algal photosynthesis. Photosynthesis Research **106**, 179–189.

Ballottari M, Mozzo M, Girardon J, Hienerwadel R, Bassi R. 2013. Chlorophyll triplet quenching and photoprotection in the higher plant monomeric antenna protein Lhcb5. The Journal of Physical Chemistry B **117**, 11337–11348.

Bennoun P. 1982. Evidence for a respiratory chain in the chloroplast. Proceedings of the National Academy of Sciences of the United States of America **79**, 4352–4356.

Berges JA, Charlebois DO, Mauzerall DC, Falkowski PG. 1996. Differential effects of nitrogen limitation on photosynthetic efficiency of Photosystems I and II in microalgae. Plant Physiology **110**, 689–696.

de Bianchi S, Dall'Osto L, Tognon G, Morosinotto T, Bassi R. 2008. Minor antenna proteins CP24 and CP26 affect the interactions between Photosystem II subunits and the Electron Transport Rate in grana membranes of *Arabidopsis*. The Plant Cell **20**, 1012–1028.

Bilger W, Björkman O. 1990. Role of the xanthophyll cycle in photoprotection elucidated by measurements of light-induced absorbance changes, fluorescence and photosynthesis in leaves of *Hedera canariensis*. Photosynthesis Research **25**, 173–185.

Bonente G, Ballottari M, Truong TB, Morosinotto T, Ahn TK, Fleming GR, Niyogi KK, Bassi R. 2011. Analysis of LHcSR3, a protein essential for feedback de-excitation in the green alga

Chlamydomonas reinhardtii. PLoS Biology **9**.

Bonente G, Pippa S, Castellano S, Bassi R, Ballottari M. 2012. Acclimation of *Chlamydomonas reinhardtii* to different growth irradiances. Journal of Biological Chemistry **287**, 5833–5847.

Borowitzka MA, Huisman JM, Osborn A. 1991. Culture of the astaxanthin-producing green alga *Haematococcus pluvialis*. Effects of nutrients on growth and cell type. Journal of Applied Phycology **3**, 295–304.

Boussiba S. 2000. Carotenogenesis in the green alga *Haematococcus pluvialis*: Cellular physiology and stress response. Physiologia Plantarum **108**, 111–117.

Boussiba S, Bing W, Yuan JP, Zarka A, Chen F. 1999. Changes in pigments profile in the green alga *Haeamtococcus pluvialis* exposed to environmental stresses. Biotechnology Letters **21**, 601–604.

Boussiba S, Vonshak A. 1991. Astaxanthin accumulation in the green alga *Haematococcus pluvialis*. Plant and Cell Physiology **32**, 1077–1082.

Cakmak T, Angun P, Demiray YE, Ozkan AD, Elibol Z, Tekinay T. 2012. Differential effects of nitrogen and sulfur deprivation on growth and biodiesel feedstock production of *Chlamydomonas reinhardtii*. Biotechnology and bioengineering **109**, 1947–1957.

Cardol P, Alric J, Girard-Bascou J, Franck F, Wollman F-A, Finazzi G. 2009. Impaired respiration discloses the physiological significance of state transitions in *Chlamydomonas*. Proceedings of the National Academy of Sciences **106**, 15979–15984.

Cazzaniga S, Dall'Osto L, Szaub J, Scibilia L, Ballottari M, Purton S, Bassi R. 2014. Domestication of the green alga *Chlorella sorokiniana*: reduction of antenna size improves light-use efficiency in a photobioreactor. Biotechnology for Biofuels **7**, 157.

Chen G, Wang B, Han D, Sommerfeld M, Lu Y, Chen F, Hu Q. 2015. Molecular mechanisms of the coordination between astaxanthin and fatty acid biosynthesis in *Haematococcus pluvialis* (Chlorophyceae). The Plant journal : for cell and molecular biology **81**, 95–107.

Chen Z, Wang G, Niu J. 2012. Variation in Rubisco and other photosynthetic parameters in the life cycle of *Haematococcus pluvialis*. Chinese Journal of Oceanology and Limnology **30**, 136–145.

Choi Y-E, Rhee J-K, Kim H-S, Ahn J-W, Hwang H, Yang J-W. 2015. Chemical genetics approach reveals importance of cAMP and MAP Kinase signaling to lipid and carotenoid biosynthesis in microalgae. Journal of microbiology and biotechnology **25**, 637–647.

Collins AM, Jones HDT, Han D, Hu Q, Beechem TE, Timlin JA. 2011. Carotenoid distribution in living cells of *Haematococcus pluvialis* (Chlorophyceae). PLOS ONE **6**, e24302.

Dall'Osto L, Holt NE, Kaligotla S, Fuciman M, Cazzaniga S, Carbonera D, Frank HA, Alric J, Bassi R. 2012. Zeaxanthin protects plant photosynthesis by modulating chlorophyll triplet yield in specific light-harvesting antenna subunits. Journal of Biological Chemistry **287**, 41820–41834.

Dong H-P, Williams E, Wang D, Xie Z-X, Hsia R, Jenck A, Halden R, Li J, Chen F, Place AR. 2013. Responses of *Nannochloropsis oceanica* IMET1 to Long-Term Nitrogen Starvation and Recovery. Plant physiology **162**, 1110–1126.

Elrad D. 2002. A major Light-Harvesting polypeptide of Photosystem II functions in thermal dissipation. the Plant Cell Online **14**, 1801–1816.

Fan L, Vonshak A, Gabbay R, Hirshberg J, Cohen Z, Boussiba S. 1995. The biosynthetic pathway of astaxanthin in a green alga *Haematococcus pluvialis* as indicated by inhibition with diphenylamine. Plant and Cell Physiology **36**, 1519–1524.

Fan L, Vonshak A, Zarka A, Boussiba S. 1998. Does astaxanthin protect *Haematococcus* against light damage? Zeitschrift fur Naturforschung. C, Journal of biosciences **53**, 93–100.

Ferrante P, Ballottari M, Bonente G, Giuliano G, Bassi R. 2012. LHCBM1 and LHCBM2/7 polypeptides, components of major LHCII complex, have distinct functional roles in photosynthetic antenna system of *Chlamydomonas reinhardtii*. Journal of Biological Chemistry **287**, 16276–16288.

Formighieri C, Cazzaniga S, Kuras R, Bassi R. 2013. Biogenesis of photosynthetic complexes in the chloroplast of *Chlamydomonas reinhardtii* requires ARSA1, a homolog of prokaryotic arsenite transporter and eukaryotic TRC40 for guided entry of tail-anchored proteins. The Plant journal : for cell and molecular biology **73**, 850–861.

Gao Z, Meng C, Gao H, Zhang X, Xu D, Su Y, Wang Y, Zhao Y, Ye N. 2013. Analysis of mRNA expression profiles of carotenogenesis and astaxanthin production of *Haematococcus pluvialis* under exogenous 2, 4-epibrassinolide (EBR). Biological research **46**, 201–206.

Garab G, Lajkó F, Mustárdy L, Márton L. 1989. Respiratory control over photosynthetic electron transport in chloroplasts of higher-plant cells: evidence for chlororespiration. Planta **179**, 349–358.

Giannelli L, Yamada H, Katsuda T, Yamaji H. 2015. Effects of temperature on the astaxanthin productivity and light harvesting characteristics of the green alga *Haematococcus pluvialis*. Journal of bioscience and bioengineering **119**, 345–350.

Grünewald K, Hagen C. 2001. β-carotene is the intermediate exported from the chloroplast during accumulation of secondary carotenoids in *Haematococcus pluvialis*. Journal of Applied Phycology **13**, 89–93.

Gu W, Li H, Zhao P, Yu R, Pan G, Gao S, Xie X, Huang A, He L, Wang G. 2014. Quantitative proteomic analysis of thylakoid from two microalgae (*Haematococcus pluvialis* and *Dunaliella salina*) reveals two different high light-responsive strategies. Scientific Reports **4**, 6661.

Gu W, Xie X, Gao S, Zhou W, Pan G, Wang G. 2013. Comparison of different cells of *Haematococcus pluvialis* reveals an extensive acclimation mechanism during its aging process: from a perspective of photosynthesis. PloS one **8**, e67028.

Guerin M, Huntley ME, Olaizola M. 2003. *Haematococcus* astaxanthin: applications for human health and nutrition. Trends in Biotechnology **21**, 210–216.

Hagen C, Grünewald K, Schmidt S, Müller J. 2000.

Accumulation of secondary carotenoids in flagellates of *Haematococcus pluvialis* (Chlorophyta) is accompanied by an increase in per unit chlorophyll productivity of photosynthesis. European Journal of Phycology **35**, 75–82.

Harker M, Young AJ. 1995. Inhibition of astaxanthin synthesis in the green alga, *Haematococcus pluvialis*. European Journal of Phycology **30**, 179–187.

Havaux M, Niyogi KK. 1999. The violaxanthin cycle protects plants from photooxidative damage by more than one mechanism. Proceedings of the National Academy of Sciences **96**, 8762–8767.

Higuera-Ciapara I, Felix-Valenzuela L, Goycoolea FM. 2006. Astaxanthin: a review of its chemistry and applications. Critical reviews in food science and nutrition **46**, 185–196.

Hockin NL, Mock T, Mulholland F, Kopriva S, Malin G. 2012. The response of diatom central carbon metabolism to nitrogen starvation is different from that of green algae and higher plants. Plant Physiology **158**, 299–312.

Holtin K, Kuehnle M, Rehbein J, Schuler P, Nicholson G, Albert K. 2009. Determination of astaxanthin and astaxanthin esters in the microalgae *Haematococcus pluvialis* by LC-(APCI)MS and characterization of predominant carotenoid isomers by NMR spectroscopy. Analytical and bioanalytical chemistry **395**, 1613–1622.

Joet T, Genty B, Josse E-M, Kuntz M, Cournac L, Peltier G. 2002. Involvement of a plastid terminal oxidase in plastoquinone oxidation as evidenced by expression of the *Arabidopsis thaliana* enzyme in tobacco. The Journal of biological chemistry **277**, 31623–31630.

Josse E-M, Simkin AJ, Gaffé J, Labouré A-M, Kuntz M, Carol P. 2000. A plastid terminal oxidase associated with carotenoid desaturation during chromoplast differentiation. Plant Physiology **123**, 1427–1436.

Kakizono T, Kobayashi M, Nagai S. 1992. Effect of carbon/nitrogen ratio on encystment accompanied with astaxanthin formation in a green alga, *Haematococcus pluvialis*. Journal of Fermentation and Bioengineering **74**, 403–405.

Kobayashi M, Kakizono T, Nishio N, Nagai S. 1992. Effects of light intensity, light quality, and illumination cycle on astaxanthin formation in a green alga, *Haematococcus pluvialis*. Journal of Fermentation and Bioengineering **74**, 61–63.

Kobayashi M, Katsuragi T, Tani Y. 2001. Enlarged and astaxanthin-accumulating cyst cells of the green alga *Haematococcus pluvialis*. Journal of Bioscience and Bioengineering **92**, 565–568.

Lemoine Y, Schoefs B. 2010. Secondary ketocarotenoid astaxanthin biosynthesis in algae: a multifunctional response to stress. Photosynthesis research **106**, 155–177.

Li Y, Sommerfeld M, Chen F, Hu Q. 2008. Consumption of oxygen by astaxanthin biosynthesis: a protective mechanism against oxidative stress in *Haematococcus pluvialis* (Chlorophyceae). Journal of plant physiology **165**, 1783–1797.

Li Y, Sommerfeld M, Chen F, Hu Q. 2010. Effect of photon flux densities on regulation of carotenogenesis and cell viability of *Haematococcus pluvialis* (Chlorophyceae). Journal of Applied Phycology **22**, 253–263.

Li J, Zhu D, Niu J, Shen S, Wang G. 2011. An economic assessment of astaxanthin production by large scale cultivation of *Haematococcus pluvialis*. Biotechnology Advances **29**, 568–574.

Lorenz RT, Cysewski GR. 2000. Commercial potential for Haematococcus microalgae as a natural source of astaxanthin. Trends in Biotechnology **18**, 160–167.

Niyogi KK. 2000. Safety valves for photosynthesis. Current Opinion in Plant Biology **3**, 455–460.

Peers G, Truong TB, Ostendorf E, Busch A, Elrad D, Grossman AR, Hippler M, Niyogi KK. 2009. An ancient light-harvesting protein is critical for the regulation of algal photosynthesis. Nature **462**, 518–21.

Pinnola A, Dall'Osto L, Gerotto C, Morosinotto T, Bassi R, Alboresi A. 2013. Zeaxanthin binds to Light-Harvesting Complex Stress-Related Protein to enhance Nonphotochemical Quenching in *Physcomitrella patens*. The Plant Cell **25**, 3519–3534.

Qiu B, Li Y. 2006. Photosynthetic acclimation and photoprotective mechanism of *Haematococcus pluvialis* (Chlorophyceae) during the accumulation of secondary carotenoids at elevated irradiation. Phycologia **45**, 117–126.

Recht L, Topfer N, Batushansky A, Sikron N, Gibon Y, Fait A, Nikoloski Z, Boussiba S, Zarka A. 2014. Metabolite profiling and integrative modeling reveal metabolic constraints for carbon partitioning under nitrogen starvation in the green algae *Haematococcus pluvialis*. The Journal of biological chemistry **289**, 30387–30403.

Rippka R, Deruelles J, Waterbury JB, Herdman M, Stanier RY. 1979. Generic assignments, strain histories and properties of pure cultures of Cyanobacteria. Microbiology **111**, 1–61.

La Rocca N, Sciuto K, Meneghesso A, Moro I, Rascio N, Morosinotto T. 2014. Photosynthesis in extreme environments: responses to different light regimes in the Antarctic alga *Koliella antarctica*. Physiologia Plantarum **153**, 654–667.

Rumeau D, Peltier G, Cournac L. 2007. Chlororespiration and cyclic electron flow around PSI during photosynthesis and plant stress response. Plant, cell & environment **30**, 1041–1051.

Schmollinger S, Muhlhaus T, Boyle NR, *et al.* 2014. Nitrogen-sparing mechanisms in *Chlamydomonas* affect the transcriptome, the proteome, and photosynthetic metabolism. The Plant cell **26**, 1410–1435.

Schoefs B, Rmiki N, Rachadi J, Lemoine Y. 2001. Astaxanthin accumulation in *Haematococcus* requires a cytochrome P450 hydroxylase and an active synthesis of fatty acids. FEBS letters **500**, 125–128.

Shahbazi M, Gilbert M, Labouré A-M, Kuntz M. 2007. Dual role of the plastid terminal oxidase in tomato. Plant Physiology **145**, 691–702.

Steinbrenner J, Sandmann G. 2006. Transformation of the green alga *Haematococcus pluvialis* with a phytoene desaturase for accelerated astaxanthin biosynthesis. Applied and Environmental Microbiology **72**, 7477–7484.

Tan S, Cunningham FX, Youmans M, Grabowski B, Sun Z, Gantt E. 1995. Cytochrome f loss in astaxanthin-accumulating red cells of *Haematococcus pluvialis* (chlorophyceae): comparison of photosynthetic activity, photosynthetic enzymes, and thylakoid

membrane polypeptides in red and green cells. Journal of Phycology **31**, 897–905.

Tjahjono AE, Hayama Y, Kakizono T, Terada Y, Nishio N, Nagai S. 1994. Hyper-accumulation of astaxanthin in a green alga *Haematococcus pluvialis* at elevated temperatures. Biotechnology Letters **16**, 133–138.

Torzillo G, Göksan T, Isik O, Gökpinar Ş. 2005. Photon irradiance required to support optimal growth and interrelations between irradiance and pigment composition in the green alga *Haematococcus pluvialis*. European Journal of Phycology **40**, 233–240.

Wan M, Hou D, Li Y, Fan J, Huang J, Liang S, Wang W, Pan R, Wang J, Li S. 2014*a*. The effective photoinduction of *Haematococcus pluvialis* for accumulating astaxanthin with attached cultivation. Bioresource technology **163**, 26–32.

Wan M, Zhang J, Hou D, Fan J, Li Y, Huang J, Wang J. 2014*b*. The effect of temperature on cell growth and astaxanthin accumulation of *Haematococcus pluvialis* during a light-dark cyclic cultivation. Bioresource technology **167**, 276–283.

Wang S-B, Chen F, Sommerfeld M, Hu Q. 2004. Proteomic analysis of molecular response to oxidative stress by the green alga *Haematococcus pluvialis* (Chlorophyceae). Planta **220**, 17–29.

Wang J, Sommerfeld M, Hu Q. 2009. Occurrence and environmental stress responses of two plastid terminal oxidases in *Haematococcus pluvialis* (Chlorophyceae). Planta **230**, 191–203.

Wang B, Zarka A, Trebst A, Boussiba S. 2003. astaxanthin accumulation in *Haematococcus pluvialis* (chlorophyceae) as an active photoprotective process under high irradiance. Journal of Phycology **39**, 1116–1124.

Wang B, Zhang Z, Hu Q, Sommerfeld M, Lu Y, Han D. 2014. Cellular capacities for high-light acclimation and changing lipid Profiles across life cycle stages of the green alga *Haematococcus pluvialis*. PLOS ONE **9**, e106679.

Xue X, Gauthier DA, Turpin DH, Weger HG. 1996. Interactions between photosynthesis and respiration in the green alga C*hlamydomonas reinhardtii* (Characterization of light-enhanced dark respiration). Plant Physiology **112**, 1005–1014.

Yuan J-P, Peng J, Yin K, Wang J-H. 2011. Potential health-promoting effects of astaxanthin: a high-value carotenoid mostly from microalgae. Molecular nutrition & food research **55**, 150–165.

Zhang W, Wang J, Wang J, Liu T. 2014. Attached cultivation of *Haematococcus pluvialis* for astaxanthin production. Bioresource technology **158**, 329–335.

Zhekisheva M, Boussiba S, Khozin-Goldberg I, Zarka A, Cohen Z. 2002. Accumulation of oleic acid in *Haematococcus pluvialis* (chlorophyceae) under nitrogen starvation or high light is correlated with that of astaxanthin esters. Journal of Phycology **38**, 325–331.

Zhu S, Huang W, Xu J, Wang Z, Xu J, Yuan Z. 2014. Metabolic changes of starch and lipid triggered by nitrogen starvation in the microalga *Chlorella zofingiensis*. Bioresource technology **152**, 292–298.

Zlotnik (Shmerler) I, Sukenik A, Dubinsky Z. 1993. physiological and photosynthetic changes during the formation of red aplanospores in the chilorophyte *Haematococcus pluvialis*. Journal of Phycology **29**, 463–469.

Supplementary data

Figure S1: Cells of H. pluvialis in different growth conditions.

Transmission light microscopy images of H. pluvialis cells grown for 8 days under different conditions. Growth conditions analyzed: control light (40 µmol photons m^{-1} s^{-1}) with (CL) and without (CL-N) nitrogen and high light (400 µmol photons m^{-1} s^{-1}) with (HL) and without nitrogen in presence (HL-N+DPA) or absence (HL-N) of diphenylamine.

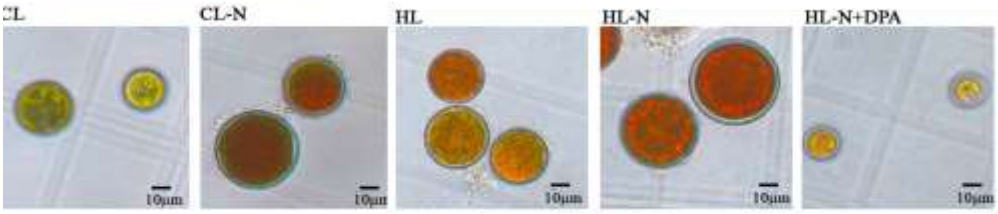

Figure S2: HPLC analysis of pigment extracts from H. pluvialis cells

Pigments were extracted from H. pluvialis cells as described in Materials and Methods Section (paragraph 2.2) and analyzed by HPLC. HPLC results are reported for cells grown in the different growth conditions for eight days as 2D-maps with elution time and wavelength of absorption on X e Y axes respectively. Growth conditions analyzed are: control light (40 µmol photons m^{-1} s^{-1}) with (CL) and without (CL-N) nitrogen and high light (400 µmol photons m^{-1} s^{-1}) with (HL) and without nitrogen in presence (HL-N+DPA) or absence (HL-N) of diphenylamine. For each condition the chromatogram obtained by measuring the absorption at 440 nm is reported with the indication of the corresponding molecule: N, neoxanthin; V, violaxanthin; L, lutein; A, anteraxanthin; Z, zeaxanthin; Chl a, chlorophyll a; Chl b, chlorophyll b; β-Car, β-carotene; As, Astaxanthin. The different elution time of astaxanthin is due to esterification with different fatty acids: "free" astaxanthin can be found only as the peak in the chromatogram between the violaxanthin and the lutein peaks (Holtin *et al.*, 2009).

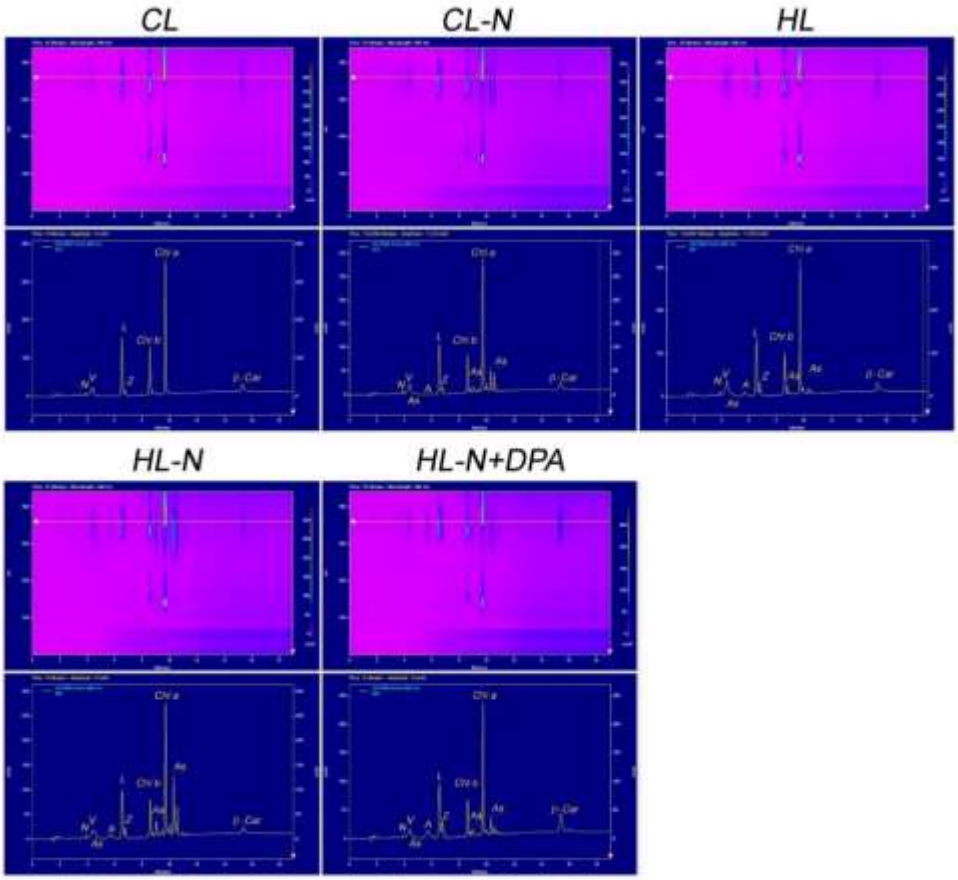

Section D

Functional analysis of photosynthetic pigment binding complexes in the green alga *Haematococcus pluvialis* reveals distribution of astaxanthin in Photosystems[6]

Astaxanthin is a ketocarotenoid, with strong anti-oxidant capacity produced in high levels in *Haematococcus pluvialis* upon stress condition. In this work, we investigate the biochemical and spectroscopic properties of the *H. pluvialis* pigment binding complexes responsible for light harvesting and energy conversion. Our findings demonstrate that the main features of chlorophyll and carotenoid binding complexes previously reported for higher plants or *Chlamydomonas reinhardtii* are preserved under control conditions. Transition to astaxanthin rich cysts however leads to destabilization of the Photosystems but, also, partially substituting β-carotene in both Photosystem I and II. However, astaxanthin binding to Photosystems does not improve their photoprotection, but rather reduces the efficiency of excitation energy transfer to the reaction centers.

In this work I helped in the experiments design, paper writing and antenna size sample production and analysis.

Abbreviations**:** Car, Carotenoid; PSI/II, Photosystem I/II; Chl Chlorophyll; RC Reaction Center; LHC, Light Harvesting Complex; DCMU, (3-(3,4-dichlorophenyl)-1,1-dimethylurea); DBMIB, (2,5-dibromo-3-methyl-6-isopropylbenzoquinone); ROS, Reactive Oxygen Species; $^1O_2$, singlet oxygen;

---

[6]This section is based on the published article: Mascia F, **Girolomoni L**, Alcocer MJP, Bargigia I, Perozeni P, Cazzaniga S, Cerullo G, D'Andrea C, Ballottari M; Functional analysis of photosynthetic pigment binding complexes in the green alga *Haematococcus pluvialis* reveals distribution of astaxanthin in Photosystems, Scientific Reports, Volume 7, Issue 1, 1 November 2017, Pages 16319.

Introduction

Haematococcus pluvialis is a photosynthetic fresh-water microalga which accumulates a high level of the ketocarotenoid astaxanthin (up to 5% DW) (Boussiba and Vonshak, 1991; Lemoine and Schoefs, 2010; Ambati *et al.*, 2014; Shah *et al.*, 2016). Astaxanthin is mainly used as coloring agent in aquaculture but it has been also reported to be a strong antioxidant, preventing production of reactive oxygen species (ROS) and lipid peroxidation in solution and in several biologic systems (Terao, 1989; Kurashige *et al.*, 1990; Guerin *et al.*, 2003; Stahl and Sies, 2005; Daubrawa *et al.*, 2005). Numerous studies have shown that astaxanthin has health-promoting effects in the prevention and treatment of various diseases such as cancers, chronic inflammations, metabolic syndrome, cardiovascular and gastrointestinal diseases, as well as enhancing the immune system and protecting the skin from radiation injury (Yuan *et al.*, 2011). Astaxanthin cannot be manufactured in animals and therefore must be consumed in the diet. This carotenoid (Car) is thus of great interest for several industrial sectors and has a high market potential. Many studies have addressed the role of astaxanthin in *H. pluvialis* and the phenotypical characterization of this alga (Boussiba and Vonshak, 1991; Kobayashi *et al.*, 2001; Wang *et al.*, 2004; Lemoine and Schoefs, 2010; Gao *et al.*, 2012*a*,*b*; Scibilia *et al.*, 2015; Shah *et al.*, 2016; Li *et al.*, 2017). The lifecycle of *H. pluvialis* includes four phases and astaxanthin is accumulated only in the aplanospores phase, which is induced under stress conditions such as high light intensity, nutrient starvation, high salinity or low/high temperatures (Boussiba and Vonshak, 1991; Wang *et al.*, 2009; Scibilia *et al.*, 2015; Hong *et al.*, 2015). Astaxanthin production from *H. pluvialis* mass cultivation is commonly carried out in a two-stage batch culture; biomass production occurs in the first stage (green stage), while in the second stage (red stage) the cultures are stressed to induce astaxanthin accumulation (Aflalo *et al.*, 2007). Astaxanthin is accumulated mainly at the level of the endoplasmatic reticulum in the form of mono- and di-esters by using β-carotene as precursor (Grunewald *et al.*, 2000, 2001). While several reports focused on astaxanthin production and its application for humans as a nutraceutic, details regarding the role of this Car in *H. pluvialis* cells are still not complete (Boussiba and Vonshak, 1991; Fan *et al.*, 1998; Kobayashi *et al.*, 2001; Wang *et al.*, 2004; Ambati *et al.*, 2014; Wan *et al.*, 2014; Su *et al.*, 2014; Scibilia *et al.*, 2015). The astaxanthin biosynthetic pathway depends on carbon fixation by the photosynthetic process in the

chloroplasts. During transition to astaxanthin rich cysts, Car biosynthesis is triggered and the plastids are degraded (Collins *et al.*, 2011). Photosynthetic processes are functionally divided in two phases; the light phase and dark phase. The light phase takes place in the thylakoid membranes, with light energy being harvested and converted into chemical energy in the form of NADPH and ATP. The subsequent dark phase is where NADPH and ATP are used in the stroma by Calvin-Benson cycle for enzymatic CO_2 fixation and reduction to carbohydrates. PSII and PSI are responsible for energy conversion, cytochrome $b_{6/f}$ contributes to electron transport and proton translocation in the lumen, and ATPase catalyzes ATP synthesis using the energy derived from the transmembrane proton gradient. PSI and PSII are pigment binding proteins composed of a *core* complex and antenna proteins called Light Harvesting Complexes (LHC) (Ben-Shem *et al.*, 2003; Caffarri *et al.*, 2009; van Amerongen and Croce, 2013; Drop *et al.*, 2014). The *core* complex binds chlorophyll (Chl) *a* and β-carotene, whilst the antenna proteins bind Chl *a*, Chl *b*, and xanthophylls (Ben-Shem *et al.*, 2003; Wei *et al.*, 2016). Pigments bound by the photosystems absorb photons and transfer excitation energy to the reaction centers. In particular PSI was observed to trap excitation energy at the reaction center (RC) faster than PSII (Croce and Van Amerongen, 2013). Higher plants and unicellular microalgae show some differences in both PSII and PSI supramolecular organization, with different stoichiometries of LHC proteins per PSI(II) core complexes. Four LHC subunits, called Lhca1-4, were found bound to PSI core complex of *A. thaliana*, while 7 to 9 different Lhca complexes were identified in the PSI-LHCI complexes from the green alga *Chlamydomonas reinhardtii*. In the case of PSII, the number of LHC complexes bound, called Lhcb, is more variable and depends on growth conditions (Stauber *et al.*, 2009; Caffarri *et al.*, 2009; Drop *et al.*, 2014; Wei *et al.*, 2016; Mazor *et al.*, 2017). Very little information is available regarding the photosynthetic complexes of the green alga *H. pluvialis* and how they are modulated during cyst formation and astaxanthin accumulation. Moreover, it is still under debate if astaxanthin accumulation has some photoprotective function at the level of the chloroplast (Fan *et al.*, 1998; Gu *et al.*, 2013, 2014; Scibilia *et al.*, 2015). The aim of this work is to characterize the photosynthetic complexes in *H. pluvialis* and the possible role of astaxanthin in the photosynthetic apparatus during acclimation to high light and transition to the red stage.

Materials and methods

Strain and culture conditions

Haematococcus pluvialis strain K-0084 was obtained from Scandinavian Culture Collection of Algae & Protozoa. Liquid cultures were grown photoautotrophically at 40 µmol photons $m^{-2}s^{-1}$ on BG-11 medium at 22 °C in flasks (Scibilia *et al.*, 2015). Culture mixing was provided by bubbling filtered (0,2 µm) air. High light treatment at 400 µmol photons $m^{-2}s^{-1}$ was applied to cell cultures in their exponential phase (approximately 5×10^5 cells ml^{-1}). Each experiment was repeated in at least five independent experiments with three biological replicates for each sample.

Cell concentration and pigment analysis

Cell concentrations (cells mL^{-1}) were determined manually using a Neubauer counting chamber as described in Scibilia *et al.* (2015). Pigment analysis were performed by reverse phase HPLC as described in Lagarde *et al.* (2000). In particular, pigment extracts in acetone 80% were analyzed by Thermo-Fisher HPLC system equipped with a C18 column using a 15-min gradient of ethyl acetate (0 to 100%) in acetonitrile-water-triethylamine (9:1:0.01, vol/vol/vol) at a flow rate of 1.5 ml/min. Only in the case of whole cells pigmentation extraction was performed in DMSO as described in Scibilia *et al.* (2015). Pigment detection was done by a Thermo-Fisher 350-750nm diode array detector.

Thylakoid membranes and pigment binding complexes isolation

Thylakoid membranes were isolated from *H. pluvialis* cells as described in Cazzaniga *et al.* (2014), with some modifications. *H. pluvialis* cells, were harvested by centrifugation (1500 g, 3 min) and resuspended in B1 buffer (50 mM tricine pH 7.9, 0.35 M sorbitol, 10 mM NaCl, 5 mM $MgCl_2$, 0.5% dried powdered milk, 1 mM aminocaproic acid, 0.2 mM aminobenzamidine, and 0.2 mM phenylmethylsulfonyl fluoride) at a final concentration of 10^6 cells/ml and then passed through a prechilled (4°C) Cell-disrupter (Constant Systems, Northants, UK) at 2.5 kbar. The resulting homogenate was subsequently centrifuged at 1500 g for 3 min at 4°C, to remove intact cells. The supernatant was collected and centrifuged at 12000 g for 15 minutes at 4°C. The resulting thylakoid membrane pellet was resuspended in B2 buffer (20 mM tricina

pH 7.9, 50% glycerol, 10 mM NaCl, 5 mM $MgCl_2$, 1 mM aminocaproic acid, 0.2 mM aminobenzamidine, and 0.2 mM phenylmethylsulfonyl fluoride) and immediately used for analysis, or stored at -80°C, after freezing it in liquid nitrogen. Isolated thylakoids were cleaned by ultracentrifugation in a sucrose step gradient formed by 1.9 M, 1.3 M and 1.14 M sucrose, 25 mM Hepes pH 7.0 and 10 mM EDTA. Clean thylakoid membranes were recovered from the 1.3 M layer, diluted to reduced sucrose concentration and precipitated by centrifugation. Isolated thylakoids were then solubilized at a concentration of 1 mg/ml of Chls (200 µg of Chls in total), with β-DM 1% and loaded onto a sucrose gradient (0.1-1 M) in presence of 0.06% β-DM and 10 mM Hepes pH 7.5. Protein fractions were isolated upon ultracentrifugation, collected from sucrose gradient and then cleaned by anion exchange chromatography as described in Ballottari *et al.* (2009). Anion exchange chromatography was performed on TOYOPEARL DEAE-650S resin (Sigma-Aldritch) equilibrated with 0.06% β-DM and 10 mM Hepes pH 7.5: protein elution was achieved using an elution buffer composed by 0.5M NaCl, 0.06% β-DM and 10 mM Hepes pH 7.5.

Absorption and fluorescence spectroscopy

Absorption spectra were measured by DW2000 Aminco spectrophotometer as described in Cinque *et al.* (2000). 77K steady state emission spectra were recorded using a Fluoromax3 equipped with an optical fiber (Horiba Jobin Yvon) as described in Grewe *et al.* (2014). Emission spectra were performed by exciting the sample at 440 nm with an excitation bandwidth of 5 nm and recording emission in the 650-800-nm range (emission bandwidth of 1 nm). Excitation spectra at 77K were performed upon excitation in the 400-550 nm range (excitation bandwidth of 2 nm) measuring the fluorescence emitted at 680 or 715 nm (emission bandwidth of 3 nm) as described in the text.

SDS-PAGE analysis

Denaturing SDS-PAGE was performed with Tris-Tricine buffer systems (Schagger and von Jagow, 1987).

PSI functional antenna size

Relative PSI antenna size was estimated from kinetics of P700 oxidation in limiting orange light (12 µE m^{-2} s^{-1}) in whole cells treated with DCMU (3-(3,4-dichlorophenyl)-

1,1-dimethylurea), DBMIB (2,5-dibromo-3-methyl-6-isopropylbenzoquinone), ascorbate and methyl-viologen, as described in Bonente *et al.* (2012).

Time resolved fluorescence measurements

Time-resolved fluorescence measurements were performed using a femtosecond laser excitation at 440 nm and a streak camera detection system, as reported in Ballottari *et al.* (2014). Briefly, an unamplifed Ti:sapphire laser (Coherent Chameleon Ultra II) operating at 80 MHz was tuned to provide pulses with central wavelengths of 880 nm, energies of 30 nJ, and temporal and spectral bandwidths of 140 fs and 5 nm, respectively. A β-barium borate crystal provided type I phase-matched second harmonic generation, leading to pulses with central wavelengths of 440 nm. These were focused onto the sample, maintaining a low fluence (<30 mJ/cm^2, 100 mm spot diameter) in order to avoid saturation and degradation effects in the sample. The samples were kept at a constant temperature of 11°C by a temperature controlled cuvette cooled by a peltier system. The resulting collected emission was analyzed by a spectrograph (Princeton Instruments Acton SP2300) coupled to a streak camera (Hamamatsu C5680) equipped with a synchroscan voltage sweep module. In this way, measurements of photoluminescence intensity as a function of both wavelength and time were obtained with spectral and temporal resolutions of ~1 nm and ~3 ps respectively. Temporal broadening of the pump pulses caused by dispersive elements was confirmed to be well below the response time of the detection system.

Global analysis

Streak camera fluorescence decay maps were globally fitted with exponential functions as previously reported (Van Stokkum *et al.*, 2004; Ballottari *et al.*, 2014). Briefly, the experimental datasets were fitted using a multi-exponential function as described by equation (1)

$$I(\lambda, t) = \sum_{i=1}^{n} A_i(\lambda)\ e^{-t/\tau_i} \quad (1)$$

with $I(\lambda, t)$ the wavelength- and time-resolved fluorescence intensity, and A_i the amplitude of the exponential decay e^{-t/τ_i}. Whilst the amplitudes were treated as wavelength dependent ($A_i = A_i(\lambda)$), the exponential decay constants were assumed to be wavelength independent $\tau_i \neq \tau_i(\lambda)$. The resulting wavelength dependent amplitudes, $A_i(\lambda)$, are referred to as Decay Associated Spectra (DAS), with each DAS being

associated with a particular exponential decay constant, τ_i. It is important to note that DAS are simply parameterisations of a time-resolved fluorescence dataset in a multi-exponential temporal basis, and so most often cannot be assigned a physical origin.

Average fluorescence lifetimes were calculated as described by equation (2):

$$\tau_{AV} = \sum_{i=1}^{n} A_i \tau_i / \sum_{i=1}^{n} A_i \qquad (2)$$

where A_i is the spectrally integrated amplitude over the spectral range 650-780 nm.

Singlet oxygen production

Singlet oxygen production was measured *in vivo* by following the 532 nm fluorescence emission of a singlet oxygen sensor green probe (Flors *et al.*, 2006). In particular, samples were diluted to in order to reach the same maximum at 0.15 OD in the Qy region and Singlet Oxygen Sensor Green was added to a final concentration of 5 µM. Samples were then illuminated with red light (2000 µE m^{-2} s^{-1} in the case of isolated complexes, 6000 µE m^{-2} s^{-1} in the case of thylakoids) and a regular time intervals, fluorescence at 532 nm was registered. Data were analyzed as increase in percentage of fluorescence, compared to time 0. Experimental data were then fitted with exponential functions.

Results

Astaxanthin accumulation in H. pluvialis

Haematococcus pluvialis cells were grown in BG11 medium at 50 µE for 7 days (hereafter, referred as G/Green), at 400 µE for 3 days (hereafter, referred as O/Orange) and at 400 µE for 6 days (hereafter, referred as R/Red). As reported in Figure 1, a clear change in the culture color appeared under the three different growth conditions, from green, to brownish, to red for G, O and R conditions respectively.

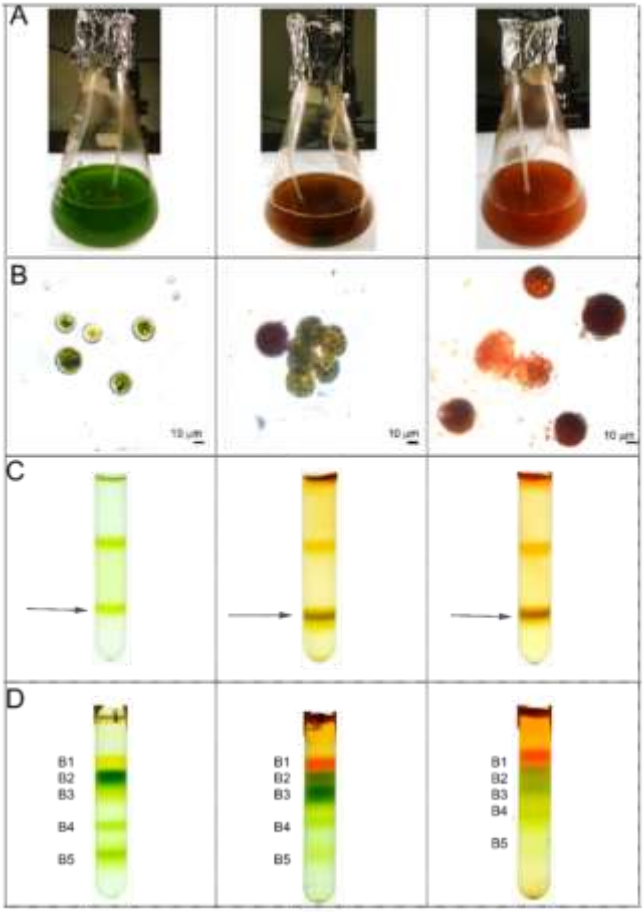

Figure 1: *Cell cultivation, membranes and pigment binding complexes isolation. (A) H. pluvialis cultures grown under 3 different stress conditions. Green: 50 µmol* $m^{-2}s^{-1}$ *for 7 days; Orange: 400 µmol* $m^{-2}s^{-1}$ *for 3 days; Red: 400 µmol* $m^{-2}s^{-1}$ *for 6 days. (B) Microscope observation of cells grown as in Panel A. (C) Isolation of plastid membranes from G, O and R cells. Purified membranes are indicated by the arrow. (D): Sucrose gradient ultracentrifugation separation of pigment binding complexes from plastid membranes solubilized in β-DM 1%.*

H. pluvialis cells grown were then observed in bright-field microscopy (Figure 1B). Cells grown in the G condition were round green cells with a distinct cell wall layer; in the O condition, cells became reddish, likely due to astaxanthin accumulation, but green chloroplasts were still visible; some cells in O and all cells R were characterized by a complete transition into a red stage, with strong astaxanthin accumulation. In this condition, partial cell degradation was also evident. Pigment composition was investigated by HPLC and reported in Figure 2.

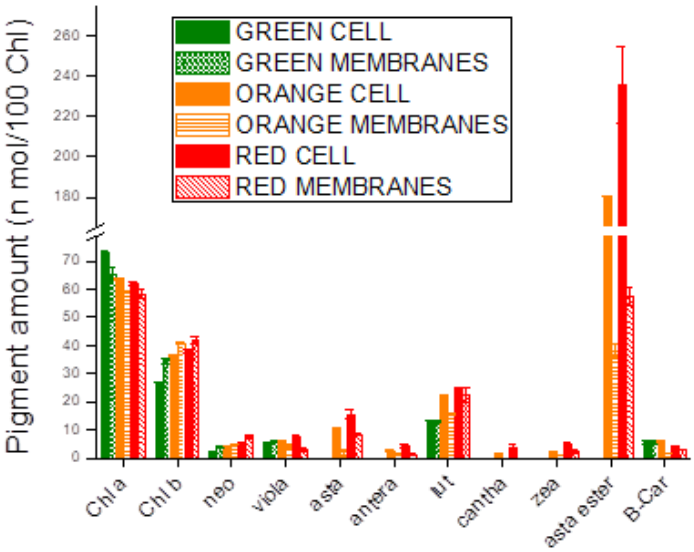

Figure 2. *Pigment analysis on H. pluvialis whole cells and isolated membranes. Pigment extracts were analyzed by HPLC. Pigment data were normalized to 100 chlorophylls. Chl: chlorophyll; Car: carotenoid; Neo: neoxanthin; Viola: violaxanthin; Lute: Lutein; Antera: anteraxanthin; Cantha: canthaxanthin; Zea: zeaxanthin; B-Car: β-carotene; Asta: astaxanthin; Asta ester: esterified forms of astaxanthin. Standard deviation (s.d.) are reported (n=3).*

A strong reduction of chlorophyll to carotenoid (Chl/Car) ratio was observed in O and R cells with the higher Car accumulation in R cells. Astaxanthin esters were the predominant Car species found in O and R cells, while no traces of astaxanthin were found in G cells. Traces of canthaxanthin, a precursor of astaxanthin, were also found in O and R cells. Incidentally finding of Chls, β-carotene and xanthophylls in O and R cells suggested the residual presence of photosynthetic complexes, responsible for the photosynthetic activity previously reported for *H. pluvialis* during transition to the red stage (Scibilia *et al.*, 2015). Lutein and neoxanthin were more abundant on a Chl basis in O and R conditions, while beta-carotene was reduced in R cells. Since lutein and neoxanthin are bound only to LHC complexes, while beta-carotene is essentially bound only to PSI or PSII core subunits, the increased neoxanthin or lutein to beta carotene ratios imply a partial degradation of core subunits during high light exposure.

Isolation and characterization of pigment binding complexes of H. pluvialis in different growth conditions

Thylakoid membranes of G, O and R cells were isolated by mechanical cell disruption followed by selective centrifugations with a final purification step by ultracentrifugation

in a sucrose step gradient. As reported in Figure 1C, membranes at similar sucrose densities were recovered from both G, O and R samples. Pigment composition of the purified membranes was then investigated by HPLC and reported in Figure 2. In O and R samples, the Chl/Car ratio was significantly reduced in purified thylakoid membranes as compared to whole cells. The observed reduction is mainly related to a strong decrease of astaxanthin, either in free or esterified forms, as compared to pigment extracts from whole cells. A reduction of β-carotene, anteraxanthin, zeaxanthin, canthaxanthin and lutein was also observed in O and R membranes as compared to whole cells, even if it was less pronounced when compared to astaxanthin. Since it has been reported that astaxanthin is accumulated only outside the plastids in *H. pluvialis* (Grunewald *et al.*, 2000, 2001; Collins *et al.*, 2011), the results obtained could be due to a co-purification of thylakoid membranes and astaxanthin rich oil droplets of similar densities. Since the presence of astaxanthin in thylakoid membranes has been reported for transgenic plants accumulating this Car (Zhong *et al.*, 2011; Roding *et al.*, 2015; Fujii *et al.*, 2016), the possible presence of astaxanthin molecules bound to pigment binding complexes was investigated using treated membranes. Purified membranes were solubilized and the Chl binding complexes were isolated by ultracentrifugation in a sucrose gradient (Grewe *et al.*, 2014). This ultracentrifugation step allowed a separation of the different photosynthetic complexes, based on their molecular density. Five bands (B1, B2, B3, B4, B5) were observed in every condition (G, O, R) (Figure 1D). B1-5 fractions were recovered and their absorption spectra investigated. The B1 band was composed of free pigments, as indicated by the Chl Qy absorption peak below 670 nm (Supplemental data, Figure S1). Absorption spectra of B2 and B3 fractions (Figure 3A-B) were similar in G, O and R conditions, resembling the features of LHC antenna proteins with two peaks in the Qy region attributable to Chl *a* (672 nm) and *b* (650 nm).

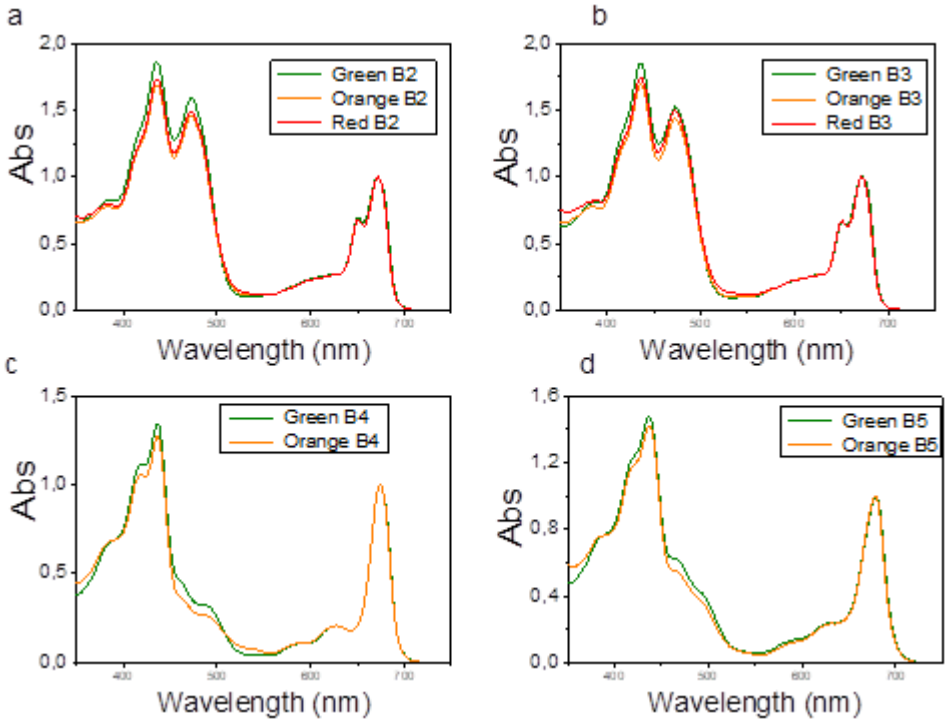

Figure 3. *Absorption spectra of pigment binding complexes isolated from H. pluvialis.* ***Absorption spectra of*** *B2, B3, B4 and B5 fraction (Figure 1D) were normalized to the maximum absorption peak in the 600 nm and 700 nm region.*

Based on their molecular density, B2 and B3 were composed of monomeric and trimeric LHC proteins respectively. B4 spectra showed an almost complete absence of the 470 nm and 650 nm peaks (Figure 3C), which are both related to Chl *b*. This indicates a high Chl *a*/*b* ratio, and hints at the presence of PSII-core in this fraction. Comparing O B4 with G B4, it is possible to notice a decreased absorbance at ~ 470 nm coupled with an increased absorbance at ~ 530 nm, which suggests the presence of astaxanthin. B5 spectra (Figure 3D) reveal the predominance of Chl a with a maximum absorbance in the Qy region at 679 nm, although Chl *b* contributions at 650 and 470 nm were still present in a lower amount. B5 was thus likely composed of the PSI-LHCI supercomplex. PSII-core (B4) and PSI (B5) fractions from R were not harvested since the bands in sucrose gradient were fuzzier and not well defined, suggesting partial degradation of these complexes in these conditions. The protein composition of B2-B5 from G and O samples was subsequently investigated by SDS-PAGE (Figure 4).

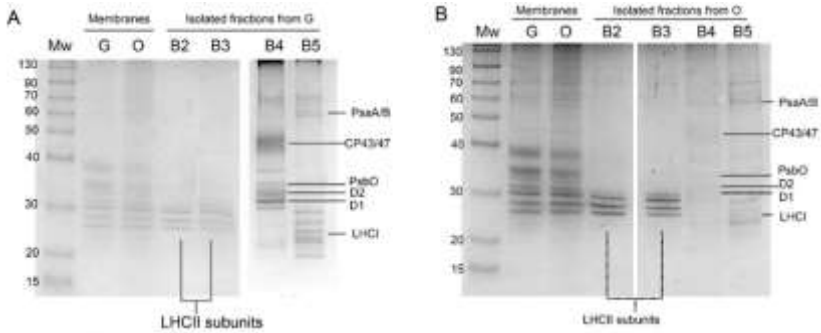

Figure 4. *SDS-PAGE of H. pluvialis purified membranes and isolated pigment binding complexes. (A) Isolated B2-5 fractions from Green cells (Figure 1) samples; (B) Isolated B2-5 fraction from Orange cells. SDS-PAGE gels were Coomassie stained. Lanes loaded in separate gels are divided by white spaces. Mw: molecular weight marker; G: proteins from "Green" cells grown at 50 µE; O: proteins from "Orange" cells grown at 400 µE for 3 days.*

B2 and B3 were characterized by four bands migrating at around 30 kDa, as expected for LHC antenna proteins. Interestingly, the two bands at lower molecular weight (MW) were more abundant in B2 than in B3 for both G and O samples, suggesting the preferential monomeric state of some specific LHC proteins as in the case of CP26 and CP29 in *C. reinhardtii* (Tokutsu *et al.*, 2009; Drop *et al.*, 2014). In B4 fractions, PSII-core proteins such as CP43, CP47, D1, D2 and PsbO subunits were identified on the basis of their apparent MW (Caffarri *et al.*, 2009). In B5 fractions (PSI-LHCI), high MW bands (60-70 KDa) could be attributed to PsaA and PsaB, together with bands at low MW (<30KDa) attributable to LHCI antenna proteins and other PSI core subunits. The pigment binding properties of the different isolated fractions were then analyzed by HPLC (Table 1).

	Chl	Chla/Chlb	Chl a	Chl b	Chl/Car	Neo	Viola	Asta	Antera	Lute	Zea	Asta ester	β-Car
GREEN B1	100	2.8	73.7	26.3	0.8	6.9	36.9	n.d.	n.d.	73.8	n.d.	n.d.	6.2
ORANGE B1	100	3.3	76.9	23.2	0.2	11.5	59.6	10.2	11.8	69.6	8.0	434.6	6.6
RED B1	100	4.2	80.9	19.1	0.1	12.0	105.2	17.8	23.1	91.4	14.7	1352.5	27.3
GREEN B2	14	1.6	8.6	5.4	4.0	0.7	0.7	n.d.	n.d.	2.7	n.d.	n.d.	n.d.
ORANGE B2	14	1.5	8.4	5.6	4.7	0.9	0.2	<0.1	n.d.	2.3	0.1	<0.1	<0.1
RED B2	14	1.5	8.4	5.6	4.5	0.9	0.2	<0.1	n.d.	2.4	0.1	0.1	<0.1
GREEN B3	14	1.7	8.8	5.2	3.8	0.7	0.8	n.d.	n.d.	2.8	n.d.	n.d.	n.d
ORANGE B3	14	1.5	8.5	5.5	4.8	0.8	0.3	<0.1	n.d.	2.3	0.1	n.d.	n.d.
RED B3	14	1.5	8.4	5.7	4.4	0.9	0.2	0.1	n.d.	2.3	0.1	0.1	n.d.
GREEN B4	72	22.6	68.9	3.1	4.3	0.3	1.0	n.d.	n.d.	3.3	n.d.	n.d.	12.1
ORANGE B4	72	29.4	69.6	2.4	6.3	0.6	0.6	0.6	n.d.	2.2	n.d.	1.9	5.4
GREEN B5	170	7.1	149.1	20.9	4.4	0.2	8.2	n.d.	n.d.	17.0	n.d.	n.d.	13.5
ORANGE B5	170	7.0	148.7	21.3	4.4	0.8	6.0	1.9	n.d.	18.0	1.0	0.9	10.6

Table 1. *Pigment analysis of isolated photosynthetic complexes. Pigment extracts were analyzed by HPLC. Pigment data from B2 and B3 fractions were normalized to 14 chlorophylls; pigments from B4 fractions were normalized to 72 chlorophylls; pigments from B5 fractions were normalized to 170 chlorophylls. Chl: chlorophyll; Car: carotenoid; Neo: neoxanthin; Viola: violaxanthin; Antera: anteraxanthin; Lute: Lutein; Zea: zeaxanthin; β-Car: β-carotene; Asta: astaxanthin; Asta ester: esterified forms of astaxanthin. Standard deviations are below 8% for each value reported in the table (n=3).*

Pigment results from B2 and B3 fractions were normalized to 14 Chls, as previously reported for LHCII subunits from higher plants (Liu *et al.*, 2004). Chl a/Chl b ratios were similar in B2 and B3 fractions from G, O or R samples, while Chl/Car ratios were increased in O and R as compared to G. This was mainly due to a strong reduction in violaxanthin content which is likely related to reduced stability of the V1 site in the presence of zeaxanthin, as previously reported for LHC proteins isolated from higher plants (Caffarri *et al.*, 2001; Johnson *et al.*, 2007). Traces of zeaxanthin were indeed detected in B2 and B3 from O and R cells. Zeaxanthin accumulation at the V1 sites of the LHC protein is likely due to xanthophyll cycle activation during high light stress or zeaxanthin accumulation in O and R membranes as a precursor to astaxanthin (Caffarri *et al.*, 2001; Grunewald *et al.*, 2001; Wehner *et al.*, 2004; Ballottari *et al.*, 2014). The reduced stability of the V1 site in B2 and B3 complexes from O and R cells could also be the reason for the reduced content of lutein in these fractions as compared to B2 and B3 fractions from G samples. Since more than 2 luteins were found in B2 and B3 fractions, the extra lutein is likely bound to the peripheral site V1 (Fiore *et al.*, 2012), which however is partially empty in O and R samples. Astaxanthin was almost completely absent in LHC proteins, even if traces of this ketocarotenoid were present only in O/R B2 and B3 fractions. The possible affinity of LHCII complexes for

astaxanthin has indeed been previously investigated by *in vitro* reconstitution (Phillip *et al.*, 2002). B4 fractions were characterized by a high Chl a/b ratio (>20), as expected for PSII-core. Traces of Chl b, neoxanthin and violaxanthin were also detected, and are likely to arise from the residual presence of antenna proteins. The most evident difference between G and O of B4 fractions is a decrease in β-carotene which is partially replaced in O by astaxanthin. In particular ≈ 2.5 molecules of astaxanthin were bound by PSII-core in O, mainly in its esterified form. It is worth noting that violaxanthin and lutein were also found in decreased quantities in O B4 as compared to G B4. These xanthophylls are likely related to residual LHC proteins bound to B4, and it is not possible exclude a possible substitution of these pigment with astaxanthin in O B4. PSI-LHCI fractions (B5 fraction) were characterized by a Chl a/b ratio of ≈7, an intermediate value between the Chl a/b ratio previously measured in the case of PSI-LHCI isolated from higher plants (Croce and Van Amerongen, 2013) and *C. reinhardtii* (Le Quiniou *et al.*, 2015*b*). The lower Chl a/b ratio observed in *C. reinhardtii* is due to an increased content of Lhca proteins, with 7-9 Lhca subunits bound per reaction center as compared to the 4 Lhca subunits found in the case of *A. thaliana* (Ballottari *et al.*; Ben-Shem *et al.*, 2003; Stauber *et al.*, 2009; Le Quiniou *et al.*, 2015*b*). In order to estimate the Lhca content associated to the PSI reaction center in *H. pluvialis*, we assumed 3.4 Cars per Lhca subunit as previously reported in the case of *A. thaliana* and *C. reinhardtii* (Le Quiniou *et al.*, 2015*b*) and 100 Chl a molecules per PSI core complex (Jordan *et al.*, 2001; Qin *et al.*, 2015; Mazor *et al.*, 2015, 2017). From the Chl a/b and Chl/Car ratios of the B5 fractions, we estimated 5 Lhca proteins per P700, with 14 Chls and 3.4 Cars bound by each subunit and 170 Chls bound by the PSI-LHCI complex. An intermediate value of Lhca content per PSI-LHCI complex in *H. pluvialis* as compared to higher plants and *C. reinhardtii* was then confirmed by PSI-LHCI functional antenna size measurement on whole cells (Supplemental data, Figure S2). Comparing B5 from G and O samples, a ~21% decrease in β-carotene content was evident, with a loss of ~2.9 molecules per P700. Conversely, ~2.8 astaxanthin molecules were found bound to each O B5 complex, suggesting a possible substitution of β-carotene with astaxanthin. A 28% decrease in violaxanthin was also observed in O B5 as compared to G B5, coupled with a rise in zeaxanthin, lutein and neoxanthin. A general re-organization of Car binding sites was thus evident in O samples even if the same total amount of Car was found in G or O B5 complexes. The markedly increased carotenogenesis observed in O cells leading

to high accumulation of lutein, zeaxanthin and astaxanthin in thylakoid membranes is likely to be the reason for the different pigment binding properties of B4 and B5 complexes.

Excitation energy transfer in astaxanthin binding complexes

The functional properties of astaxanthin bound to photosynthetic complexes were initially investigated by fluorescence measurements at 77K, where emission is mainly attributed to the lowest Chl excited states. When exciting Chl a at 440 nm, B2 and B3 fractions from G cells showed similar emission peaks at 680 nm and similar excitation spectra characterized by a high Chl b contribution (Figure 5).

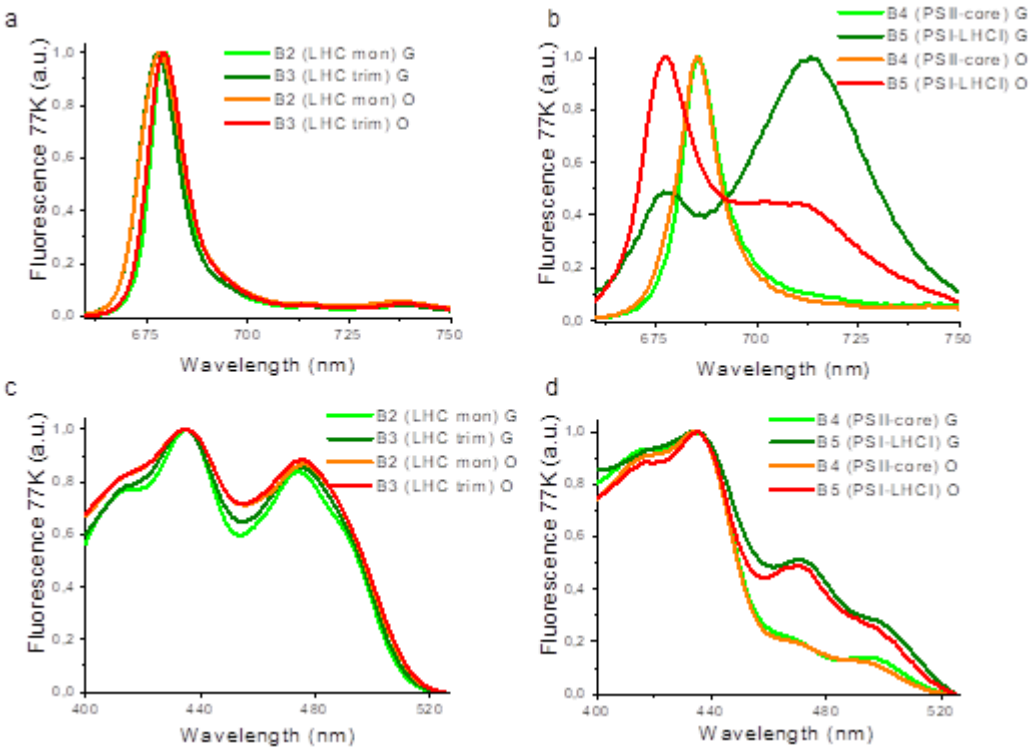

Figure 5. *77K Fluorescence emission and excitation spectra of isolated pigment binding complexes. Panel A/B:77K fluorescence emission spectra of B2-3 (A) and B4-5 (B) fractions, upon excitation at 440 nm. (C/D) 77K fluoresce excitation spectra of B2-3 (C) and B4-5 (D) fractions. Emission wavelengths were set at 680 nm for B2 and B3, 687 for B4 and 715 for B5 fractions.*

The traces of astaxanthin found in LHC proteins (Table 1) do not influence the fluorescence properties of these fractions. PSII-core fractions (B4) from both G and O

samples were characterized by an emission spectrum peaking at 686 nm and an excitation spectrum almost absent of Chl b contribution, as expected for a PSII-core. Even in this case, astaxanthin binding to PSII core did not influence the fluorescence properties of the complex. PSI-LHCI complex (B5) isolated from G cells presented two separated peaks; a major peak at 715 nm related to emission from the low energy Chls bound to the complex, and a minor peak at 680 nm associated to partially dissociated antenna proteins. In PSI-LHCI from O cells, the 680 nm emission peak was more dominant than the 715 nm peak, suggesting a higher proportion of detached LHCI subunits. The excitation spectra of the 715 nm emission peaks associated to the intact PSI-LHCI complex were similar for both G and O samples. Astaxanthin binding to the different complexes does not alter the energy of the emitting state, but could be involved in a partial disconnection of LHC proteins from PSI core complex. Excitation energy transfer dynamics were subsequently investigated by time resolved fluorescence spectroscopy with a streak camera based set up. Streak camera detection allows simultaneous acquisition of fluorescence decays at different wavelengths. The resulting datasets were analyzed by global analysis, resulting in decay associated spectra (DAS) for each sample – wavelength dependent amplitudes for each time-constant in a multi-exponential decay (Van Stokkum *et al.*, 2004). DAS identified in each sample were normalized to the total DAS amplitude of that sample. As reported in Figure 6, two components were sufficient to fit B2 and B3 decays, with a shorter redder component at ~ 200 ps ($DAS1_{B2/3}$) and a longer bluer component at ~4 ns ($DAS2_{B2/3}$). $DAS1_{B2/3}$ and $DAS2_{B2/3}$ could be assigned to two different LHC protein conformations with different non photochemical quenching properties, as previously reported (Moya *et al.*, 2001).

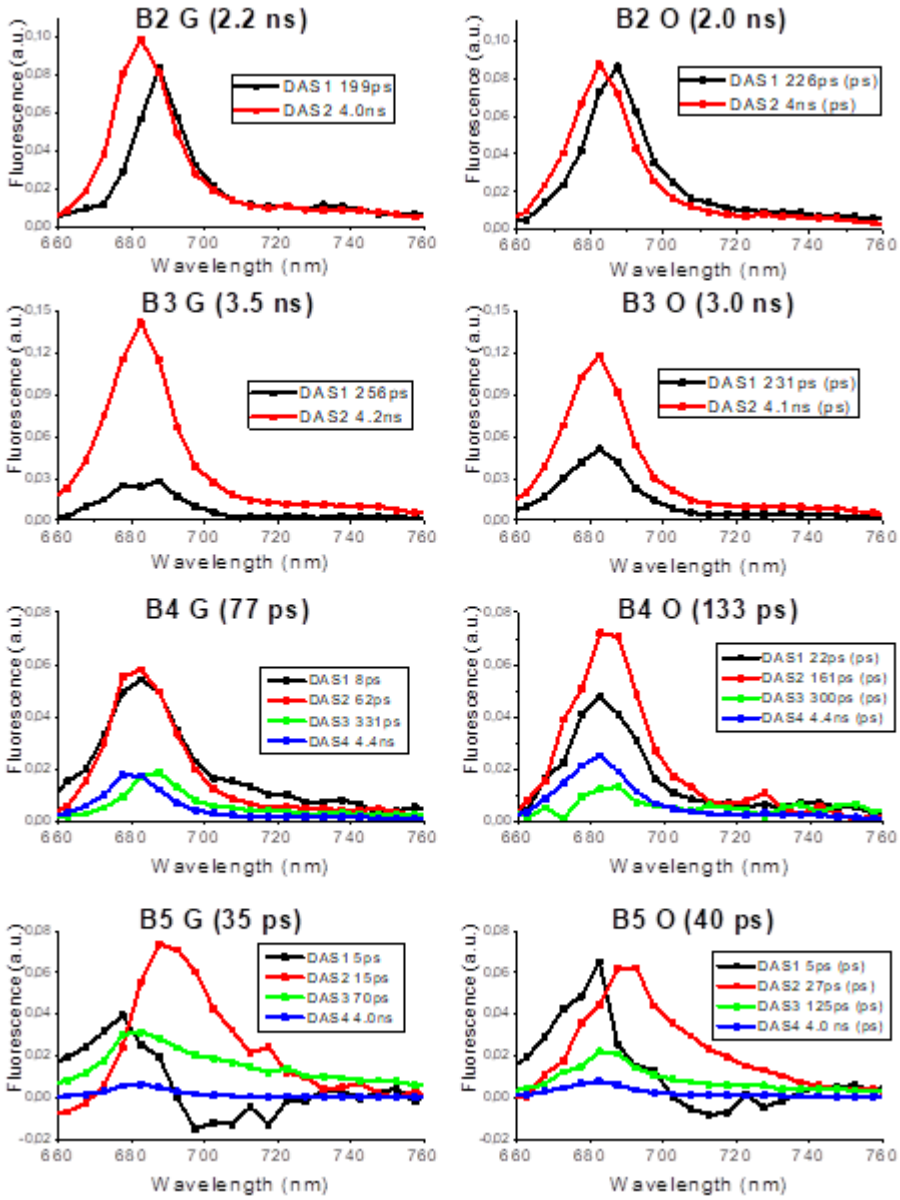

Figure 6. *Decay Associated Spectra (DAS) resulting from Global Analysis of fluorescence decay maps of isolated pigment binding complexes. 2D Streak camera maps were fitted with a multi-exponential decay function with a Global Analysis approach. The resulting wavelength dependent amplitudes, $A_i(\lambda)$, are referred to as Decay Associated Spectra (DAS), with each DAS being associated with a particular exponential decay constant, τ_i. Decay Associated Spectra (DAS) of each sample are reported with associated decay constants indicated in the legend. Average fluorescence lifetimes for each sample is reported in brackets and calculated as $\Sigma A_i\tau_i/\Sigma A_i$. Two exponential decay components were required to adequately fit the decay maps recorded for B2 and B3, whilst four were required for B4 and B5.*

DAS1 was higher in B2 than in B3 fractions and stronger in O than in G samples, indicating stronger quenching properties in B2 and in O samples. Accordingly, average fluorescence decay times (τ_{AV}) were shorter in B2 than in B3 fractions and in O than in G samples (Figure 6). The results obtained in the case of B2 and B3 are consistent with fluorescence decay kinetics of LHC monomers and LHCII trimers respectively (Moya *et al.*, 2001; Xu *et al.*, 2015). The reduced τ_{AV} observed in the case of O fractions is unlikely to be related to the traces of astaxanthin or zeaxanthin bound to the complexes, but rather to varying protein compositions of these fractions induced by the different growth conditions and accumulation of protein subunits with stronger quenching properties (Moya *et al.*, 2001). In the case of B4 fractions, four DAS were identified. Differences were found mainly in the first two fast decaying $DAS1_{B4}$ and $DAS2_{B4}$, with decay constants of 8/22 ps, and 62/161 ps for Green/Orange B4 respectively. $DAS1_{B4}$ and $DAS2_{B4}$ amplitudes were similar in G samples, while in O samples $DAS2_{B4}$ had an increased weight as compared to $DAS1_{B4}$. $DAS3_{B4}$ and $DAS4_{B4}$ on the other hand exhibited similar time constants (300 ps and 4.4 ns respectively) in both G and O samples, with $DAS4_{B4}$ being more represented in O samples. DAS1-4_{B4} identified for B4 are consistent with components previously reported for PSII core complexes, even if it is difficult to associate components unambiguously to Chl or protein moieties (Caffarri *et al.*, 2011). Only the weak 4.4 ns component ($DAS4_{B4}$), most clearly visible in the O sample, can be safely associated to partially detached antenna proteins or free Chls found in B4. A 77 ps τ_{AV} was calculated for B4 isolated from G cells, consistent with previous reports for PSII core (van Amerongen and Croce, 2013). The longer τ_{AV} determined in the case of B4 isolated from O cells (136 ps) suggests that excitation energy transfer to the PSII reaction center is partially disturbed in this complex. Four DAS components were also identified for the PSI-LHCI complexes (B5). In particular a short (5 ps) component, $DAS1_{B5}$, with positive/negative amplitude was found in both G and O PSI-LHCI complexes and are attributed to energy equilibration within the complex (Wientjes *et al.*, 2011). The 13 ps $DAS2_{B5}$ found in B5 from G samples has been usually associated to emission from PSI-core. In the case of B5 from O cells, $DAS2_{B5}$ is characterized by time constant of 27 ps which is longer than that in G samples and thus indicates an alteration of excitation energy transfer to the reaction center. $DAS3_{B5}$ found in the B5 fraction from G cells has a time constant of 70 ps and a spectrum which is more enriched in forms emitting above 700 nm. This component is related to energy transfer from

peripheral LHCI complexes. In PSI-LHCI from O cells, the time constant associated with $DAS3_{B5}$ is increased to 125 ps whilst the DAS amplitude is reduced. This indicated some alterations in energy transfer from antenna complexes to the PSI reaction center. Finally, a small 4 ns component ($DAS4_{B5}$) was identified in both B5 fractions from G and O cells, and was attributed to detached antenna proteins as previously observed in PSI-LHCI preparations (Wientjes *et al.*, 2011; Croce and Van Amerongen, 2013; Jennings *et al.*, 2013; Ballottari *et al.*, 2014; Le Quiniou *et al.*, 2015*b*). This ns component was almost 50% stronger in PSI-LHCI from O cells. Astaxanthin binding PSI-LHCI complexes from O cells were thus characterized by reduced excitation energy transfer to the reaction center from both the Chl moieties bound to the core complex and to the peripheral antenna proteins. They also contain a higher amount of partially disconnected LHCI proteins emitting in the ns time range, in agreement with the low temperature emission florescence spectra reported in Figure 5. In the case of PSI-LHCI, the photochemical efficiency (ϕPSI) of the complex can be estimated from the τ_{AV} (35 and 40 ps respectively for G and O samples), which in turn can be interpreted as the time required to transfer energy to the reaction center of the complex. ϕPSI calculated from PSI-LHCI τ_{AV} and disregarding the ns component (as previously reported in Wientjes *et al.* (2011)) were in both cases higher than 98%. Inclusion of the ns component reduced the excitation energy transfer efficiency to 92% and 95% for the O and G samples respectively. Astaxanthin binding PSI-LHCI is thus characterized by a partial disconnection of LHCI proteins, whilst maintaining more than 90% of excitation energy transfer efficiency, as previously observed for PSI-LHCI complexes (Croce and Van Amerongen, 2013; Le Quiniou *et al.*, 2015*b*,*a*).

Photoprotective functions of astaxanthin in the plastids

The photoprotective role of astaxanthin bound to Chl binding subunits was evaluated by measuring $^1O_2$ production under high irradiance (2000 µmol $m^{-2}s^{-1}$) of red light (>600 nm) and application of a fluorescent probe (Singlet Oxygen Sensor Green, SOSG) whose fluorescence increases upon $^1O_2$ production (Flors *et al.*, 2006). The use of red light, which is absorbed only by Chls, enables selective investigation of the photoprotective role of astaxanthin without regard to its absorption properties (Dall'Osto *et al.*, 2012; Ballottari *et al.*, 2013). As reported in Figure 7, after 30 minutes of illumination no

significant differences were observed among G and O B2, B3 and B4 fractions (Figure 7A-C).

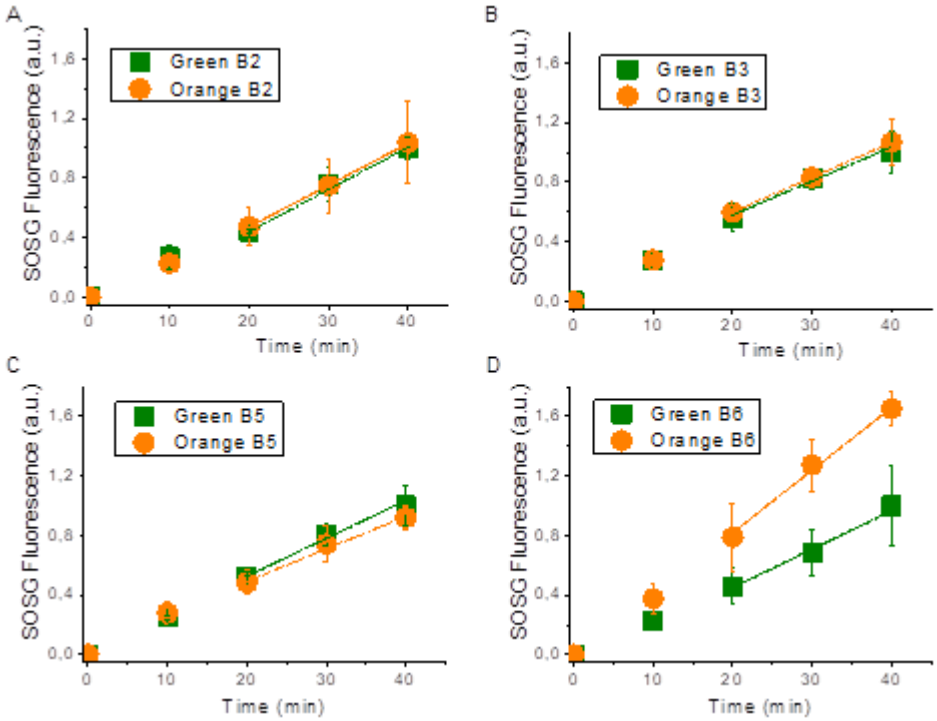

Figure 7: *Singlet oxygen production in isolated complexes upon red light treatment***.** *Singlet oxygen production was indirectly determined following the increase of fluorescence of Singlet Oxygen Sensor Green (SOSG), a fluorescent probe increasing its fluorescence in presence of singlet oxygen. Isolated complexes were illuminated with red light at 2000 µmol* $m^{-2}s^{-1}$*. All data were normalized to chlorophyll content and to the SOSG fluorescence of the green samples after 40' of illumination. Standard deviations are indicated in each panel (n=3).*

In the case of PSI-LHCI complexes, O B5 showed a higher $^1O_2$ production than G B5 (Figure 7D). This can be explained by the presence of some antenna proteins in O B5 which transfer excitation energy less efficiently to the PSI reaction center, in agreement with 77K steady state and time resolved fluorescence results: these antenna proteins are more prone to produce ROS upon high light illumination. In every case tested, no significant improvements in photoprotection were attributable to astaxanthin binding. Since most of the astaxanthin was found not bound to Photosystems, the same SOSG analysis was performed on isolated membranes illuminated with red light at 6000 µmol $m^{-2}s^{-1}$ for 40 minutes (Figure 8A).

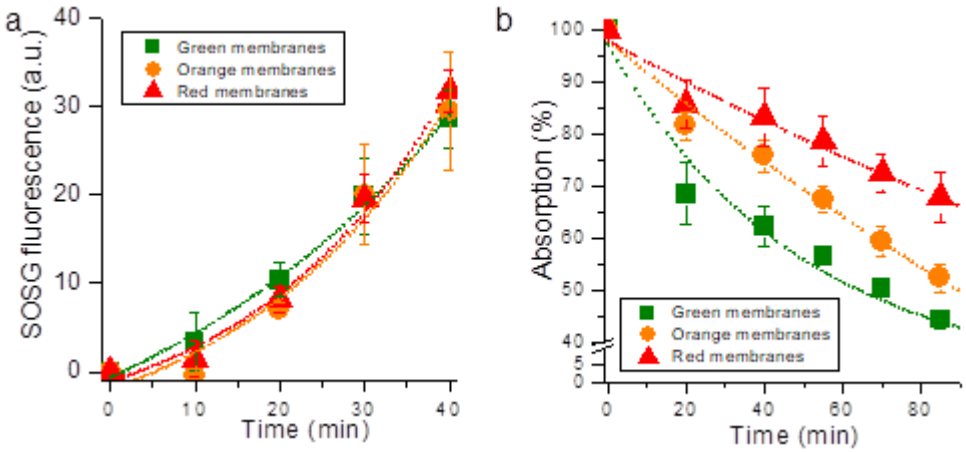

Figure 8. *Singlet oxygen production and chlorophyll photo-bleaching in isolated membranes. (A) Singlet oxygen production indirectly determined following the increase of fluorescence of Singlet Oxygen Sensor Green (SOSG), a fluorescent probe increasing its fluorescence in presence of singlet oxygen. Isolated membranes were illuminated with red light at 6000 µmol $m^{-2}s^{-1}$. All data were normalized to chlorophyll content and to the SOSG fluorescence of green membranes after 30' of illumination. (B) Chlorophylls photo-bleaching induced in isolated membranes upon illumination with white light at 6000 µmol $m^{-2}s^{-1}$. Standard deviations are indicated in both panels (n=3).*

Despite the huge amount of astaxanthin in O and R membranes, $^1O_2$ production comparable with G thylakoids was found after normalization to Chl content, suggesting a minor role of astaxanthin as scavenger of $^1O_2$. Moreover, astaxanthin in plastids could act as a light filter: in order to investigate this point, Chl bleaching was measured in these membranes upon white light treatment at 6000 µmol $m^{-2}s^{-1}$. As reported in Figure 8B, Chl absorption in G thylakoids was reduced by 60% after 80 minutes due to Chl degradation, while the O and R Chl bleaching kinetics were much slower, especially in the case of R samples. Astaxanthin thus improves photoprotection in thylakoid membranes only through its absorption properties, acting as a light filter.

Discussion

In this work, we presented the biochemical and spectroscopic properties of photosynthetic complexes responsible for light harvesting and energy conversion in *H. pluvialis*. In the case of cells grown in control conditions (G), monomeric and trimeric LHC proteins isolated from *H. pluvialis* present features consistent with previous report for LHC proteins purified from *A. thaliana* or *C. reinhardtii*. Interestingly, monomeric

LHC proteins from *H. pluvialis* were characterized by a shorter fluorescence lifetime as compared to LHCII trimers. This finding is likely related to a somewhat different protein composition of B2 fractions as compared to B3 (Figure 4), with B2 containing some LHC proteins more abundant in monomeric form, such as the minor monomeric LHC subunits identified in *A. thaliana* (Lhcb4-6 subunits) and *C. reinhardtii* (CP26 and CP29) (Moya *et al.*, 2001; van Amerongen and Croce, 2013). PSII core complexes were also isolated and analyzed, demonstrating conservation of pigment binding properties and similar biochemical and spectroscopic properties as compared to PSII cores purified from cyanobacteria or higher plants. The evolution of the photosynthetic process therefore mainly addressed the peripheral light harvesting complexes rather than core complexes (Croce and Van Amerongen, 2013; van Amerongen and Croce, 2013). In the case of PSI-LHCI, 77K fluorescence demonstrates that *H. pluvialis* lacks Lhca proteins with so called "red-forms" which emit above 730 nm and are found in higher plants but not in green algae (Croce and Van Amerongen, 2013; Le Quiniou *et al.*, 2015*b*). It is postulated that the absence of far red light in water did not lead microalgae to evolve LHC proteins which absorb above 700 nm. Chl a/b and Chl/Car ratios measured in the case of B5 fractions suggest the presence of 5 Lhca proteins per reaction center, however additional biochemical and structural work is required to support this hypothesis. Nevertheless, the PSI functional antenna size measured following P700 oxidation kinetics indicated an intermediate value between *A. thaliana* (4 Lhca per P700) (Ben-Shem *et al.*, 2003) and *C. reinhardtii* (7/9 Lhca per P700) (Stauber *et al.*, 2009; Le Quiniou *et al.*, 2015*b*) (Supplemental data, Figure S2). *H. pluvialis* PSI-LHCI was characterized by a very short τ_{AV} (<40ps), indicating a ϕPSI higher than 98% and consistent with similar analysis performed on PSI-LHCI complexes purified from other organisms (Wientjes *et al.*, 2011; Le Quiniou *et al.*, 2015*b*). The photosynthetic machinery is reorganized when *H. pluvialis* cells are stressed and astaxanthin is accumulated. Oxidative stress and ROS accumulation are indeed the triggers for activation of the astaxanthin biosynthetic pathway, with β-carotene over-production in the chloroplast followed by export to the cytosol and conversion to astaxanthin. In particular, while the different enzymes involved in β-carotene accumulation are localized in the plastids, the key enzyme β-carotene oxygenase (CRTO), which produces astaxanthin from β-carotene or zeaxanthin, was found both in the plastid and in lipid vesicles in the cytosol, despite its activity only having been previously reported in the

cytosol compartment (Grunewald *et al.*, 2001). Our findings of traces of astaxanthin in the plastids suggests that a low activity of CRTO was present also in these organelles. The photosynthetic machinery continues to work even in cysts (Scibilia *et al.*, 2015), but the chloroplasts reduce their volume and the thylakoid membranes become degraded (Collins *et al.*, 2011; Wayama *et al.*, 2013). In this work, we demonstrated that acclimation to high light induced a destabilization of the PSI-LHCI supercomplex and PSII core, especially after six days of high irradiance (Figure 1). Rapid turnover of PSII core subunits is likely to be the reason for the rapid destabilization observed for the PSII core. In addition, isolated PSII cores from O cells were characterized by a slower excitation energy transfer to the reaction center. In the PSII core complex, β-carotene molecules are in close contact with Chls and are required for effective quenching of ^{3}Chl* and scavenging of $^{1}O_2$ produced during charge recombination. Therefore, depletion of β-carotene produces a strong photooxidation in both PSII and PSI core complexes (Cazzaniga *et al.*, 2012). In the case of PSI-LHCI, high light acclimation caused a destabilization of the interaction between peripheral antenna complexes and PSI core, as demonstrated by both 77K steady state and time resolved fluorescence. Moreover, the reduced energy connection between antenna proteins and PSI reaction center decreased the photochemical quenching of the LHCI proteins, exposing them to a higher risk of photooxidation, as measured using SOSG (Figure 7). The molecular mechanism by which PSII core and PSI-LHCI are destabilized cannot be easily identified and additional work is required to elucidate this point. The loss and partial substitution of β-carotene with astaxanthin in PSII core and PSI-LHCI could however be involved in the destabilization of Photosystems. Astaxanthin binding to Photosystems I been reported for Chlrophyceae species such as *Eremosphaera viridis* (Vechtel *et al.*, 1992), however no information was available for the main species used in astaxanthin production, *H. pluvialis*. *H. pluvialis* astaxanthin binding complexes were not more photoprotected as compared to the control samples and their excitation energy transfer dynamics were even slower when compared to the same complexes isolated in the absence of astaxanthin. It is thus difficult to claim that astaxanthin binding to PSI or PSII has a photoprotective role. However, considering the higher level of $^{1}O_2$ produced in astaxanthin binding PSI-LHCI and the similar $^{1}O_2$ production observed in isolated membranes, it cannot be excluded that astaxanthin found free in the thylakoid membranes could have a role as scavenger of $^{1}O_2$ produced by Photosystems. Rather,

considering the important role of β-carotene for the assembly and function of PSI and PSII (Telfer, 2005; Mazor *et al.*, 2017), its substitution by astaxanthin could be the key to core complex destabilization. Indeed, astaxanthin was found in PSI and PSII cores even in its esterified form. Interactions between the fatty acids esterified to astaxanthin and the protein subunits of photosystems could impact the interactions at the base of the PSI and PSII assemblies. These results are indeed consistent with the observation of reduced photochemical efficiency in higher plants engineered to accumulate astaxanthin (Hasunuma *et al.*, 2008; Roding *et al.*, 2015; Fujii *et al.*, 2016). Considering the ratio between astaxanthin and Chls in whole cells and in isolated fractions, less than 1% of the total astaxanthin accumulated in *H. pluvialis* was found bound to PSI or PSII, while almost all astaxanthin is accumulated in the cytoplasm. Astaxanthin rich oil droplets accumulated in the cytoplasm could have a specific role as antioxidants to protect the nucleus. Moreover, the astaxanthin oil droplets act as a light filter, reducing the excitation pressure on photosynthetic subunits and their risk of photodamage (Figure 8B) (Scibilia *et al.*, 2015). The presence of astaxanthin in *H. pluvialis*, even in photosynthetic pigment binding complexes, raises the question whether these astaxanthin molecules are synthetized in the plastid or, perhaps more likely, in the cytoplasm and then imported back to the plastid.

References

Aflalo C, Meshulam Y, Zarka A, Boussiba S. 2007. On the relative efficiency of two- vs. one-stage production of astaxanthin by the green alga *Haematococcus pluvialis*. Biotechnology and bioengineering **98**, 300–305.

Ambati RR, Phang S-M, Ravi S, Aswathanarayana RG. 2014. Astaxanthin: Sources, Extraction, Stability, Biological Activities and Its Commercial Applications—A Review. Marine Drugs **12**, 128–152.

van Amerongen H, Croce R. 2013. Light harvesting in photosystem II. Photosynthesis Research **116**, 251–263.

Ballottari M, Alcocer MJP, D'Andrea C, Viola D, Ahn TK, Petrozza A, Polli D, Fleming GR, Cerullo G, Bassi R. 2014. Regulation of photosystem I light harvesting by zeaxanthin. Proceedings of the National Academy of Sciences **111**, E2431–E2438.

Ballottari M, Govoni C, Caffarri S, Morosinotto T. 2004. Stoichiometry of LHCI antenna polypeptides and characterization of gap and linker pigments in higher plants Photosystem I. European Journal of Biochemistry **271**, 4659–4665.

Ballottari M, Mozzo M, Croce R, Morosinotto T, Bassi R. 2009. Occupancy and Functional Architecture of the Pigment Binding Sites of Photosystem II Antenna Complex Lhcb5. Journal of Biological Chemistry **284**, 8103–8113.

Ballottari M, Mozzo M, Girardon J, Hienerwadel R, Bassi R. 2013. Chlorophyll Triplet Quenching and Photoprotection in the Higher Plant Monomeric Antenna Protein Lhcb5. The Journal of Physical Chemistry B **117**, 11337–11348.

Ben-Shem A, Frolow F, Nelson N. 2003. Crystal structure of plant photosystem I. Nature **426**, 630–635.

Bonente G, Pippa S, Castellano S, Bassi R, Ballottari M. 2012. Acclimation of *Chlamydomonas reinhardtii* to different growth irradiances. Journal of Biological Chemistry **287**, 5833–5847.

Boussiba S, Vonshak A. 1991. Astaxanthin Accumulation in the Green Alga *Haematococcus pluvialis*. Plant and Cell Physiology **32**, 1077–1082.

Caffarri S, Broess K, Croce R, van Amerongen H. 2011. Excitation energy transfer and trapping in higher plant Photosystem II complexes with different antenna sizes. Biophysical journal **100**, 2094–2103.

Caffarri S, Croce R, Breton J, Bassi R. 2001. The major antenna complex of photosystem II has a xanthophyll binding site not involved in light harvesting. Journal of Biological Chemistry **276**, 35924–35933.

Caffarri S, Kouřil R, Kereïche S, Boekema EJ, Croce R. 2009. Functional architecture of higher plant photosystem II supercomplexes. The EMBO Journal **28**, 3052–3063.

Cazzaniga S, Dall'Osto L, Szaub J, Scibilia L, Ballottari M, Purton S, Bassi R. 2014. Domestication of the green alga *Chlorella sorokiniana*: reduction of antenna size improves light-use efficiency in a photobioreactor. Biotechnology for Biofuels **7**, 157.

Cazzaniga S, Li Z, Niyogi KK, Bassi R, Dall'Osto L. 2012. The *Arabidopsis* szl1 mutant reveals a critical role of beta-carotene in photosystem I photoprotection. Plant physiology **159**, 1745–1758.

Cinque G, Croce R, Bassi R. 2000. Absorption spectra of chlorophyll a and b in Lhcb protein environment. Photosynthesis Research **64**, 233–242.

Collins AM, Jones HDT, Han D, Hu Q, Beechem TE, Timlin JA. 2011. Carotenoid Distribution in Living Cells of *Haematococcus pluvialis* (Chlorophyceae). PLOS ONE **6**, e24302.

Croce R, Van Amerongen H. 2013. Light-harvesting in photosystem I. Photosynthesis Research **116**, 153–166.

Dall'Osto L, Holt NE, Kaligotla S, Fuciman M, Cazzaniga S, Carbonera D, Frank HA, Alric J, Bassi R. 2012. Zeaxanthin protects plant photosynthesis by modulating chlorophyll triplet yield in specific light-harvesting antenna subunits. Journal of Biological Chemistry **287**, 41820–41834.

Daubrawa F, Sies H, Stahl W. 2005. Astaxanthin diminishes gap junctional intercellular communication in primary human fibroblasts. The Journal of Nutrition **135**, 2507–2511.

Drop B, Webber-Birungi M, Yadav SKN, Filipowicz-Szymanska A, Fusetti F, Boekema EJ, Croce R. 2014. Light-harvesting complex II (LHCII) and its supramolecular organization in *Chlamydomonas reinhardtii*. Biochimica et biophysica acta **1837**, 63–72.

Fan L, Vonshak A, Zarka A, Boussiba S. 1998. Does astaxanthin protect *Haematococcus* against light damage? Zeitschrift fur Naturforschung. C, Journal of biosciences **53**, 93–100.

Fiore A, Dall'Osto L, Cazzaniga S, Diretto G, Giuliano G, Bassi R. 2012. A quadruple mutant of *Arabidopsis* reveals a β-carotene hydroxylation activity for LUT1/CYP97C1 and a regulatory role of xanthophylls on determination of the PSI/PSII ratio. BMC Plant Biology **12**, 50.

Flors C, Fryer MJ, Waring J, Reeder B, Bechtold U, Mullineaux PM, Nonell S, Wilson MT, Baker NR. 2006. Imaging the production of singlet oxygen in vivo using a new fluorescent sensor, Singlet Oxygen Sensor Green®. Journal of Experimental Botany **57**, 1725–1734.

Fujii R, Yamano N, Hashimoto H, Misawa N, Ifuku K. 2016. Photoprotection vs. photoinhibition of photosystem II in transplastomic lettuce (Lactuca sativa) dominantly accumulating astaxanthin. Plant and Cell Physiology **57**, 1518–1529.

Gao Z, Meng C, Zhang X, Xu D, Miao X, Wang Y, Yang L, Lv H, Chen L, Ye N. 2012*a*. Induction of salicylic acid (SA) on transcriptional expression of eight carotenoid genes and astaxanthin accumulation in *Haematococcus pluvialis*. Enzyme and Microbial Technology **51**, 225–230.

Gao Z, Meng C, Zhang X, Xu D, Zhao Y, Wang Y, Lv H, Yang L, Chen L, Ye N. 2012*b*. Differential expression of carotenogenic genes, associated changes on astaxanthin production and photosynthesis features induced by JA in *H. pluvialis*. PLOS ONE **7**, 1–9.

Grewe S, Ballottari M, Alcocer M, D'Andrea C, Blifernez-Klassen O, Hankamer B, Mussgnug JH, Bassi R, Kruse O. 2014. Light-Harvesting Complex Protein LHCBM9 Is Critical for Photosystem II Activity and Hydrogen Production in *Chlamydomonas reinhardtii*. The Plant cell **26**, 1598–1611.

Grunewald K, Eckert M, Hirschberg J, Hagen C. 2000. Phytoene desaturase is localized exclusively in the chloroplast and up-regulated at the mRNA level during accumulation of secondary carotenoids in *Haematococcus pluvialis* (Volvocales, chlorophyceae). Plant physiology **122**, 1261–1268.

Grunewald K, Hirschberg J, Hagen C. 2001. Ketocarotenoid biosynthesis outside of plastids in the unicellular green alga *Haematococcus pluvialis*. The Journal of biological chemistry **276**, 6023–6029.

Gu W, Li H, Zhao P, Yu R, Pan G, Gao S, Xie X, Huang A, He L, Wang G. 2014. Quantitative proteomic analysis of thylakoid from two microalgae (*Haematococcus pluvialis* and *Dunaliella salina*) reveals two different high light-responsive strategies. Scientific Reports **4**, 6661.

Gu W, Xie X, Gao S, Zhou W, Pan G, Wang G. 2013. Comparison of different cells of *Haematococcus pluvialis* reveals an extensive acclimation mechanism during its aging process: from a perspective of photosynthesis. PloS one **8**, e67028.

Guerin M, Huntley ME, Olaizola M. 2003. *Haematococcus* astaxanthin: applications for human health and nutrition. Trends in Biotechnology **21**, 210–216.

Hasunuma T, Miyazawa S-I, Yoshimura S, Shinzaki Y, Tomizawa K-I, Shindo K, Choi S-K, Misawa N, Miyake C. 2008. Biosynthesis of astaxanthin in tobacco leaves by transplastomic engineering. The Plant journal : for cell and molecular biology **55**, 857–868.

Hong M-E, Hwang SK, Chang WS, Kim BW, Lee J, Sim SJ. 2015. Enhanced autotrophic astaxanthin production from *Haematococcus pluvialis* under high temperature via heat stress-driven Haber-Weiss reaction. Applied microbiology and biotechnology **99**, 5203–5215.

Jennings RC, Zucchelli G, Santabarbara S. 2013. Photochemical trapping heterogeneity as a function of wavelength, in plant photosystem I (PSI-LHCI). Biochimica et biophysica acta **1827**, 779–785.

Johnson MP, Havaux M, Triantaphylidès C, Ksas B, Pascal AA, Robert B, Davison PA, Ruban A V, Horton P. 2007. Elevated Zeaxanthin Bound to Oligomeric LHCII Enhances the Resistance of Arabidopsis to Photooxidative Stress by a Lipid-protective, Antioxidant Mechanism. Journal of Biological Chemistry **282**, 22605–22618.

Jordan P, Fromme P, Witt HT, Klukas O, Saenger W, Krauß N. 2001. Three-dimensional structure of cyanobacterial photosystem I at 2.5 Å resolution. Nature **411**, 909.

Kobayashi M, Katsuragi T, Tani Y. 2001. Enlarged and astaxanthin-accumulating cyst cells of the green alga *Haematococcus pluvialis*. Journal of Bioscience and Bioengineering **92**, 565–568.

Kurashige M, Okimasu E, Inoue M, Utsumi K. 1990. Inhibition of oxidative injury of biological membranes by astaxanthin. Physiological chemistry and physics and medical NMR **22**, 27–38.

Lagarde D, Beuf L, Vermaas W. 2000. Increased production of zeaxanthin and other pigments by application of genetic engineering techniques to *Synechocystis* sp. strain PCC 6803. Applied and environmental microbiology **66**, 64–72.

Lemoine Y, Schoefs B. 2010. Secondary ketocarotenoid astaxanthin biosynthesis in algae: a multifunctional response to stress. Photosynthesis research **106**, 155–177.

Li K, Cheng J, Ye Q, He Y, Zhou J, Cen K. 2017. *In vivo* kinetics of lipids and astaxanthin evolution in *Haematococcus pluvialis* mutant under 15% CO2 using Raman microspectroscopy. Bioresource technology **244**, 1439—1444.

Liu Z, Yan H, Wang K, Kuang T, Zhang J, Gui L, An X, Chang W. 2004. Crystal structure of spinach major light-harvesting complex at 2.72 Å resolution. Nature **428**, 287.

Mazor Y, Borovikova A, Caspy I, Nelson N. 2017. Structure of the plant photosystem I supercomplex at 2.6 A resolution. Nature plants **3**, 17014.

Mazor Y, Borovikova A, Nelson N. 2015. The structure of plant photosystem I super-complex at 2.8 Å resolution. eLife **4**.

Moya I, Silvestri M, Vallon O, Cinque G, Bassi R. 2001. Time-resolved fluorescence analysis of the photosystem II antenna proteins in detergent micelles and liposomes. Biochemistry **40**, 12552–12561.

Phillip D, Hobe S, Paulsen H, Molnar P, Hashimoto H, Young AJ. 2002. The Binding of Xanthophylls to the Bulk Light-harvesting Complex of Photosystem II of Higher Plants: A specific requirement for carotenoids with a 3-hydroxy-β-end group . Journal of Biological Chemistry **277**, 25160–25169.

Qin X, Suga M, Kuang T, Shen J-R. 2015. Photosynthesis. Structural basis for energy transfer pathways in the plant PSI-LHCI supercomplex. Science (New York, N.Y.) **348**, 989–995.

Le Quiniou C, van Oort B, Drop B, van Stokkum IHM, Croce R. 2015*a*. The high efficiency of Photosystem I in the green alga *Chlamydomonas reinhardtii* is maintained after the antenna size is substantially increased by the association of Light-harvesting Complexes II. Journal of Biological Chemistry **290**, 30587–30595.

Le Quiniou C, Tian L, Drop B, Wientjes E, van Stokkum IHM, van Oort B, Croce R. 2015*b*. PSI-LHCI of *Chlamydomonas reinhardtii*: Increasing the absorption cross section without losing efficiency. Biochimica et biophysica acta **1847**, 458–467.

Roding A, Dietzel L, Schlicke H, Grimm B, Sandmann G, Buchel C. 2015. Production of ketocarotenoids in tobacco alters the photosynthetic efficiency by reducing photosystem II supercomplex and LHCII trimer stability. Photosynthesis research **123**, 157–165.

Schagger H, von Jagow G. 1987. Tricine-sodium dodecyl sulfate-polyacrylamide gel electrophoresis for the separation of proteins in the range from 1 to 100 kDa. Analytical biochemistry **166**, 368–379.

Scibilia L, Girolomoni L, Berteotti S, Alboresi A, Ballottari M. 2015. Photosynthetic response to nitrogen starvation and high light in *Haematococcus pluvialis*. Algal Research **12**, 170–181.

Shah MMR, Liang Y, Cheng JJ, Daroch M. 2016. Astaxanthin-producing green microalga *Haematococcus pluvialis*: From single cell to high value commercial products. Frontiers in Plant Science **7**, 531.

Stahl W, Sies H. 2005. Bioactivity and protective effects of natural carotenoids. Biochimica et Biophysica Acta - Molecular Basis of Disease **1740**, 101–107.

Stauber EJ, Busch A, Naumann B, Svatos A, Hippler M. 2009. Proteotypic profiling of LHCI from *Chlamydomonas reinhardtii* provides new insights into structure and function of the complex. Proteomics **9**, 398–408.

Van Stokkum IHM, Larsen DS, Van Grondelle R. 2004. Global and target analysis of time-resolved spectra. Biochimica et Biophysica Acta - Bioenergetics **1657**, 82–104.

Su Y, Wang J, Shi M, Niu X, Yu X, Gao L, Zhang X, Chen L, Zhang W. 2014. Metabolomic and network analysis of astaxanthin-producing *Haematococcus pluvialis* under various stress conditions. Bioresource technology **170**, 522–529.

Telfer A. 2005. Too much light? How β-carotene protects the

photosystem II reaction centre. Photochemical & Photobiological Sciences **4**, 950–956.

Terao J. 1989. Antioxidant activity of β-carotene-related carotenoids in solution. Lipids **24**, 659–661.

Tokutsu R, Iwai M, Minagawa J. 2009. CP29, a monomeric light-harvesting complex II protein, is essential for state transitions in *Chlamydomonas reinhardtii*. Journal of Biological Chemistry **284**, 7777–7782.

Vechtel B, Pistorius EK, Ruppel HG. 1992. Occurrence of Secondary Carotenoids in PS I Complexes Isolated from *Eremosphaera viridis* De Bary (Chlorophyceae). **56**, 51–56.

Wan M, Zhang J, Hou D, Fan J, Li Y, Huang J, Wang J. 2014. The effect of temperature on cell growth and astaxanthin accumulation of *Haematococcus pluvialis* during a light-dark cyclic cultivation. Bioresource technology **167**, 276–283.

Wang S-B, Chen F, Sommerfeld M, Hu Q. 2004. Proteomic analysis of molecular response to oxidative stress by the green alga *Haematococcus pluvialis* (Chlorophyceae). Planta **220**, 17–29.

Wang J, Sommerfeld M, Hu Q. 2009. Occurrence and environmental stress responses of two plastid terminal oxidases in *Haematococcus pluvialis* (Chlorophyceae). Planta **230**, 191–203.

Wayama M, Ota S, Matsuura H, Nango N, Hirata A, Kawano S. 2013. Three-Dimensional ultrastructural study of oil and astaxanthin accumulation during encystment in the green alga *Haematococcus pluvialis*. PLOS ONE **8**, e53618.

Wehner A, Storf S, Jahns P, Schmid VHR. 2004. De-epoxidation of violaxanthin in Light-harvesting Complex I proteins. Journal of Biological Chemistry **279**, 26823–26829.

Wei X, Su X, Cao P, Liu X, Chang W, Li M, Zhang X, Liu Z. 2016. Structure of spinach photosystem II-LHCII supercomplex at 3.2 A resolution. Nature **534**, 69–74.

Wientjes E, Van Stokkum IHM, Van Amerongen H, Croce R. 2011. Excitation-energy transfer dynamics of higher plant photosystem i light-harvesting complexes. Biophysical Journal **100**, 1372–1380.

Xu P, Tian L, Kloz M, Croce R. 2015. Molecular insights into Zeaxanthin-dependent quenching in higher plants. Scientific Reports **5**, 13679.

Yuan J-P, Peng J, Yin K, Wang J-H. 2011. Potential health-promoting effects of astaxanthin: a high-value carotenoid mostly from microalgae. Molecular nutrition & food research **55**, 150–165.

Zhong Y-J, Huang J-C, Liu J, Li Y, Jiang Y, Xu Z-F, Sandmann G, Chen F. 2011. Functional characterization of various algal carotenoid ketolases reveals that ketolating zeaxanthin efficiently is essential for high production of astaxanthin in transgenic *Arabidopsis*. Journal of experimental botany **62**, 3659–3669.

Supplementary data

Figure S1. Absorption spectra of B1 fraction isolated from H. pluvialis.

Absorption spectra of B1, fractions (Figure 1D) were normalized to the maximum absorption peak in the 600 nm and 700 nm region.

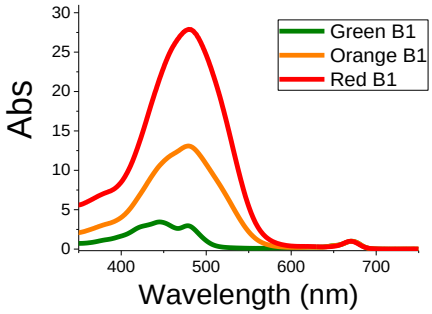

Figure S2. Functional antenna size of Photosystem I in H. pluvialis compared to Arabidopsis thaliana and Chlamydomonas reinhardtii.

(A) P700 oxidation kinetics measured on whole cells in presence of DCMU and DBMIB, in order to block linear and cyclic electron transfer, and ascorbate and methyl viologen as electron donor and acceptor. Measurements were performed at 12 µmol $m^{-2}s^{-1}$. Traces representative of 5 independent biological replicates are reported. (B)Functional antenna size of PSI-LHCI calculated as $1/\tau_{2/3}$, where $\tau_{2/3}$ is the time required to reach 2/3 of the maximum P700 oxidation. A.t.: Arabidopsis thaliana; C.r.: Chlamydomonas reinhardtii. H.p. G/O: H. pluvialis in Green/Orange stage as in Figure 1 main text. Standard deviations are indicated (n=5).

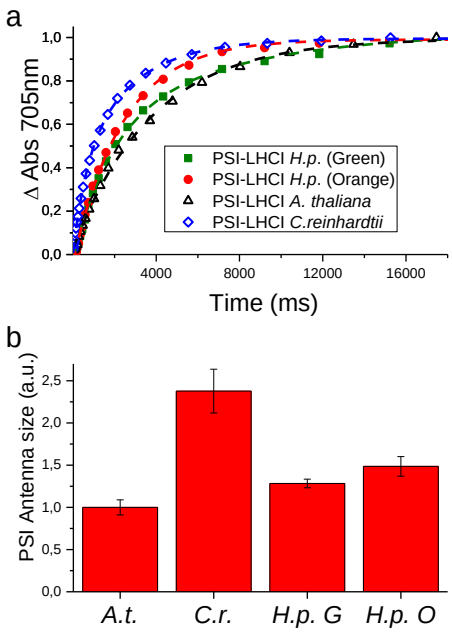

5.Conclusion

The aim of this thesis was to gain a deeper understanding of the Non-Photochemical Quenching regulation in microalgae. In the first part of this project, major attention was focused on the model organism *C. reinhardtii*, due to the large knowledge presents in literature about its genetics and physiology. In *C. reinhardtii*, NPQ is mainly activated by two pigments binding proteins called LHCSR3 and LHCSR1 induced after high light treatment. NPQ can be calculated from quenching of chlorophyll fluorescence, based on room temperature measurements which monitor changes of PSII fluorescence. In this condition, PSI is characterized by a low fluorescence quantum yield preventing analysis in presence of strong fluorescence emission by PSII, explaining why few information about PSI quenching are present in literature. Therefore, NPQ regulation at the level of PSI was studied at 77K, where fluorescence quantum yield is high for both PSI and PSII allowing for proper quantification of both emissions. The role of LHCSRs subunit in quenching of PSI and PSII was investigated in WT and mutant cells (*npq4, npq4 lhcsr1*, *C-lhcsr3-4/24*, *stt7, npq1* and *stt7 npq4)* in quenched and unquenched states. The results presented in this work demonstrate a LHCSR-dependent quenching on PSII and on LHCII bound to PSII-complex, but also on LHC bound to PSI-complex. The LHCSRs quenching activity can occurs at PSII supercomplexes, at LHC complexes bound to PSI or to LHCII "mobile" fraction loosely connected to the Photosystems. Moreover, the PSII and PSI quenching differ in the activation time, where PSII quenches rapidly, while PSI shows a slower activation rate probably due to the time needed to LHCII protein detachment from PSI (Chapter I, section A).

It is important to notice that LHCII proteins, in this contest, could act as interactor with LHCSRs subunits or have a role as quenchers themselves. Their involvement in NPQ regulation was already established in the case of LHCBM1, where knock out mutant showed an impaired NPQ phenotype. In this thesis LHCBM4/6/8 were functionally characterized by analysing their biochemical and spectroscopic features *in vitro* and by studying their function *in vivo* using a reverse genetic approach (Chapter I, section B). *In vitro* analysis of re-folded LHCBM4 and LHCBM6 show a low fluorescence yield, which is modulated by the activity of the concurrent heat dissipation channel, meaning that LHCBM4 and LHCBM6 are characterized by high quenching activity. Phenotypical characterization of silenced strains on *Lhcbm4/6/8* genes confirmed those findings

showing a reduce NPQ amplitude in the mutant strains compared to the WT. All these data confirm their function not only in photon capture, but also in photoprotective mechanisms within a pool of LHCII proteins free or very loosely connected to the PSII supercomplex.

In the second part of this thesis the attention was focused on *C. vulgaris* and *H. pluvialis*, microalgae species use for industrial application, in which a deeper understanding of the regulative mechanisms, could be essential in developing new technology for improve their productivity. For this purpose, the development of new genetics tool based on the identification of potential targets for a biotechnological manipulation is of a strong interest. For this reason, in the Chapter II section A the *C. vulgaris* genome was presented. The combination of several techniques allows the assembly of ~40Mb genome, composed by 14 pseudo-molecules with a GC content comparable to *C. variabilis* or *C. reinhardtii*. The genome assembly data combined with the functional annotation evidenced a horizontal transfer from chloroplast to the mitochondria typical of higher plants but not present in *C. reinhardtii*. Differently from *C. reinhardtii*, *psbs* and *lhcsr*, the main genes related proteins involved in photoprotection in higher plants and microalgae respectively, were found to be expressed in both low and high light. Furthermore, the VDE (violaxanthin de-epoxidase) enzyme, which de-epoxidase violaxanthin into zeaxanthin, was found to be overexpressed in high light, reveling a divergency in the evolution in the green lineage of the enzyme carrying the VDE catalytic activity. In the Chapter II section B, the VDE of *C. vulgaris* was functionally characterized *in vitro* and *in vivo* in order to assess its function in *C. vulgaris.* Multiple alignment of *C. vulgaris* VDE sequences from several organisms showed a high identity compared to *A. thaliana* with the conservation of all the key residues involved in protein structure stability and catalytic activity. *In vitro* expression of the VDE enzyme and enzymatic assay demonstrate its ability in converting violaxanthin into zeaxanthin. *In* vivo measurements show an exponential correlation between the NPQ induction and the zeaxanthin accumulation, activity that is reduced in presence of DTT demonstrating a partial role of zeaxanthin in NPQ induction in *C. vulgaris*.

In the section C and D of the Chapter II we focused our attention on the photosynthetic regulation in stress condition of *H. pluvialis*. In the section C of Chapter II two different stresses were applied: high light and nitrogen starvation. Phenotypic analysis of stressed cell revel that nitrogen starvation inhibits chlorophyll biosynthesis, induces chlorophyll b

degradation with a consequent PSII antenna proteins destabilization. In this condition PTOX activity and the cyclic electron transport are also inhibited with the simultaneously increase of dark respiration activity again photosynthesis, while high light induces the xanthophyll cycle activation and carotenogenesis. The combination of high light and nitrogen starvation induce the acclimation of photosynthetic apparatus increasing the resistance to the photo-oxidative stress with astaxanthin accumulation and PSII antenna size reduction. In the section D of the Chapter II more attention was focused on the effect of stressing conditions on isolated complexes from *H. pluvialis.* Complexes isolated from cells grown in control condition show features reliable with proteins purified from higher plants or *C. reinhardtii*. In this Chapter was demonstrated that the acclimation to high light, in *H. pluvialis*, induces a destabilization of the PSI-LHCI supercomplex and PSII core probably due to the rapid PSII core turnover and partially substitution of astaxanthin to β-carotene bind to the Photosystems. The β-carotene absence causes a destabilization of the interaction between antenna protein complexes and PSI core. But only 1% of the total astaxanthin produced in *H. pluvialis* is bound to PSI or PSII, while almost all astaxanthin is accumulated in the cytoplasm having a specific role as antioxidant to protect the nucleus and filtering light with the consequent reduction of excitation pressure on the photosynthetic subunits.

Abbreviations

Ax	Antheraxanthin
APX	Ascorbate peroxide
ATP	Adenosine triphosphate
ATPase	Atp synthase
β-Car	β -Carotene
Car	Carotenoids
CEF	Cyclic electron flow
Chl	Chlorophyll
CP24	Chlorophyll binding protein of 24 kda
CP26	Chlorophyll binding protein of 26 kda
CP29	Chlorophyll binding protein of 29 kda
Cyt b_6f	Cytochrome b_6f complex
DTT	DL-dithiothreitol
F0	Minimal fluorescence of dark-adapted leaves
FLV	Flavodiiron
Fm	Maximum fluorescence of dark-adapted leaves
Fm’	Maximum fluorescence light adapted leaves
Fv	Variable florescence ($Fm-F_0$) of dark-adapted leaves
LEF	Linear electron flow
LHC	Light harvesting complex
LHCI	Photosystem I light harvesting complex
LHCII	Photosystem II light harvesting complex
Lut	Lutein
MDA	Monodehydroascorbate
$NADP^+$	Nicotinamide adenine dinucleotide phosphate oxidized
$NADPH_2$	Nicotinamide adenine dinucleotide phosphate reduced
NDH	NAD(P)H dehydrogenase
Neo	Neoxanthin
NPQ	Non photochemical quenching
OEC	Oxygen evolving complex
P680	Photosystem II reaction center
P700	Photosystem I reaction center
PAR	Photosynthetically Active Radiation
PC	Plastocyanin
PTOX	Plastoquinone terminal oxidase

PSI	Photosystem I
PSII	Photosystem II
Qa	plastoquinone A
Qb	plastoquinone B
Qy region	spectrum region between 630-675nm
ROS	reactive oxygen species
SOD	SupeOxide Dismutase
Soret region	spectrum region between 450-475nm
Vx	Violaxanthin
VDE	Violaxanthin De-Epoxidase
WT	Wild-type strain
Zx	zeaxanthin